AD-A032 635 AEROJET SOLID PROPULSION CO SACRAMENTO CALIF F/G 21/9.2
FLEXIBLE CASE - GRAIN INTERACTION IN BALLISTIC WEAPON SYSTEMS. --ETC(U)
OCT 76 K W BILLS, S W JANG, H LEEMING F04611-72-C-0055
UNCLASSIFIED ASPC-1953-81-F-VOL-1 AFRPL-TR-76-57-VOL-1 NL

1 OF 3
AD
A032635

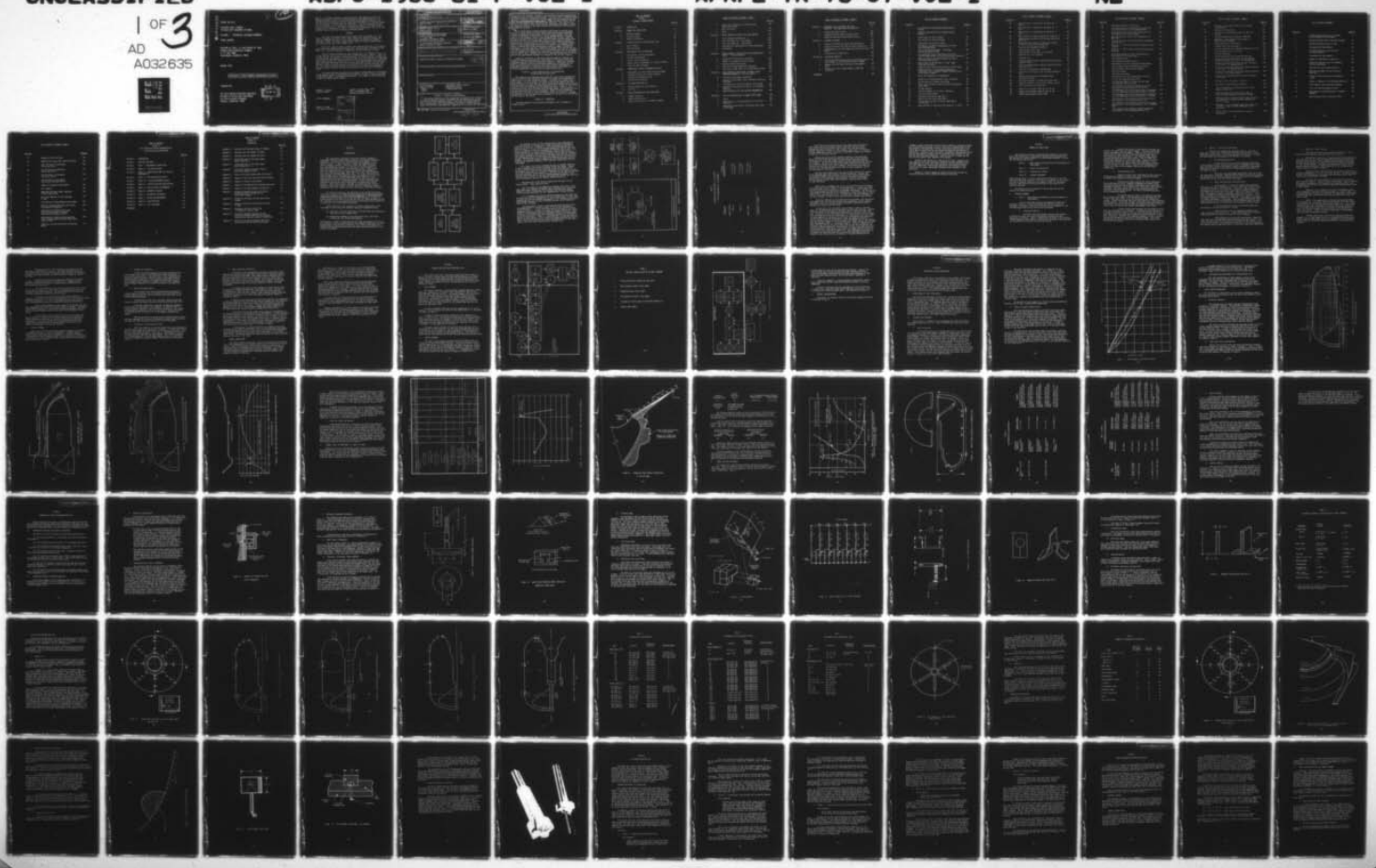

AFRPL-TR-76-57

FLEXIBLE CASE - GRAIN IN BALLISTIC WEAPON SYSTEMS

VOLUME I - TECHNICAL ACCOMPLISHMENTS

FINAL REPORT

Kenneth W. Bills, Jr. and Samuel W. Jang
Aerojet Solid Propulsion Company
P. O. Box 13400
Sacramento, California, 95813

October 1976

Prepared for:

Air Force Rocket Propulsion Laboratory
Director of Science and Technology
Air Force Systems Command
Edwards, California, 93523

When U. S. Government drawings, specifications, or other data are used for any purpose other than a definitely related Government procurement operation, the Government thereby incurs no responsibility nor any obligation whatsoever, and the fact that the Government may have formulated, furnished, or in any way supplied the said drawings, specifications, or other data, is not to be regarded by implication or otherwise, or in any manner licensing the holder or any other person or corporation, or conveying any rights or permission to manufacture, use or sell any patented invention that may in any way be related thereto.

FOREWORD

This report was submitted by Aerojet Solid Propulsion Company, P. O. Box 13400, Sacramento, California, 95813, under Contract No. F04611-72-C-0055, Job Order No. 305910WA with the Air Force Rocket Propulsion Laboratory, Edwards, California, 93523. The report summarizes the technical efforts conducted under this contract from April 1972 to March 1976.

The efforts reported herein represent the combined activities of the Aerojet Solid Propulsion Company, Harold Leeming, Ph.D. and Associates, Konigsberg Instruments, Inc., the Texas A&M Research Foundation, and the University of Texas.

The key technical personnel on this program were: Mr. Kenneth W. Bills, Jr., of ASPC, who was the Principal Investigator on the Program; Mr. Samuel W. Jang, also of ASPC, who was the program's Principal Engineer; Dr. Harold Leeming, of HL&A, who coordinated the instrumentation of the motors and, later the acquisition of gage data during motor testing; Mr. Eph Konigsberg, of KII, who supplied the stress and strain gages and supporting consultation; Dr. Scott W. Beckwith, of TAMRF, who provided an extensive study of flexible case materials and their constitutive relations; and Drs. Eric Becker and Robert Dunham, of the University of Texas, who developed an advanced computer code for the structural analysis of grains held in fiberglass cases.

This report has been reviewed by the Information Office/DOZ and is releasable to the National Technical Information Service (NTIS). At NTIS it will be available to the general public, including foreign nations. This report is unclassified and suitable for general public release.

Durwood I. Thrasher
Project Engineer

Charles E. Payne, Major, USAF
Chief, Surveillance and
Mechanical Behavior Section

FOR THE COMMANDER

Charles R. Cooke
Solid Rocket Division

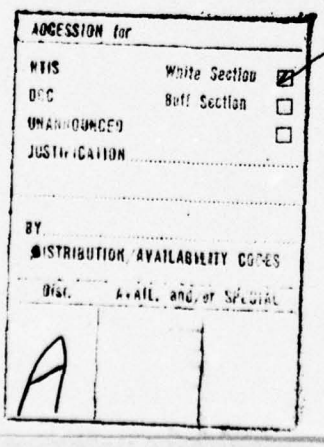

SECURITY CLASSIFICATION OF THIS PAGE (When Data Entered)

REPORT DOCUMENTATION PAGE

READ INSTRUCTIONS BEFORE COMPLETING FORM

1. REPORT NUMBER: AFRPL-TR-76-57-Vol-1	2. GOVT ACCESSION NO.
3. RECIPIENT'S CATALOG NUMBER	
4. TITLE (and Subtitle): Flexible Case-Grain Interaction in Ballistic Weapon Systems, Volume I. Technical Accomplishments.	5. TYPE OF REPORT & PERIOD COVERED: Final Report, Apr 1972 - Mar 1976
	6. PERFORMING ORG. REPORT NUMBER: 1953-81-F
7. AUTHOR(s): Kenneth W. Bills, Jr., Samuel W. Jang, Harold Leeming	8. CONTRACT OR GRANT NUMBER(s): F04611-72-C-0055
9. PERFORMING ORGANIZATION NAME AND ADDRESS: Aerojet Solid Propulsion Company, P. O. Box 13400, Sacramento, California, 95813	10. PROGRAM ELEMENT, PROJECT, TASK AREA & WORK UNIT NUMBERS: Job Order No. 305910JU
11. CONTROLLING OFFICE NAME AND ADDRESS: Air Force Rocket Propulsion Laboratory, Edwards, California, 93523	12. REPORT DATE: Oct 1976
	13. NUMBER OF PAGES: 749
14. MONITORING AGENCY NAME & ADDRESS (if different from Controlling Office): ASPC-1953-81-F-Vol-1	15. SECURITY CLASS. (of this report): Unclassified
	15a. DECLASSIFICATION/DOWNGRADING SCHEDULE

16. DISTRIBUTION STATEMENT (of this Report)

Approved for public release; distribution unlimited.

250 p.

17. DISTRIBUTION STATEMENT (of the abstract entered in Block 20, if different from Report)

18. SUPPLEMENTARY NOTES

19. KEY WORDS (Continue on reverse side if necessary and identify by block number)

Solid Propellant
Sensors or Gages
Stress
Strain
Experimental Stress Analysis
Structural Testing
Filament-Wound Case

20. ABSTRACT (Continue on reverse side if necessary and identify by block number)

Volume I - Technical Accomplishments

The original objective of this program was to establish the reliability of existing structural analysis techniques for the prediction of stresses and strains in solid propellant grains. This was to be accomplished by fully instrumenting a full-scale Minuteman III Stage III motor with the latest stress-strain instrumentation, subjecting it to various test conditions

DD FORM 1 JAN 73 1473 EDITION OF 1 NOV 65 IS OBSOLETE

UNCLASSIFIED

SECURITY CLASSIFICATION OF THIS PAGE (When Data Entered)

405 706

(thermal cycling, handling, vibration, pressurization) and then comparing the experimental results with predicted values. This was to be a "closed envelope" approach in which the reduced data from the gages were to be kept secret until the final assessment phase of the program. Midway through the motor testing phase serious anomalies were detected in the gage data. This led to a suspension of the original plan and an eventual redirection and change in scope to concentrate efforts on the identification and correction of the sources of the anomalies observed.

The revised program included diagnostic evaluations to isolate error sources, a system rework to correct and/or modify questionable components, a parallel laboratory investigation of specific gage characteristics and, finally, verification of the stability of the reworked system. From the results of the diagnostic tests it was determined that the major anomalies observed could be traced to the gages-lead-wire-solder junction combinations. Use of an acid flux in soldering the stainless steel leadwires provided a potential for corrosion to occur as the junction aged. The reworked system, which included crimped spade-lug junctions in place of the leadwire solder joints, a new DAS and revised operational procedures showed a substantial improvement in system stability, exhibiting an average drift rate of 0.5% of full scale output per month. This value is consistent with that for the gages alone as quoted by the manufacturer, and converts to about 0.75 psi per month for the 150 psi gage. However, this drift is considered excessive for measurement of long term thermal stresses (as required by the original program).

Laboratory evaluations of the gages addressed potential problems associated with exposed semi-conductor strain gages on the normal stress gage diaphragm, gage self-heating and hysteresis effects. These tests indicated potential transducer response differences between the calibration and the high rate pressurization situations which would require experimentally determined corrections to achieve the accuracy required to accomplish the original program goals for the high rate pressurization tests.

Volume II - Solid Propellant Grain Instrumentation
System Design and Application

The experience and knowledge gained from this and similar programs were compiled in this volume, which was designed as a guide to the experimental stress analysis of solid propellant grains. The effort was divided into six major phases. The first phase is directed to the program manager and the project engineer, who must make the initial decision to conduct such an effort. The second and third phases are more elaborate versions of Phase I, but involve realistic plans for instrumenting and testing the units. Phase III is an evaluation of these plans to assure that the measurements can be obtained with the available facilities and test equipment. Phases IV and V define the extensive work required to carry out the test plans, while Phase VI includes the reduction of the test data and an assessment of the quality of the testing and the value of the results.

Volume III - Appendices

Seventeen appendices give detailed supplemental data in support of Volumes I and II.

TABLE OF CONTENTS

VOLUME I

TECHNICAL ACCOMPLISHMENTS

TABLE OF CONTENTS OF VOLUME I (CONT.)

TABLE OF CONTENTS OF VOLUME I (CONT.)

LIST OF FIGURES OF VOLUME I

LIST OF FIGURES OF VOLUME I (CONT.)

LIST OF FIGURES OF VOLUME I (CONT.)

LIST OF FIGURES OF VOLUME I (CONT.)

LIST OF TABLES OF VOLUME I

LIST OF TABLES OF VOLUME I (CONT.)

TABLE OF CONTENTS

VOLUME II

SOLID PROPELLANT GRAIN INSTRUMENTATION SYSTEM DESIGN AND APPLICATION

TABLE OF CONTENTS

VOLUME III

APPENDICES

SECTION 1

INTRODUCTION

This program was conceived as part of an overall transducer development and applications effort by the Air Force Rocket Propulsion Laboratory. The place of this program within that framework is best shown by Figure 1, which presents a simple flow diagram relating the key programs involved. Starting in 1967, the AFRPL instituted four instrumentation programs (1-4) for the in-situ measurement of bond shear and normal stresses and inner-bore strains. Then, having shown an acceptable level of success, the efforts were extended to full-scale motor applications, beginning with a first stage Minuteman motor (5,6) and the Bomb Dummy Unit (7,8). The initial successes from these programs led to more ambitious efforts to develop an in-situ surveillance gage (9,10), a three-dimensional stress gage (11), and a highly sophisticated data acquisition system (12) for monitoring tests conducted on full-scale, instrumented motors. Finally, the gages were directed to the more practical applications of experimental stress analyses. These latter efforts involved, in addition to the Flexible Case-Grain Interaction studies, Project SALE (13), SRAM (14), Ambient Temperature Cure (15), and the Ballistic and Tactical HTPB Motor programs.

As originally conceived, the objective of the Flexible Case-Grain Interaction program was to establish the reliability of existing analytical techniques to predict the stress and strain behaviors in solid propellant rocket motors with flexible cases under the wide variety of loading conditions normally anticipated in the service life of a deployed weapon system. This objective was to be accomplished using the previously proven capability of grain stress and strain measuring devices.

Stated differently, this program was originally dedicated to the assessment of grain structural analyses; the basic assumptions being:

(1) The stress and strain gages were fully developed and sufficiently qualified for the planned effort.

(2) Conventional methods of data acquisition were sufficiently accurate for the required measurements.

Unfortunately, a number of gage anomalies and other measurement difficulties associated with the data acquisition and data reduction techniques precluded accomplishment of the original objectives. As a result the program was redirected to concentrate efforts upon the definition and correction of the problems encountered.

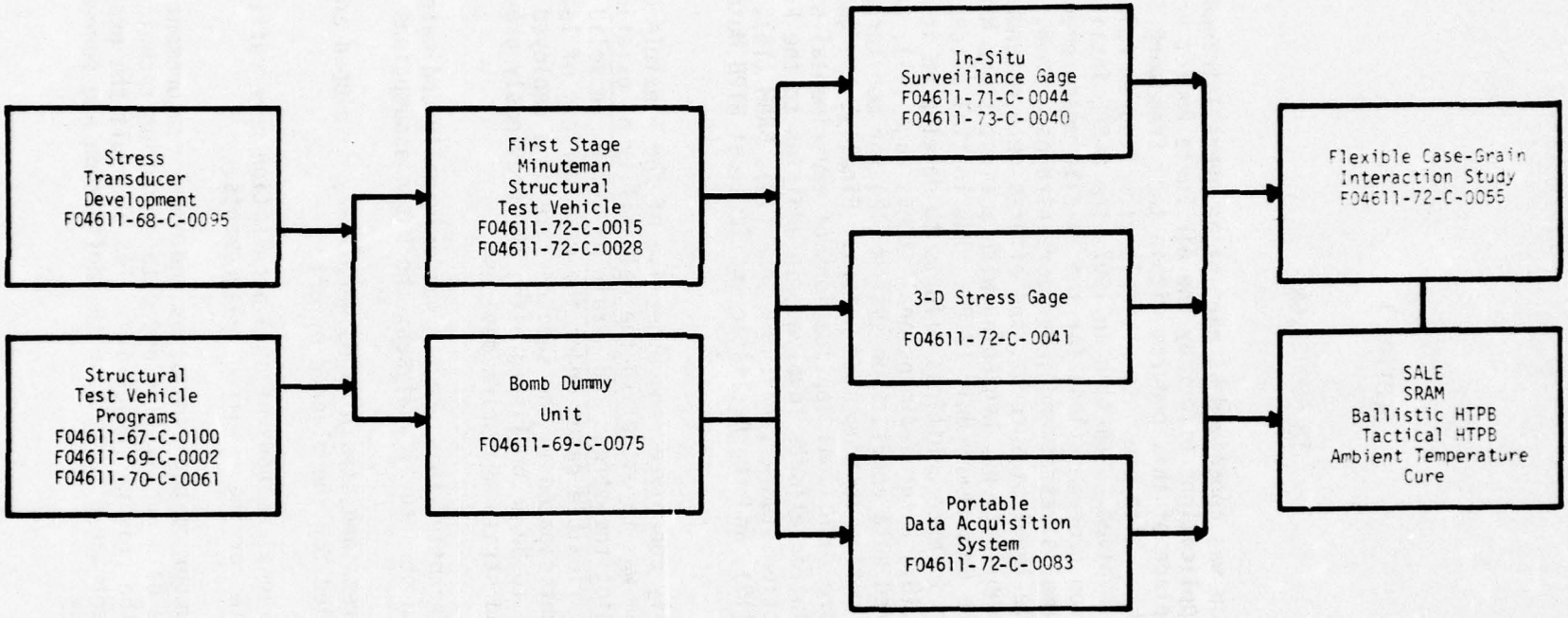

FIGURE 1. INSTRUMENTATION DEVELOPMENT AND APPLICATION EFFORTS

The problems in the original program efforts were compounded by a "closed envelope" philosophy which allowed unrecognized measurement anomalies to continue. A schematic of the closed envelope approach is given in Figure 2. In the first envelope measurements made on the motor were to be reduced to give the observed grain stresses and strains. The second envelope was to contain the predicted values of these stresses and strains as derived from structural analyses (using material properties from samples obtained by dissection of the motor after the test program). The two envelopes were not to be opened and compared until the end of the program. This approach further required that the measurements and data reduction be conducted separately (ASPC and HL&A, respectively) with no interchange.

This latter restriction prevented the type of feedback necessary to permit immediate correction of problems within the system. Because of this difficulty ASPC and HL&A requested relief from AFRPL of this requirement after review of the data measured during the thermal cycling tests had disclosed serious anomalies. Therefore, by the time the problems had been recognized and the closed envelope approach discarded it was realized that a solution to the gage and measurement problem was essential before continuing to pursue the original program objectives.

The objectives of the revised program form the basis for the ensuing report. Those objectives were:

(1) To isolate the instrumentation problems which exist in the motor under test; demonstrate whether these problems can be eliminated; demonstrate means of detecting such problems; and determine whether criteria can be established for the 'repairability' of such problems.

(2) To document the fullest possible guidance for the proper use of stress and strain instrumentation in solid rocket motors so that other programs may avoid the problems encountered in this program; also provide some insight into ways in which transducer designs can be improved to minimize these problems.

The measurement accuracies which were believed attainable with the embedded gages in the early stages of the original program are listed in Table 1. It was later realized that an order of magnitude improvement would be required to achieve the program objectives. Consequently, a considerable effort was expended during the revised program in setting up an appropriate data acquisition system and in developing proper use procedures. Table 1 is provided here to show the state of the art at the inception of the Flexible Case-Grain Interaction program. These values do not necessarily reflect the capabilities of the transducers, since the limits represent total system errors.

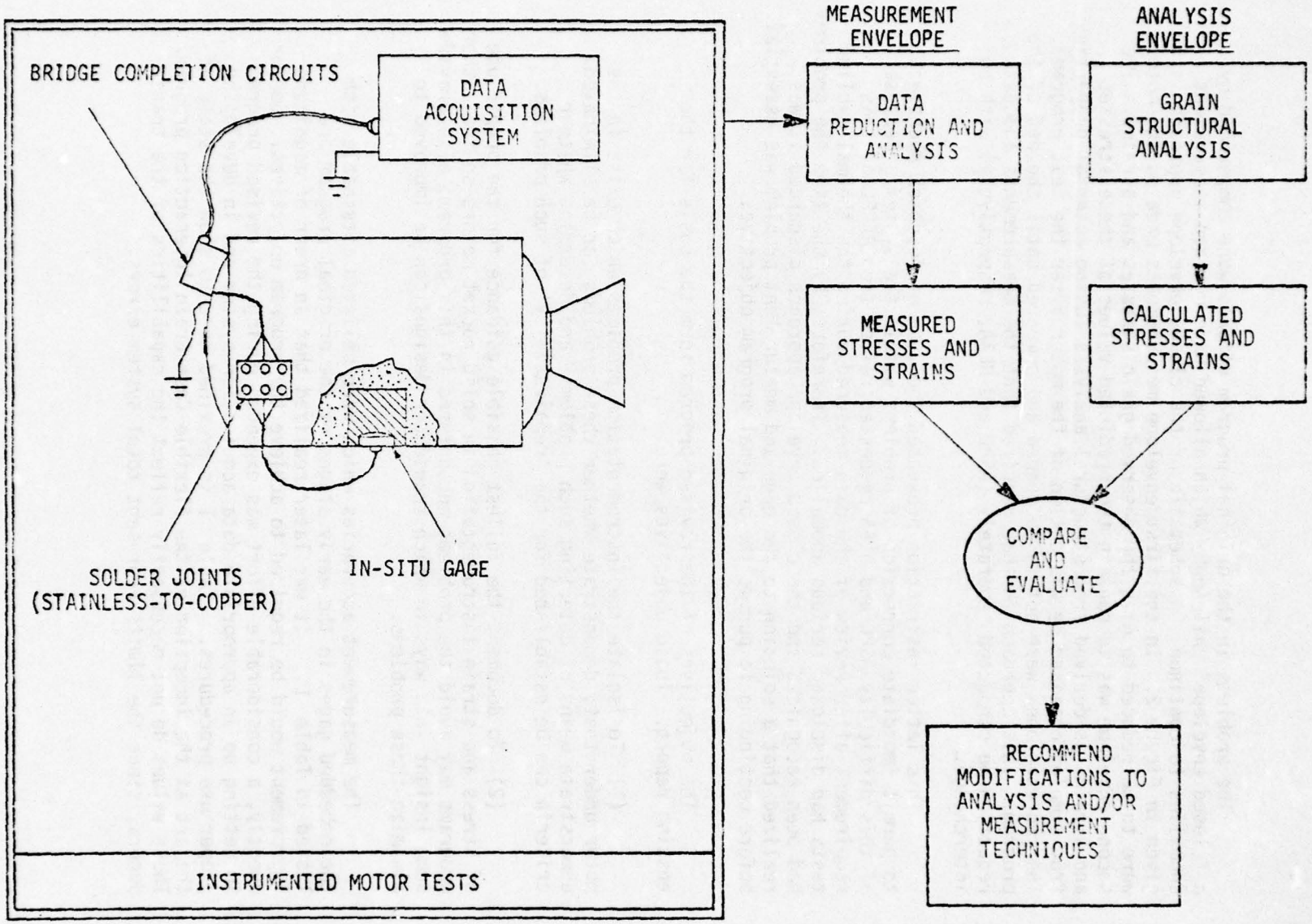

FIGURE 2. SCHEMATIC REPRESENTATION OF CLOSED ENVELOPE APPROACH

TABLE 1

ESTIMATED SYSTEM ACCURACY IN THE MOTOR

AT THE BEGINNING OF THE PROGRAM

Transducer	Original Measurement Limits
Normal Stress	
150 psi	± 10% of rdg or ± 2 psi*
450 psi	± 10% of rdg or ± 4 psi*
Shear Cubes	± 30% of rdg or ± 5 psi*

* Whichever is larger.

After the revised program was put into effect and the necessary modifications made on the motor external electrical system and DAS, measurements taken revealed that data scatter and drift were greatly reduced, though not eliminated. This residual "gage drift" is a mixture of motor temperature change, propellant viscoelastic response and inherent instability in the gage circuits.

Concern was expressed that adiabatic heating of the propellant during the rapid motor pressurization associated with firing simulation would generate a transient thermal gradient in the propellant adjacent to the gages. The resulting gage output comprising pressurization stresses plus transient thermal error signals would then prove too inaccurate for resolution of the small deviatoric stresses. The difficulty of ensuring rational high rate pressurization data from the gages eventually led to the termination of the effort.

One final gage problem which was not resolved concerns the response of the embedded gages under thermal transient conditions. Because the gage sensing elements for each bridge circuit are situated both internal and external to the diaphragm, they experience different environments during transient thermal tests which produces a spurious output under no load conditions.

ASPC strongly recommends the use of in-situ stress and strain gages for experimental stress analyses of solid propellants. In many cases large deviations from existing analyses are expected, and the actual values can only be approximated by some direct experimental techniques. The difficulties experienced on this program are all manageable by proper techniques of fabrication, test, and data acquisition. In some cases, the best techniques are yet to be learned, so the Air Force could do well to support such efforts.

Certainly, improved in-situ gages would be desirable, but significant improvements over the existing designs would undoubtedly require advanced development efforts by the most capable instrument companies and would probably cost several million dollars.

For the most part, this report was outlined in terms of the major events of the program and follows the order in which they occurred. However, since the anomalies encountered invalidated most of the early motor test data, discussion of the associated efforts has been limited to that information considered necessary for completeness or of potential use to the reader. The major emphasis in the report is given to a presentation and evaluation of the results of the revised program. After the summary, Section 2, a special section (Section 3) briefly outlines the complex flow of the program, then two sections summarize the anticipated grain loads and the plan followed when instrumenting the motor (Sections 4 and 5). Section 6 summarizes the structural test vehicles used to develop some of the new installation and testing procedures planned for this program. Section 7 describes the fabrication of two full-scale motors, while Section 8 summarizes the results of the original tests conducted on Motor No. 1 (only abbreviated test data are presented, and these are given only to show the measurement anomalies). Sections 9 and 10 describe the assessment of the gage problems and the

attempts at their correction, while Section 11 presents a suggested method for re-calibrating the gages in place. Section 12 considers some of the environmental conditions where the full-scale motor might develop stress levels that are sufficient to give useful correlations with analytical predictions. Section 13 gives an overall assessment of the measured stress data and the potential future value of structural test vehicles for predicting full-scale motor behaviors. Finally, Section 14 summarizes the work of three studies that supported this program.

Volume II was prepared as a "How to do it" book. Attempts have been made to distill the significant findings from this program and use that knowledge to refine and update previously established procedures to give a simplified, step-by-step approach to the planning of tests, installation of gages, measurement procedures and assessment of the gage data.

Volume III contains Appendices which provide detailed data and background material which support the Volume I discussion.

SECTION 2

SUMMARY AND CONCLUSIONS

The program as originally structured was intended to be a four-phase effort consisting of experimental and analytical evaluations of the stresses and strains produced in a Third Stage Minuteman III motor. The four phases consisted of:

Phase I - Anticipated Load Definition and Instrumentation Requirements

Phase II - Design and Fabrication

Phase III - Experimental Testing

Phase IV - Program Assessment

Midway through Phase III serious anomalies were detected in the data from full-scale motor testing. This led to a suspension of the original plan and an eventual redirection and change in scope to concentrate efforts on the identification and correction of the source of the anomalies observed.

The major activities completed in the original and revised programs are summarized below.

A. ORIGINAL PROGRAM

1. Phase I - Anticipated Load Definition and Instrumentation Requirements

In this report two sections are devoted to discussion of the Phase I efforts. Section 4 provides the analytical basis for placement of the gages, and Section 5 details the instrumentation plan, including gage selection and installation techniques.

a. Structural Analysis

Available static and dynamic analyses were employed to define the stress and strain distributions expected for motor operational conditions. Special consideration was given to the flexible filament-wound case which exerts a significant influence on the magnitude and distribution of the grain stresses and strains.

Based on the results of the analysis the motor was divided into eight zones for gage placement. Each zone represented unique instrumentation requirements. Zones A, B and C were on the outer surface of the case and included the forward dome, barrel section and aft dome, respectively. The remaining zones were at the grain bondline and inner bore surface. Zone D covered the forward boot termination, a high stress area. Zone E was at mid barrel bond interface, an area of low stress gradients. Zone F included the critical aft dome bondline where the maximum stresses occur and failure is most likely. Zones G and H encompassed the finocyl slot region and axisymmetric portion of the inner bore, respectively.

b. Instrumentation Plan

Specific criteria were established to guide selection of the types and numbers of gages to be used, locations for their placement, and associated wiring and hardware.

The principal gages selected for stress measurement were a miniature (0.310 in. diameter) diaphragm type normal stress transducer manufactured by Konigsberg Instruments, and a shear gage developed by Leeming. Failure event gages, fabricated from conductive elastomers, were developed by ASPC for this program and used for detection of bondline separations. All other instrumentation used was of conventional design.

The general approach taken in placement of the gages was to place stress gages of the appropriate type and range near the critical high stress areas in the aft dome and at the forward boot release. Failure event gages were also used liberally in these potential failure regions. In addition a number of bondline gages were placed near the center of the barrel section where the gradients are small and most nearly ideal for correlations between measurements and analyses.

A unique installation procedure for the bondline stress gages was developed for this program. It involved potting the gages in a castable insulation material prior to calibration by the manufacturer. Upon return the potted gages were bonded into pre-milled holes in the motor insulation. Leadwires were channeled through a 0.060 in. diameter hole drilled through the case directly below the gage. This unique through-the-case wiring technique was developed by ASPC specifically for use on this program.

2. Phase II - Design and Fabrication

Phase II was comprised of two major efforts. The first, summarized in Section 6, involved the fabrication and testing of structural test vehicles (STV). The second, discussed in Section 7, included the fabrication and instrumentation of the full scale motors.

a. STV Fabrication and Test

A total of five STV's were fabricated and tested early in the program to verify that the several types of embedded stress transducers and their installation methods could be successfully used without affecting the integrity of the grain or filament-wound glass chamber of the Stage III motor.

These tests provided needed experience in the use of the new installation techniques, demonstrated the feasibility of the pre-potting and through-the-case wiring techniques, and verified the failure detection capabilities of the shear and failure event gages.

b. Motor Instrumentation and Fabrication

Two Minuteman III, Stage III chambers were purchased, hydrotested and then instrumented per the plan developed in Phase I and procedures verified in STV evaluations. Motor No. 1 was designed to be structurally tested but not fired so the external hardware components were taken from a previously fired motor. Motor No. 2 was an "all up" motor instrumented to permit measurements during static firing. It has been in storage since completion of propellant cure. (Motor No. 2 was instrumented about five months after Motor No. 1 and received the benefit of several improvements in technique. These improved methods were subsequently applied to the instrumentation of the Minuteman Stage III motor fabricated and tested on the Strategic HTPB program at Thiokol-Wasatch).

Prior to propellant casting the installed gages were calibrated by step pressurization to 15 psig.

Both motors were cast with ANB-3066 propellant made from a production lot of materials. Carton samples were taken from each propellant batch and placed in storage for later evaluation.

After propellant cure the grain was cooled, X-rayed and then inner bore instrumentation and associated wiring was installed. The motor was then placed in 110°F storage to be aged for four months. This was to allow the post-cure hardening to take place at the cure temperature and thereby prevent significant shifts in the grain stress-free temperature.

3. Phase III - Motor Testing

The major structural tests performed on Motor No. 1 were thermal cycling, handling, transportation, and vibration.

The testing of Motor No. 1 actually started during processing since the output of the gages was monitored during grain cure and cool-down and core extraction. After trimming and radiographic inspection a pressure calibration was performed and the motor was placed in storage at 110°F for four months. The gages were monitored daily for the first week and monthly thereafter. After completion of the storage period thermal cycling tests were initiated.

Thermal testing involved storage for 10 days at each of the following temperatures: 80°, 60°, 110°, 80° and 60°F. The grain stresses/strains, case deformations, and temperatures were monitored at three discrete times in each thermal transient.

The motor was then subjected to the conditions typical of motor handling; namely: lifting, tip over and rolling. This was followed by storage-to-transporter and transporter-to-transporter tests. Case deformations and the grain stress/strain gages were monitored during each of these events.

Motor No. 1 was subjected to a series of vibration survey tests conducted in the thrust (Y) and transverse (Z, 90-270°) axes. The resonant frequency response characteristics and mode shapes of the motor and propellant due to sinusoidal excitation was monitored in the 10-to-300-cps range.

ASPC's first opportunity to evaluate the data from these tests on Motor No. 1 came when the motor was mounted in the test stand in preparation for the planned rapid pressurization test. This review showed that the first indication of anomalous behavior occurred during a 15 psig pressurization following installation of bridge completion units. In this case a number of gages showed significant shifts in "zero load" output. Similar shifts were noted again in measurements made just prior to propellant casting.

Readings taken while the grain was subjected to the cure pressure (15 $\pm$ 1 psig) showed that all of the gages responded to the pressure, but the magnitudes varied from somewhat less to considerably greater than the sum of the propellant hydrostatic head and the cure pressure.

Following gelation of the propellant, the behavior of the transducers become much more regular. The gages generally reacted in the expected direction to applied loadings, and the traces for companion bridges on each gage remained very nearly parallel through the rest of the tests.

From this point on most of the gage responses to pressure, or stress, differentials generally remained fair. Although erratic behaviors occurred in some tests, reasonably good differential data were obtained in most cases.

This also seemed to be the case for the handling tests during part of which the motor is rolled about its longitudinal axis while the transducers were being monitored. The results obtained are consistent with those predicted analytically for this motor.

In general, the limited testing performed on Motor No. 2 appeared to yield data which were more reproducible and consistent than those obtained from Motor No. 1. This is attributed to the use of improved motor instrumentation techniques learned from the work on Motor No. 1

It was clearly apparent at this stage in the program that the gage measurements were exhibiting marked calibration changes. The overall system needed evaluation to correct the problems encountered, determine their sources and document them to help avoid similar problems in the future.

In the ensuing revised program the roles of the gages, DAS, and the electrical systems on the observed anomalies were ascertained through diagnostic studies on the motor and reinforced by laboratory evaluations. From this point on the closed envelope restriction was removed from the program and ASPC became directly involved in data acquisition procedures and gage data reduction.

B. REVISED PROGRAM

The scope of the revised program included diagnostic evaluations to identify the sources of the system anomalies, a system rework to correct and/or modify questionable components, a parallel laboratory investigation of specific gage characteristics, and finally, verification of the stability of the reworked system. These efforts are described in detail in Sections 9 and 10.

1. Diagnostic Evaluations

A total of twelve diagnostic tests were conducted on the motor ranging from simple visual inspection through evaluations of system drift and stability. From the results it was determined that the major anomalies observed could be traced to the gages-leadwire-solder junction combinations. Investigation revealed that an acid flux had been used to solder the stranded stainless steel leadwires which provided a potential for corrosion to occur as the junctions aged.

2. Motor and System Rework

All stainless steel solder junctions were replaced with crimped spade-lug terminals and the junction strips were modified to allow a complete electrical drift and calibration check prior to and following each measurement.

A divider was placed across the power supply and one DAS channel to permit continuous checking of gage energization power level.

A new data acquisition system was designed and assembled. It consisted of a Varian 620 i mini-computer, an interface with an analog to digital converter, and a 64 channel multiplexer. The system was designed to guarantee precision and accuracy of the results within a specified limit of $\pm$ 0.2 mv or 3% of the reading, whichever was greater.

Revised operational procedures were formulated which required that each component of the system be checked for proper operation during each data run, and specified an operating cycle for the gages.

3. Evaluation of the Reworked System

Drift and stability and pressurization tests were conducted on the motor using the revised operational procedures. A substantial improvement in system stability was observed, i.e. an average drift rate of 0.5% of full scale output per month. This value is consistent with that for the gages alone as quoted by the manufacturer. This converts to about 0.75 psi per month for a 150 psi gage, however, which is a significant error when attempting to measure thermal stresses which do not exceed 5 psi.

4. Gage Laboratory Evaluations

To provide a more fundamental assessment of the normal stress gages and the factors which might cause them to exhibit anomalous behavior a series of laboratory experiments were conducted which addressed specific gage and system characteristics which had been previously identified as possible contributors to the overall problem - areas studied included the stainless steel solder junctions, the exposed semi-conductor strain gages on the gage diaphragm, gage self-heating, hysteresis effects, and gage pre-potting.

An accelerated aging test was conducted in which various types of junctions, soldered and mechanical, were exposed to 160°F and 100% R.H. for eleven days. Both stainless steel and copper wire were evaluated. Upon drying for eight hours the stainless steel soldered junction exhibited a change in resistance of 13%, while the remaining junctions showed no significant effects.

Cooling of the transducer from the epoxy adhesive cure temperature to ambient produces differential thermal stresses between the semi-conductors and the diaphragm which could cause creep of the semi-conductor and long term drift of the zero stress output. Limited experiments suggested that cumulative errors due to creep of gage elements may become significant if the gages experience repeated exposure to temperatures above 130°F.

The construction of the normal stress gage and its embedment in an insulating material lend themselves to the development of thermal gradients across the diaphragm, due to external transient effects or gage self-heating. Measurements made when such gradients are present will be subject to error since the resistance of the semi-conductor strain gages is strongly affected by temperature. Experiments to evaluate the self-heating effect indicated temperature increases in the strain gage elements of between 11 and 21°F, with the external gage showing about a 3°F higher increase.

A large number of pressurization tests at moderate rates were conducted which showed that hysteresis occurs in the transducer measurements. The results suggested that this effect could significantly alter transducer response under the high pressurization rates experienced in a simulated motor firing. Calibration corrections would be required to obtain acceptable accuracy from tests of this type.

C. OVERALL CONCLUSIONS

The subject program experienced a series of problems which ultimately led to the abandonment of the original objectives and a redirection of the effort. Some of the problems stemmed from a certain naivete and lack of experience with an instrumentation job of this complexity. For the most part these problems could have been corrected in a timely manner if the "closed envelope" philosophy had not prevented immediate feedback when anomalies occurred in the data.

Unfortunately, as shown by the results of the revised program, even with all circuitry faults corrected the system still shows drift and rate dependency, simply because the gages available at the beginning of this program were not designed to exhibit the inherent stability needed for this application. These features prevented measurements of the grain stresses to the degree of accuracy required to accomplish the original objectives.

This latter observation exemplifies perhaps the most important lesson learned from this effort, and one which has been strongly emphasized in Volume II of this report. It's crucial that, at the outset of an undertaking of this type, the accuracy required be clearly defined and judged to be achievable. Detailed specifications must then be written which will tell the gage manufacturer exactly what is wanted, what the limits of acceptability will be, and what level of testing and certification is required.

It is felt that the redirected effort was quite successful and has contributed to a better understanding of the capabilities and limitations of grain instrumentation, which, in turn, will provide the basis for future improvements in the gages and methods for their application.

Numerous applications still exist where in-situ stress and strain gages can provide useful information obtainable by no other means. It is hoped that the experience and knowledge gained from this program will encourage wider use of this type of instrumentation, while at the same time providing the guidance needed to ensure that valid data are the result.

SECTION 3

PROGRAM FUNCTIONS AND OPERATIONAL FLOW

The Flexible Case-Grain Interaction program was quite complex in that it initially involved many activities and technologies, and midway through the effort a major change was made in the scope and direction of the program. The following section was specifically written for the reader, to put the program activities into perspective and to guide him through the report.

A. BASIC PROGRAM

This effort involved a "closed-envelope" approach where one company, HL&A, was responsible for the gages, their installation, calibration, data reduction, and data analyses. The second company, ASPC, was responsible for structural analyses, motor fabrication, testing, and data acquisition. A flow diagram for the basic program which shows this division of responsibility, is given in Figure 3. The two envelopes, experimental stress/strain measurements and the analytical predictions were to be kept secret until the end of the program when they would be opened and compared by AFRPL.

Sections 4 through 8 describe the basic program as far as it was pursued. The function and the section of the report where it is described are shown in Figure 3.

A number of new gage concepts were used on this program; see Table 2 and Section 5. Before they could be used in full-scale motors it was necessary to test the concepts in structural test vehicles (STV's). These STV's were fiberglass cylinders 5 in. I.D. by 20 in. long. Their fabrication, testing, gage test results and data analyses are reported in Reference 16 and summarized in Section 6.

The basic program continued to the point where the motor was to be pressurized to grain failure. At that time the program was put on a "Hold" status for five months to allow assessments of various questions pertaining to gage anomalies and measurement accuracy. The result of these and some later evaluations was the "Revised" program described below.

B. REVISED PROGRAM

This part of the program revolved around the isolation and correction of the gage measurement anomalies. The closed envelope secrecy had been removed and all of the data were available for review. Assessments by ASPC, AFRPL, and an independent consultant provided the impetus for planning efforts that led to diagnostic studies on Motor No. 1 and a preliminary corrective action plan, Figure 4. Implementation of this plan gave an accurate DAS and versatile diagnostic capabilities to

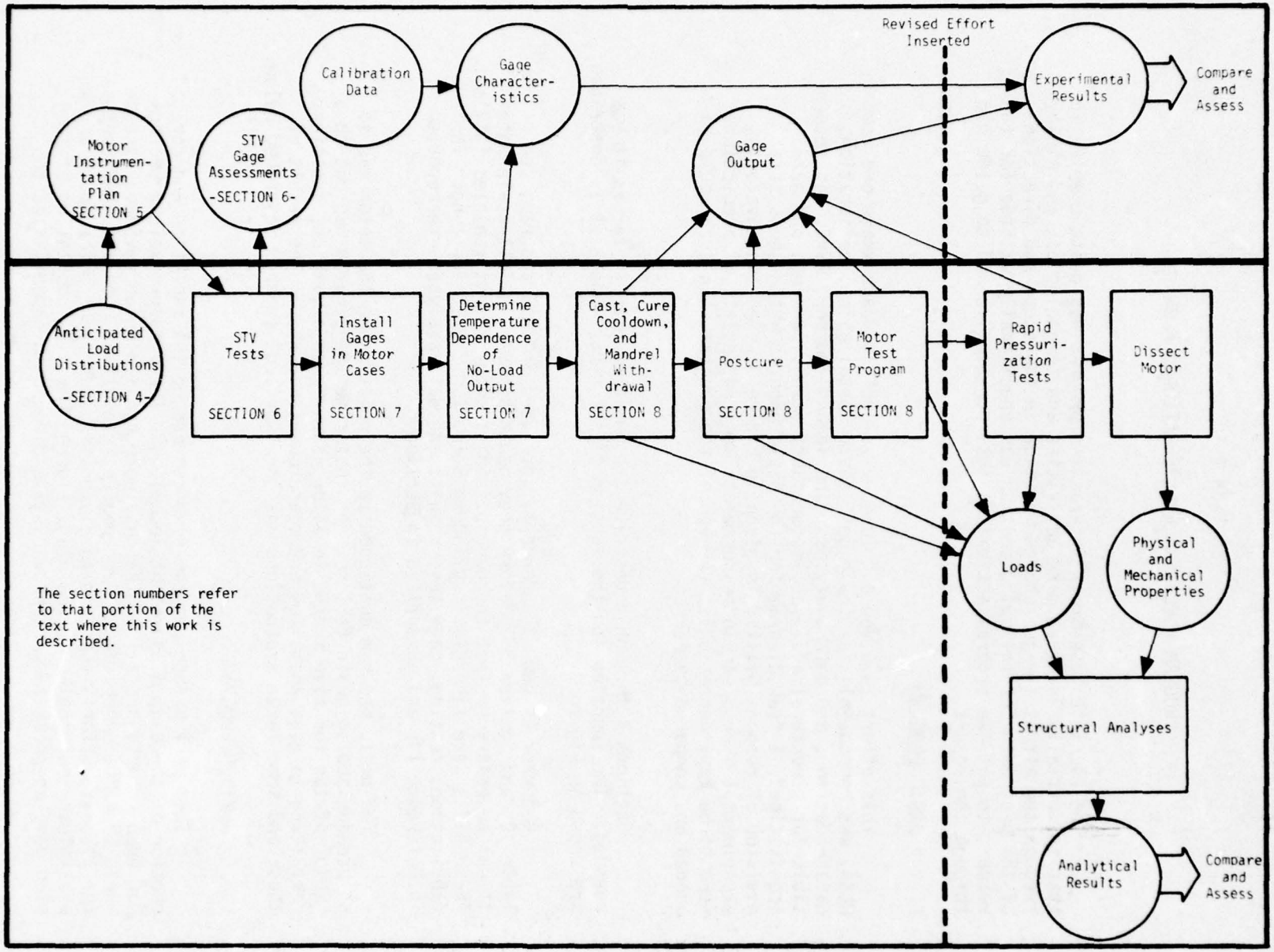

FIGURE 3. FLOW DIAGRAM FOR BASIC PROGRAM

TABLE 2

NEW GAGE CONCEPTS USED ON THE BASIC PROGRAM

1. Exiting lead wires through the case wall.

2. Small diameter normal stress gages.

3. Ruggedized shear stress gages.

4. Pre-potting of normal stress gages.

5. Elastomeric failure gages for bondline separations.

6. Three-D gage (HL&A).

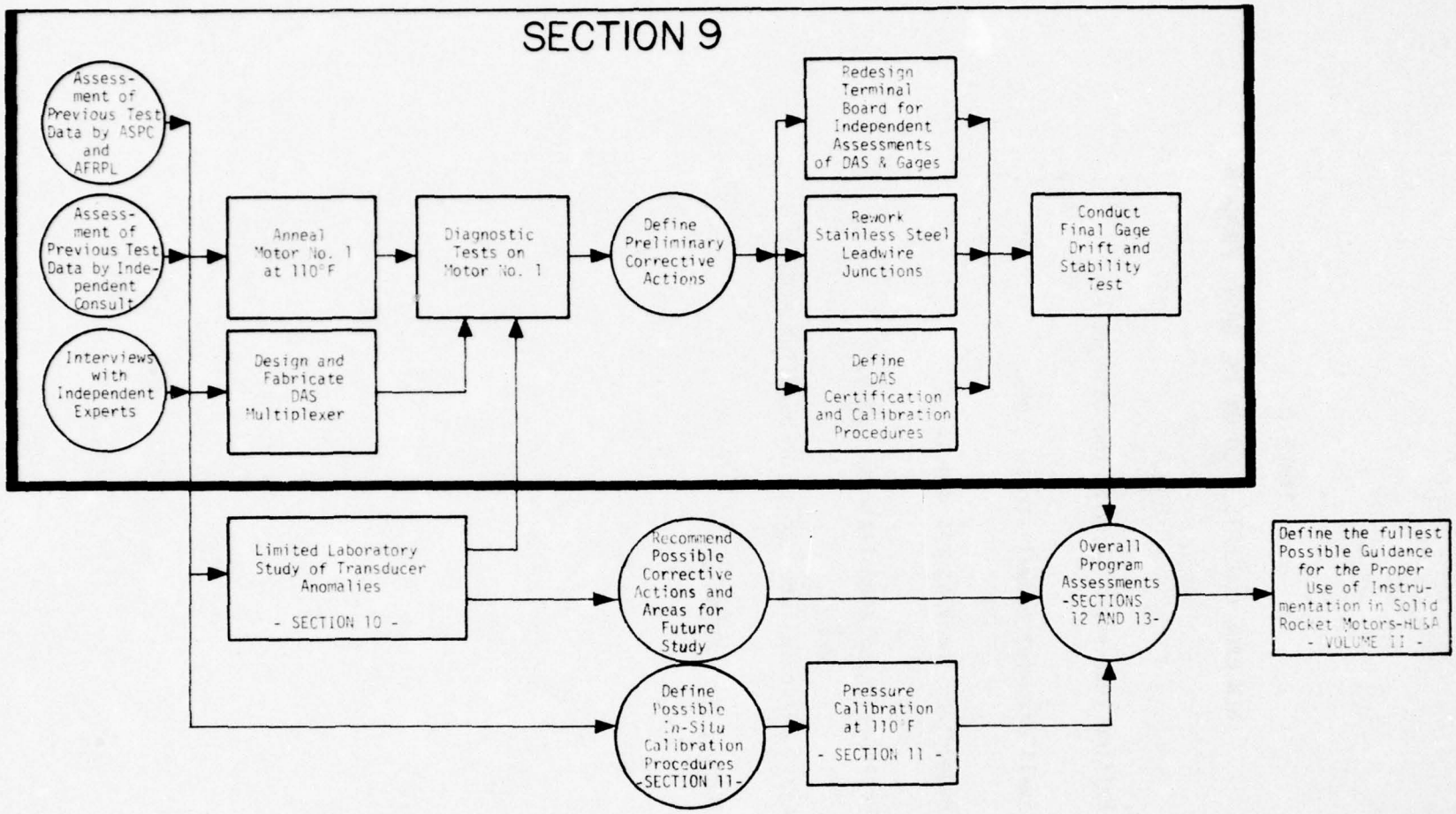

FIGURE 4. FLOW DIAGRAM FOR REVISED PROGRAM

isolate anomalous areas of the gage measuring network. Rigorous DAS certification and calibration procedures were implemented and the overall measurement system (gage plus the DAS) were subjected to long term drift and stability tests. All of this work is reported in Section 9.

Section 10 summarizes a limited laboratory study which investigated, among other factors, gage self-heating, hysteresis, and rate dependency.

Section 11 considers possible procedures for the recalibration of normal stress gages while they remain implanted in the grain. This is followed by a limited example that is also described in Section 11.

C. OVERALL CONSIDERATIONS

Assessments of different factors of the overall program are given in Sections 12 and 13.

SECTION 4

ANTICIPATED LOAD DISTRIBUTIONS

This effort, conducted at the beginning of the program, was designed to guide the placement of gages in the grain and on the motor case. It employed available static and dynamic structural analyses and test data to define the stress and strain distributions within the motor when placed under various loading conditions. Because of the flexibility of the fiberglass motor case, separate considerations were made to account for its special characteristics. The following subsections summarize these considerations, beginning with those for the fiberglass case.

A. DESCRIPTION OF THIRD STAGE MOTOR

The Third Stage Minuteman III motor has a 52-inch OD S-994 preimpregnated glass roving case (UTS 440 ksi), with a composite wall thickness of 0.1605 inch in the basic chamber where 0.1005 inch is hoop wrap and 0.060 inch is longitudinal wrap. The ANB-3066 propellant grain is axisymmetric and cylindrical throughout its length, except at the forward end where a six-slot finocyl design is incorporated; it is released over the entire forward head of the motor and is bonded from the forward equator to the aft nozzle boss attachment. The bond system is ANB-3066 propellant/SD-851-2 liner/V-45 insulation. Insulation at the forward end is 0.165 inch thick and tapers to 0.030 inch in the cylindrical section of the motor; the 0.050 inch thick forward boot is V-45 rubber bonded to the grain.

B. FLEXIBLE CASE BEHAVIOR

This section is intended to give background data that helps define the filament-wound motor case as a special problem area requiring careful attention.

1. Case Flexibility

Since the flexibility of a rocket motor case is a relative matter it is desirable to make some comparison between filament-wound cases, which are generally regarded as "flexible", and the more conventional homogeneous metal chambers. A review of operational motors indicate the working level of hoop strain for various case materials to be as follows: steel 0.4 to 0.7%, titanium 0.5 to 1.0%, glass 1.0 to 2.0%. On the basis of the above numbers it would appear that there is a certain amount of overlap and no sharp demarcation between case material and stiffness. In reality, however, the difference between homogeneous metal and filament-wound motor cases is more pronounced than the comparable strength and moduli ratios would indicate. This results from the longitudinal deformations of a filament-wound case being proportionally higher than the previously mentioned hoop strain levels would suggest. The problems becomes quite apparent when one examines the detailed design of a motor such as the third stage Minuteman.

The total longitudinal deformation is a summation of the individual cylindrical and dome deflections. The cylinder is a layered orthotropic shell with hoop and longitudinal windings oriented to carry hoop and longitudinal loads respectively. As a result hoop windings contribute very little to the longitudinal stiffness and the longitudinal strains are of the same order of magnitude as the hoop strains. This is in decided contrast to a homogeneous case where the longitudinal strain is less than 25 percent of the hoop strain under pressure loading. The longitudinal deflections of the domes or end closures is dependent on the shape and wrap angle. In general the shape is selected to minimize hoop stresses while the wrap angle is determined by the overall length and opening diameters. This design also results in considerably more longitudinal deflection than a comparable metal dome. Comparing total deformations it can be shown that the initial design pressure of 411 psi causes an empty third stage case to deflect approximately 1.34 inches "boss-to-boss" (Figure 5). This is in contrast to a predicted deflection of only 0.30 inches for a comparable case designed with high strength (220 ksi ultimate) steel.

On the basis of this comparison a flexible case was tentatively defined as one of glass filament-wound construction.

2. Effects of Motor Pressurization

The large deformations allowed by flexible cases during motor pressurization cause significantly higher grain inner bore strains and bond stresses than are experienced in equivalent metal cases. Since the propellant is practically incompressible at the pressure levels associated with motor operation, the volume of propellant remains constant while the volume of the container, i.e. motor case, expands significantly. For the third stage Minuteman motor this change in volume has been recorded as approximately 2.3 cubic feet during hydrotest at 600 psi. In order to maintain compatibility at the bonded surfaces this requires fairly large distortions at the bond termination points as well as of the entire free surface of the propellant.

By releasing the entire forward dome, and carefully tailoring the fin slot configurations, the inner bore strain levels were kept within estimated allowables and no evidence of grain cracking has been experienced. The local distributions at the bond termination has proven to be a more serious problem however. These distortions produce shear stresses which are almost directly proportional to propellant modulus, and the unexpected age hardening of the ANB-3066 propellant resulted in a very marginal condition for fully aged motors.

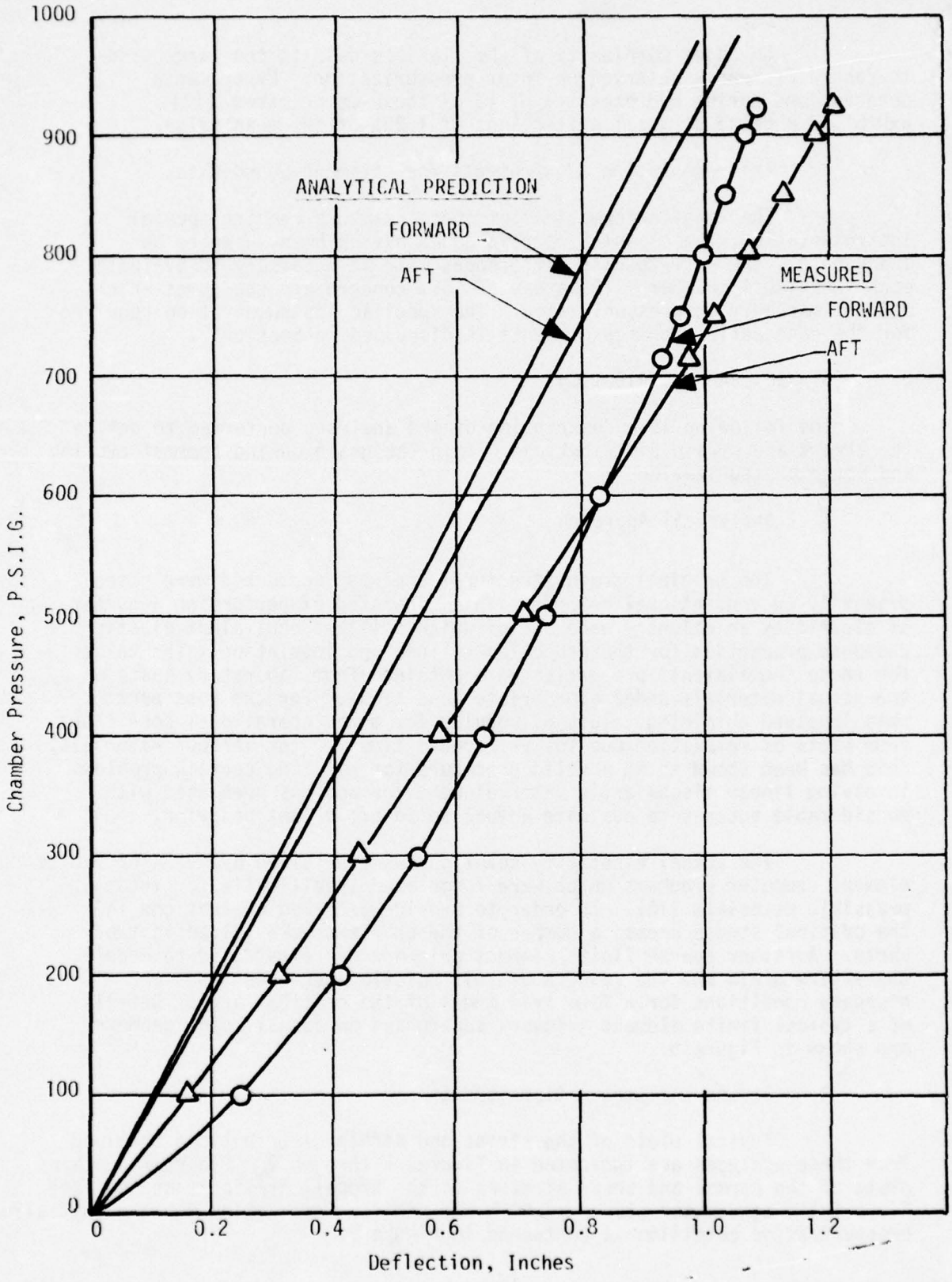

FIGURE 5. LONGITUDINAL DEFLECTION OF BOSSES

An added complexity of the flexible case is the large case-to-case differences observed on motor pressurization. Experimental observations during hydrotesting of 13 of these motor cases (17) exhibited a range of axial deflections of $\pm$ 20% of the mean value.

3. Instrumentation Requirements for Filament-Wound Cases

The large deformations of these chambers require special instrumentation, the classical strain gages having been shown to be inadequate. The case-to-case differences make it necessary to evaluate each individual chamber. The areas of most concern are the domes which deflect markedly on pressurization. The specific instrumentation required for the case deflection measurements is discussed in Section 5.

C. STATIC LOAD DISTRIBUTIONS

The following is a description of the analyses performed to define the stress and strain distributions within the grain during thermal cycling and motor pressurization.

1. Analytical Approach

The original grain structural analyses conducted were based primarily on conventional methods. This consisted of performing a number of elasticity solutions - each one of which utilized equivalent elastic response properties for the propellant, liner and insulation. The values for these "equivalent" properties were obtained from laboratory tests on the actual materials under appropriate conditions. For the most part this involved obtaining values of modulus for motor operational conditions from plots of relaxation modulus vs reduced time for the various materials. This has been shown to be a valid procedure for handling certain problems involving linear viscoelastic material behavior and has been used with considerable success to evaluate actual solid propellant behavior.

The actual elasticity solutions were obtained by means of finite element computer programs which were formulated specifically for incompressible materials (18). In order to provide detailed evaluations in the critical stress areas, a number of the problems were solved in two parts. A rather coarse finite element gridwork was first used to model the entire grain and the results of this solution were then used as boundary conditions for a fine grid model of the critical area. Details of a typical finite element gridwork superposed on actual motor geometry are shown in Figure 6.

2. Stress and Strain Distributions

Typical plots of the stress and strain distributions obtained from these analyses are indicated in Figures 7 through 9. Figure 7 contains plots of the normal and shear stresses at the propellant/liner bond surface for a fully aged motor stored at 60°F and similar information for the initial pressurization condition is contained in Figure 9.

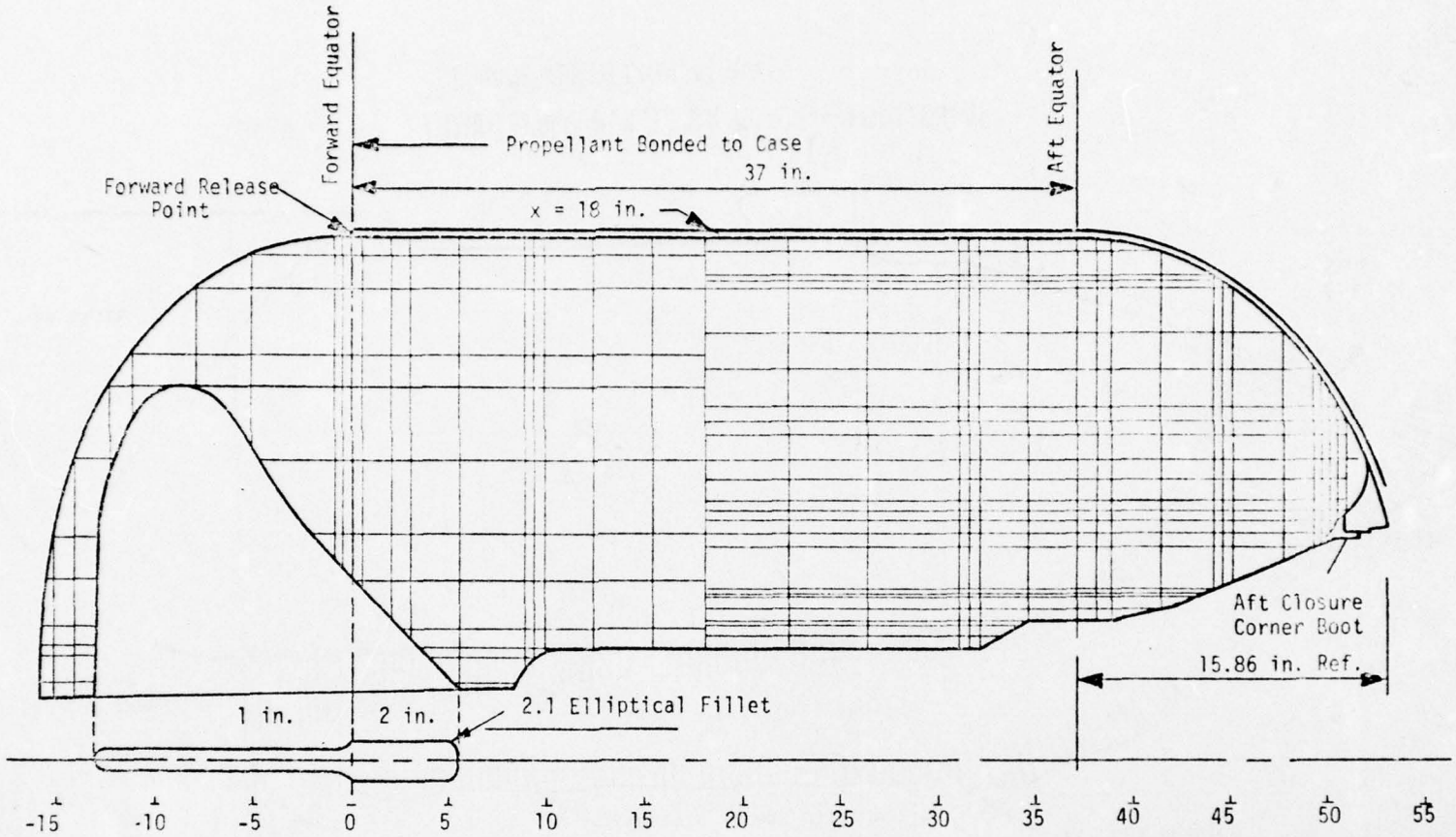

FIGURE 6. GRID NETWORK AND GRAIN CONFIGURATION OF THIRD STAGE MINUTEMAN MOTOR

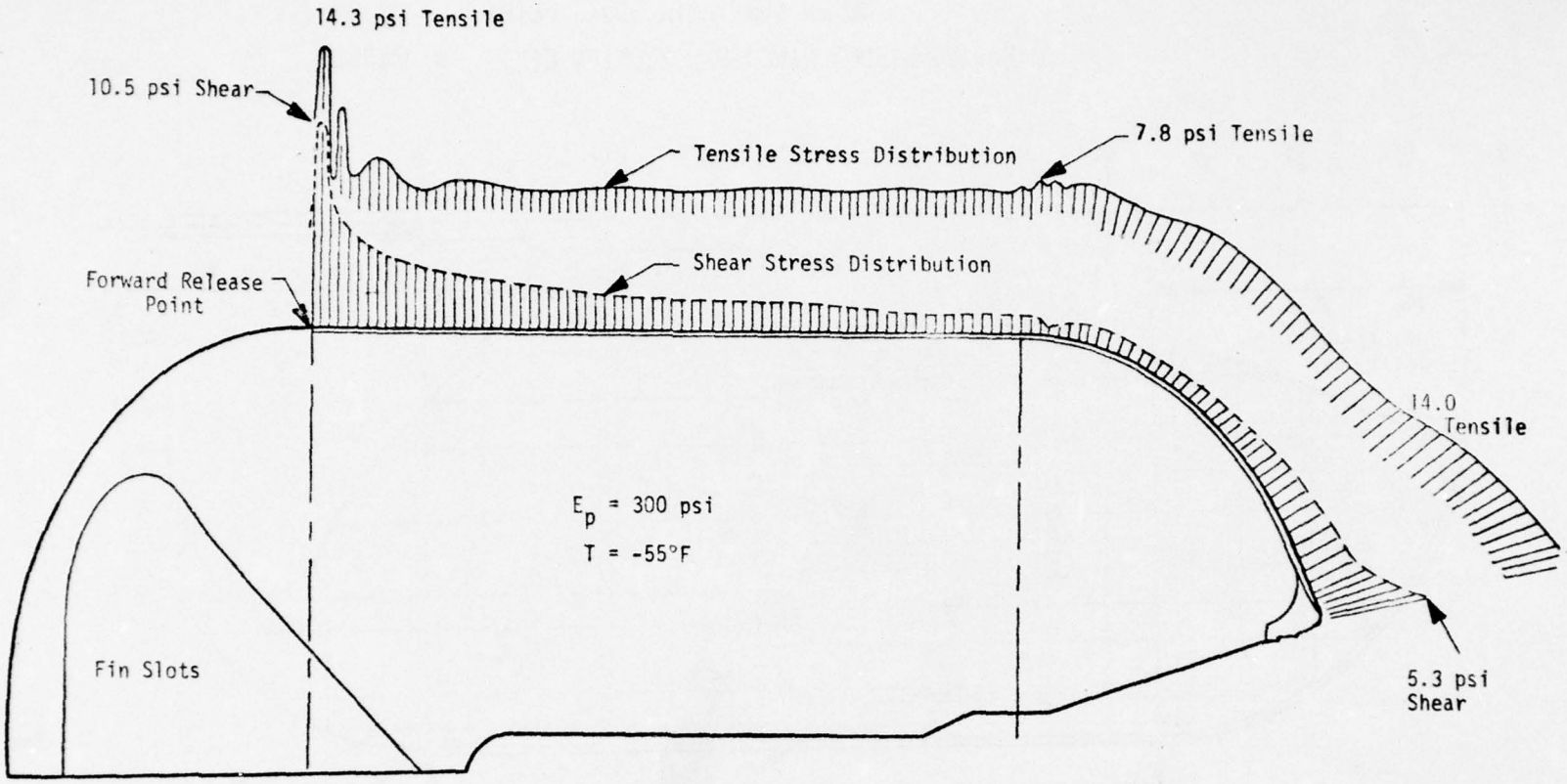

FIGURE 7. THIRD STAGE MINUTEMAN MOTOR - HORIZONTAL STORAGE CONDITION AT 60°F

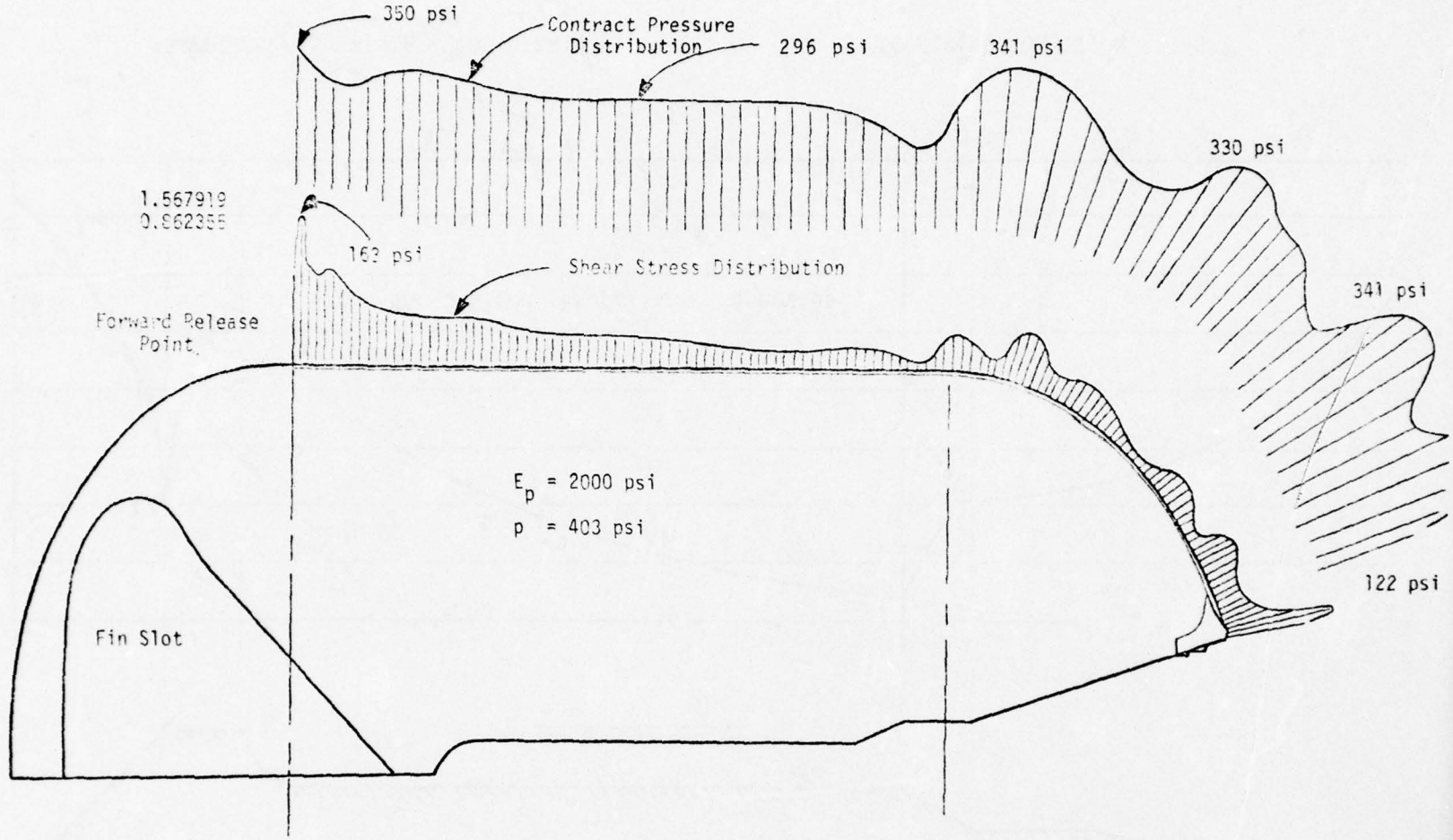

FIGURE 8. CALCULATED BOND STRESS DISTRIBUTION FOR THIRD STAGE MINUTEMAN MOTOR INITIAL PRESSURIZATION CONDITION

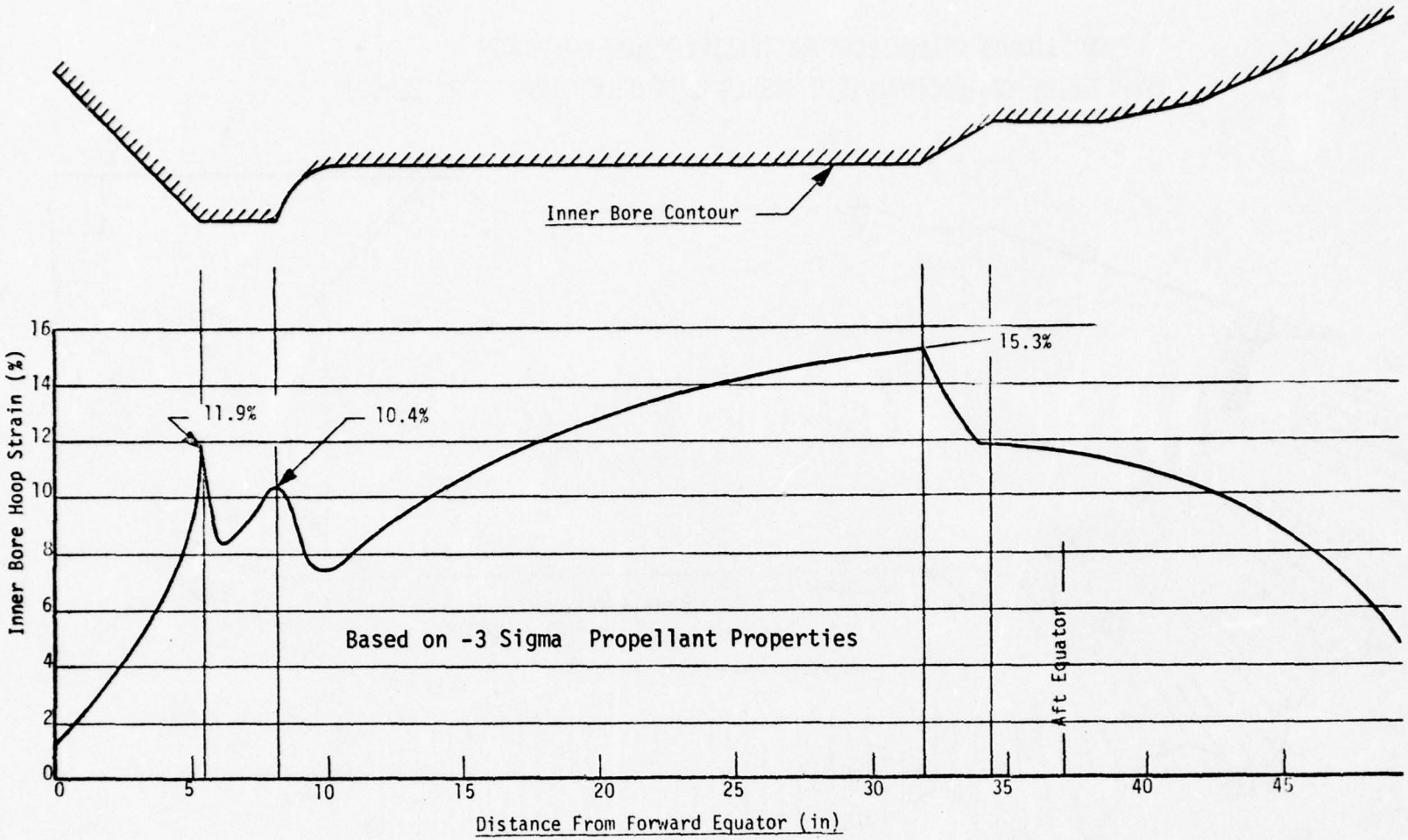

FIGURE 9. INNER BORE HOOP STRAIN DISTRIBUTION FOR STATIC FIRING CONDITION AT 60°F

The oscillatory nature of the calculated pressurization stresses in the aft dome area is considered to be due primarily to the manner in which the Rohm and Haas computer program handles the case behavior. This program ignores the non-linear stiffening effect due to membrane loads acting on the finite deformations which results in an unrealistic oscillation in the calculated case deflection pattern. The peak shear stress of 122 psi is considered valid since the case deflections in this area were adjusted to match static test measurements.

A summary of the maximum stresses and strains obtained from consideration of various loadings applied to the initial grain geometry, along with comparable allowables and margins of safety, is contained in Table 3. It will be noted that a negative margin of safety is indicated at the forward boot release point and the actual probability of failure at this location was computed as 0.3 percent. This behavior results from the increase in modulus due to aging of the ANB-3066 propellant.

3. Effect of Propellant Burning

A more detailed analysis of the grain for the firing condition revealed that the maximum shear stress in the aft end of the motor during pressurization does not occur near the original propellant surface. Due to the complex geometry of the aft nozzle boss and insulation, the maximum stress occurs at a point just opposite the outer corner of the forward face of the aluminum boss. In addition, the stress-time history of this critical point is rather complex. As indicated in Figure 10 the shear stress at this point rises rapidly at ignition, then decays as the propellant modulus relaxes, and finally again increases rapidly as the burning front approaches this location. When the burn front arrives at this location it encounters the shear stress distribution along the aft dome given in Figure 11.

D. DYNAMIC LOADS IN MINUTEMAN III, STAGE III MOTOR

During the Stage III development program steady state dynamic analyses were performed only to the level of complexity required to define motor test requirements. As a result detailed calculations of the dynamic response characteristics and grain stresses are not available. However, a summary of the principal results obtained from the longitudinal axis analysis of the Minuteman Stage III motor is provided in the following table.

TABLE 3
IMPROVED MINUTEMAN STAGE III GRAIN

CONDITION	INTERFACE TENSILE STRESS (psi) MAX.	ALLOW.	M.S.	INTERFACE SHEAR STRESS (psi) MAX.	ALLOW.	M.S.	INNER BORE HOOP STRAIN (ε) MAX.	ALLOW	M.S.
A. STORAGE AT 60°F $\Delta T = -55°F$, $a_T = 3.0$									
I. Short-Term Storage 1 Day ≤ t < 3 months $+3\sigma E_p = 155$ psi									
a. Horizontal Position	7.4	19.5(1)	+1.64	5.4			4.01	14.0(1)	+2.49
b. Vertical Position (Nozzle Down)	7.3			6.0	11.5(1)	+0.92	2.80		
II. Long-Term Storage 1 Year ≤ t ≤ 10 Years $+3\sigma E_p = 300$ psi $-3\sigma E_p = 90$ psi									
a. Horizontal Position	14.3	19.6(2)	+0.37	10.5			4.01	11.1(3)	+1.77
b. Vertical (Nozzle Down)	14.1			11.6	11.8(2)	+0.02	3.42		
B. AXIAL ACCELERATION AT 60°F $\Delta T = -55°F$, $a_T = 3.0$									
I. Handling Vibrations at + 15 g's (Horizontal Motor Position) $+3\sigma E_p = 2330$ psi at 0.10 sec $-3\sigma E_p = 800$ psi at 0.10 sec	29.0	154.5	+4.33	48.0	94.2	+0.96	7.01 ($-3\sigma E_p$)	14.4(3)	+1.05
II. Booster Flight at -8.4 g's (Vertical Motor Positon) $+3\sigma E_p = 780$ psi at 47 sec $-3\sigma E_p = 260$ psi at 47 sec	16.4	91.0	+4.55	20.6	53.4	+1.59	2.29 ($+3\sigma E_p$)	13.1(3)	+4.72
C. PRESSURIZATION CONDITION AT 60°F P = 403 psi, t = 0.20 sec								INCREMENTAL STRAINS	
I. Static Firing Condition at 60°F $+3\sigma E_p = 2000$ psi, $-3\sigma E_p = 700$ psi	COMPRESSION			174	153(2) 196(3)	-0.12* +0.13	15.3 ($-3\sigma E_p$)	17.3(3)	+0.14
II. Flight Condition at 60°F $\Delta T = -55°F$, a = 3.4 g's $+3\sigma E_p = 2000$ psi $-3\sigma E_p = 700$ psi	COMPRESSION			177	153(2) 196(3)	-0.14* +0.11	14.4 ($-3\sigma E_p$)	17.3(3)	+0.20

(1) 3-month allowable.
(2) 1-year allowable.
(3) 10-year allowable.

*NOTE: Probability of Failure = -0.3% for shear stress at forward release point during flight condition.

Probability of Failure = 6.7% for shear stress at aft end at 11.36 sec firing time.

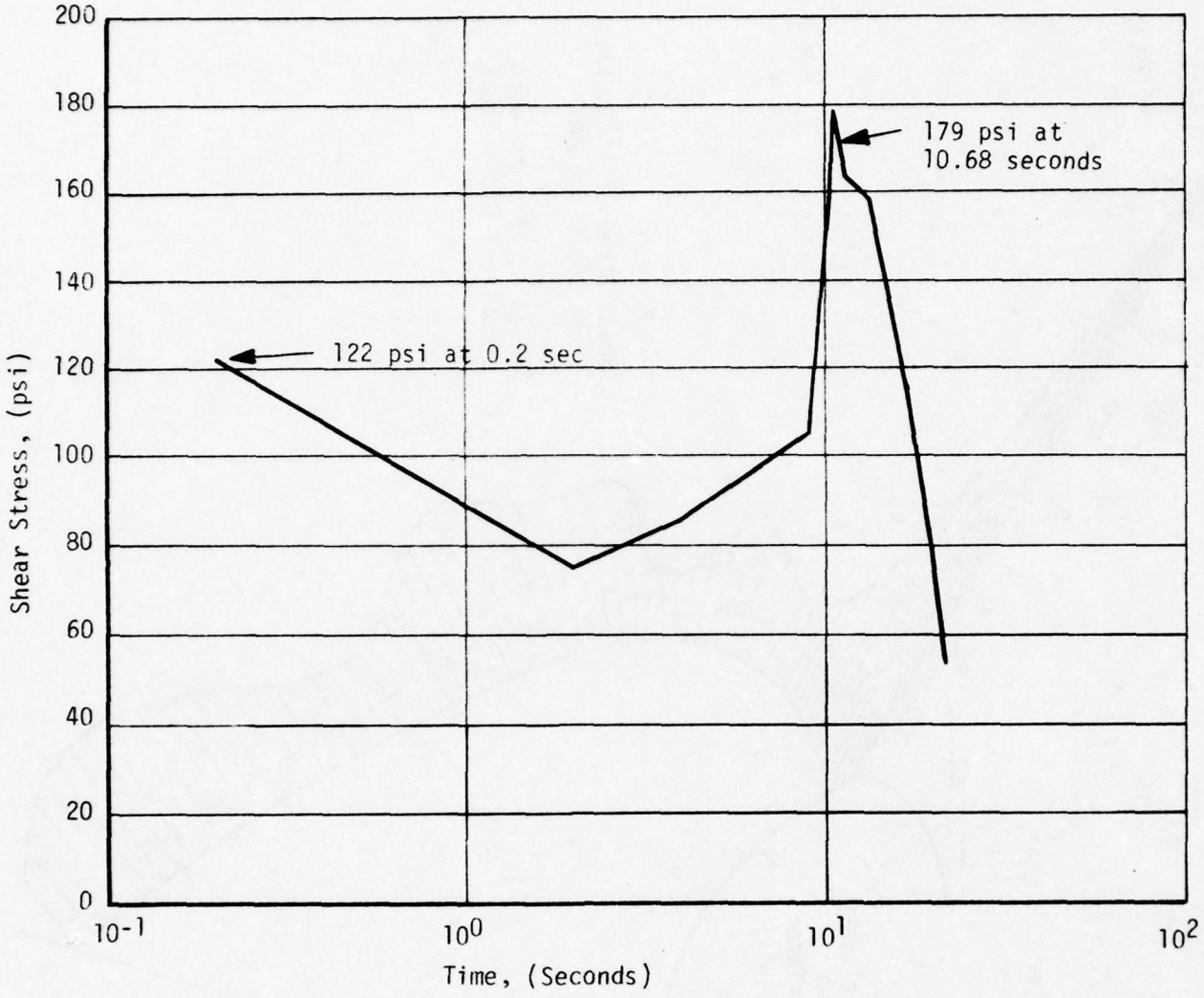

FIGURE 10. SHEAR STRESS AT THE AFT BOSS VS. TIME - AGED PROPELLANT PROPERTIES

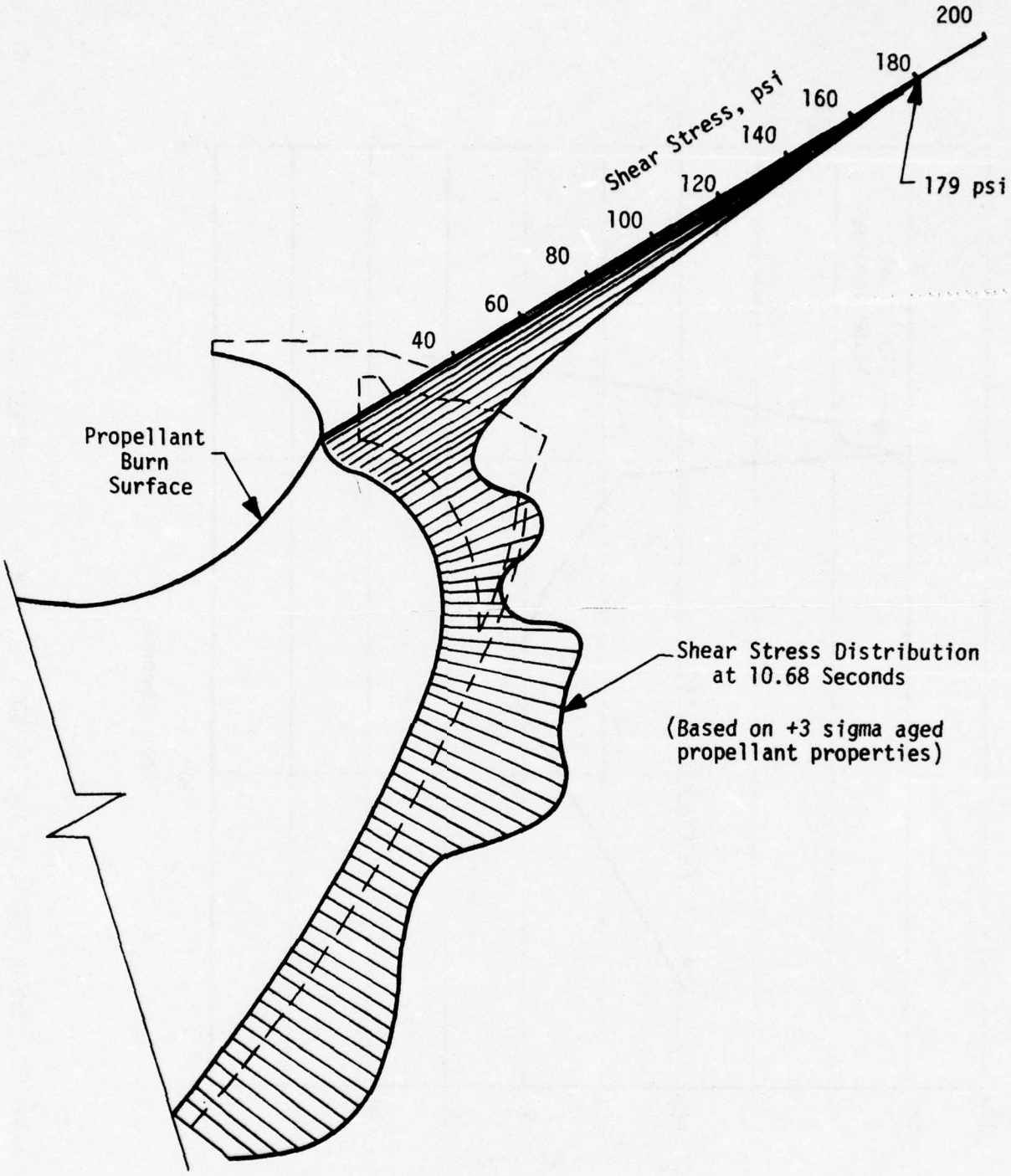

FIGURE 11. PREDICTED SHEAR STRESS DISTRIBUTION AT THE AFT DOME

Resonant Frequency (Hz)	Dynamic Amplitude Factor	Max. Calculated Dynamic Stresses	
		Direct Stress	Shear Stress
38	6.2	6.34 psi/g	5.12 psi/g
(Propellant Axial Shear Mode)	(At propellant node at forward region of motor near bore centerline)		

The maximum propellant dynamic stresses calculated in the longitudinal axis analysis of the motor occurred near the junction between the case and the propellant at the aft end of the motor adjacent to the junction of the case and aft dome.

That the analyses were essentially correct was shown by excellent correlations made in some full spectrum dynamic surveys on Minuteman Wing VI motors. The second stage motor 52-TET-1 gave the correlations shown below and in Figure 12. The calculated and measured results compare quite well.

Resonant Frequency (H_z) of 1st Axial Propellant Shear Mode		Amplification Factor of Propellant Mode 1022	
Calculated	Measured	Calculated	Measured
49	42	4.9	4.6

Comparison between results from the preliminary dynamic analysis of the Stage II motor and tests of Motor 52-TET-1 (19) also showed good agreement. For example, a value of 39 Hz was predicted by the analysis for the first axial shear mode of the propellant, while 35 Hz was observed.

The past experience in the instrumentation of motors for dynamic testing was fully utilized in this case. The same instrumentation plan that had been fully satisfactory in previous motor tests was used here. This approach had the advantage of allowing direct comparisons with past motor test results to evaluate possible measurement anomalies.

E. ZONES FOR GAGE PLACEMENTS

For simplicity in defining the problem, the motor was divided into zones. These are shown in Figure 13, while the requirements, expected range, and purpose of the instrumentation that was used in each of these zones is specified in Table 4.

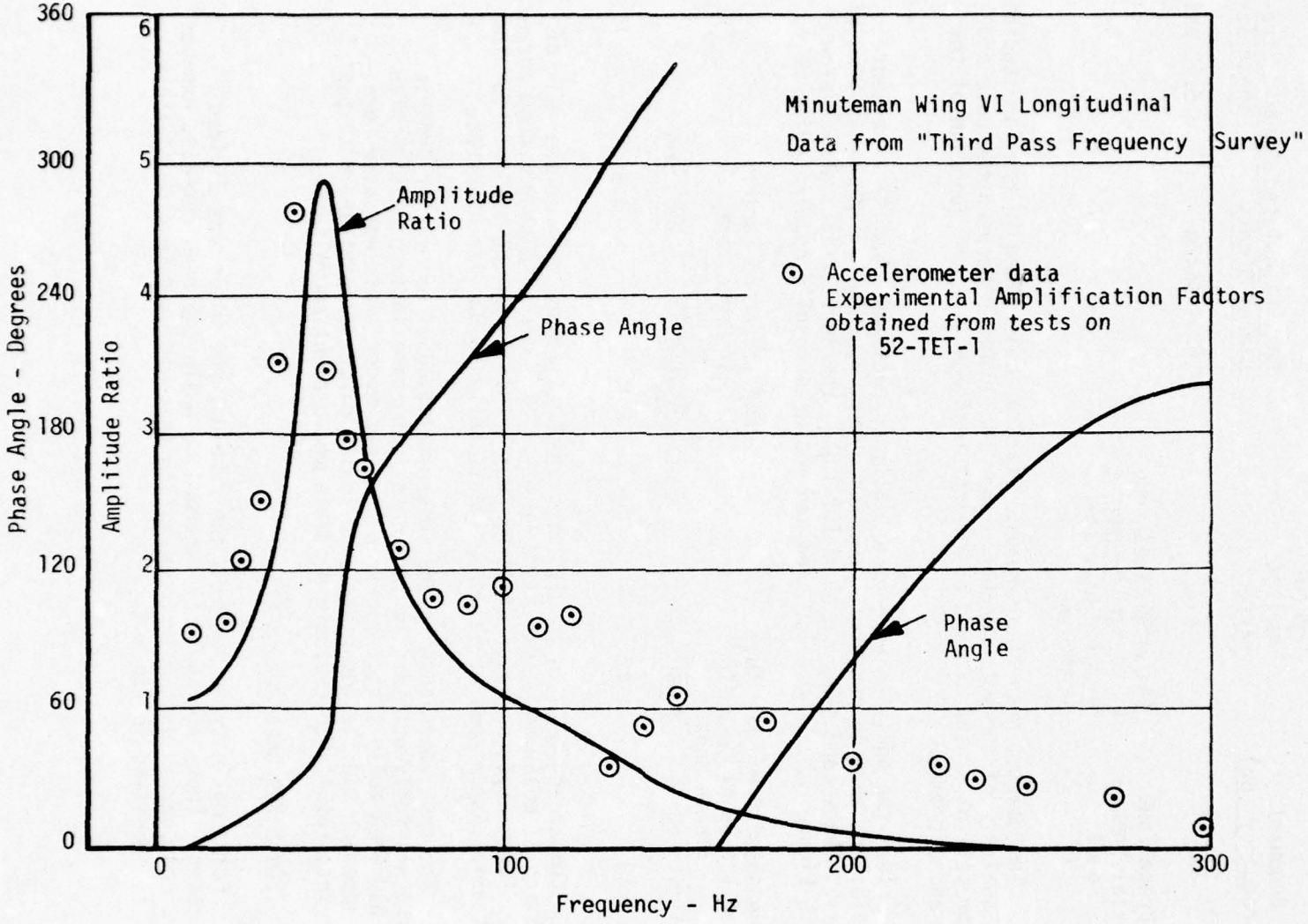

FIGURE 12. COMPARISON PLOTS OF CALCULATED AND MEASURED LONGITUDINAL AXIS FREQUENCY RESPONSE CHARACTERISTICS OF THE 52-TET-1 MOTOR

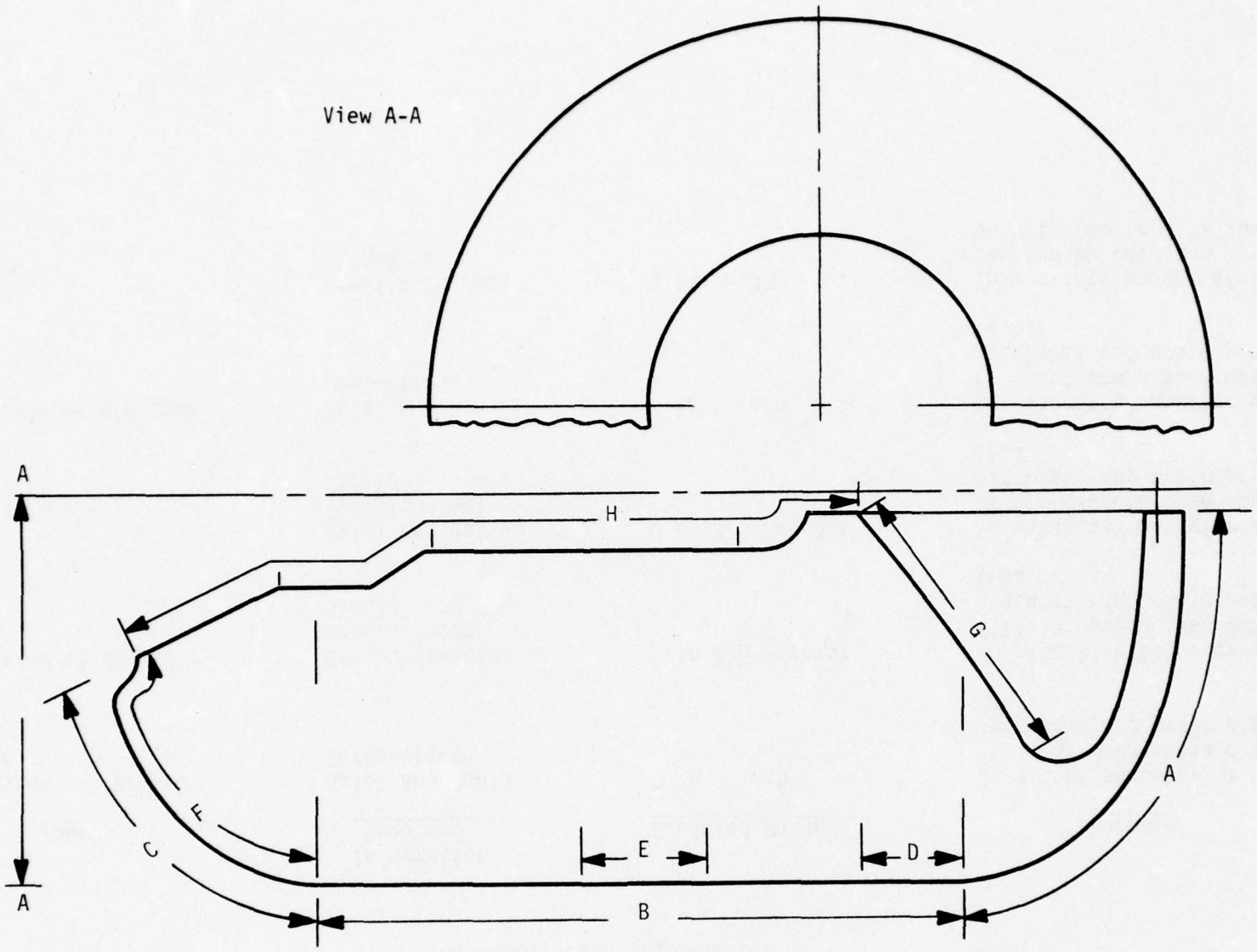

FIGURE 13. MOTOR ZONES REQUIRING INSTRUMENTATION

TABLE 4

INSTRUMENTATION REQUIREMENTS

Zone	Information Required	Expected Range	Purpose
A. Outside of Forward Dome	Axial and Radial Deflections	0 to 1 inch	To establish behavior of filament wound case during hydrotest and grain pressure test.
B. Outside of Cylinder	Circumferential Growth (Hoop Strain)	0 to 2.5 Percent	To establish behavior of filament wound case during hydrotest and grain pressure test.
	Axial Deflection (Longitudinal Strain)	0 to 2.5 Percent	To establish behavior of filament wound case during hydrotest and grain pressure test.
C. Outside of Aft Dome	Axial and Radial Deflections	0 to 1 inch	To establish behavior of filament wound case during hydrotest and grain pressure test.
	Strains in Case Filaments	0 to 15,000 μ in.	To indicate amount of load carried by case and to detect some bond failures.

TABLE 4 (CONT.)

INSTRUMENTATION REQUIREMENTS

Zone	Information Required	Expected Range	Purpose
D. Inside Case Near Forward Boot Release Point	Bond Tension	0-25 psi Cure, Thermal and Inertia: 0-725 psi Pressure	To detect build-up of stresses at forward boot release point and to detect failure.
	Bond Shear	0-25 psi Cure, Thermal and Inertia: 0-250 psi Pressure	To detect build-up of stresses at forward boot release point and to detect failure.
E. Inside Case Near Center of Motor	Bond Tension	0-25 psi Cure, Thermal and Inertia: 0-725 psi Pressure	To check structural analysis in area of approximate plane strain.
F. Inside Aft Dome	Bond Tension	0-25 psi Cure, Thermal and Inertia: 0-725 psi Pressure	To check structural analysis of critical area and to detect failure.
	Bond Shear	0-25 psi Cure, Thermal and Inertia: 0-250 psi Pressure	To check structural analysis of critical area and to detect failure.
G. Forward Fin Slots	Local Strains	0 to 20%	To check structural analysis in slot area.
H. Circular Inner Bore	Bore Deflections	0-10% Thermal 0-25% Pressure	To check structural analysis of axisymmetric geometry.

1. Static Loadings

Extensive deflection measurements of the chamber in Zones A, B, and C during hydrotest, as well as during the grain pressure test, were considered essential. The hydrotest data may be used to verify the structural description of the case as used in the grain analysis and comparison of these data with those from the grain test, may give a good indication of the pressure drop through the web of the propellant grain. In addition, the deflection gages in Zone C were expected to be useful in detecting aft end bond failures.

Zone D was considered to be a critical area due to the forward boot release point. Gages in this area were considered mandatory for failure detection. The stresses at this location have large gradients, but judicious spacing of gages were expected to provide valuable information on stress distributions.

Zone E was considered to be a key area for the evaluation of analytical techniques. This is the area most nearly representative of plane strain conditions and the circular cross section makes it amenable to analyses. The simplicity of the geometry makes it possible to consider sophisticated material behaviors, so comparisons of predicted and measured behaviors in this area were considered essential.

Zone F was considered to be critical for both bond stress magnitudes and failure initiation. Both shear and normal stress gages were used in this area with the objective of determining stress magnitudes, stress distribution, failure initiation, and failure propagation.

Surface strain gages were placed in Zone G to evaluate the "strain concentrations" associated with the finocyl slots. This represents a truly three dimensional problem area where estimates of these local strains had been based on approximate two dimensional models.

The large axisymmetric region of inner bore surface indicated by Zone H provided an excellent opportunity for evaluating the overall structural behavior of the grain under both thermal and pressurization loading. Hoop strains over this entire area were directly obtainable from diametral measurements and the results were expected to be valuable in evaluating analytical predictions based on axisymmetric geometry.

2. Dynamic Loadings

The results of steady-state dynamic analyses performed on the Minuteman III, Stage III motor indicated that the maximum dynamic stress produced in the propellant occurs under steady-state vibration conditions corresponding to the longitudinal shear mode of the grain. The location of the maximum dynamic stress is at the propellant-liner interface. The maximum dynamic displacements of the propellant grain occur on the inner-bore surface and in the region of the fin.

The selection of the optimum gage location for the full-scale motor considered the results of the available dynamic analysis and the dynamic response anticipated in the full-scale motor test program. Since the dynamic loading conditions are much less severe than the static condition, preference was given to providing optimum gage location for the evaluations of the anticipated static loads. Special instrumentation for the dynamic full-scale motor tests were limited to the addition of accelerometers to the center bore and externally to the motor case and handling fixtures.

SECTION 5

FORMULATING A MOTOR INSTRUMENTATION PLAN

Having established the general instrumentation needs the next step was to identify the specific gages, their locations in the motor, and the associated wiring and hardware. The following section describes the instrumentation plan beginning with the overall ground rules guiding the effort.

A. GROUND RULES FOR GAGE SELECTION AND PLACEMENT

The specific criteria followed in making these selections were:

(1) The primary objective is to evaluate the actual stress/strain distributions.

(2) The monitoring of grain failures is of secondary importance.

(3) Only limited gage redundancy may be used in the motor layout (in addition to that built into the gages themselves).

(4) No structural failure of any kind is expected in the grain prior to the final pressurization tests.

(5) The majority of the gages used in meeting these ground rules are expected to break prior to grain failure. This necessitates the use of some special gages for the failure observations.

(6) Most of the transducers shall be of the type that have been previously developed, calibrated, evaluated and found to give reliable, meaningful measurements.

(7) The gages will be calibrated using the simplest methods available, consistent with established requirements for meaningful measurements in the propellant grain.

B. TRANSDUCER DESIGNS AT PROGRAM INCEPTION

An excellent summary of the transducer designs available at the beginning of this program is given in Reference 20. The reader is referred to that document for a more complete review of the transducers and their methods of use.

1. Gage-Grain Interactions

The insertion of any solid object into a propellant grain must significantly affect the local stress/strain conditions. It is within this disturbed stress/strain field that the stress transducers must function. The techniques required to handle this gage-grain interaction are discussed in Reference 20, where Leeming has made the following overall assessment of the problem:

> "The key factor in any successful measuring device is that it should measure what is required without modifying the system it is measuring, i.e., maximum information content with minimum energy transfer. Very few devices approach this ideal so that the problem becomes one of determining in what manner the presence of the measuring device influences the system and from this fact calculating the correct magnitude of the response as if the instrument were not present. An understanding of the manner in which the transducer itself modifies the stress-strain state enables improved transducer performance to be obtained."

> "The complete gage-grain interaction problem consists of two separate parts; the influence of the surrounding material (propellant) on the response of the gage, and the effect of the embedded gage on the stress-strain field within the grain. Though these two effects are considered separately, the interaction problem consists of the sum of the two effects."

2. Through-the-Case Stress Transducers

The essential features of this class of instruments (which have been used most effectively by Rocketdyne (2) are illustrated in Figure 14. A hole is drilled in the case and a steel plug, which is a clearance fit in the hole and is attached to the transducer, is mounted flush with the inner case surface. The strain gaged element is attached to a stiff housing, which is attached rigidly to the outer surface of the case. Thus, any force applied to the steel plug causes a slight deflection of the strain gaged element that can be interpreted as a stress across the plug diameter. By making use of small dimensioned, sensitive, semiconductive strain gages, the compliance of the strain gage section can be kept to an extremely low value (dependent upon the required gage sensitivity). Transducers of this type can be made with virtually no change in properties over a wide temperature range. They also have the advantage that local perturbations in the grain stress field are kept to a negligible level. However, they must operate through a large hole drilled through the case, which is unacceptable for simulated or actual firing tests; therefore, they were not considered for use in the present program.

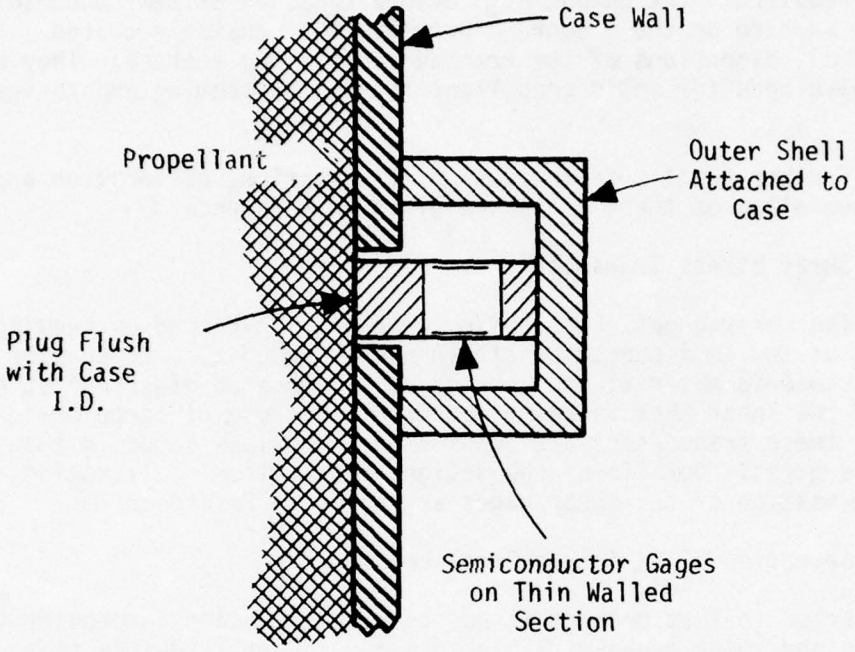

FIGURE 14. SCHEMATIC OF THROUGH-THE-CASE STRESS TRANSDUCER

3. Miniature Diaphragm Transducers

The diaphragm type normal stress transducer (1) is shown in Figure 15. These transducers are simply conventional diaphragm-type pressure gages that have been modified to minimize the grain-gage interaction; i.e. they are as small as possible consistent with the output sensitivity required. The output of a bridge composed of semiconductor strain gages mounted on the diaphragm provides the sensing required. The remarkably small dimensions of the transducer is a key feature. They were originally developed for solid propellant testing by Leeming and Konigsberg (1).

Further details on the design, fabrication, calibration and thermal compensation of these gages are given in Reference 11.

4. Shear Stress Transducers

The shear gages, Figure 16, were also developed by Leeming (1) They consist of two semi-conductor strain gages bonded to a triangular shaped piece of elastomeric material and mounted at 90° to each other and at 45° to the plane of the shear that is being measured. Because of large grain-gage interactions these transducers are considered to be less accurate than the normal stress gages. Details of the design, fabrication, calibration, and thermal compensation of the shear gages are given in Reference 16.

5. Selection of Stainless Steel Leadwires

Prior to this program it had been the practice to provide the normal stress and shear gages with high quality copper leadwires that were specifically designed for taking electro-cardiograms (EKG). But the motors fabricated on this program were expected to undergo prolonged storage (more than two years) and to be subjected to harsh testing environments. Also, in the planning period there was a strong possibility that the leadwires might have to be layed-up along the insulation-to-propellant interface where the environment could be quite corrosive to the copper wires. (As it turned out, this approach was not followed).

These concerns for possible leadwire corrosion and low strength were expressed to the gage supplier, who recommended a stainless steel, 33 gage stranded wire with a very thin Teflon insulation. This is a standard wire used in biomedical instrumentation. Since the procedures for the use of this wire were supposedly developed for other electronic uses, the leadwire was accepted for use on the Flexible Case-Grain Interaction program. As it turned out, this was an unfortunate choice. Some of the problems associated with the soldering of these wires are discussed in Section 10.

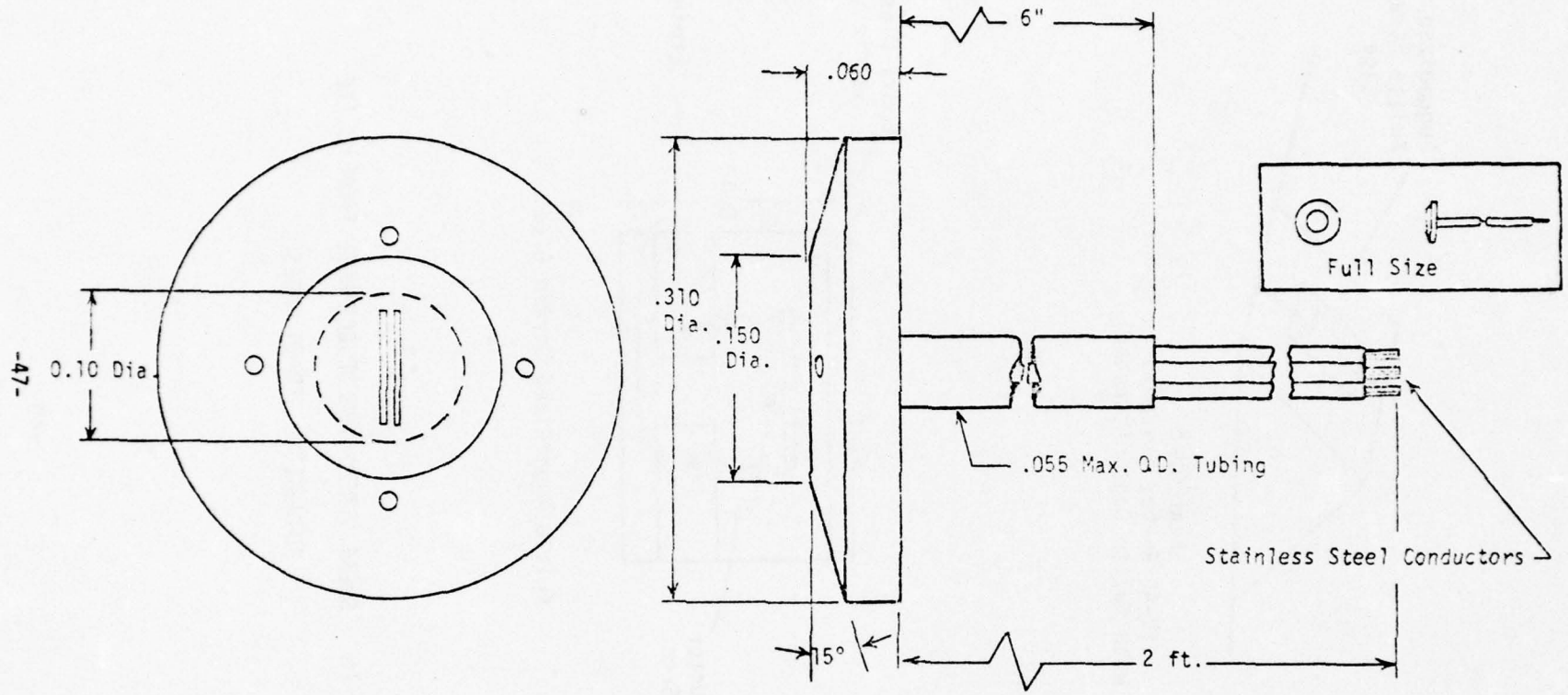

FIGURE 15. OUTLINE DRAWING OF NORMAL STRESS GAGE

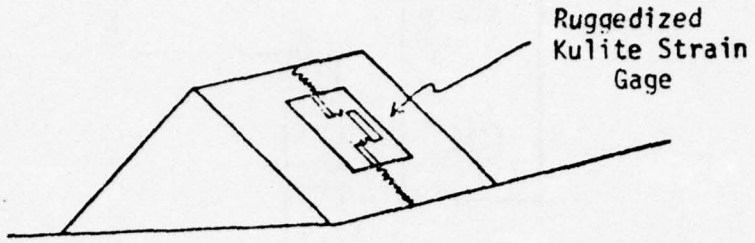

Shear Gage
(V-45 Rubber Triangle
with Kulite Gages Attached)

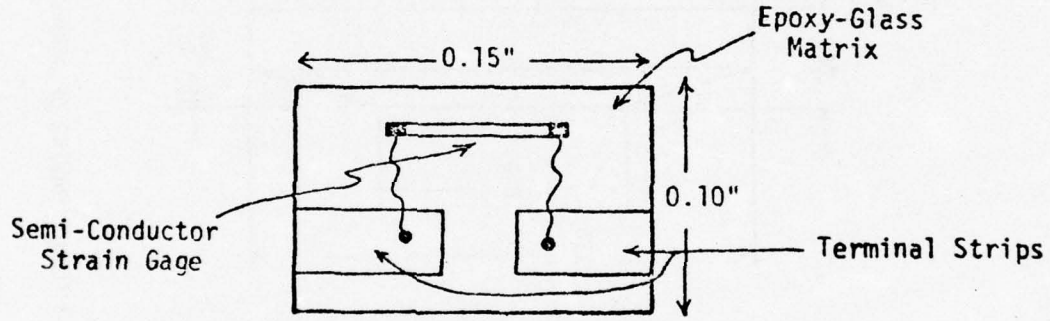

Kulite Ruggedized Strain Gage

FIGURE 16. SHEAR STRESS TRANSDUCER MADE FROM KULITE RUGGEDIZED STRAIN GAGES

6. 3D Stress Gage

An experimental gage to measure three dimensional stress components under development at HL&A (11) was used in the motor. A schematic of the device is shown in Figure 17 and the wiring diagram in Figure 18. Six stress sensing elements oriented in the directions shown were mounted near the center of a 1-1/2 inch cube of inert propellant. When calibrated by the application of three orthogonal normal stresses and three planes of shear stress it is possible to resolve an unknown stress load into its normal and shear stress components. Because the 3D gage is insensitive to hydrostatic pressures a miniature diaphragm normal stress gage was embedded close to the 3D gage to monitor the pressure component. The voltages across the sensing elements were measured with respect to a dummy gage element to provide thermal compensation.

7. Clip Strain Gages

Deformation measurements in the fin slot of the third stage motor was accomplished using clip strain gages. These gages were of a conventional type designed by ASPC and fabricated by Konigsberg Instruments, Inc. (their Model J1C). The specific design is given in Figure 19. Basically, it consists of a full bridge (four semiconductor gages) mounted onto the flexure portion of a clip gage. It was designed with an operating range of plus and minus .200 inch.

8. Bondline Failure Event Gages

These gages were developed at ASPC to measure the passage of a bondline separation in the motor. They were fabricated from conductive elastomers which exhibit a marked rise in electrical resistance as the tear front approaches and passes through the gage (see Reference 16 for a more complete description of this gage).

Two types of failure event gages were developed for use on this program. The first failure event gage was made of a CTPB binder filled with conductive silver and was made in the design given in Figure 20. The gage, which is 1/4 in. x 1 in., was cut from pre-molded .030-inch thick sheet and wire terminations were bonded to the gage with a similar material. The failure gage strips were then bent into a configuration resembling an inverted "Tee" or trouser leg, such that when placed perpendicular to the direction of separation growth, the leg portion of the inverted tee (embedded in the propellant) would tear.

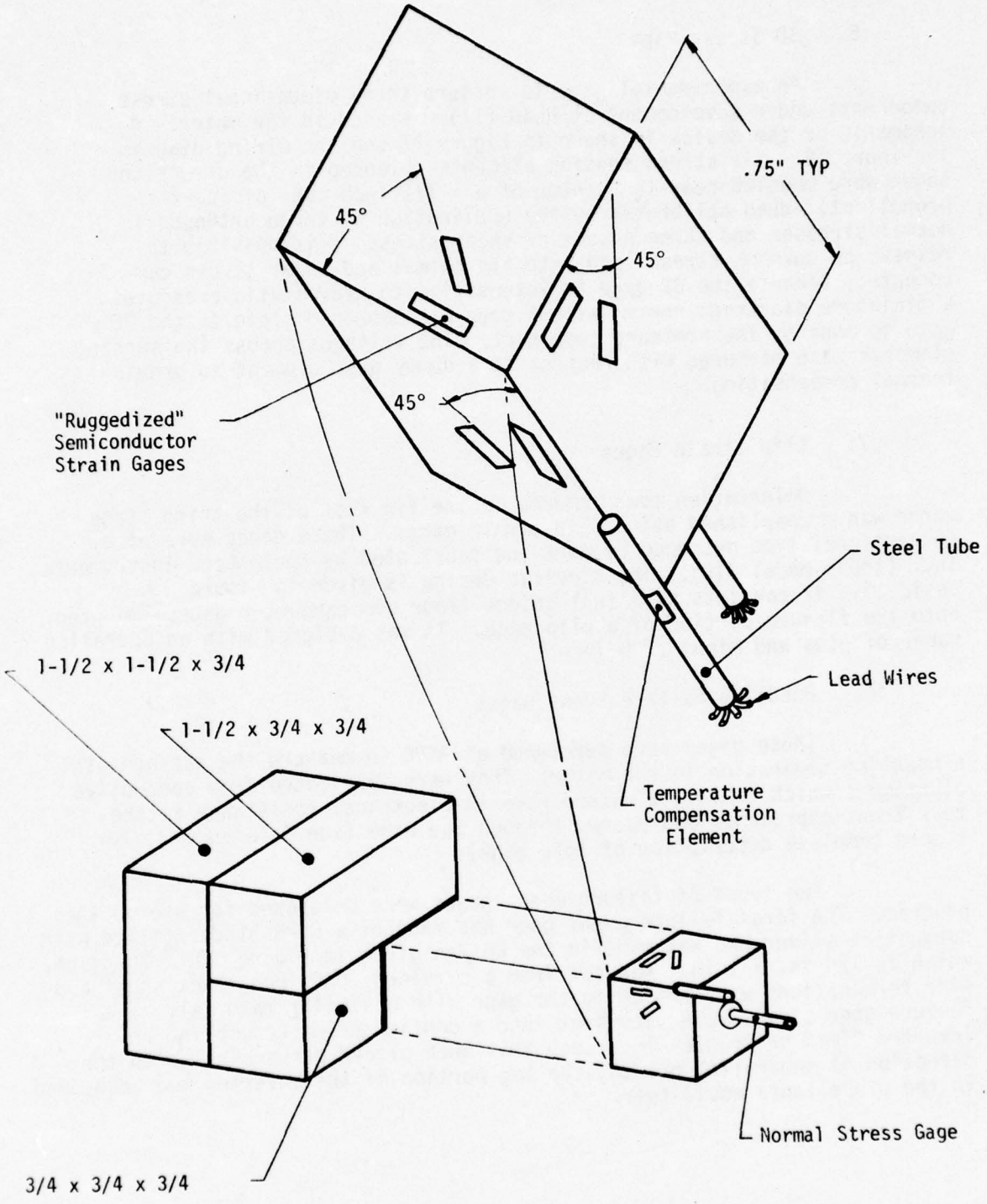

FIGURE 17. 3D GAGE SCHEMATIC

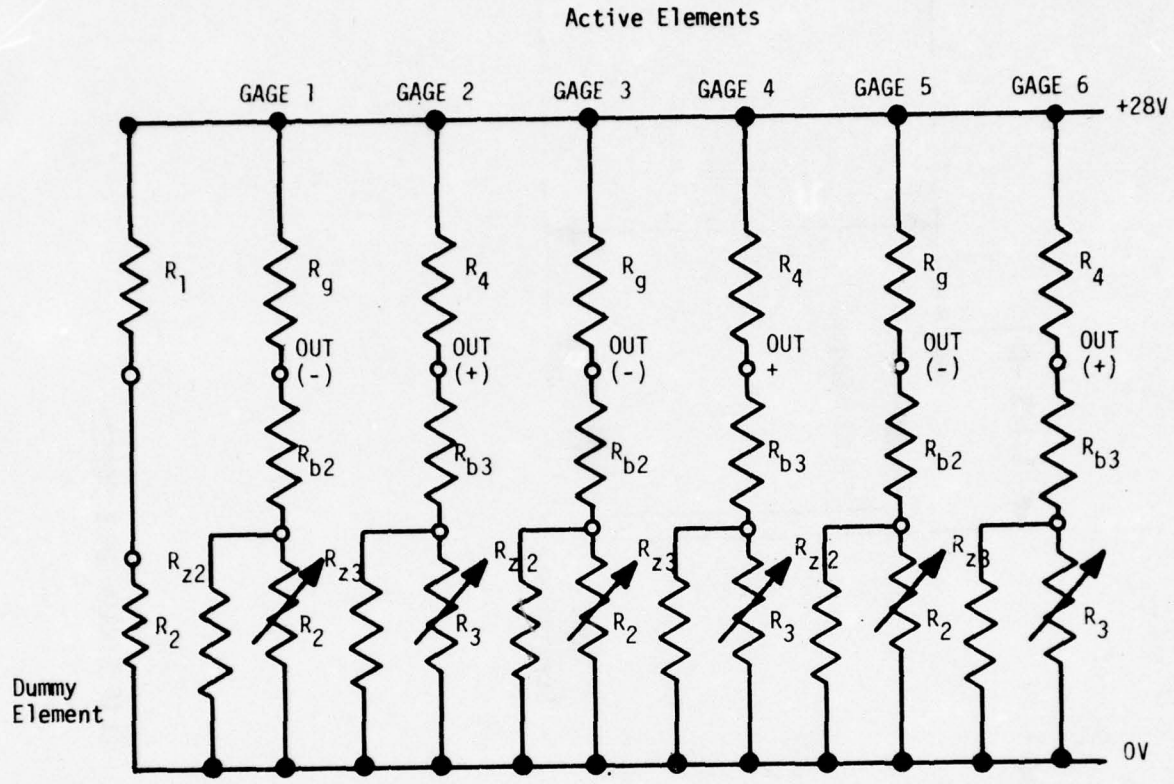

FIGURE 18. TYPICAL SCHEMATIC OF 3-D STRESS TRANSDUCER

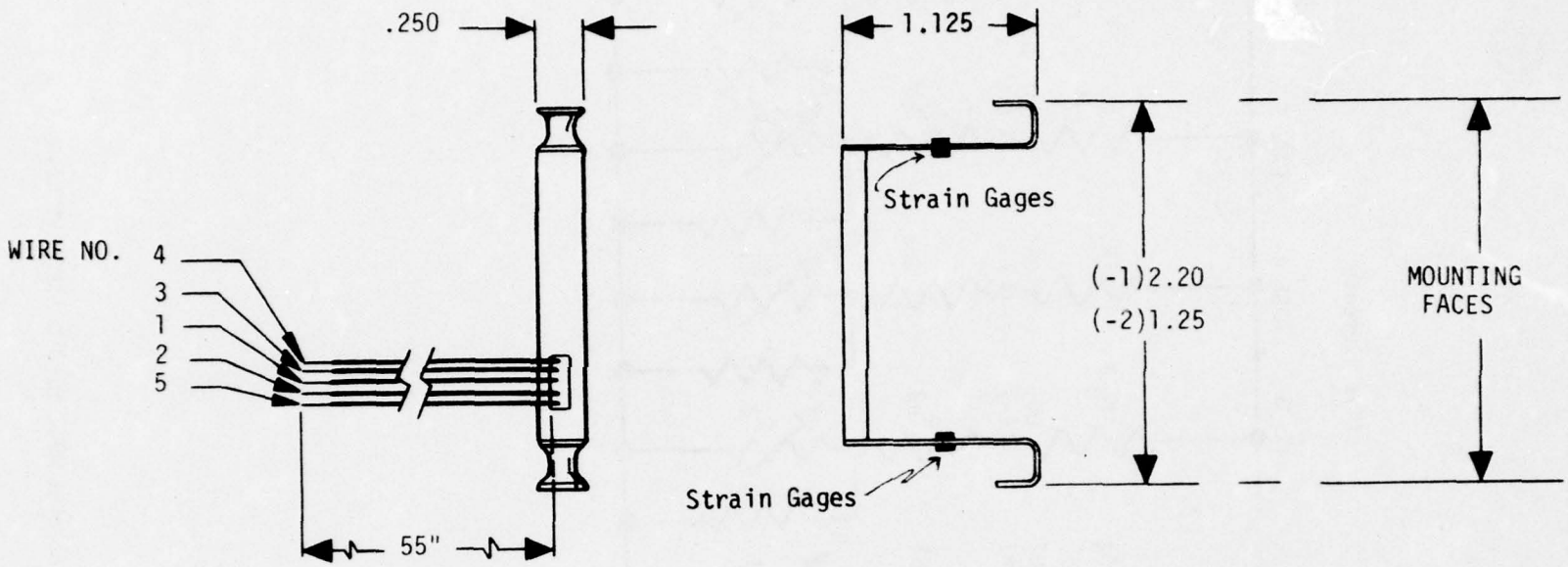

FIGURE 19. CLIP STRAIN GAGE DESIGN

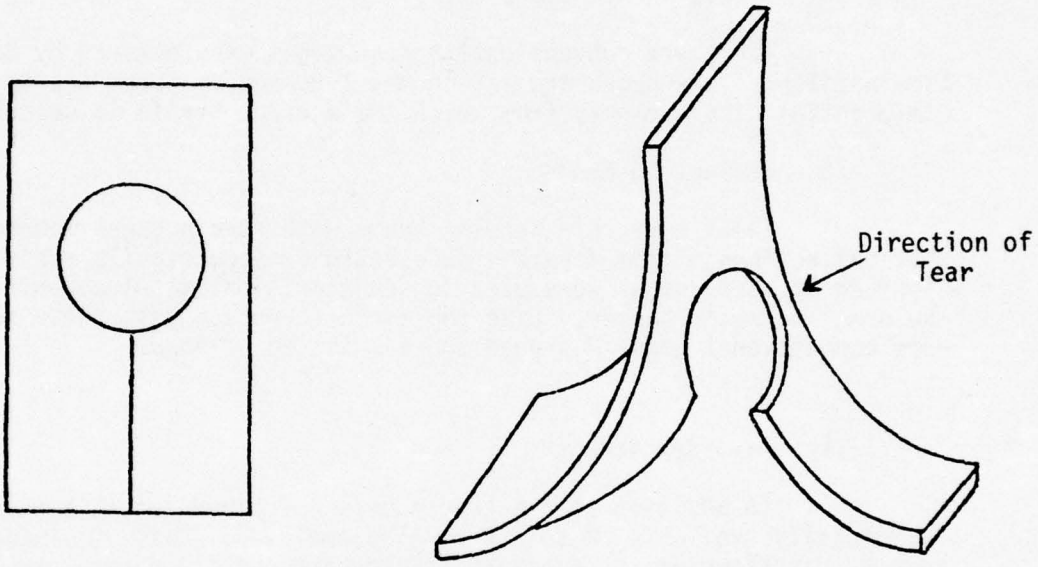

FIGURE 20. BONDLINE FAILURE EVENT GAGE TYPE I

The second type of failure event gage tested was the Technit Products model made with a commercial conductive elastomer (Consil G). Its configuration is shown in Figure 21.

Later work by Thiokol Chemical Company improved the method for bonding the leadwires to these gages (21).

9. Circumference Gages

These are conventional strain gages manufactured by Baldwin-Lima Hamilton. The gages are 120 inches long and measured the total circumferential displacement, from which the average strain is calculated.

10. Deflection Reeds

These were thin bending beams with strain gages mounted so that deflections of the flexible case could be electrically monitored. Eighteen of these gages were used to sense critical displacements of the dome and metal bosses. Like the circumference gages, these reeds were conventional gages designed and fabricated at ASPC.

11. Assorted Sensors

In addition to the transducers described above, a number of commercially available sensors were also employed. These included thermocouples, accelerometers, pressure transducers, strain gages, and linear variable differential transformers (LVDT's).

12. Transducer Accuracies and Precisions

A statement of the accuracies of absolute values and of the precisions that can be expected of the several transducers used for this program are shown in Table 5. It must be emphasized that the stated accuracies are for the transducer in service in, or on, propellant and that they reflect the uncertainty associated with the reduced data output compared to the magnitude of the sensed quantity in the complete absence of the gage. These data have been obtained in measurements made over a broad range of temperatures and the accuracies were expected to be significantly better on the Flexible Grain-Case Program where a temperature range of only 60 to 110°F was planned.

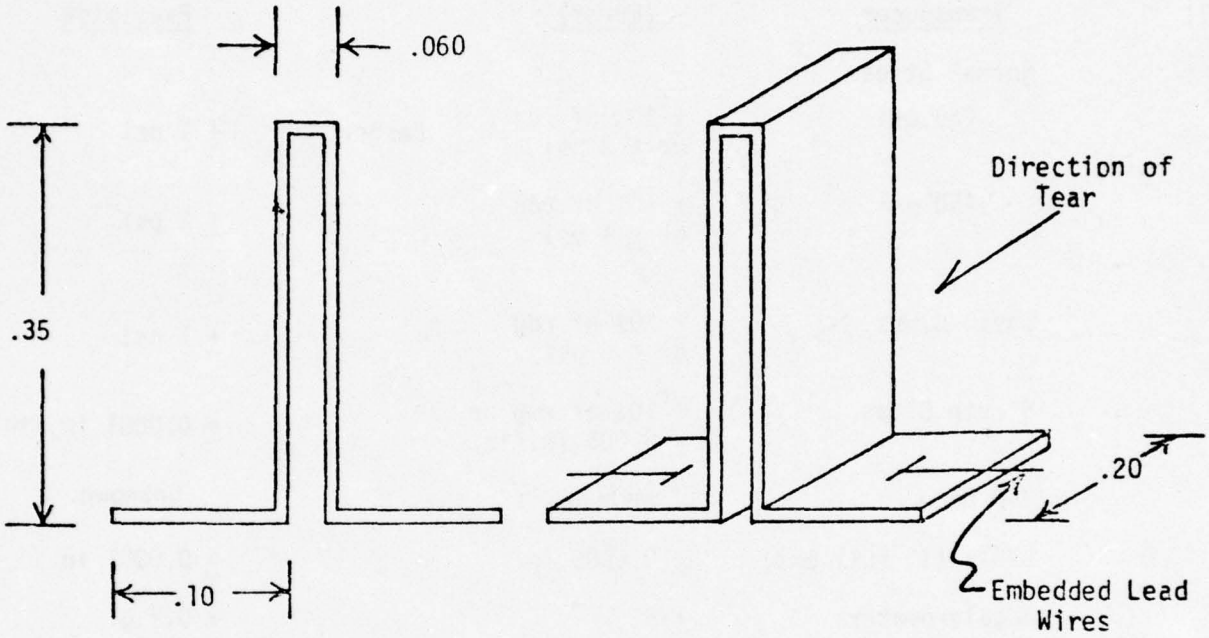

FIGURE 21. BONDLINE FAILURE EVENT GAGE-TYPE II

TABLE 5

ESTIMATED* ACCURACIES AND PRECISION OF SINGLE READINGS

Transducer	Accuracy (Error)		Precision
Normal Stress			
150 psi	± 10% of rdg or ± 2 psi	} Larger	± 1 psi
450 psi	± 10% of rdg or ± 4 psi		± 2 psi
Shear Cubes	± 30% of rdg or ± 5 psi		± 1 psi
Strain Clips	± 10% of rdg or ± 0.005 in./in.		± 0.0001 in./in.
3-D Gage	Unknown		Unknown
LVDTs (1" Full Ext)	± 0.0005 in.		± 0.0001 in.
Accelerometers	± 5%		± 0.2 g
Thermocouples	± 2 F		± 0.2 F
Circumference Gages (2 in.)	± 0.001 in.		± 0.0005 in.
Strain Gages (1 in. on Case)	± 0.0001 in./in.		± 0.00001 in./in.
Deflection Reeds	Unknown		Unknown

* These estimates are purposely large and are based on personal experience with these transducers.

C. SELECTED INSTRUMENTATION PLAN

The previous considerations led to the following plans for selecting the transducers and placing them in the two Third Stage motors. The plan for Motor No. 2 was the same as that for Motor No. 1, except for the addition of five stress transducers and five thermocouples.

The instrumentation plans given here involve only the internally mounted gages. The case deflection gages used in the hydrotest and the accelerometers used in the vibration testing are described along with the testing efforts.

1. Motor No. 1

The gage layout for this full-scale motor is given in Figures 22 through 26 while Table 6 contains a summary of the number and types of transducers and the code designation of each instrument or transducer, its relative location in the motor, type of information required during testing, and the expected range.

Figure 22 is a view looking from the aft end and shows an array which includes four 450-psi F.S. normal stress sensors, eight shear stress transducers, and 16 failure event gages. Figures 23 through 26 indicate some of the locations in the radial planes. These aft end gage locations were positioned primarily to detect and define an unzipping failure at the bondline that was expected to occur during pressurization. Further, the shear cubes and the normal stress transducers were to collect data during all tests for comparison with the calculated values at these critical locations.

A boot releases the forward end of the grain back to the point labeled forward equator. Just aft of this point, the root of the relief boot, indications of cohesive propellant failures have been found. As discussed previously, the calculated stresses and stress gradients in this region are severe for most loading conditions. To measure the corresponding values in the motor, as well as the normal stresses, and to detect the time and extent of any failures, one 150 psi FS normal gage, one shear cube, the 3-D gage and four failure gages were positioned just aft of this release. The 3-D gage was positioned here to assess a 3-D stress field in which significant shears are present. The lone thermocouple was mounted on its interior face only because it provided a convenient way to suspend it four inches away from the case into the web during casting. The locations of failure gages placed in the forward dome region are indicated in Figure 27.

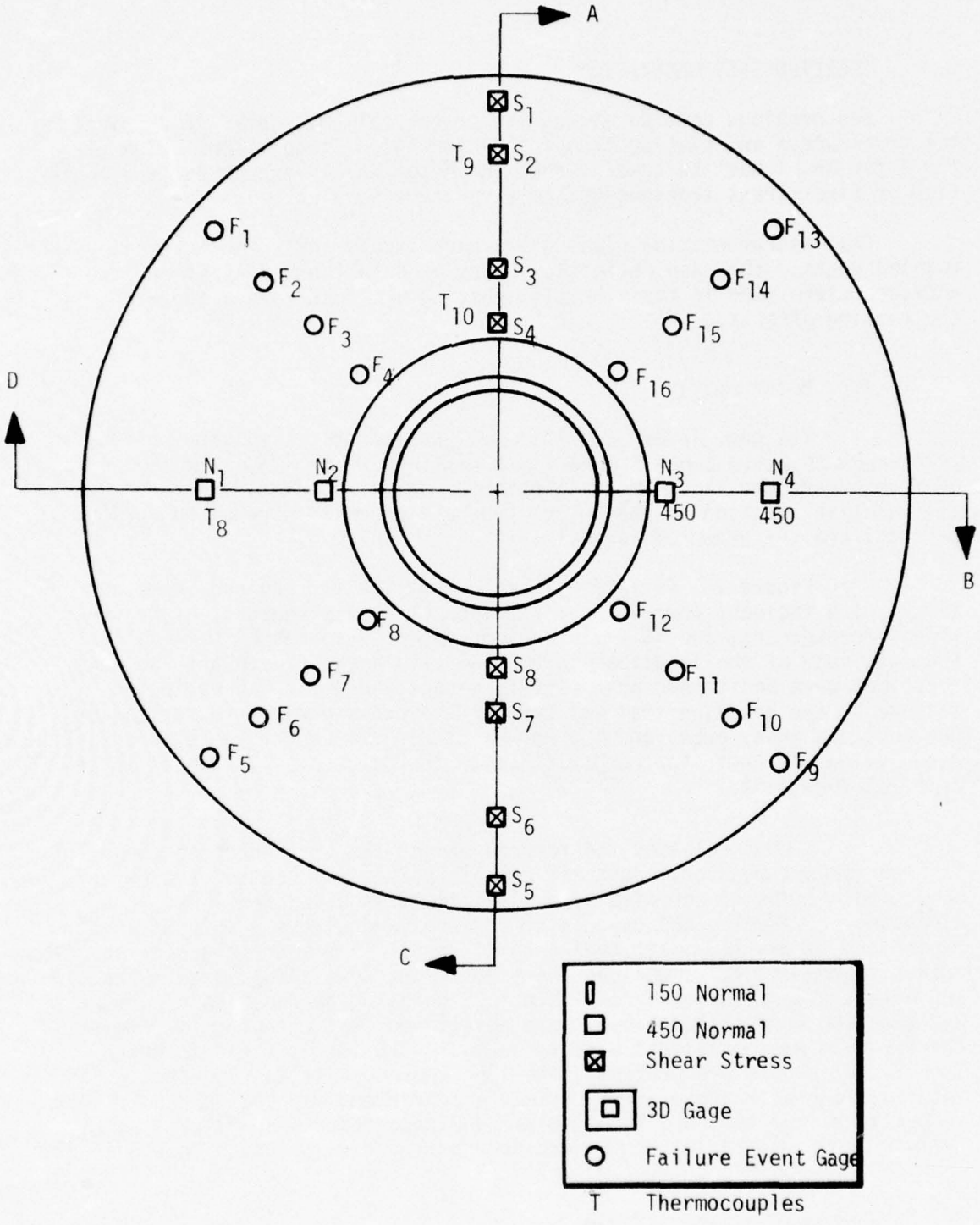

FIGURE 22. PLANNED GAGE LOCATIONS IN THE AFT DOME REGION FOR MOTOR NO. 1

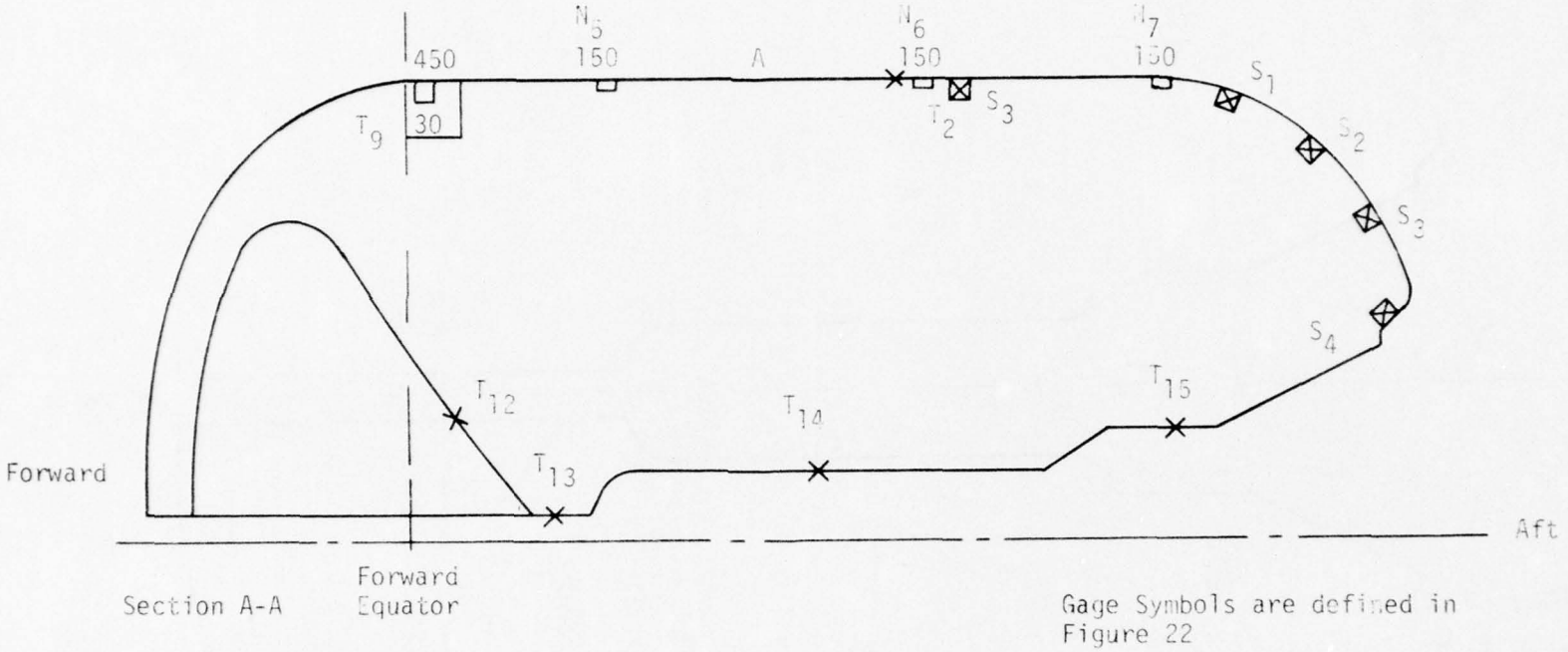

FIGURE 23. GAGE LOCATIONS IN SECTION A-A FOR MOTOR NO. 1 (130°)

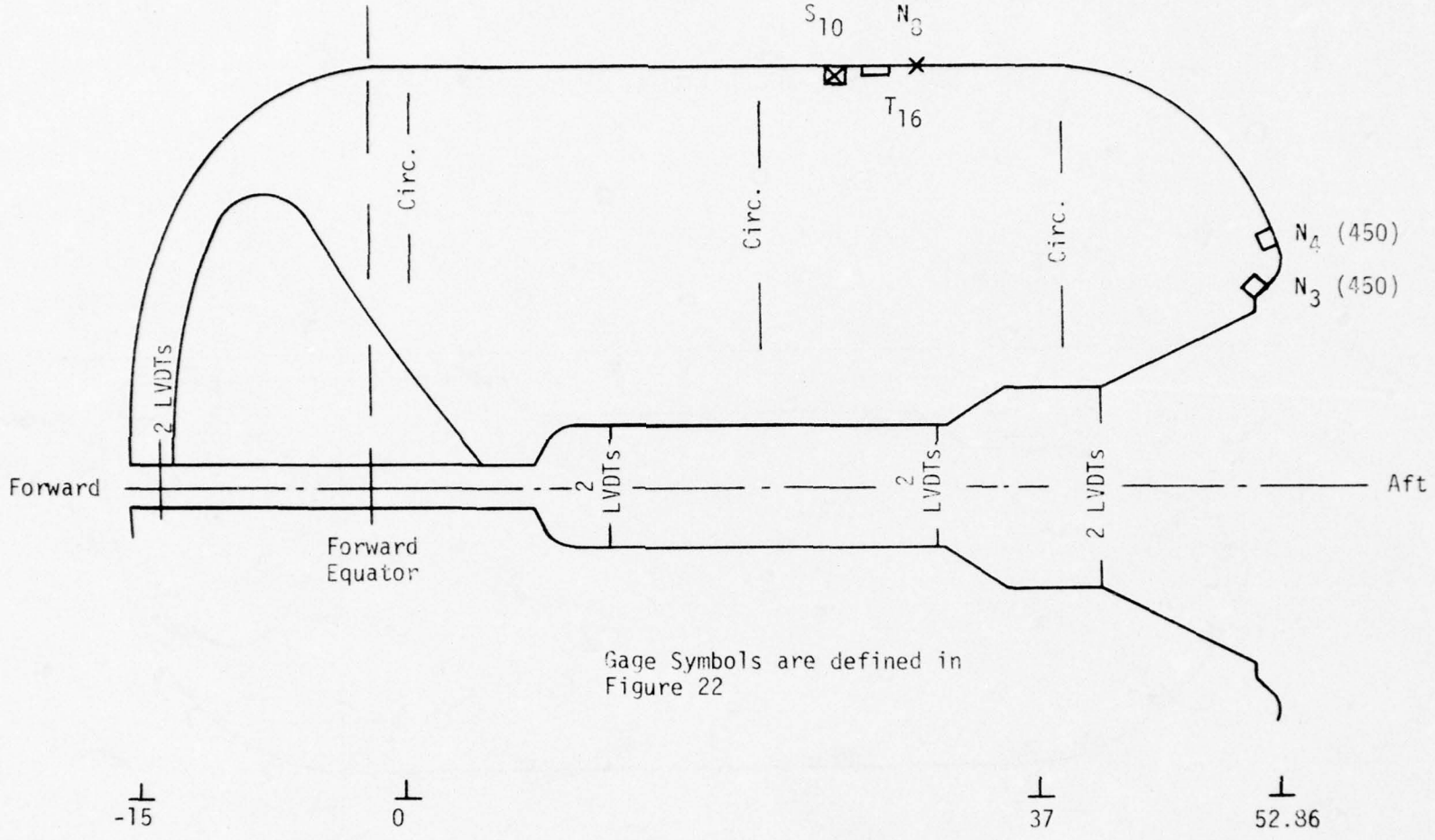

FIGURE 24. GAGE LOCATIONS IN SECTION B-B FOR MOTOR NO. 1 (270°)

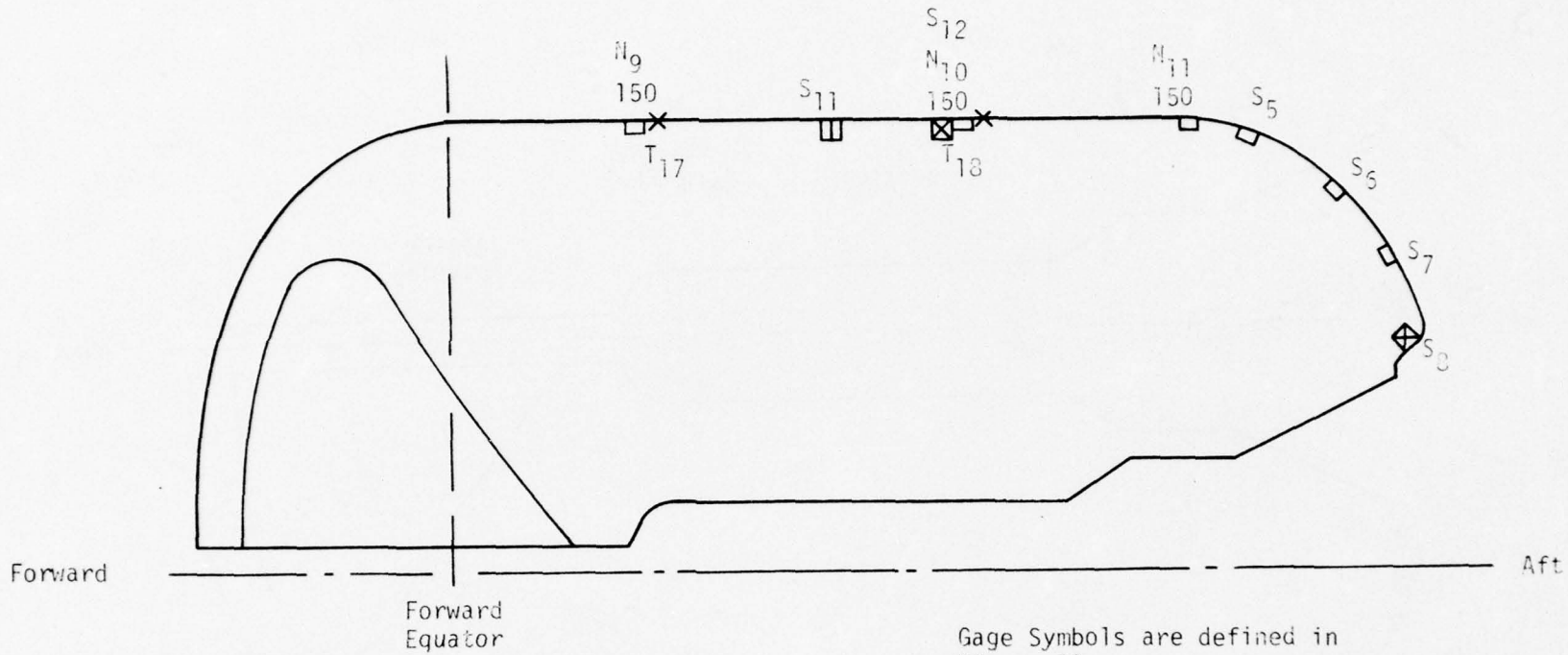

FIGURE 25. GAGE LOCATIONS IN SECTION C-C FOR MOTOR NO. 1
(0°)

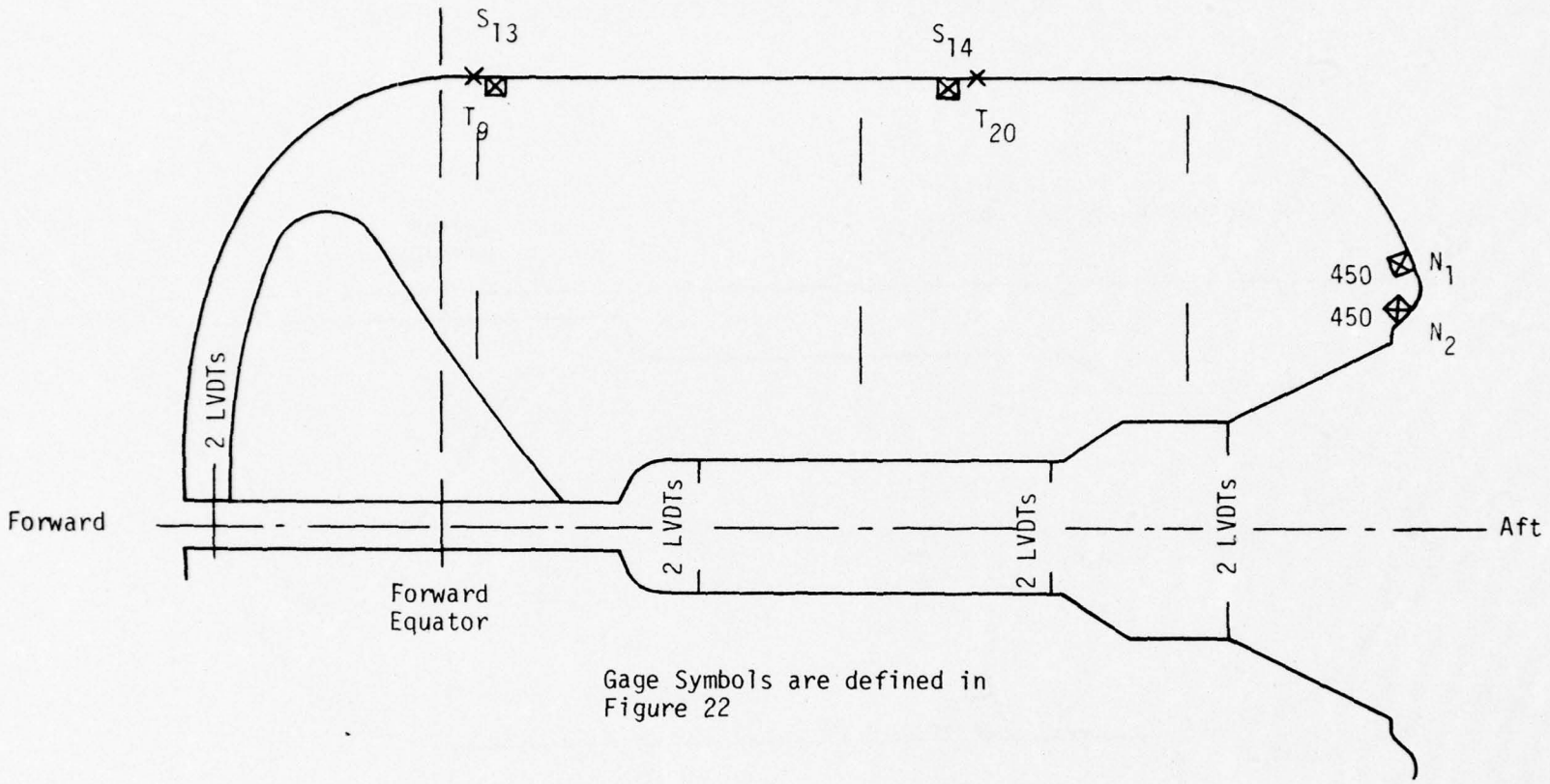

FIGURE 26. GAGE LOCATIONS IN SECTION D-D FOR MOTOR NO. 1
(90°)

TABLE 6

INSTRUMENTATION REQUIREMENTS

Type	Location	Information Required	Expected Range
Shear Gages (14)			
No. S1	Aft Head 180°	Bond Shear	0 to 500 psi, pressure tests, and 0 to 10 psi, all other tests
S2	Aft Head 180°	Bond Shear	
S3	Aft Head 180°	Bond Shear	
S4	Aft Head 180°	Bond Shear	
S5	Aft Head 0°	Bond Shear	
S6	Aft Head 0°	Bond Shear	
S7	Aft Head 0°	Bond Shear	
S8	Aft Head 0°	Bond Shear	
S9	Barrel 180°	Bond Shear	
S10	Barrel 90°	Bond Shear	
S11	Barrel 0°	Bond Shear	
S12	Barrel 0°	Bond Shear	
S13	Barrel 270°	Bond Shear	
S14	Barrel 270°	Bond Shear	
Normal Gages (11)			
N1 (450 psi)	Aft Head 90°	Bond Tension	0 to 500 psi, pressure tests, and 0 to 10 psi, all other tests
N2 (450 psi)	Aft Head 90°	Bond Tension	
N3 (450 psi)	Aft Head 270°	Bond Tension	
N4 (450 psi)	Aft Head 270°	Bond Tension	
N5 (150 psi)	Barrel 180°	Bond Tension	
N6 (150 psi)	Barrel 180°	Bond Tension	
N7 (150 psi)	Barrel 180°	Bond Tension	
N8 (150 psi)	Barrel 90°	Bond Tension	
N9 (150 psi)	Barrel 0°	Bond Tension	
N10 (150 psi)	Barrel 0°	Bond Tension	
N11 (150 psi)	Barrel 0°	Bond Tension	

TABLE 6

INSTRUMENTATION REQUIREMENTS (CONT.)

Type	Location	Information Required	Expected Range
Three-D Gages (2)			
D1	Aft Head 0°	Bond Shear and Bond Tension	0 to 500 psi, pressure tests, and 0 to 10 psi, all other tests
D2	Barrel 180°		
Failure Gages (20)			
F1	Aft Head 135°	Bond Separation	Discontinuity of circuit
F2	Aft Head 135°	Bond Separation	
F3	Aft Head 135°	Bond Separation	
F4	Aft Head 135°	Bond Separation	
F5	Aft Head 45°	Bond Separation	
F6	Aft Head 45°	Bond Separation	
F7	Aft Head 45°	Bond Separation	
F8	Aft Head 45°	Bond Separation	
F9	Aft Head 315°	Bond Separation	
F10	Aft Head 315°	Bond Separation	
F11	Aft Head 315°	Bond Separation	
F12	Aft Head 315°	Bond Separation	
F13	Aft Head 225°	Bond Separation	
F14	Aft Head 225°	Bond Separation	
F15	Aft Head 225°	Bond Separation	
F16	Aft Head 225°	Bond Separation	
F17	Forward Head 235°	Bond Separation	
F18	Forward Head 115°	Bond Separation	
F19	Forward Head 55°	Bond Separation	
F20	Forward Head 295°	Bond Separation	
LVDT (8)			
LVDT 1	Bore 0-180°	Bore Deflections	0 to 25%, pressure tests, and 0 to 10%, all other tests
LVDT 2	Bore 0-180°	Bore Deflections	
LVDT 3	Bore 0-180°	Bore Deflections	
LVDT 4	Bore 0-180°	Bore Deflections	
LVDT 5	Bore 90-270°	Bore Deflections	
LVDT 6	Bore 90-270°	Bore Deflections	
LVDT 7	Bore 90-270°	Bore Deflections	
LVDT 8	Bore 90-270°	Bore Deflections	

TABLE 6

INSTRUMENTATION REQUIREMENTS (CONT.)

Type	Location	Information Required	Expected Range
Clip Gages (3)			
C1	Aft Fin 180°	Local Deflections in Fins	0 to 20%
C2	Aft Fin 115°		
C3	Aft Fin 0°		
Thermocouples (23)			
T1	Aft Head 180° (Ext.)	Local Grain	60 ± 5°F to 110 ± 5°F
T2, T3	Aft Head 180°		
T4	Aft Head 270°		
T5, T6	Aft Head 0°		
T7	Aft Head 0° (Ext.)		
T8	Aft Head 90°		
T9, T10, T11	Barrel 180°		
T12, T13, T14, T15	Bore Surfaces		
T16	Barrel 90°		
T17, T18	Barrel 0°		
T19, T20	Barrel 270°		
T21, T22, T23	Aft Fin 175°, 115°, 355°		

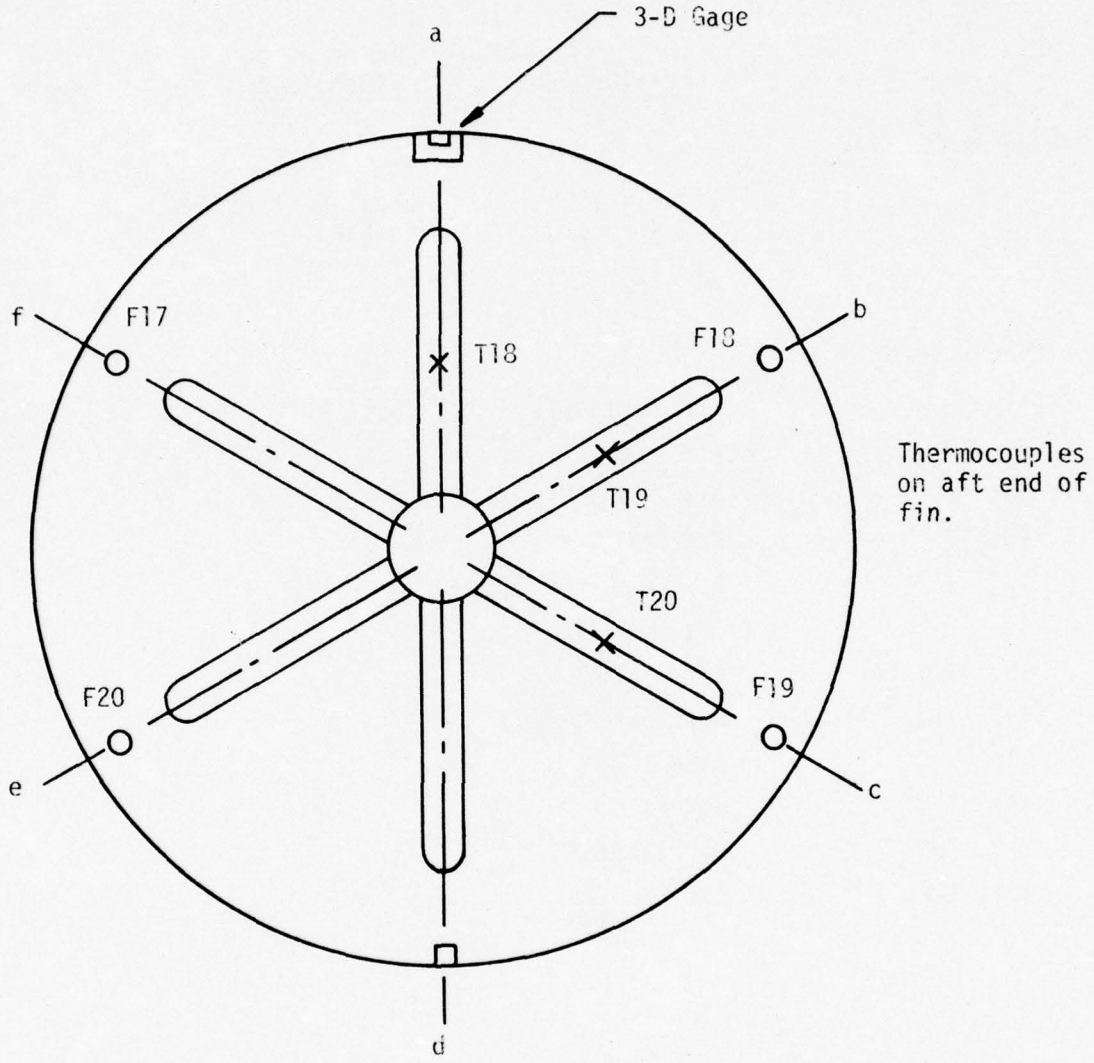

FIGURE 27. GAGE LOCATIONS IN HEAD END REGION FOR MOTOR NO. 1

All other bondline gages were placed near the center of the motor where the gradients are small and the most ideal for correlations between measurements and analyses. The geometry is such as to provide a near-plane strain (generalized) condition with a circular ported cross-section. The case deformations during axially symmetric loading could be obtained here (and at the forward and aft equators) using the circumference gages. Nearby thermocouples provided the temperature at the case wall and within the web.

The inner-bore placement of the LVDTs was the minimum number that could be used to assess the bore hoop strain distribution.

Table 7 summarizes the instrumentation plan for Motor No. 1. Of particular interest is the number of channels of data (138) required for this testing.

2. Motor No. 2

The instrumentation plan for this motor was the same as that for Motor No. 1 except for the addition of five stress gages to the aft dome; Figure 28. There was one 3-D, two normal, and two shear stress transducers. The 3-D stress gage was an experimental model, so it was planned to use it in a location where the bond stresses had only a small gradient.

The four normal and shear stress gages were added to the motor to measure stresses at the location considered to be critical in motor firings. Figure 29 illustrates the shapes of the burning surface at discrete times after ignition. The critical point occurs between 10.68 and 11.36 seconds. Thus, a gage placed at the bondline between positions 3 and 4 of Figure 29 would permit direct measurements of local stress or failure events at a point very close to that where the failure is likely to initiate.

D. INSTALLATION TECHNIQUES

The methods for preparing the gages and mounting them on the motor are described below. Because of the special procedures involved, all of them were assessed and improved upon prior to their use in full-scale motors.

TABLE 7

SUMMARY OF TRANSDUCERS IN MOTOR NO. 1

Type	No. of Transducers per Motor	No. of Channels	No. of Leads
Strain Clips (Width of Fin)	3	3	12
Normal Stress			
150 psi F.S.	7	14	42
450 psi F.S.	4	8	24
Shear Gage	14	14	42
Three-D Gage	1	7	18
Failure Event Gages	20	20	40
Thermocouples	23	23	46
Accelerometers (3 Way)			
Crystal	9	23	54
Circumference Gage	3	3	12
Deflection Reed	18	18	72
Pressure Transducer	2	2	8
LVDTs	8	8	32
Case Strain Gages	2	2	2

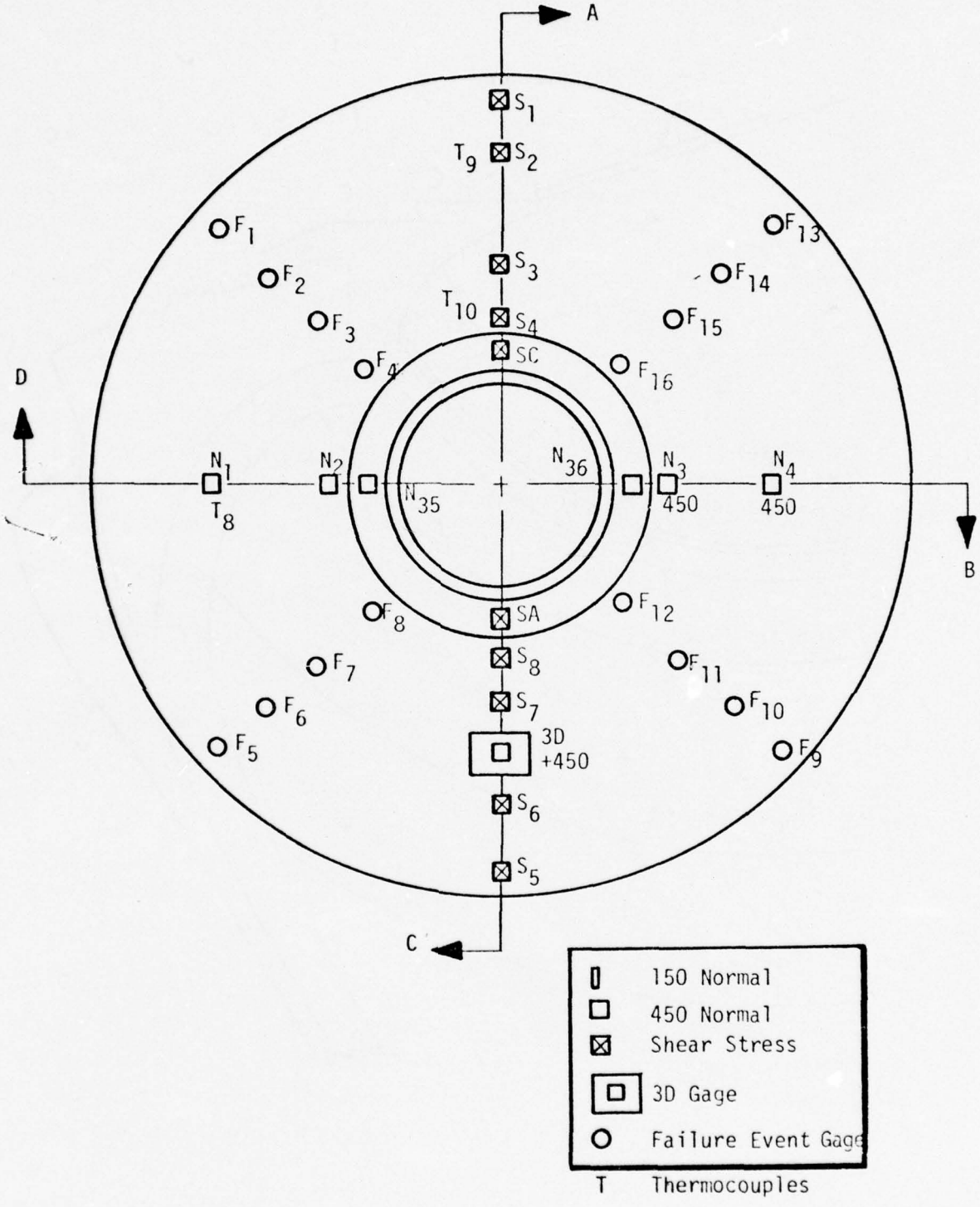

FIGURE 28. PLANNED GAGE LOCATIONS IN THE AFT DOME REGION FOR MOTOR NO. 2

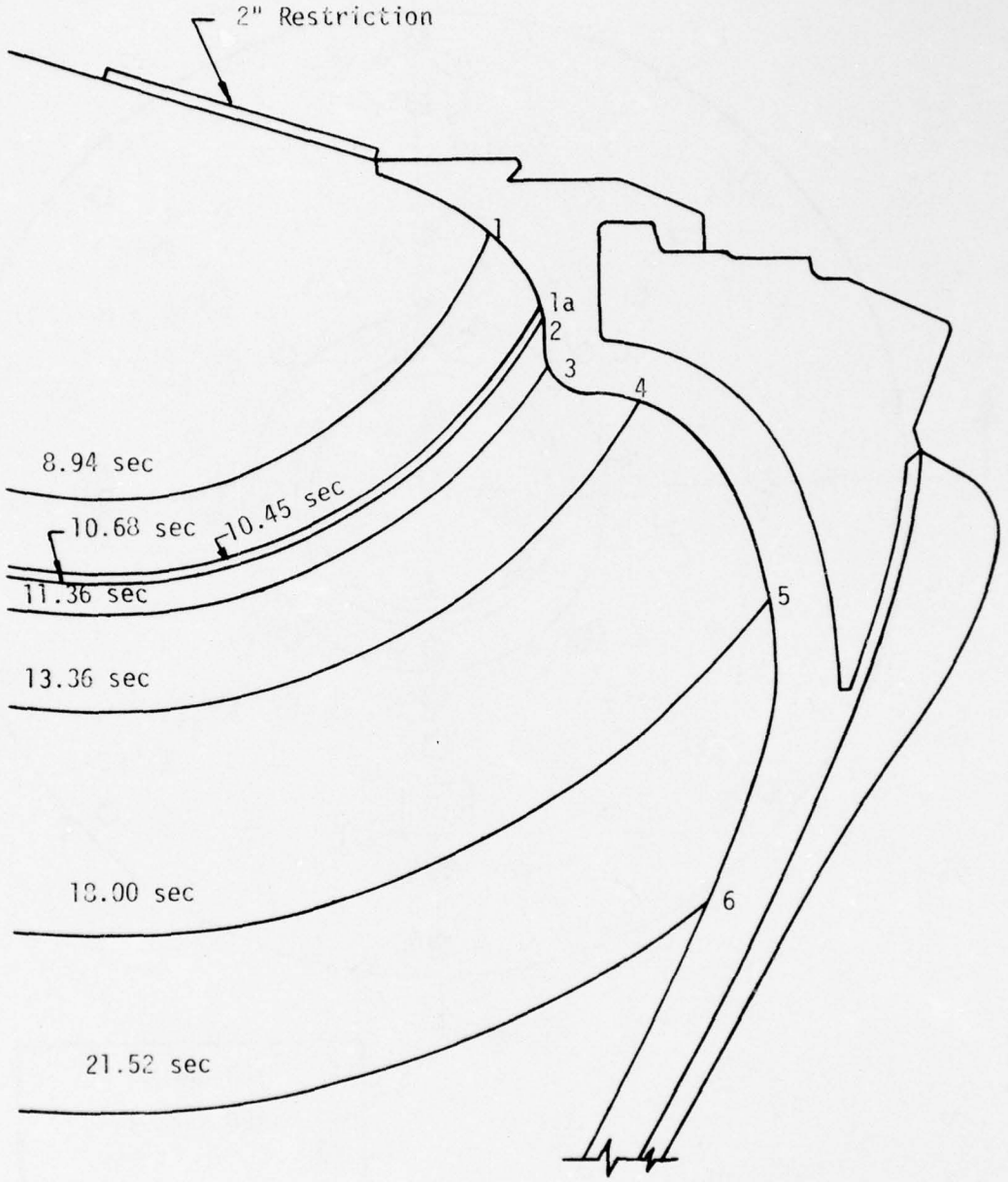

FIGURE 29. PROPELLANT BURN SURFACES VS TIME AFTER IGNITION IN THE VICINITY OF THE ALUMINUM BOSS

1. Normal Stress Gage Pre-Potting

The proposal planning efforts for this program led to the new concept of gage pre-potting. Previously the normal stress gages were mounted on the case wall, then they were potted in a cup of propellant as shown in Figure 30. After propellant cure, the gages were calibrated through internal pressurization of the motor case. Temperature compensation of the gages was performed prior to delivery by the vendor (Konigsberg Instruments, Inc.).

The new potting concept resulted from the intention to embed the gages within the insulation for thermal protection during motor firing. Since the insulation is inert it was possible to pre-pot the gages before calibration and temperature compensation by the vendor.

As noted previously, the embedded gage modifies the local grain stresses and the embedding propellant (or insulation) modifies the performance of the gage diaphragm. The 'zone of influence', which is that portion of the material surrounding the gage which contributes to the modification of its performance, is a strong function of its diameter (1, 3, 4), which is only 0.10 in. (Figure 15). A major portion of the zone of influence occurs within two radii of the edge of the diaphragm or, in this case, a region with a total diameter of about 0.30 in. Thus, much of the zone of influence for the diaphragm falls within the diameter of the base of the gage, 0.310 in. diameter.

The finally selected prepotting design, Figure 31, considerably exceeds the gage base with an overall diameter of 0.75 in. and a height of 0.375 in. This enlarged prepotting region also takes into account the discontinuity effects arising at the edge of the metal disc. These produce their own interaction stress effects which do not affect the gage performance.

The potting material was a trowelable insulation (ASPC formulation No. IBT-115), which has relaxation moduli similar to those of the ANB-3066 propellant.

2. Through-the-Case Wiring

One of the most practical accomplishments of this program was the successful installation of gages with their leadwires projecting directly through the case. A typical installation is given in Figure 32.

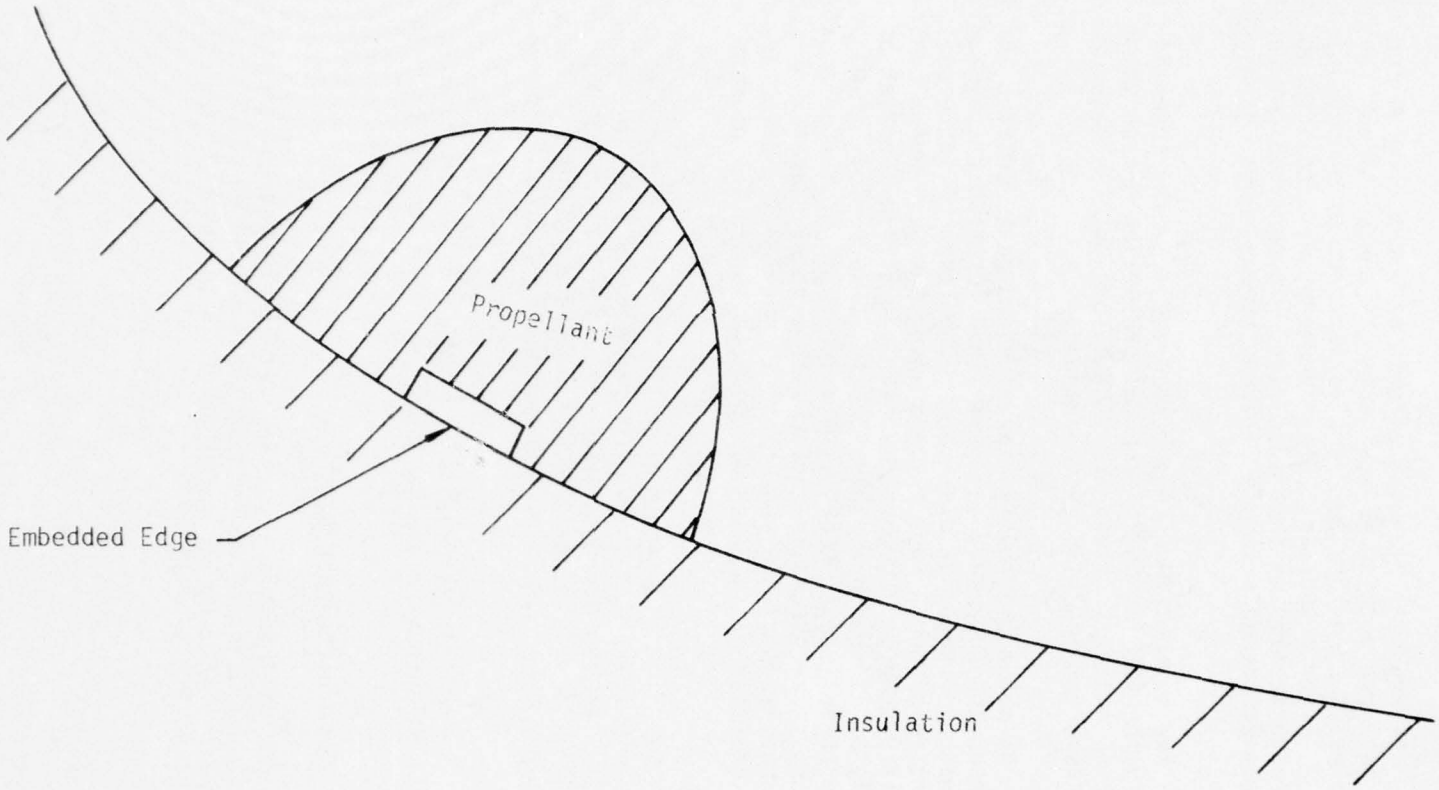

FIGURE 30. PREVIOUS GAGE EMBEDMENT PROCEDURE

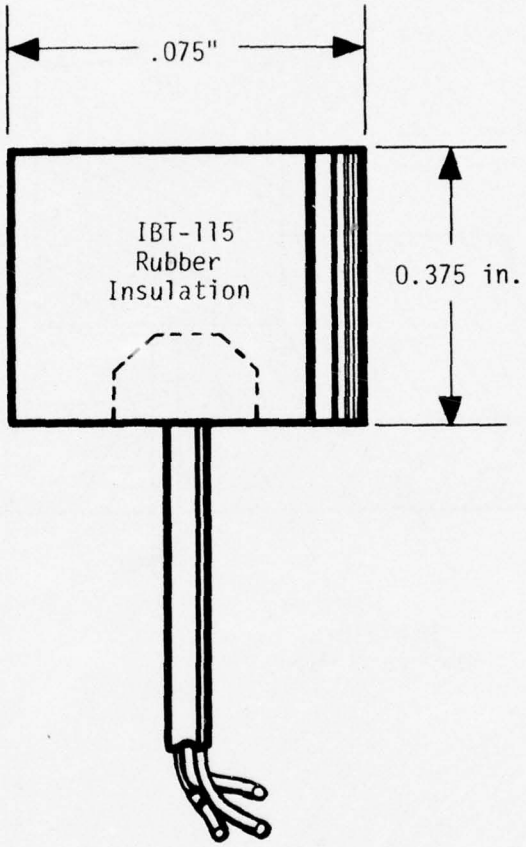

FIGURE 31. POTTED NORMAL STRESS GAGE

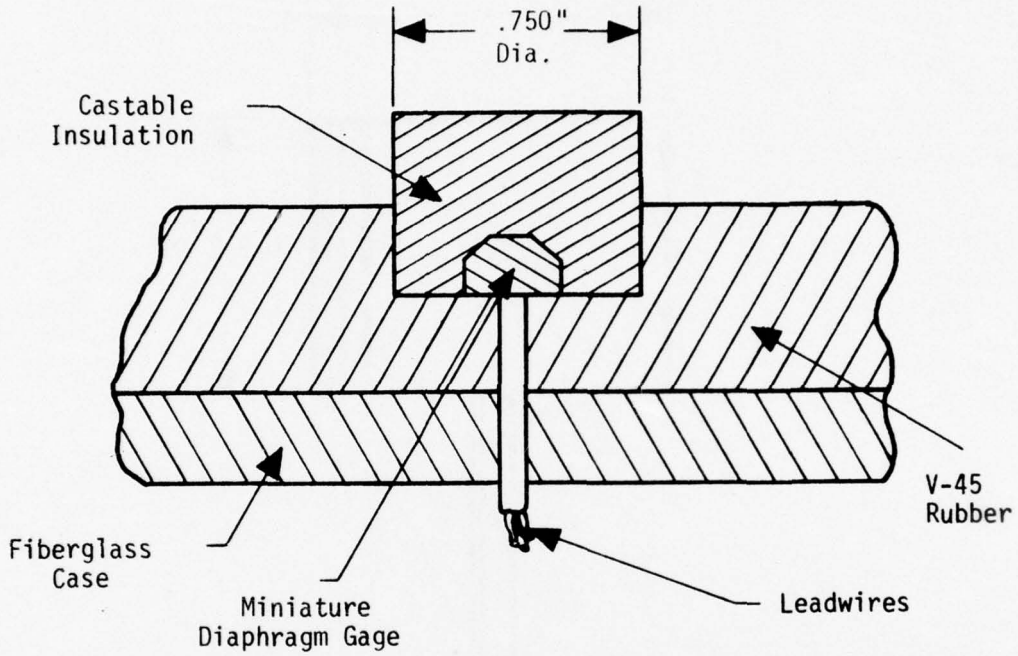

FIGURE 32. POTTED NORMAL STRESS GAGE - AS INSTALLED

Prior experience on the Polaris A-3 program (22) had demonstrated the practicality of this concept on full-scale motors. Hole sizes from 0.090 to 0.249 in. were employed in that program and the largest holes reduced case strength only 10%. The maximum hole size planned for the Flexible Case-Grain Interaction program was only 0.060 in. so negligible effects on case strength were expected.

The possibility of local case degradation leading to fissuring of the insulation and gas leaking was a real problem area still requiring evaluation. This assessment was accomplished during the STV testing (16) which showed that the soft IBT-115 adhesive made an excellent flexible seal for pressures up to 1800 psig; with case holes of 0.060 in. (Actually, the end plate unbonded from the STV chamber before failure of the case wall could take place).

3. Motor Installation Procedures

The basic problem here was to devise a practical method for drilling holes in the motor case then mill the inside rubber insulation to receive the pre-potted gages. The procedures were developed in the STV-1 tests (16), which simulated as closely as possible the operations planned for the full-scale motors.

The basic tool for this drilling was a modified 3/4 in. diameter end mill with a pilot guide welded to its center, Figure 33. The tool is driven by a high speed air drill, with the pilot guide inserted into a 0.060 in. diameter hole, previously drilled through the case. The guide automatically centers the cutting edge of the end mill making a 3/4in. diameter recess in the insulation (this accommodates the seating of the normal and shear stress gages). An excluded length was designed into the tool to provide a positive "stop". This stop prevented the end mill from cutting into the case wall (just one cut of this kind could make the case unacceptable for pressurization testing).

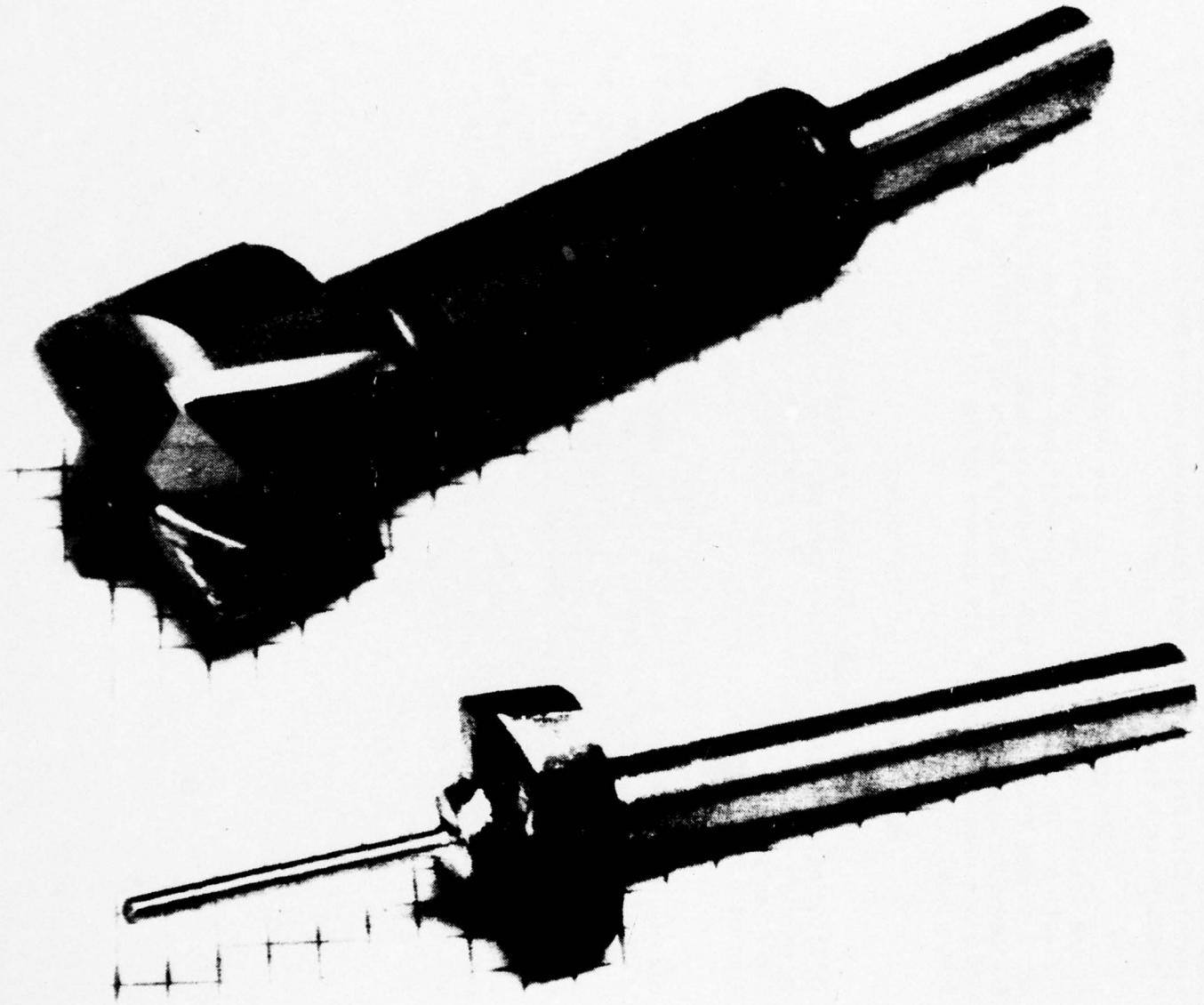

FIGURE 33. MODIFIED 3/4 IN. DIA. END MILL

SECTION 6

STV FABRICATION AND TEST

Structural test vehicle evaluations were conducted early in the program to verify that several types of embedded stress transducers and their installation methods could be successfully used without affecting the integrity of the grain or filament-wound glass chamber of the Minuteman III, Third Stage motor. The results of these tests, along with the impact on those results of the gage and system errors discovered later in the program, are discussed in detail in Special Technical Report AFRPL-TR-75-7 issued in October 1975. For the purposes of continuity and completeness the tests conducted and the significant findings are summarized in this section.

A. PROBLEMS REQUIRING STV EVALUATIONS

The required instrumentation in the full-scale motor led to a number of problems; particularly, at the propellant-insulation bondline. Here, a large number of gages (about 56) with a much larger number of leadwires (about 185 wires) were required to gain the desired data. These leadwires could have been bonded to the insulation surface and brought out through fore and aft bosses. But, that approach probably would have affected the bondline integrity of the grain; especially, where a larger number of the wires would come together. The problem was solved by bringing the leadwires out through the case wall. Such an approach had been demonstrated on other motors, but its acceptability to the Minuteman motor required further evaluation. That became one of the tasks requiring STV testing (see STV No. 1, below).

In addition, a number of technical problems had been solved on paper or in the laboratory. But, before they could be applied in the full-scale motor, these solutions had to be demonstrated and evaluated under motor use conditions. The structural test vehicles provided the testing medium for these evaluations and demonstrations.

The original plan was to use only four STV's, but a fifth was added to complete some testing requirements overlooked in the earlier STV testing. The five STV's, and the problems they were designed to address are described below, along with a brief summary of significant test results.

B. STV TESTS

1. STV No. 1 - Bonding and Case Failure Tests

Task Statement:

> Conduct bonding and case failure tests with normal stress gages and thermocouples to define the best technique for through-the-case wall installation.

This task involved two separate evaluations. First, there was the problem of drilling holes through the fiberglass case; as mentioned above.

Second, the flexibility of the case produces problems of differential deformations with respect to the rigid metal, normal stress gages. The solution to this problem involved the use of an elastomeric adhesive, whose adequacy had to be verified in an STV.

This STV gave experience in the use of the new installation techniques. Several useful procedures and special tooling were developed as a result of these studies.

The planned gage installations required that 0.060-in. diameter holes be drilled through the motor case. Prior experience on the Polaris A-3 program had demonstrated that a typical fiberglass case was not significantly weakened by small holes of this size. The tests on STV-1 provided the added demonstration that the holes would not cause case degradation leading to fissuring of the surrounding insulation with gas leaking through the holes in the fiberglass case.

2. STV No. 2 - Evaluation of Gage Potting and Calibration Methods

Task Statement:

> Pre-pot and calibrate normal stress gages and shear gages, then test under hydrostatic and differential pressures while measuring viscoelastic responses of the propellant. Also, compare the performances of gages using the pre-potting procedure with those post-potted in propellant (the conventional method).

This task involved protecting the instrumented case during motor firing. Wherever gage leadwires were brought through the case wall there existed the possibility of case burn-through. To protect against this contingency, all of the gages were to be embedded within rubber insulation material. This was accomplished partly by potting the gages and partly by embedding the gages within the V-45 insulation layer.

This task also required a performance evaluation of a new small diameter (0.1 in. diaphragm) normal stress gage. This gage was required for making measurements in high stress gradient areas. Previous to this program the normal stress gages used 0.25 in. diaphragms.

A novel technique of "pre-potting" the normal stress gages within an inert insulation material (IBT-115) was devised for the full scale motor program. The tests on this STV showed that:

(1) Pre-potting of these transducers may be satisfactory for preliminary calibrations and compensation purposes. Nevertheless, final calibrations and compensations should be made after the gage is mounted in place.

(2) To minimize material property differences the potting or prepotting material should be the live propellant or an inert version of it.

(3) Over the limited temperature range of 30° to 110°F the IBT-115 pre-potted gages and the propellant post-potted gages gave essentially the same "measured" stress data, within expected errors.

(4) Both types of gage potting are sensitive to improper preparation errors, such as voids occurring within the potting near the gage diaphragm. Careful procedures plus X-ray examinations of all potting procedures should be instituted.

The shear gage performances under differential (shear) tests within the STV were very similar to those observed during the calibration within the shear test fixture. However, apparent gage calibration factors were approximately 14% higher in the STV than those determined in the shear fixture, assuming a uniform shear stress along the length of the STV. This effect was attributed partly to voids or microvoids within the grain that produced a more compressible propellant than expected. This condition would produce the higher gage outputs (higher apparent gage calibration factors) which were observed.

3. STV No. 3 - Failure Detection Using Shear and Failure Event Gages

Task Statement:

> Verify shear gage and failure event gage performances up to failure of the grain/insulation bond.

Because of the very large bondline areas in the Minuteman III motor, it was essential that as many of the gages as possible would be able to detect local failures. This required the use of a new rugged version of the shear cube (developed by Harold Leeming, Ph.D., and Associates). All previous designs were far too fragile for this treatment.

To give an additional failure detection capability at a low price, ASPC designed an elastomeric, failure event gage. This gage is a simple device designed to detect passage of a crack or bondline separation. The gage was made of a conductive rubber, failure of the gage being determined by the loss of electrical conductivity.

The 77°F test series performed on STV No. 3 was designed to evaluate the performances of the shear and elastomeric failure gages under realistic combinations of pressure and shear loads up to failure of the propellant-liner-insulation bond. A premature failure of the bond at a shear stress of 32 psi, without a superimposed hydrostatic pressure, led to a decision to make an additional STV (No. 5) to repeat the complete sequence of failure tests.

The STV No. 3 test data showed that the new ruggedized shear gages operated satisfactorily up to bond failure. But, the earliest types of elastomeric shear gages proved to be too delicate. Later experience indicated that eight of ten of these gages would break during grain casting. On the other hand, two of the failure event gages debonded rather than break during the differential pressure tests. Clearly, more development work was required before re-evaluating the event gages in STV No. 5.

4. STV No. 4 - Investigation of Stress-Free Temperature Change

Task Statement:

> Stress-free temperature monitoring during motor storage and test at 80°F.

The behavior of the solid propellant itself is known to cause a number of analytical difficulties. One of these difficulties,changes in the stress-free temperature, is especially important to the use of stress gages in solid propellant grains. STV tests of this parameter were intended only to illustrate the problem for ANB-3066 propellant.

This background could be of value in any later evaluations of future test data from a second full-scale motor prepared on this program. That motor is expected to show significant changes in its stress-free temperature.

This STV was similar in design to the other STV's and contained two normal stress gages and two shear gages. One purpose of this STV was to determine changes in the stress-free reference temperature which would occur in ANB-3066 propellant during long term storage at 77°F. The normal stress data for STV No. 4 decayed from approximately 5 psi at the start of storage at 77°F to 0 psi then, seemingly, became compressive after 33 to 46 weeks. This behavior is attributed to changes in both the stress-free temperature of the propellant grain and the zero-stress calibration of the normal stress gages. The relative contributions of these two effects could not be estimated from the available data.

Another test performed on STV No. 4 was a week-long differential pressure test to ascertain whether plastic deformation was obtained with the propellant. Monitoring of the grain displacements after removal of the pressure showed that a small creep of approximately 0.020-in. remained 30 days after the end of the test. This small plastic deformation is probably insignificant.

5. STV No. 5 - Re-test of STV No. 3

Task Statement:

> Calibrate normal stress and shear gages using hydrostatic and differential pressure tests. Conduct failure detection tests using shear and failure event gages.

This STV was designed to evaluate the performances of the shear gages and bondline failure event gages under realistic combinations of hydrostatic and differential pressure (shear) stresses. The shear stress data from the STV gave similar gage sensitivities to those measured in the calibration shear fixture. However, precise agreement was not achieved. Observed defects in the gage installation techniques, excessive liner material surrounding the gages, and significant voids close to the gages, plus an estimated 5 vol. % level of casting voids in the grain, are considered to be factors which contribute to the apparent changes in the gage sensitivities.

A significant aspect of the STV No. 5 data was the verification that shear stress gages which exhibit a large sensitivity to hydrostatic pressure will produce spurious outputs under combined shear and pressure loads. Three of the shear gages showed an excessive response under hydrostatic pressure. One of these gages had been tested under combined hydrostatic pressure and shear during its calibration and had been rejected for use in a full-scale motor because of excessive response to hydrostatic pressure.

The STV failure tests performed with a hydrostatic pressure component of 600 psi were successfully carried out; failure occurred at a gage-measured shear stress of 22 psi. All the shear gages gave good indications of the initiation of grain failure. All four of the failure event gages also gave clear indications of the initiation of bond failure during the test.

The performance of the improved failure event gages in STV No. 5 was very encouraging and suggested that they should be satisfactory in the full scale motor applications.

SECTION 7

MOTOR INSTRUMENTATION AND FABRICATION

This section is limited to descriptions of the activities required in the selection of a chamber, instrumenting it, calibrating the transducers, and casting and curing the grain. The next section (Section 8) summarizes the testing and gage measurements made on Motor No. 1.

In this work two Minuteman III, Stage III motors of the ASPC design were fabricated using the instrumentation and gage mounting procedures defined in Section 5. Motor No. 1 was designed to be structurally tested but not fired so the associated hardware (nozzle, igniter, etc.) were used components taken from a previously fired motor. Motor No. 2 was fabricated and instrumented to permit measurements in a static firing, then it was placed in storage to await testing on a future program. The fabrication and propellant testing followed the procedures normally employed in production. Cartons of propellant were taken from each of the batches used.

Some of the key features of these two motor preparation tasks are considered below in the order in which they occurred.

A. CHAMBER PURCHASES

Two fiberglass chambers of the Minuteman III, Third Stage design were purchased from the Thiokol Corporation and delivered in August 1972. The two "as delivered" cases were of Aerojet design and acceptable for the purposes of this program. But they had small boss alignment defects that put them outside of Air Force specifications for delivery to the fleet.

B. CHAMBER HYDROTESTING

The first full scale Minuteman III, Third Stage chamber S/N 30113-1 was hydrotested on 25 September 1972, while chamber S/N 30114-1 was hydrotested the following week on 29 September 1972. The hydrotests of the full-scale chambers represented the first steps in the motor fabrication and test program. They were performed to give case deflection versus internal pressure data that would serve as boundary conditions for later structural analyses.

The hydrotest procedures, summarized in Appendix A, call for extensive instrumentation of the chamber to permit measurement of strains and deflections as a function of several levels of internal pressure. Locations of the instrumentation are summarized in Appendix A, also. Cantilever beam deflection transducers were used for measuring deflections, while the hoop strains along the barrel were obtained using long length circumferential strain gages. Longitudinal strains in the barrel were measured by pairs of deflection beams attached to the aft skirt. The pressure transducers were attached to the aft closure.

Since these chambers had already been subjected to a proof pressure of approximately 720 psi at Thiokol further testing to high pressures was expected to weaken the chambers and adversely effect correlations to structural analysis predictions. Therefore, chamber hydrotesting was limited to a maximum pressure of 200 psig.

A preliminary pressurization to 50 psig was performed to check and stabilize the instrumentation; after which the pressure was reduced to zero. Pressure was then applied, increasing in 50 psig increments to 200 psig, with a complete set of measurements made at each pressure increment. The pressure was then decreased in 50 psig increments to zero psig, while recording the gage data at each increment and at zero psig.

The results of the hydrotest are given in their entirety in Appendices B and C. During the hydrotest of Chamber S/N 30114-1, three minor leaks developed near the middle of the barrel section. These leaks were water "weeping" through the case wall. Their specific locations and the observations noted were:

(1) At 27 in. and 170° - water beads formed at 175 psig.

(2) At 26 in. and 175° - water beads formed at 155 psig.

(3) At 24 in. and 213° - water flowed in intermittent streams beginning at 150 psig, continued until pressure fell below 100 psig.

The chamber was accepted for use on the program with the specific stipulation that it was <u>never</u> to be fired.

Chamber S/N 30113-1 showed no weeping during hydrotest so it was reserved for use with Motor No. 2, which was designed for a possible future firing test. Thus, Chamber S/N 30114-1 became Motor No. 1 and is so designated for the remainder of the report.

C. GAGE INSTALLATIONS ON THE CHAMBER SIDEWALL

Motor No. 1 was instrumented in accordance with the plan given in Section 5. The instrumentation installed in this chamber consisted of 11 normal stress gages, 14 shear gages, 20 failure gages, one 3-D stress gage and 16 copper-constantan thermocouples. Four junction boxes consisting of cable terminations and bridge completions were mounted on the inside of the forward skirt approximately 90 degrees apart. The balance of the instrumentation was installed after removal of the casting core and consisted of eight LVDT's, three clip gages, and seven thermocouples. The total instrumentation of this motor, including that installed for the hydrotest measurements, is listed in Table 7.

The instrumentation plan used for Motor No. 2 was the same as that for Motor No. 1, with the addition of two shear gages, two normal stress gages (450 psi) and one 3-D stress gage.

The sequence of events in the instrumentation of these motors is given below.

1. Motor Layout for Gage Placement

A special alignment tool, Figure 34, was bolted directly to the flange in the aft boss to aid in locating the angles and distances of each transducer location. This tool consisted of a 24 in. arm, marked out in tenths of an inch throughout its entire length. The arm is pivoted about the center plate, which in turn is marked off in nearest tenths of a degree to 360 degrees. As the proper angle is determined by rotating the arm, it is locked in place by turning two set screws. The axial coordinate for each gage is then located and a marker placed on the chamber, with an accompanying gage identification. The motor was laid out in accordance with the instrumentation plan given in Section 5.

2. Drilling Through the Case Wall (External)

At each of the marked locations, pilot holes of 0.060 in. diameter were drilled perpendicularly through the case wall from the outside.

AD-A032 635 AEROJET SOLID PROPULSION CO SACRAMENTO CALIF F/G 21/9.2
FLEXIBLE CASE - GRAIN INTERACTION IN BALLISTIC WEAPON SYSTEMS. --ETC(U)
OCT 76 K W BILLS, S W JANG, H LEEMING F04611-72-C-0055
UNCLASSIFIED ASPC-1953-81-F-VOL-1 AFRPL-TR-76-57-VOL-1 NL

2 OF 3
AD
A032635

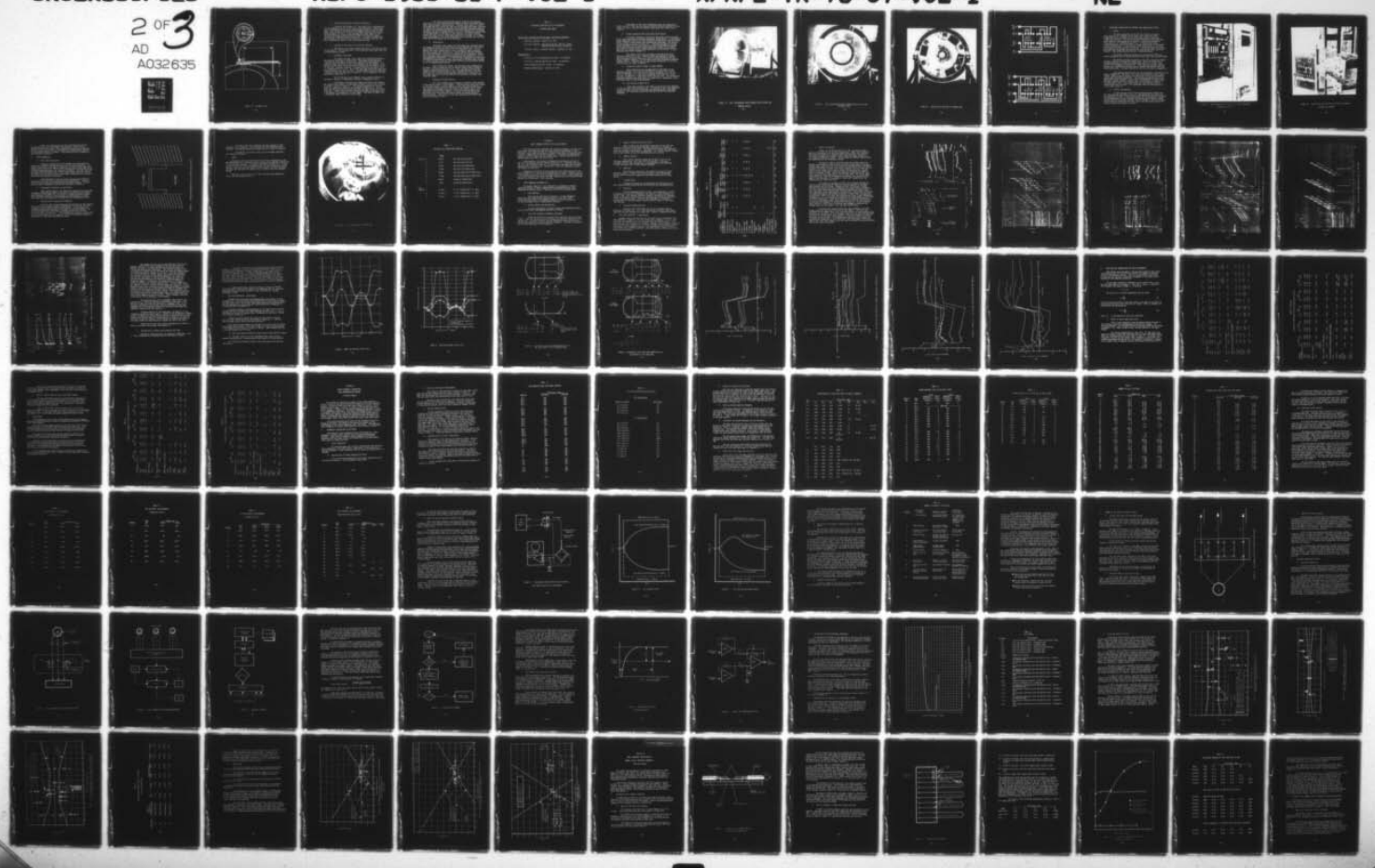

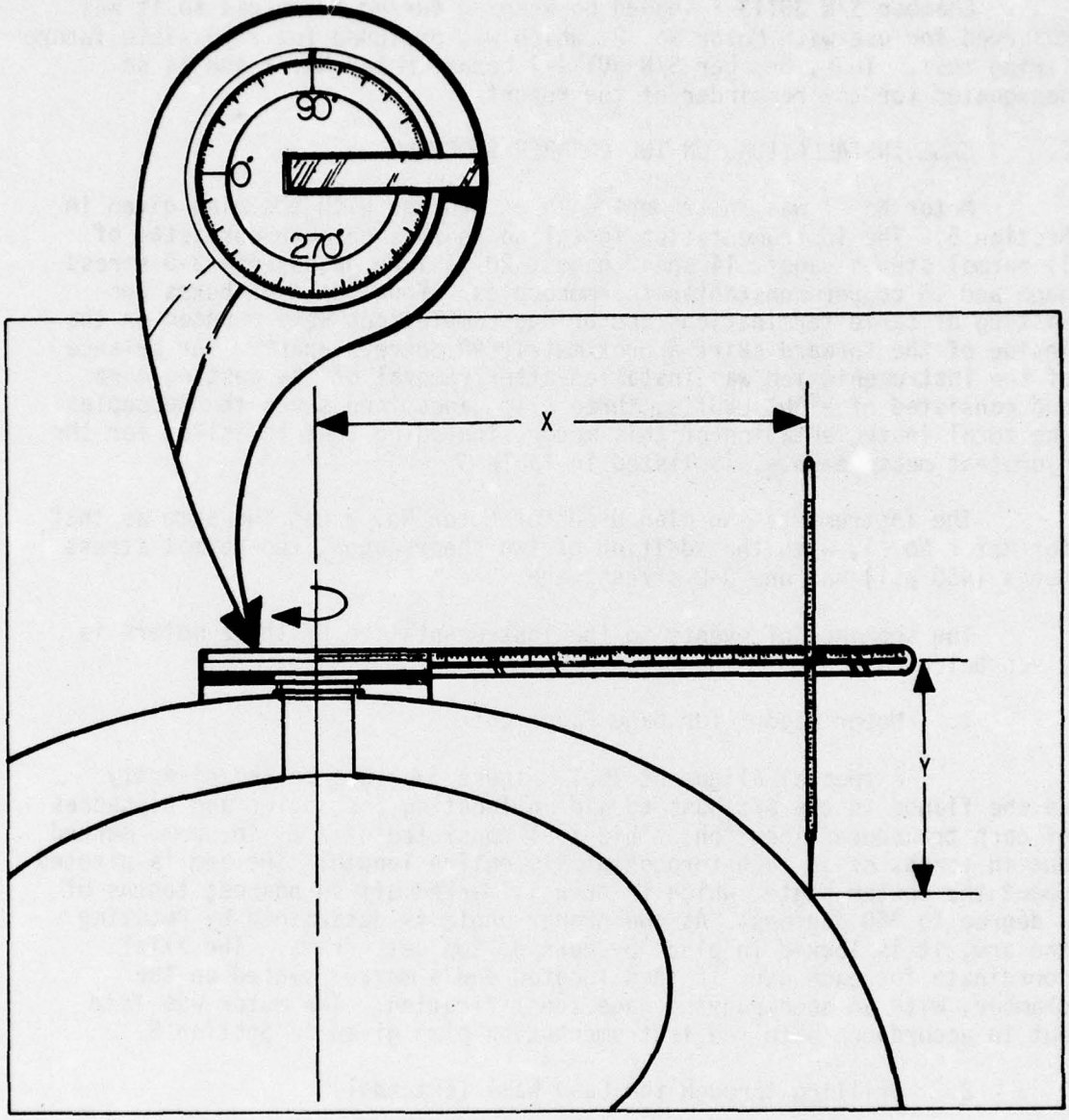

FIGURE 34. ALIGNMENT TOOL

3. Drilling Through Case Insulation (Internal)

A special tool (Figure 33) was used to drill shallow holes 7/8 in. diameter by up to 1/4 in. deep in the insulation. These holes were drilled primarily to seat the encapsulated normal stress and shear gages. The tool was a modified 7/8 in. diameter end mill with a pilot guide welded on its face. It was chucked into a high speed air drill. The pilot guide was inserted into the 0.060 inch pilot hole, which automatically centered the modified end mill. A flanged extruded area was included in the bottom face of the tool to provide a positive stop which prevented the end mill from hitting the case wall.

4. Cleaning of Case Holes and Insulation Recesses

Compressed air was blown through the holes in the case to clear out the debris. The recessed holes in the insulation were wiped clean with trichloroethylene solvent.

5. Transducer Selections

The normal and shear stress gages were selected according to the behaviors exhibited in calibration. Those gages exhibiting good linearity and the highest precision were selected for measurements in locations where the stress levels were expected to be the largest. Calibrations of the normal stress gages were conducted by the supplier at 30°, 80° and 130°F using gas pressure. A vacuum calibration was made at ASPC at a temperature of 77 + 3°F. All of the shear gage calibrations were performed by HL&A at 30°, 80° and 130°F. The calibration data are summarized in Appendix D for the gages used in Motor No. 1 and in Appendix E for the gages used in Motor No. 2.

Logs of the gage serial numbers, their assigned locations in the motors, and their calibrations are given in Appendices D and E.

Two designs of failure event gages were used on this program. The "Trouser-Leg" design is illustrated in Figure 20 while the "Inverted U" design is given in Figure 21. The Trouser-Leg design was used in Motor No. 1 while the Inverted U was employed in Motor No. 2. In each motor two different materials were used with ten gages of each kind being installed. Technical Wire Products manufactured their event gages using a low modulus, low elongation silicone rubber. ASPC made its gages from a low modulus epoxy filled with silver flake.

The failure gages manufactured by Technical Wire Products were tested in 2-inch cube propellant samples to check out safety requirements and performance characteristics. The test data, Table 8, indicate that under the worst situation, when the failure gages were open circuited or sheared off, and then re-touched to cause sparking the power required to ignite the ANB 3066 propellant was less than three watts in 60 seconds. Therefore, by using a minimum factor of 50:1, or limiting the current flow for maximum power of 0.06 watts by the insertion of current limiting diodes into each circuit, these gages could be safely used. As a redundant safety measure, low current ohm meters were stipulated for all tests where the failure gages were to be monitored.

6. Installation

The normal stress gages and shear gages were installed inside the chamber by feeding the gage leads and stems through the pilot holes, then bonding them in place with an IBT-115 trowelable liner. The air bubbles and excess bonding material were extruded by manual pressure. The failure gages were installed in a similar manner with the exception that they were bonded in place with standard AGC liner material. Fiberglass insulated copper-constantan thermocouples were employed for all of the temperature measurements. To eliminate heat conduction the installed thermocouples were made six inches long inside of the motor and laid down in a spiral pattern along the insulation surface with the junction ending up in its predesignated location.

Due to excessive lengths, the stainless steel leadwires for the gages in the aft head were cut to shorter lengths before attaching them to a case-mounted terminal strip. This required re-tinning the leadwires before soldering them to their assigned terminals. No leadwires were cut off while making the gage installations in Motor No. 2. The excess wire was coiled and bonded to the outside of the motor case using RTV rubber.

7. Routing of External Wiring

All of the leadwires were soldered to terminal strips mounted on the outside surface of the chamber. From that point, wires were routed in four main bundles, at motor angles of 0, 90, 180, and 270 degrees, to four junction boxes mounted on the inside of the forward skirt. After gage hookup was complete, continuity checks and pressure checks were performed to verify proper hookups. All wires on the surface of the motor were then coated with RTV rubber sealant to prevent possible handling damage. The terminal strips were protected with teflon tape and a thick coating of RTV.

TABLE 8

ELECTRICAL IGNITION TESTS OF ELASTOMERIC

FAILURE EVENT GAGES

Narrow Spark Gap Made by Cutting Gages and Causing Sparking:

140 V.A.C. applied - ignition in 1 min.

125 V.D.C. applied - ignition in 20 sec. (50 m.a. current observed during ignition transient)

60 V.D.C. (50 m.a. sporadic current) - ignition in 1 min.

Heating Tests:

2.41 V.D.C. at 1.5 amp applied for 5 min. - no ignition

6.5 V.D.C. at 50 amp applied for 5 min. - no ignition

6 watt soldering iron for 15 min. - no ignition

200 watt soldering gun - ignition in 1 min.

Photographs of the fully instrumented motor are presented in Figure 35 to 37. They show the potted wiring and external terminal strips, Figures 35 and 36, and the four junction boxes under the forward skirt, Figure 37.

8. Bridge Completion Units and Junction Box Design

The bridge completion circuits for the normal stress and shear stress gages employed the customary Wheatstone Bridge design. To standardize bridge completion connections, and to minimize wiring errors and poor solder joints, printed circuit boards were designed and fabricated. The printed circuit designs are shown in Figure 38. They were designed to be horizontally mounted with no socket connections which might become dislodged under some of the more severe loading conditions planned for the motor. The electrical system and the bridge completion circuit designs are more completely described in Appendix F.

The junction boxes were rectangular aluminum boxes with a separate moisture seal cover. Terminal strips were mounted to accept the input leads from the gage and to provide interconnections with the bridge completion network. All the output leads were fastened to separate terminal strips. Identification of the terminal connections in the four junction boxes are given in Appendix F.

9. Calibration Check of Gages in Empty Chamber

After completing the instrumentation of the motor it was necessary to obtain an in-situ calibration of the gages and to verify their performances. This was done at internal pressures 0, 5, 10, and 15 psig. The Motor No. 1 tests were performed at 40° and 70°F, while the tests on Motor No. 2 took place at 30°, 70° and 110°F. The calibration parameters obtained from these tests are summarized in Appendixes D and E with those taken in earlier measurements.

10. Leak Testing of Motor No. 2

Since plans called for this motor to be fired it was necessary to find and repair any detectable leak. To accomplish this the chamber was pressurized with a mixture of nitrogen and freon gases and a leak check conducted. All leaks were repaired by potting with IBT-115 trowelable insulation.

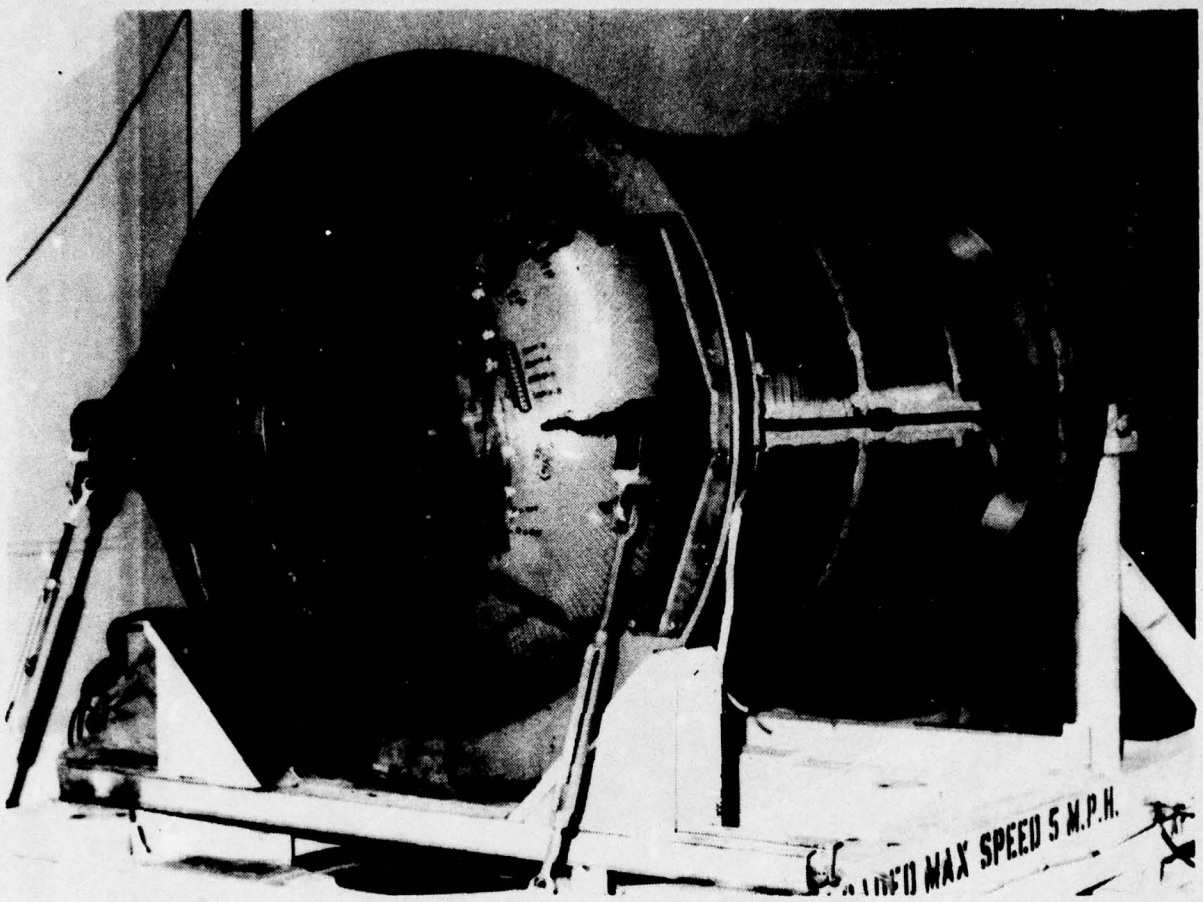

FIGURE 35. FULLY INSTRUMENTED MOTOR SHOWING POTTED WIRING AND TERMINAL STRIPS

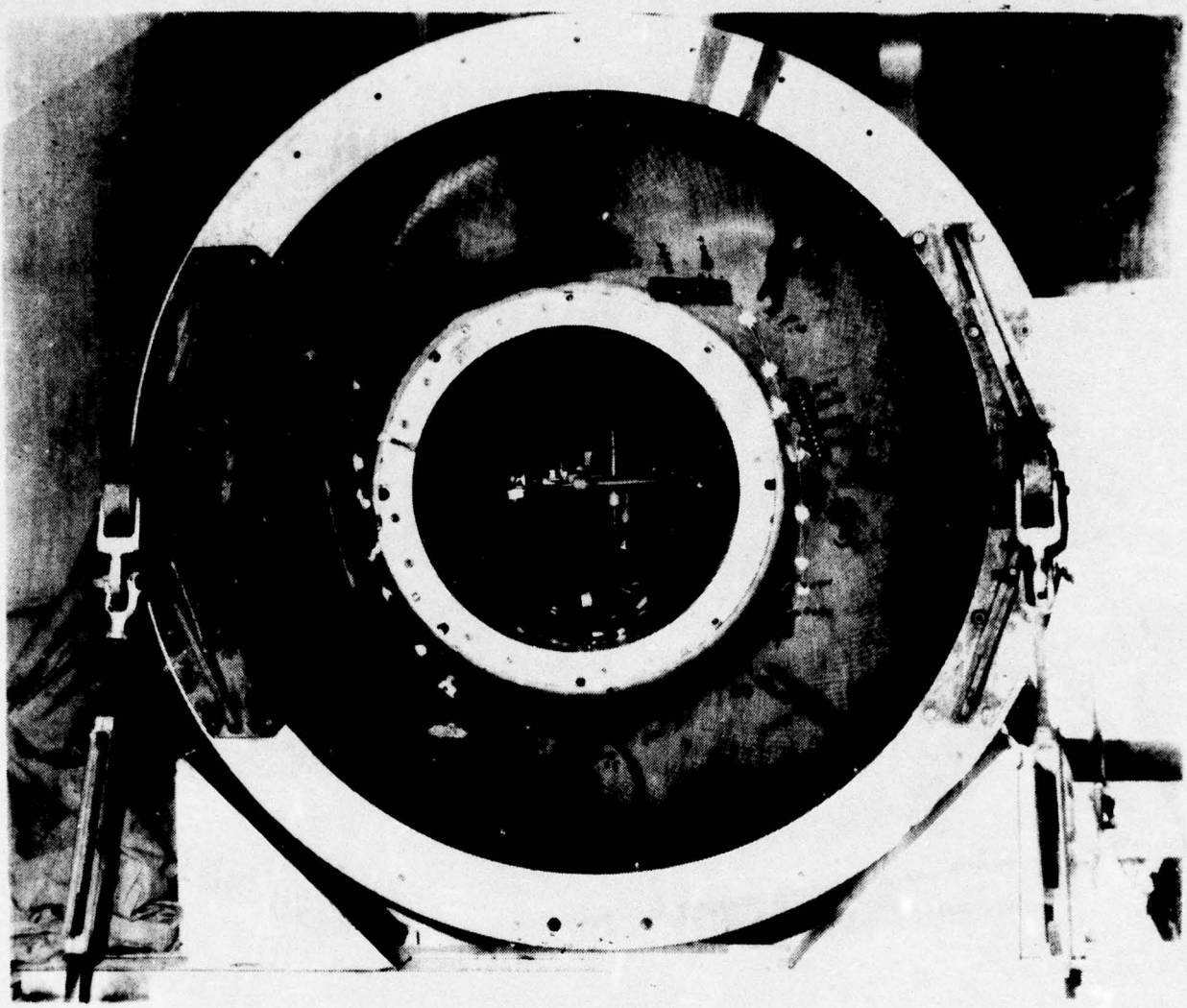

FIGURE 36. FULLY INSTRUMENTED MOTOR SHOWING POTTED WIRING AND TERMINAL STRIPS

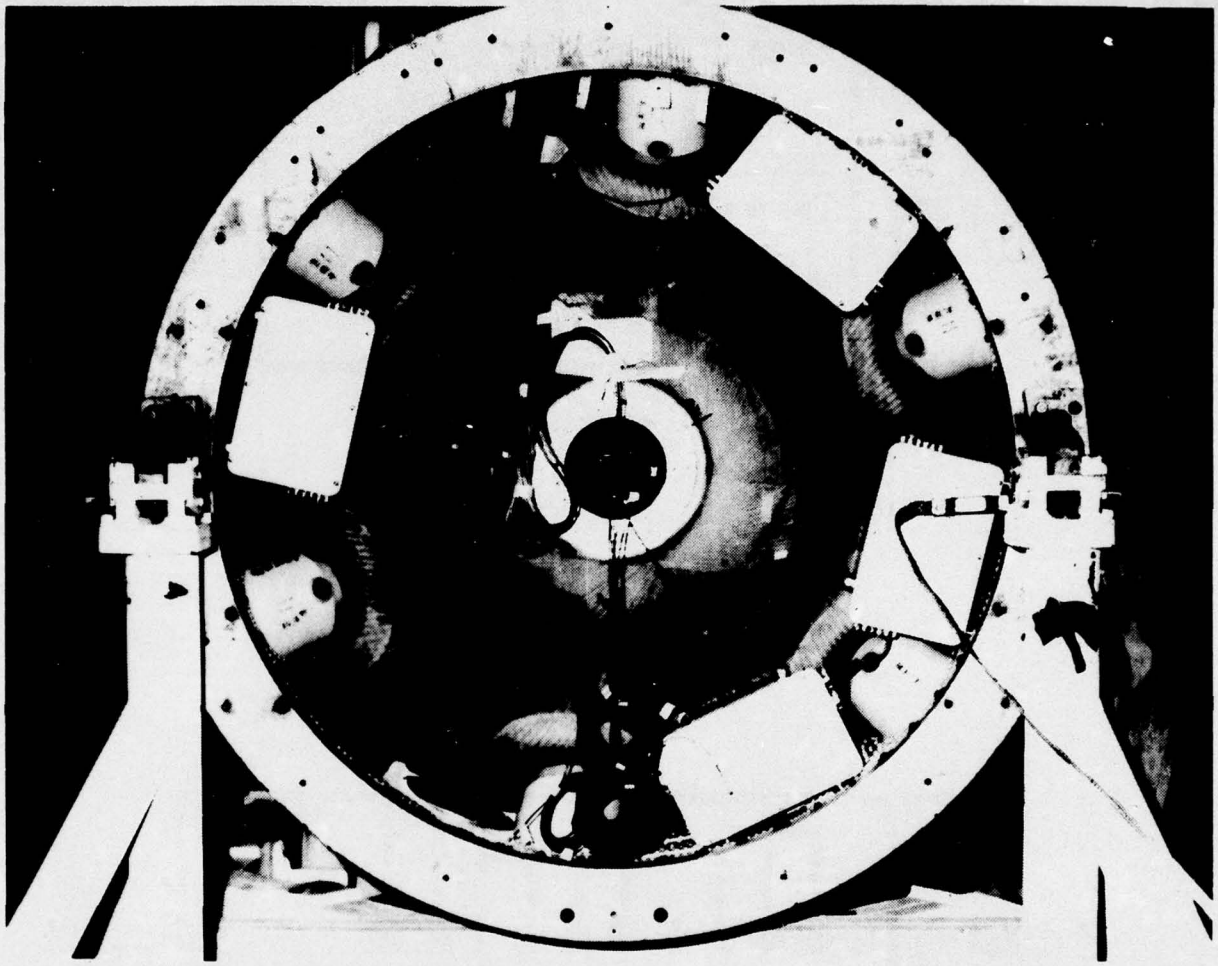

FIGURE 37. JUNCTION BOX LOCATIONS AT FORWARD DOME

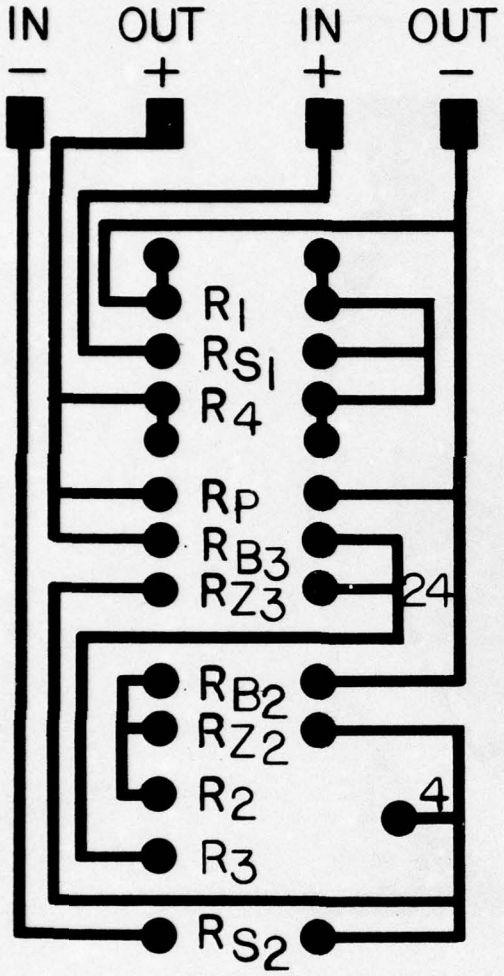

a. Normal Stress Transducers

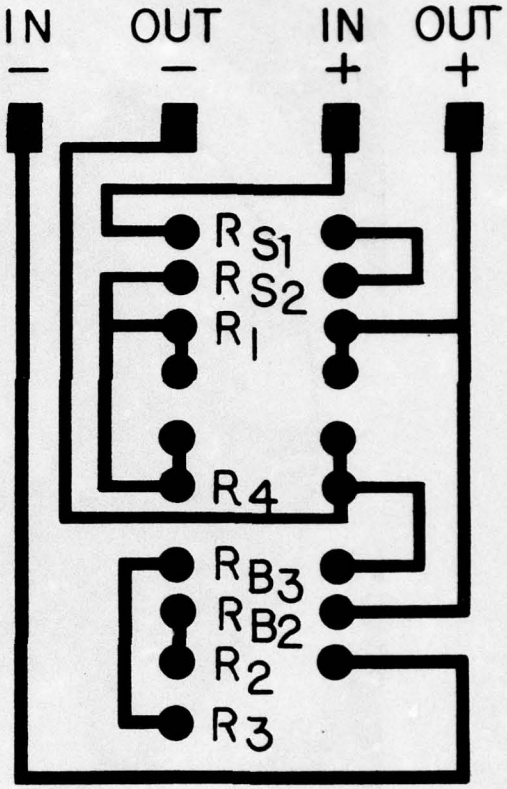

b. Shear Stress Transducer

FIGURE 38. PRINTED CIRCUIT DESIGNS USED IN BRIDGE COMPLETION UNITS

D. DESIGN AND INSTALLATION OF PORTABLE DATA ACQUISITION SYSTEM

1. Design

The data acquisition system for the flexible case static tests consisted of an HP2010 series system which utilized a 2401 Integrating Digital Voltmeter as the digitizing element, along with a 2901A Input Scanner. The 2010 series was characterized by exceptional common mode and superimposed noise rejection, selectable integration line, and built in programming capability. The Dymec 2901A Input Scanner/Programmer scans 25 channels of inputs and programs all functions of associated systems. It was expanded to 50 channels with an auxiliary system which included two banks of switches. System functions and measurement delay were programmed individually for each channel with a built-in pinboard. The maximum scanning rate was 12 channels/second.

The entire system was periodically calibrated by PATO calibration laboratory and all system simulation tests were within specifications.

The analog to digital converter on the 2401 integrating digital voltmeter featured a floated and guarded input, while the output was an average reading with an effective common mode rejection of better than 140 DB at all frequencies including DC. Since they were average readings and were fully guarded, the system greatly reduced superimposed noise and common mode errors. The specifications of the unit are given in Appendix G.

The complete specifications for the components of the DAS also are shown in Appendix G. Basically, this system scans multiple analog input signals, converts them to digital form and visual display and permanently records the resultant measurements. The recording system used was an HP Model 562A Digital Recorder, a solid state electromechanical device which provides a printed record of digital data. Its accuracy is identical to the input device used. The printing rate was five lines/sec. with a column capacity of 11 digits. The system was rated at a DC accuracy of .01% of rdg $\pm$ .005% fs.

2. Trailer Installation

A large van-type utility trailer approximately 30 feet long by 8 feet wide was obtained to house all instrumentation for monitoring and recording all tests in the various phases of the Flexible Case Program. All instrumentation was rack-mounted and included the following: Dymec Scanner and Printer System, nonlinear digital voltmeter, CEC oscillograph, Brown Multipoint Temperature Recorder, and a path and junction panel for parallel monitoring, Figures 39 and 40.

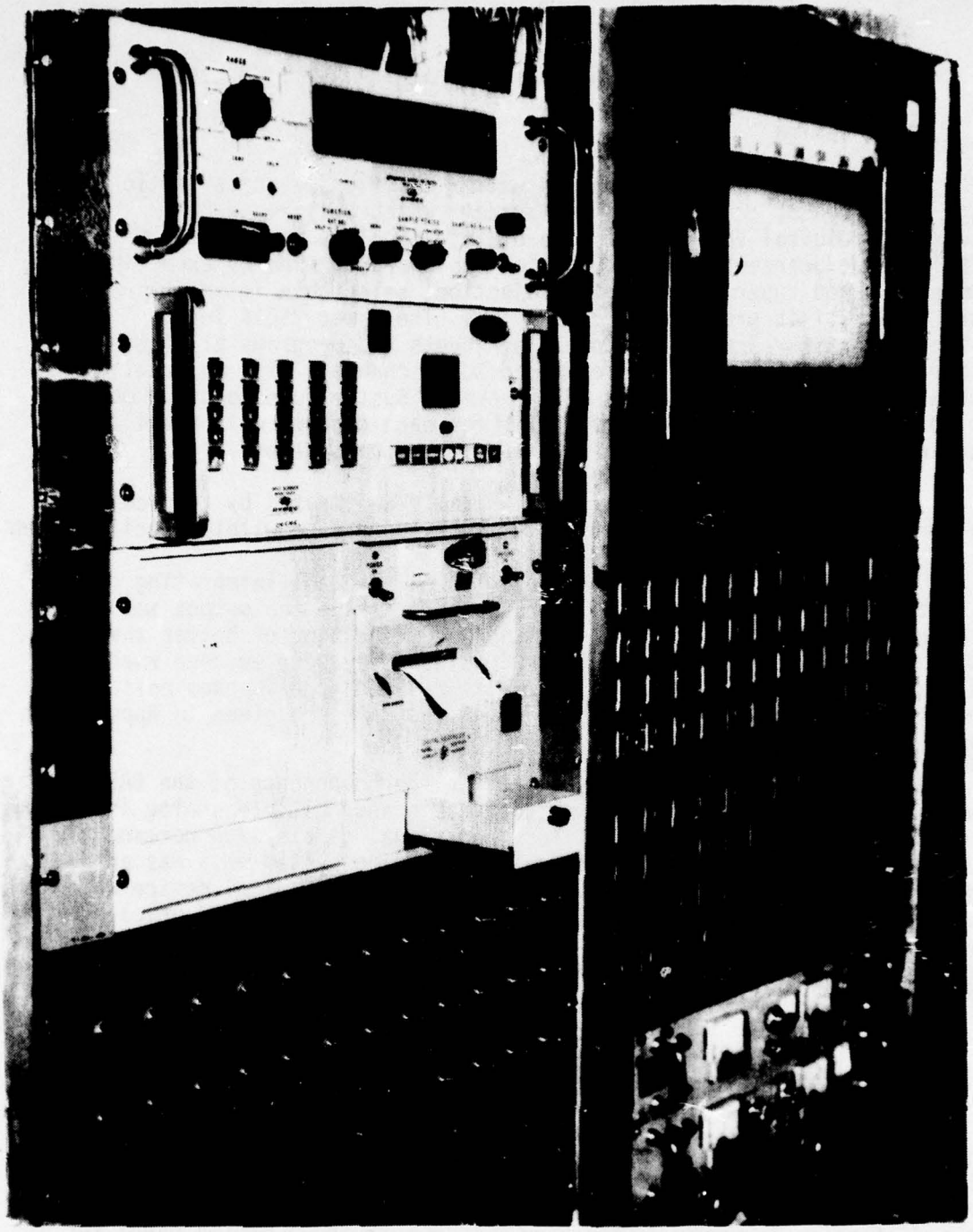

FIGURE 39. DATA ACQUISITION SYSTEM FOR FLEXIBLE CASE/GRAIN INTERACTION PROGRAM

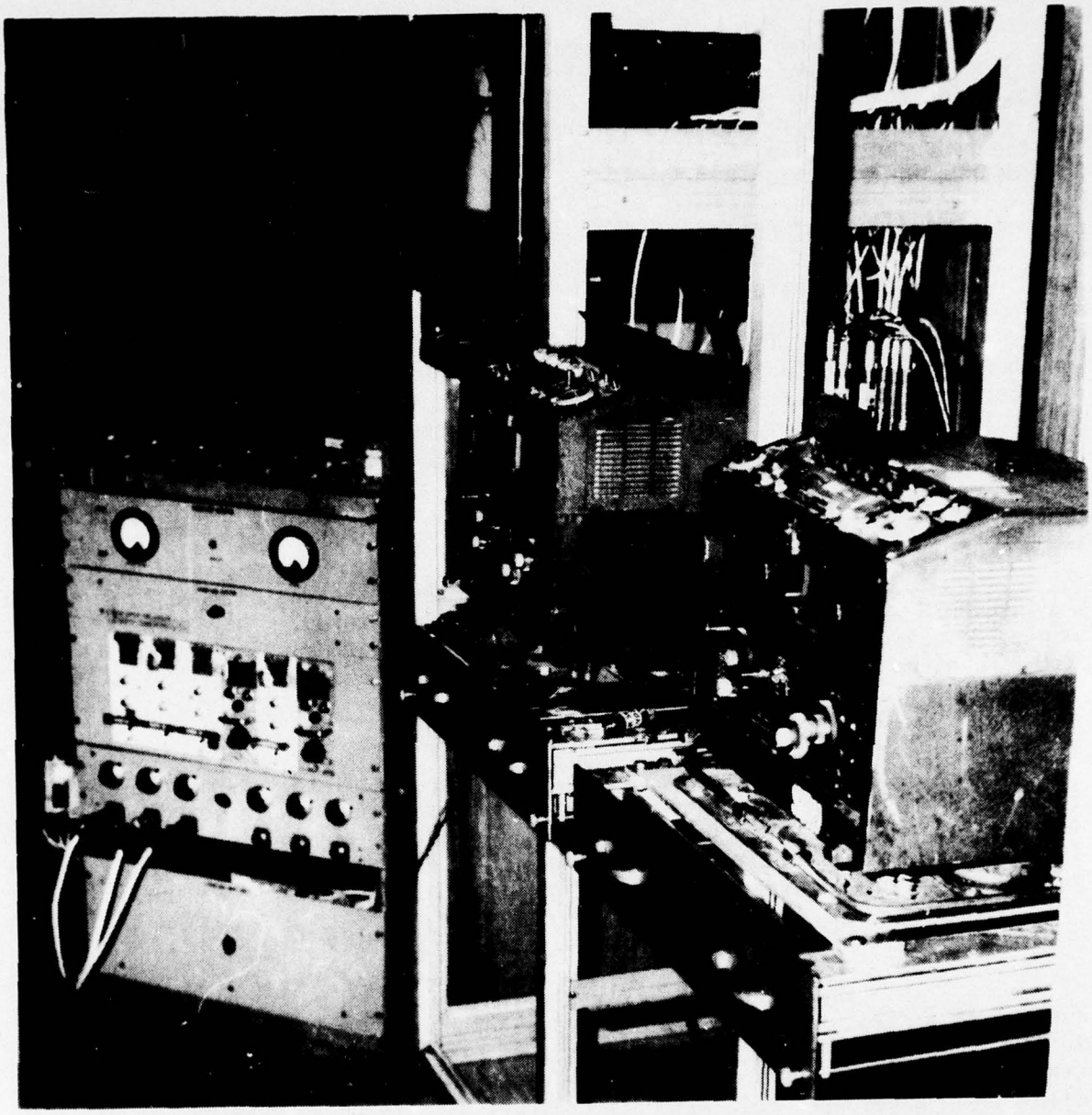

FIGURE 40. DATA ACQUISITION SYSTEM FOR FLEXIBLE CASE/GRAIN INTERACTION PROGRAM

After liner application, but prior to propellant casting, the junction boxes were connected to the recorders in the trailer through 165 foot long cables. After completion of hookup and checkout, the zero stress data prints were recorded on the Dymec Scanner and also on the redundant digital voltmeter. These data are given in Appendix H and discussed in Section 8.

E. MOTOR PROCESSING

1. Grain Casting and Cure

Following installation of the internal instrumentation the chamber was shipped to the manufacturing area for motor processing. The chamber insulation was abraded by hand while the failure event gages were protected by plastic cups. Motor lining and propellant casting and curing followed standard Minuteman III, Stage III procedures. The cure cycle for the propellant required 12 days at 110°F under 15 psig pressure. During the twelve day cure period, grain stresses were monitored on a daily basis. These data are discussed in Section 8.

Upon completion of the cure cycle, the motor was allowed to cool to 80°F while the grain stresses were being monitored. They were monitored again while the casting mandrel was being withdrawn. The test data are given in Appendix H and they are discussed in Section 8.

2. Radiographic Inspection of Cast Grains

After mandrel removal, the motors were completely X-rayed every 15 degrees around the periphery of the motor in accordance with standard specifications (AGC-3488E) for inspection of Minuteman production motors. The radiographic inspection report showed no visible defects in either motor except for the presence of the gages and the thermocouple wiring.

3. Installation of Inner-Bore Transducers

The final step in the preparation of the motor was the installation of clip strain gages to measure displacements in the fins and LVDT's to measure grain inner-bore radial displacements. The procedures were centered on bonding the footpads of the gages to the grain surface. The clip strain gages were held slightly contracted while being located in the fin area, see Figure 41. The footpads were previously coated with IBT-115, which acted as a soft adhesive; so after the gage was released it held itself in place while the adhesive cured.

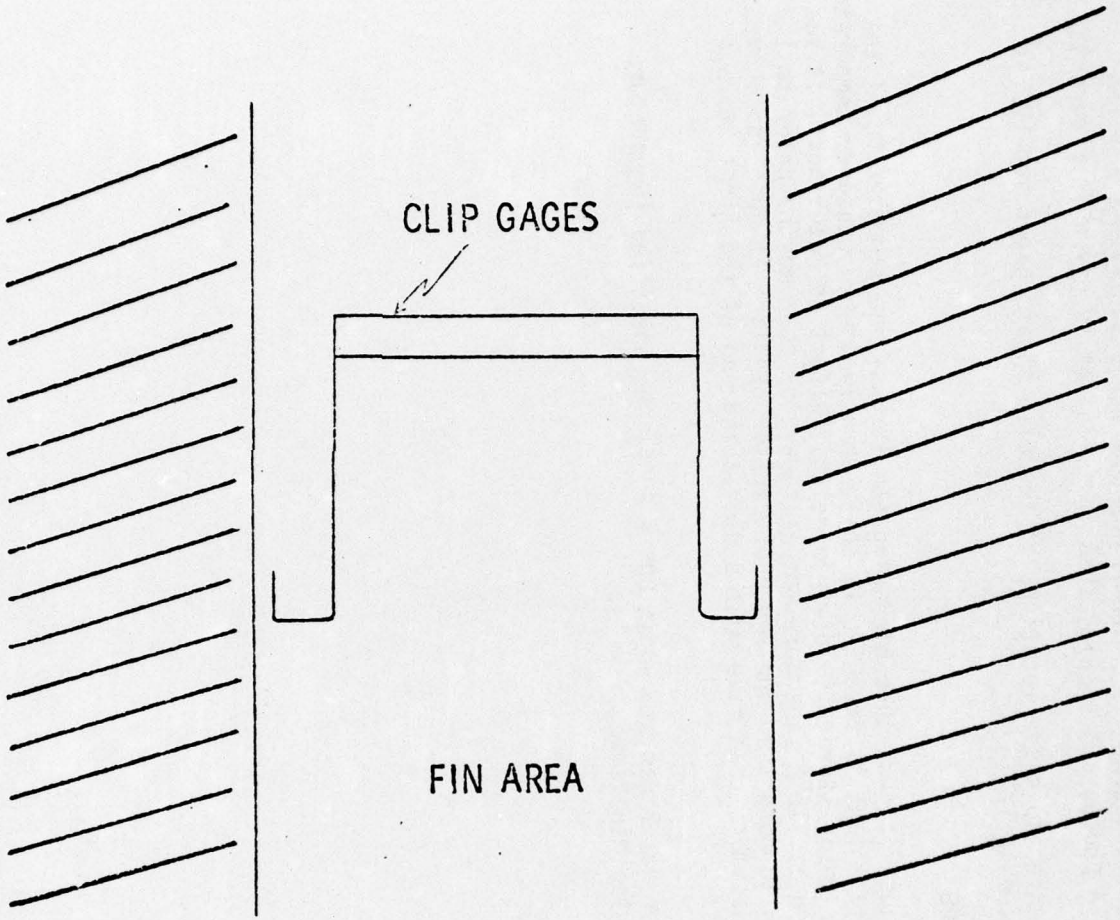

FIGURE 41. MOUNTING PROCEDURE FOR CLIP STRAIN GAGES IN FINS

The LVDT's had swivel footpads that were mounted in place using the IBT-115 adhesive. The transducer was then attached to the footpads. A photograph showing this installation is given in Figure 42.

The specific locations of the clip strain gages and LVDT's are tabulated in Table 9.

F. AGING

Because of post-cure hardening the stress-free temperature of the ANB-3066 propellant is expected to shift greatly toward whatever temperature is used for motor storage. To minimize that effect in Motor No. 1 it had to be stored at 110°F (the cure temperature) for four months prior to the testing. With more than one month of earlier handling at 80°F and above, the motor was more than five months old at the end of the first storage period.

Motor No. 2 was stored at 80° $\pm$ 20°F, the specified temperature limits for the Minuteman missile.

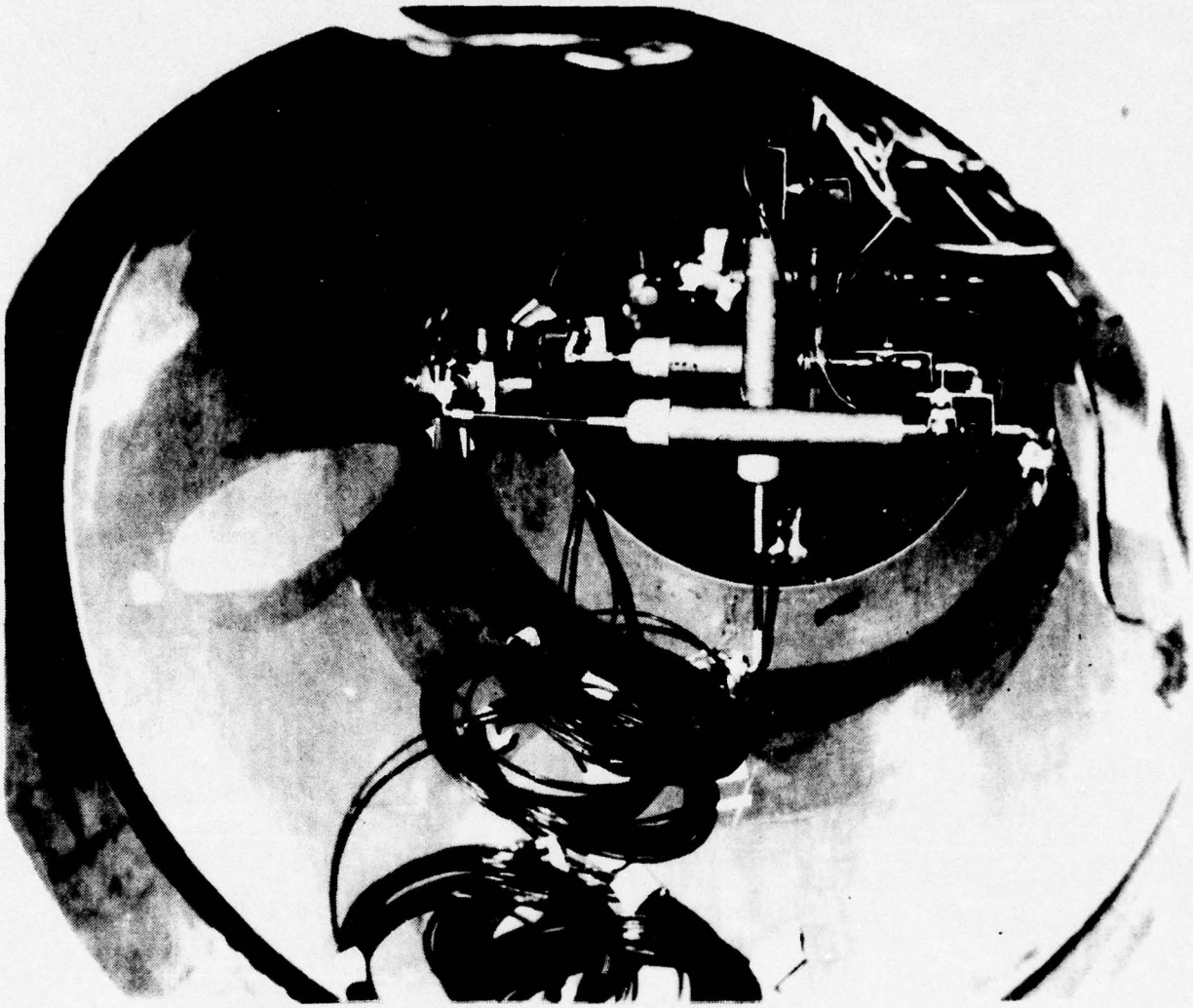

FIGURE 42. LVDT INSTALLATION AT INNER BORE

TABLE 9

LVDT AND CLIP STRAIN GAGE LOCATIONS

		Plane	
LVDT No.	1	90-270	One inch into aft bore
	2	0-180	One inch into aft bore
	3	90-270	One inch into middle bore
	4	0-180	One inch into middle bore
	5	90-270	Two inch from end of middle bore
	6	0-180	Two inch from end of middle bore
	7	90-270	Inside of forward boss
	8	0-80	Inside of forward boss
Clip Gage No.	1	Fin No. 1	1.5 in. forward and 1 in. down
	2	Fin No. 2	1.5 in. forward and 1 in. down
	3	Fin No. 3	1.5 in. forward and 1 in. down

SECTION 8

BASIC PROGRAM TESTING OF FULL-SCALE MOTORS

This section briefly highlights the testing performed on the two full-scale motors and summarizes the test data and ASPC's assessment of them. Motor No. 1 after gage installation, calibration and motor casting was cooled to ambient temperature for mandrel withdrawal. The motor was subsequently placed in a 110°F chamber for four months aging. Periodic readings of the embedded gages were taken during this time.

Simultaneously, the program continued with manufacture and test of the STV's and preparations for casting of motor No. 2. Following the casting, cure and cooldown of Motor No. 2, during which the gages were monitored, attention was transferred back to Motor No. 1 which was scheduled to begin the thermal cycling tests.

Although some problems with the gage data were noted during the 110°F aging of Motor No. 1, they were not considered very severe. However, analysis of the thermal cycling test data disclosed serious shifts in gage outputs and such erratic behavior that HL & A and ASPC requested that the closed envelope approach be discontinued. AFRPL concurred.

A. TESTS CONDUCTED ON MOTOR NO. 1

As planned, Motor No. 1 was subjected to a sequence of loading conditions typical of those encountered by an operational motor from manufacturing through firing. These tests are briefly outlined below.

1. Case Hydrotest

This test was described in Section 7. It was designed to define the static deformation characteristics of the cases, while pressurized with water, at incremental pressure levels of 50 psig up to case acceptance level of approximately 200 psig.

2. Curing Stresses and Deformations

The case deformations and grain stresses were monitored during cure at 110°F with a superimposed pressure of 15 psig.

3. Post-Cure Cooldown and Mandrel Withdrawal

After the 12-day cure cycle at 110°F, the motor was cooled down to 80°F. Then the casting core was withdrawn and the motor removed from the casting bell. The grain stresses and case deformations were monitored during the cooling period and during mandrel withdrawal. The load to remove the core was also monitored in this operation.

4. Aging of Propellant Grain at 110°F

After trimming and radiographic inspection of the grain and pressure calibration of the gages, the motor was placed in storage at 110°F for a period of four months. The stress/strain gages were monitored daily for one week, then monthly to determine: (1) initial thermal changes, and (2) the effects of post-cure hardening on grain stresses.

5. Thermal Cycling

This testing involved storage for 10 days at each of the following temperatures: 80°, 60°, 110°, 80° and 60°F. The grain stresses/ strains, case deformations, and temperatures were monitored at three discrete times in each thermal transient.

6. Handling

The motor was subjected to the conditions typical of motor handling; namely: lifting, tip over and rolling. Case deformations and the grain stress/strain gages were monitored during each of these events.

7. Transportation

Storage-to-transporter and transporter-to-transporter tests were conducted while monitoring the stress/strain and case deformations.

8. Vibration

The live Minuteman Stage III motor was subjected to a series of vibration survey tests conducted in the thrust (Y) and transverse (Z, 90-270°) axes. The resonant frequency response characteristics and mode shapes of the motor and propellant to sinusoidal excitation was monitored in the 10-to-300-cps range. The motor was suspended in a horizontal attitude from an overhead support system during all phases of the vibration testing.

9. Transducer Monitoring Plan

Because of DAS limitations, not all of the gages could be monitored in a given test. So, a plan was devised to monitor those gages that were the most relevant to a given test. Table 10 presents that plan.

B. FULL-SCALE MOTOR NO. 1 DATA REVIEW

Summary logs of the test data for the normal stress transducers have been compiled in Appendix H for the static tests, Appendix I for the vibration tests and Appendix J for the transportation and handling tests. The shear data are not included in this report. Because of the problems previously noted, the data were compiled as raw output voltages from the gages and were not reduced to give apparent stresses. The experimental results from the static tests were reviewed separately from those taken in vibration and transportation and handling.

TABLE 10

MONITORING SCHEDULE FOR THE TESTING OF MOTOR NO. 1

Type of Instrumentation to be Monitored	Channels Required for Transducer	Hydrotest to 200 psig	Channels of Instrumentation								
			Cure Cycle	Post-cure Cool-down	Mandrel With-drawal	50 psig Pressure Check	4 Mos. Aging	Handling Tests	Trans-tation-Tests	Vibra-tion	Thermal Cycle
23 Thermocouples	1	2 (ext)	19	19	10	10	23				23
1 Reference T.C.	1										
3 Circumferential Gages	1	3	3	3	1	3	3	1	1		1
8 Strain Gages	1	8	2	2	1	2	2	1	1		2
3 Clip Gages	1					3					
8 LVDT's	1					8					
14 Shear Gages	1		14	14	14	14	14	14	14	14	14
11 Normal Gages	2		22	22	22	22	22	22	22	11	22
1 3D Gage	8		16	16	16	16	16	16	16	16	16
20 Failure Gages	1					20					
25 Deflection Reeds	1	25									
1 Load Cell Visual	1				1						
2 Pressure Transducers	1	2				1					
1 Common Time Base	1									1	
22 Accelerometers	1									22	
2 Impedance Heads	1									2	
145 Transducers	-	40	76	76	65	99	80	54	54	66	78

1. Static Test Results

Figures 43 and 44 contain plots of the raw voltage output data for transducers N1 to N8 (two bridges each). Where the transducers were wired to respond in a negative electrical direction, the signs of the output voltages were changed to show a positive output change for an increasing compressive stress. This was done to simplify visualization and comparisons of the transducer actions.

The data in Figures 43 and 44 cover the original zero calibrations by Konigsberg, those at ASPC, pressure calibrations of the case-mounted gages, grain cast and cure, post-cure cooldown, mandrel withdrawal, pressure calibration testing in the grain, aging at 110°F, cycling, and the thermal stress values at the time of motor vibration testing. The data begin with the potted gage calibrations made at Konigsberg Instruments prior to shipment to ASPC. These are presented in the form of the "zero load" output at three temperatures, 30, 80, and 130°F. All of the gages showed excellent linearity of response to pressure, and, except for N2-1, they all had less than a 2 mv change in "zero load" response over the temperature span from 30 to 130°F.

On receipt of the gages at ASPC, circuit boards (bridge completion units) containing the required circuitry external to the gage were prepared for each bridge. Because of small differences in these external resistances and circuit components from those used at Konigsberg, the "zero load" values observed were generally somewhat different from those indicated in the manufacturer's calibrations. These small differences are common occurrences and standard procedure in gage usage, and they have no discernable effect on either the pressure sensitivity or the temperature compensation. All of the gages were subjected to vacuum chamber calibrations at ambient temperature. With the exception of an irregularity observed in N2-1, all of the gages showed linear response with the same sensitivities as obtained by Konigsberg in the pressure calibrations. In two instances (N4-2 and N7-1), the circuit resistances were changed to rebalance the bridges nearer to zero output. N7-1 was then recalibrated.

Following the vacuum calibrations, the transducers and their bridge completion units were installed on the chamber. The first test performed on the chamber after this installation was a 15 psig pressurization primarily for checkout of all of the gage circuits and to check the magnitude and direction of the normal gage responses. With the exception of some of the gages on the aft dome, the responses were generally quite linear with sensitivities comparable to those obtained in the "free gage" calibrations. Many of the "zero load" output values were quite different from those obtained during the vacuum calibrations.

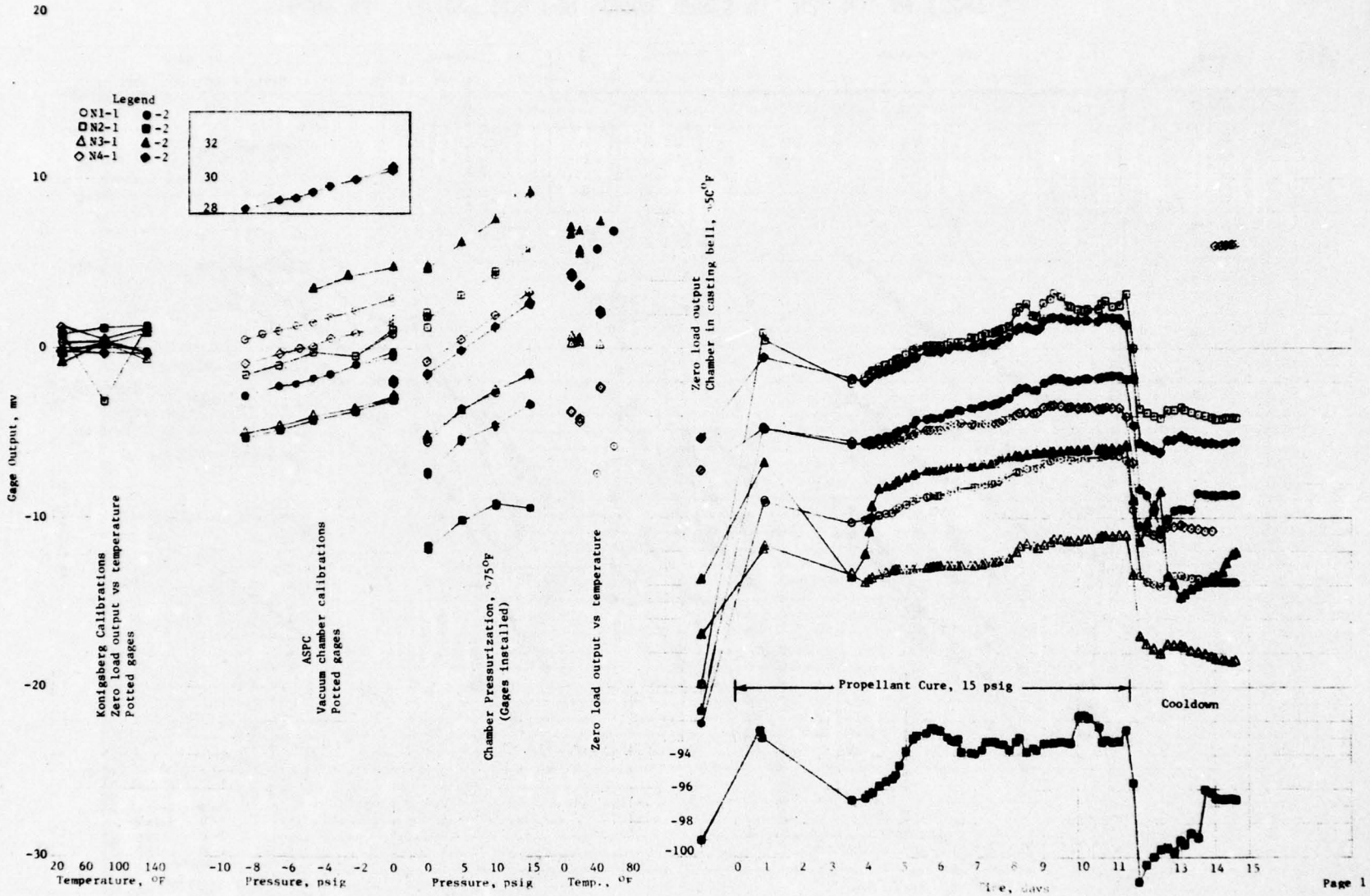

FIGURE 43. OUTPUT LOG FOR NORMAL GAGES N1, N2, N3, N4

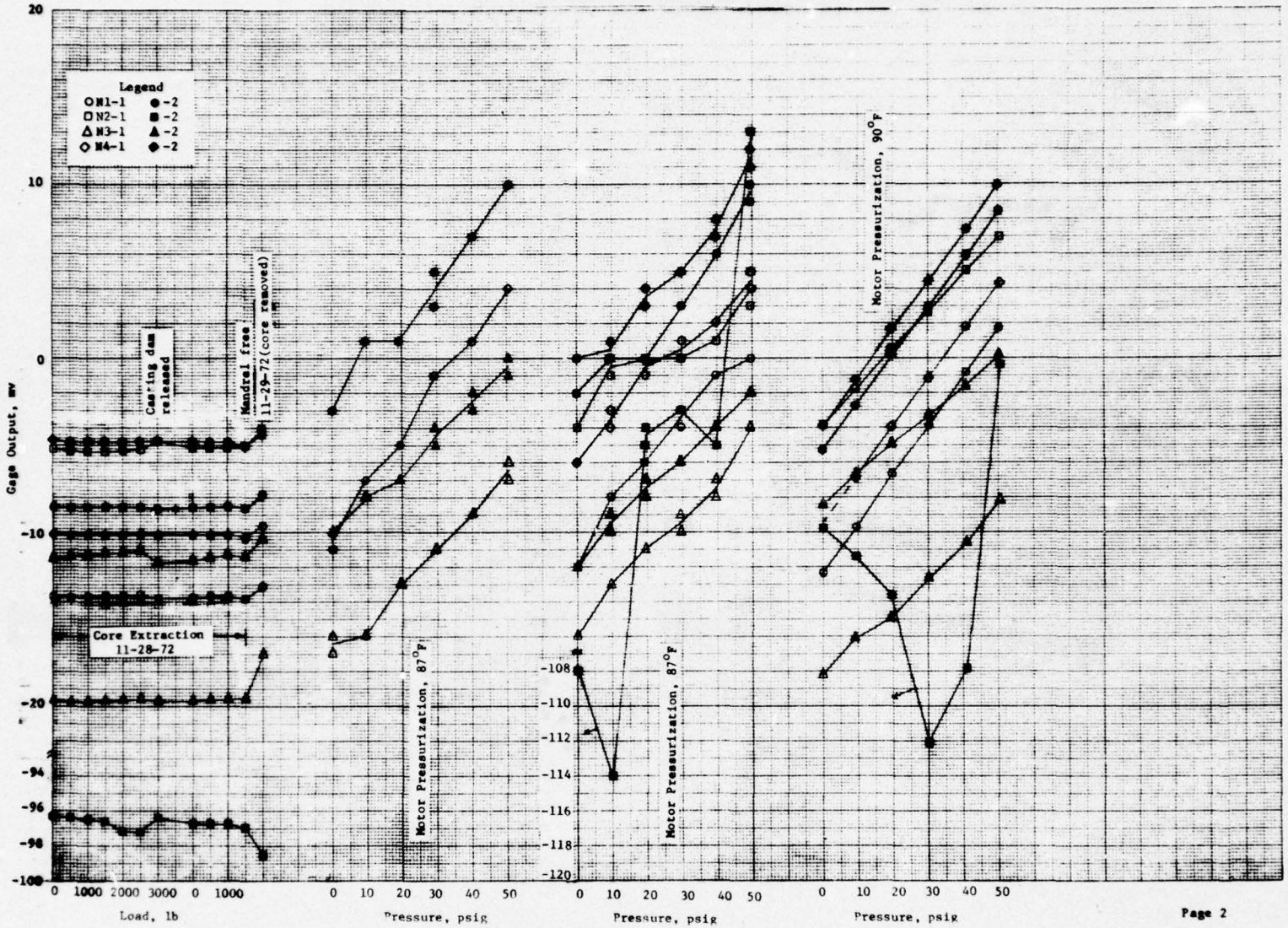

FIGURE 43. OUTPUT LOG FOR NORMAL GAGES N1, N2, N3, N4 (CONT.)

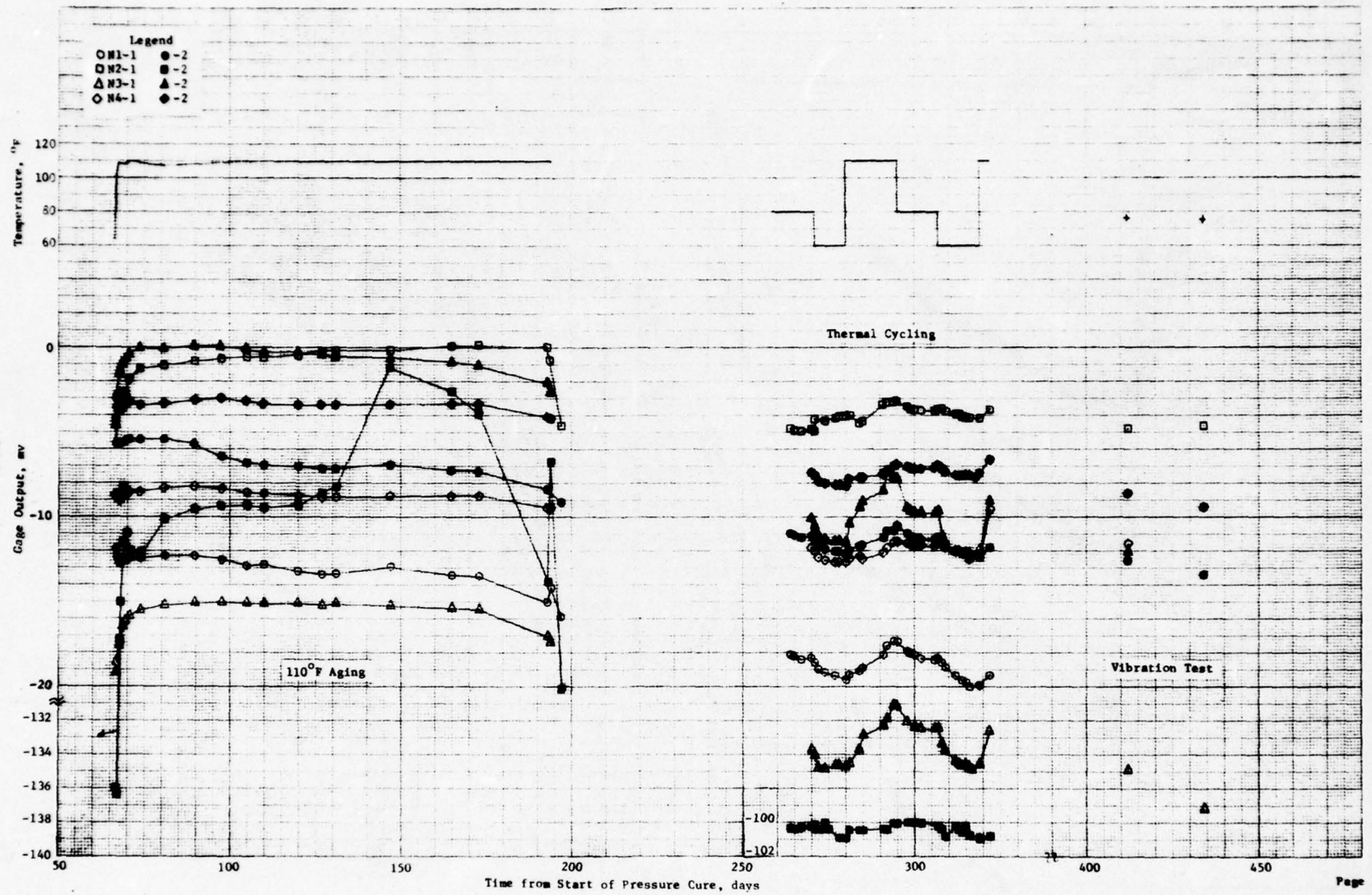

FIGURE 43. OUTPUT LOG FOR NORMAL GAGES N1, N2, N3, N4 (CONT.)

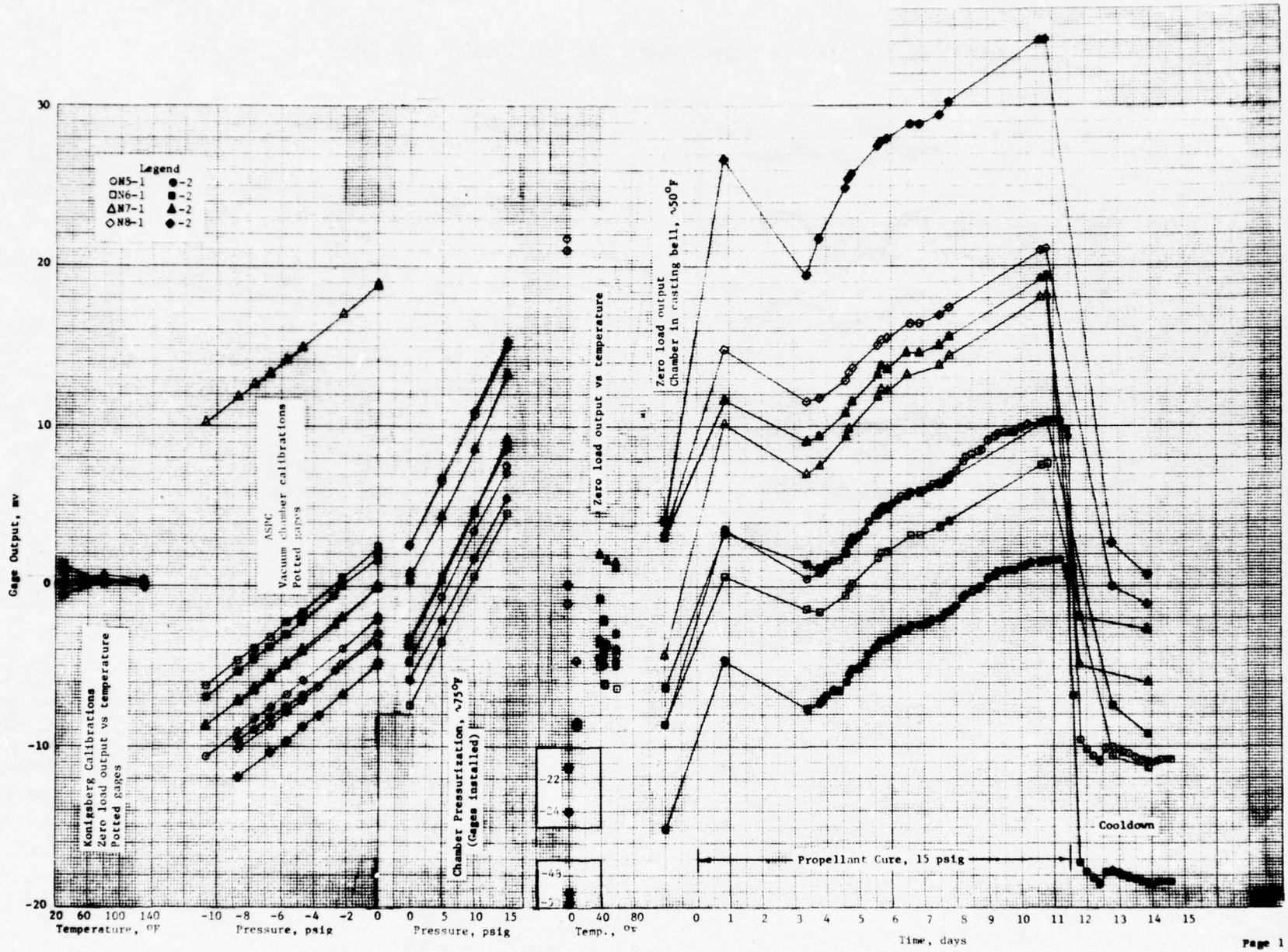

FIGURE 44. OUTPUT LOG FOR NORMAL GAGES N5, N6, N7, N8

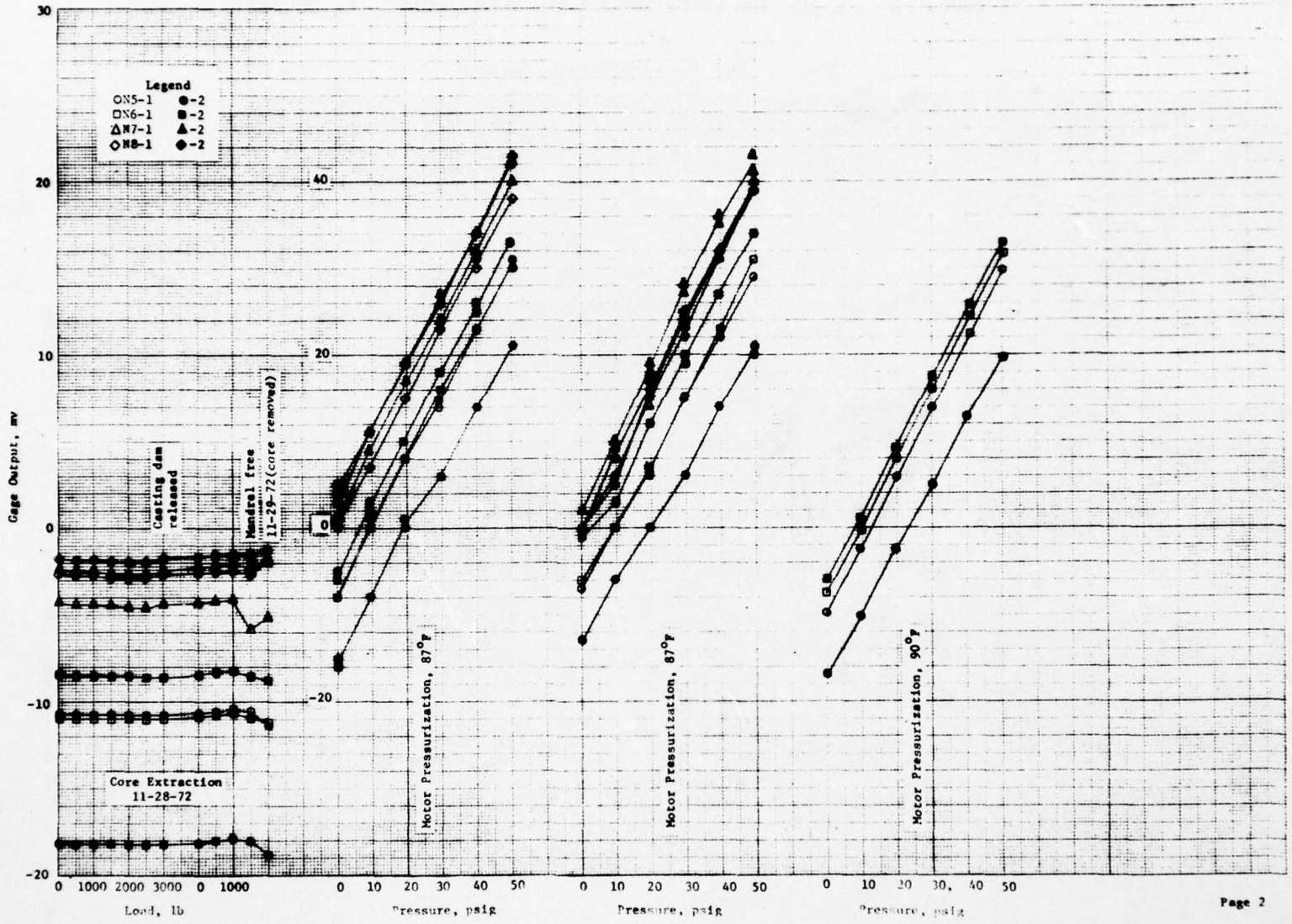

FIGURE 44. OUTPUT LOG FOR NORMAL GAGES N5, N6, N7, N8 (CONT.)

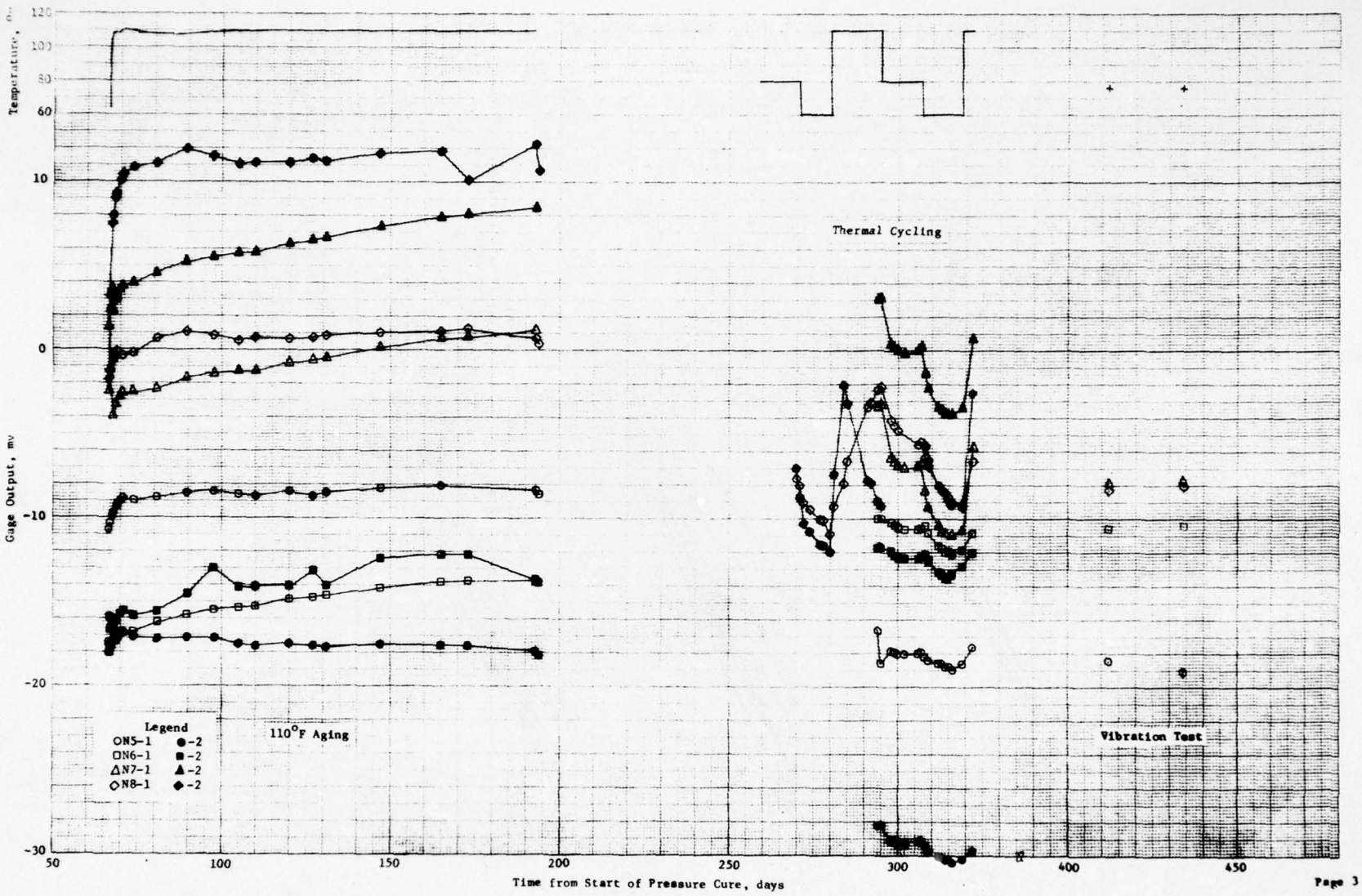

FIGURE 44. OUTPUT LOG FOR NORMAL GAGES N5, N6, N7, N8 (CONT.)

The chamber was next sent to the propellant line for processing. Handling rings were attached to the stub skirts both to maintain the case in a round condition and to provide a means of lifting and handling the loaded motor. The interior surface of the insulation was abraded, and the insulation was dried by flowing heated air (180°F) through the chamber for six days. Liner was applied to the insulation surface, and the chamber was sealed with a humidity cover having a container of desiccant attached to its inside face. The unit was then placed in the casting bell where the liner was partially cured (16-20 hours at 110°F) by circulating heated air around the chamber. In the bell, the chamber was in a vertical attitude resting on the forward handling ring. The bell temperature was lowered to 70-80°F, and the casting tooling was installed. Instrumentation cables were installed to allow remote measurement of the gage outputs, and the next set of measurements was made on 2 November 1972, just prior to the propellant casting. Again, large differences from the previous zero output values were observed. The changes ranged from 2 to 25 mv except for N2-2 which showed a change of almost 90 mv from the original chamber pressurization test. (This transducer continued to be erratic for the remainder of the program).

The propellant was cast on 2 November 1972, and the cure pressure (15 $\pm$ 1 psig) was applied at 1945 hours on that date. The next set of data was taken the afternoon of 3 November 1972. All of the gages responded to the pressure, but the magnitudes varied from somewhat less to considerably greater than the sum of the propellant hydrostatic head and the cure pressure.

Following gelation of the propellant, the behavior of the transducers became much more regular. Except for the exaggerated response of N8-2 to temperature changes and the atypical response of N2-2 to both thermal and pressure loads, the gages generally reacted in the expected direction to applied loadings, and the traces for companion bridges on each gage remain very nearly parallel through the rest of the tests.

Experience with the shear stress transducers was similar to that of the normal stress gages (see Appendix H).

2. Transportation, Handling and Vibration Test Data

The bulk of these test data are reported in Appendices I and J. Only limited data are presented here to show typical results.

In a later discussion it is pointed out that most of the gage responses to pressure, or stress, differentials generally remained fair, although erratic behaviors occurred in some tests. This seems to be the case for the handling tests. Figures 45 and 46 present plots of data from three normal and four shear stress transducers during a roll test on the motor. Here, the motor is rolled about its longitudinal axis while the transducers were being monitored. The data were reduced as the stress change observed during the test. The results given in Figures 45 and 46 are consistent with those predicted analytically for this motor, Appendix P.

Some vibration test results are given in Figures 47 and 48. The differential stress results appear to be reasonable for the conditions considered, but the dynamic analyses are not sufficient for a proper assessment of them.

C. FULL-SCALE MOTOR NO. 2 DATA REVEW

A summary log of the test measurements made on this motor is given in Appendix K. Only limited data are presented here to show testing trends. The same kind of shift in the zero-load output occurred on taking the motor from the laboratory to the casting bell and attaching the transducers to the portable DAS (see Appendix K).

In general, however, the measurements on this motor seem to be more reproducible and consistent than those obtained from Motor No. 1. This is attributed to the use of improved motor instrumentation techniques learned from the work on Motor No. 1.

Figures 49 and 50 provide data plots for the casting, pressure cure (15 psig), depressurization and cooldown of Motor No. 2. The data from the gages seem to track each other quite well.

The primary problem appears to have been the initial zero-load output shift before grain casting. This effect shows up in the data when reduced to the apparent grain stresses, Figures 51 and 52. These reduced data show a zero-load output shift, in that:

(1) The loads range to impossibly high values of the tensile stresses.

(2) The data, after an initial adjustment step, seem to track together reasonably well, showing general consistency of the measurements.

(3) The two half-bridge circuits on the same gage do not give the same results.

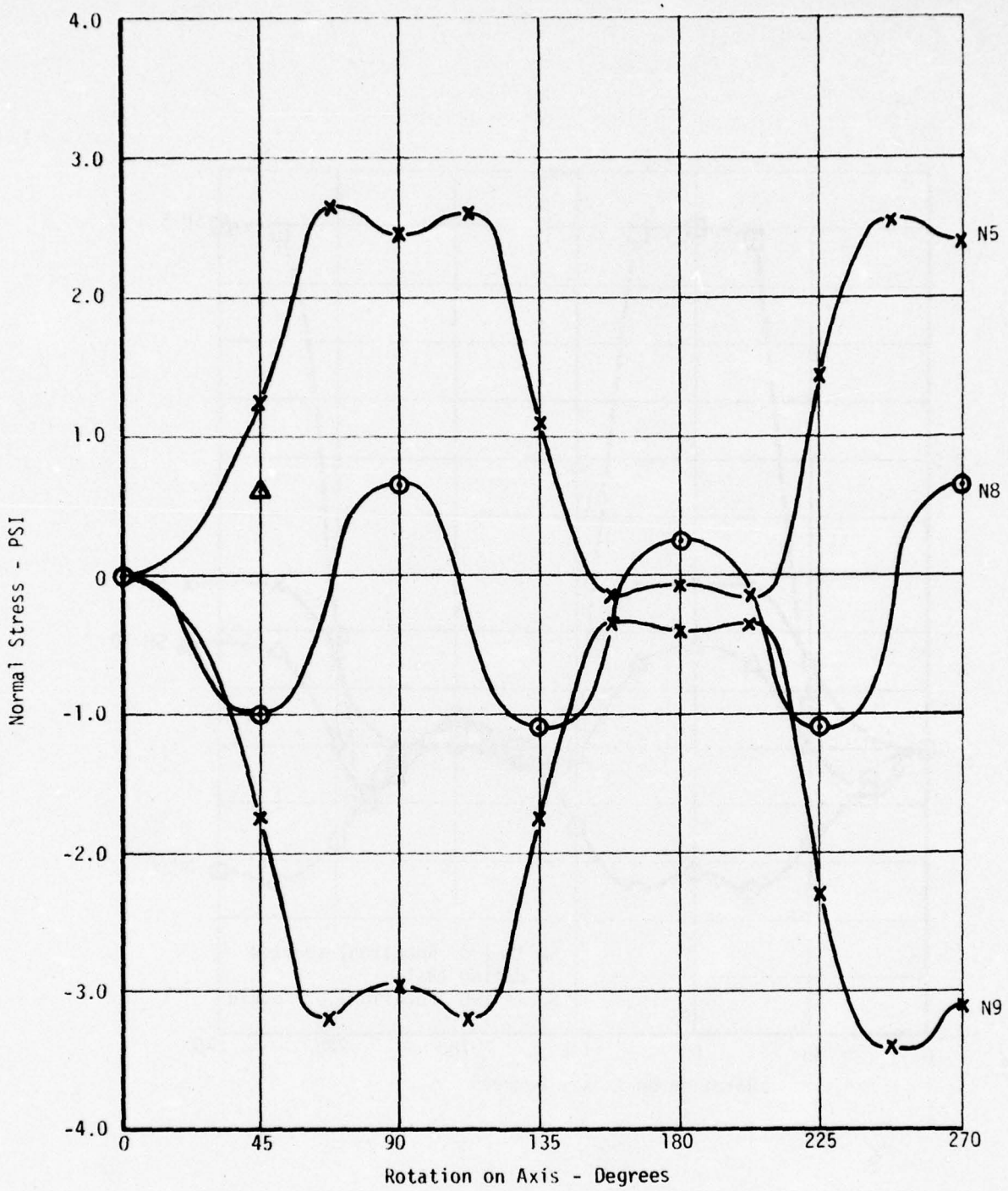

FIGURE 45. NORMAL GAGE RESPONSE TO ROLL TESTS

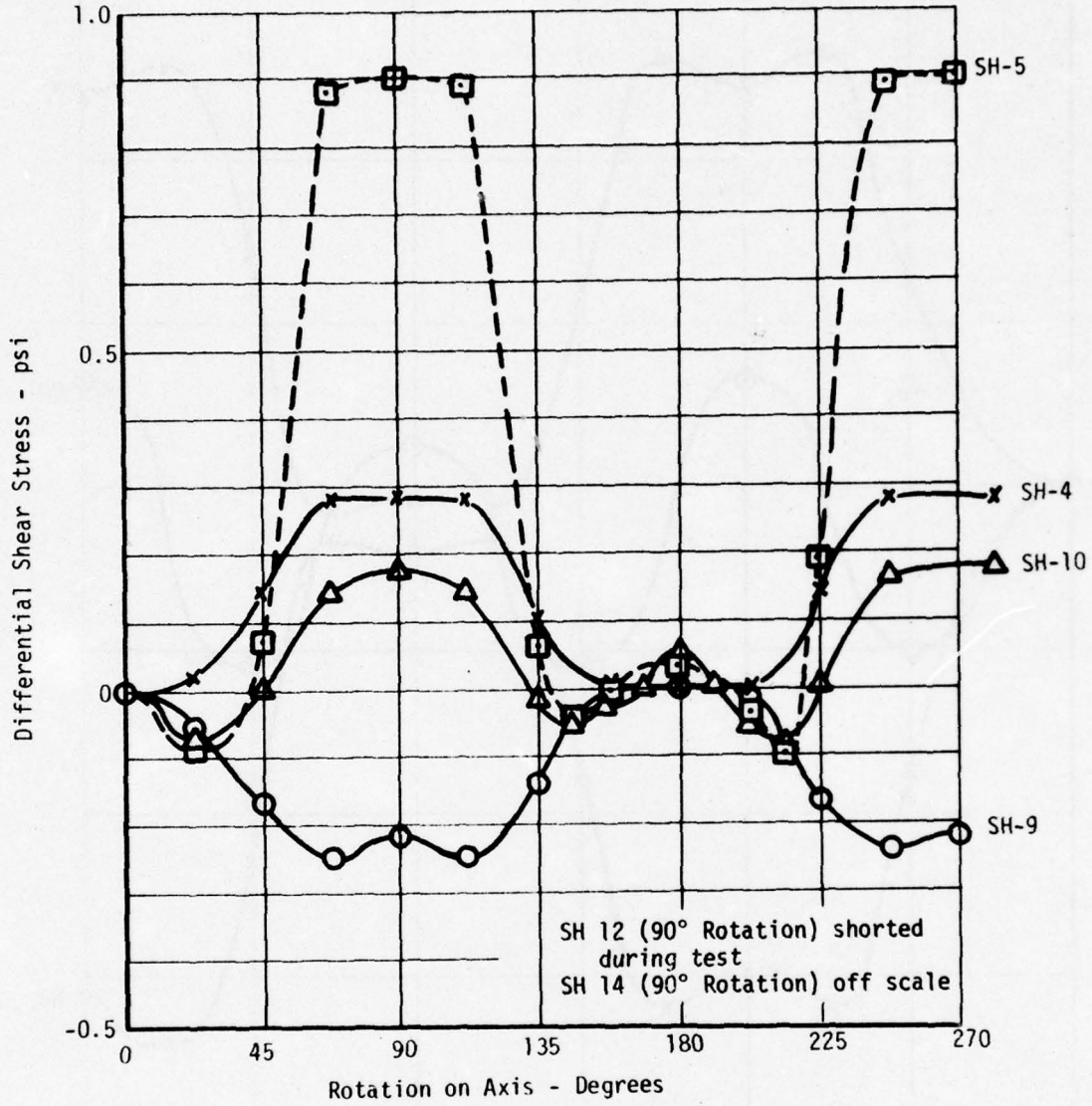

FIGURE 46. SHEAR GAGE RESPONSE TO ROLL TESTS

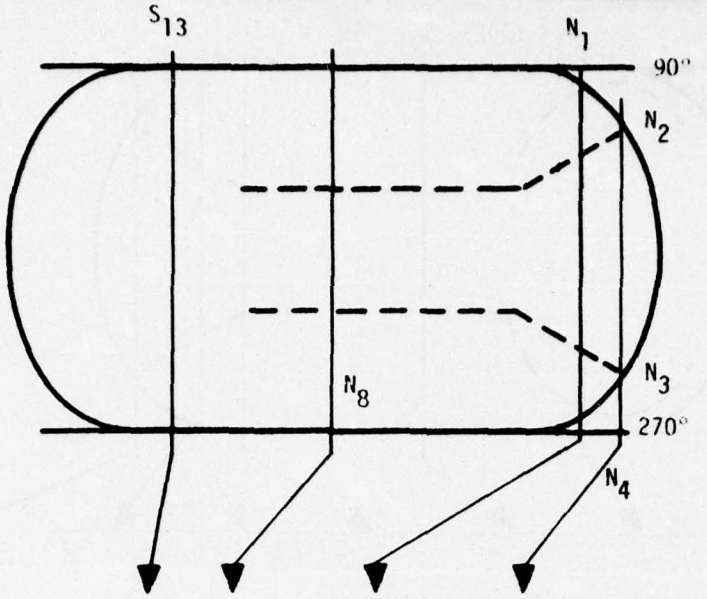

Run	g's	Hz	SH-13	N-8	-1	-4	-2	-3	
020	± 1.0	45.7	3.0 psi	1.0	0.7	Noisy	1.1	Noisy	All other normal gages were out of plane of vibration and had less than 1.0 psi
032	± 2.0	44.6	4.7	3.2	1.4	4.8	2.9	Noisy	

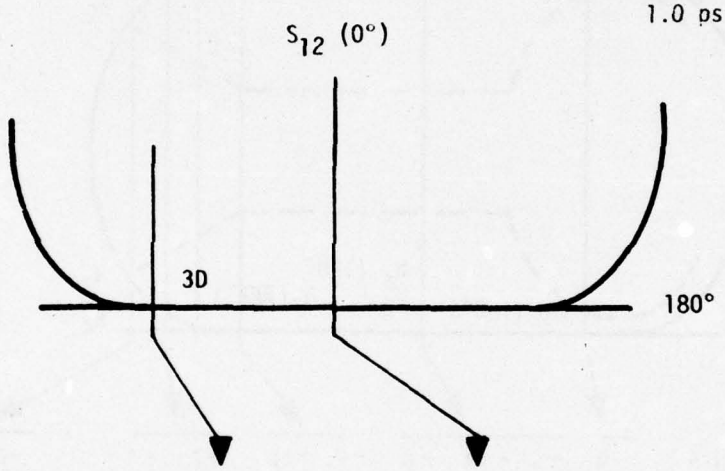

			3D Gage			Shear Gage	
Run	g's	Hz	T_{rz}	T_{zo}	T_{RO}	S-12 90° Rotation	
020	±1.0	45.7	1.4 psi	0.1	3.0	1.0	All other shear gages had less than 1.0 psi output
032	±2.0	44.6	2.2	0.1	5.0	2.0	

FIGURE 47. DIFFERENTIAL STRESS DATA FROM VIBRATION TEST OF FULL SCALE MOTOR #1 IN THE TRANSVERSE MODE

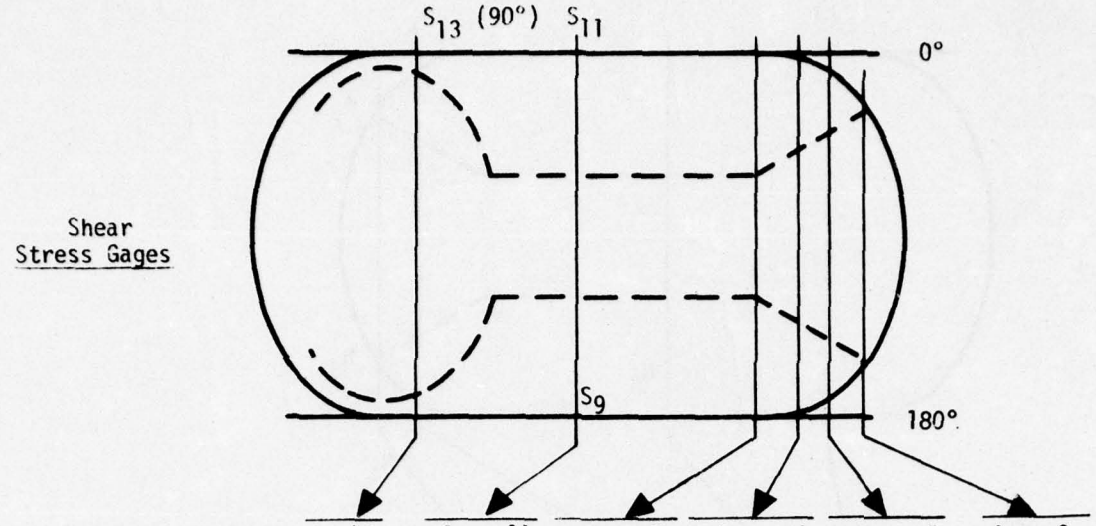

Shear Stress Gages

Run	g's	Hz	S11-13	-9	-11	-1	-5	-2	-6	-3	-7	-4	-8
05	± 1.0	44.4	3.9 psi	1.2	2.4	1.6	0.8		1.5	1.3	1.0	1.1	0.7
09	± 1.5	44.4	5.6	3.6	3.7	2.2	1.1		2.2	1.9	1.5	1.8	1.0

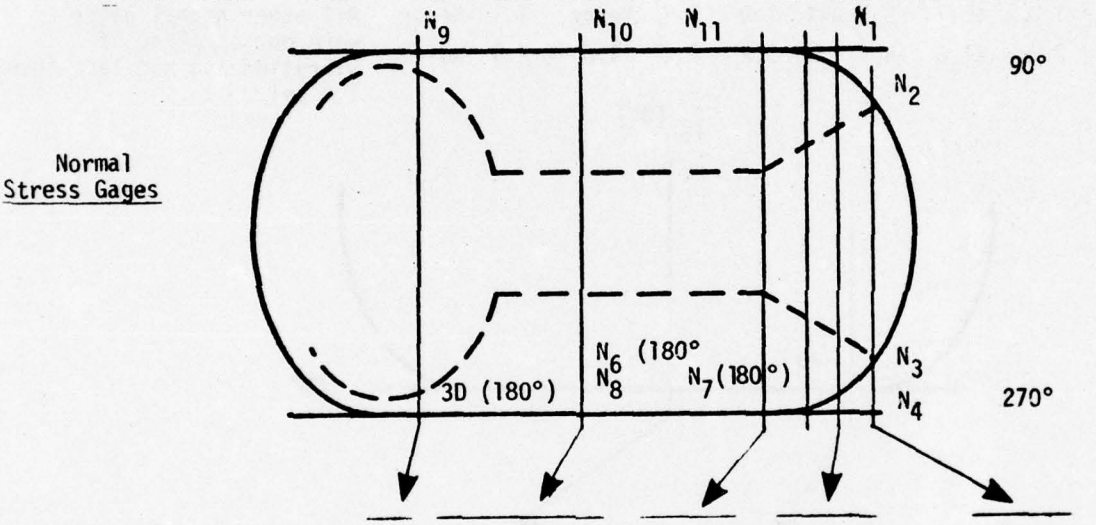

Normal Stress Gages

Run	g's	Hz	N-5	-9	-6	-10	-8	-7	-11	-1	-4	-2	-3
05	± 1.0	44.4	1.0 psi	0.7	1.6	1.0	1.2	4.9	2.2	4.2	4.1	5.1 psi	7.0
09	± 1.5		1.2	1.3	2.7	2.0	1.8	7.4	3.4	6.1	5.9	7.6	7.9

3D Gage

			T_{rz}	$T_{r\theta}$	$T_{z\theta}$
05	1.0	44.4	2.0 psi	0.1	3.9
09	1.5	44.4	3.1	0.1	5.7

FIGURE 48. DIFFERENTIAL STRESS DATA FROM VIBRATION OF FULL SCALE MOTOR #1 IN THE AXIAL MODE

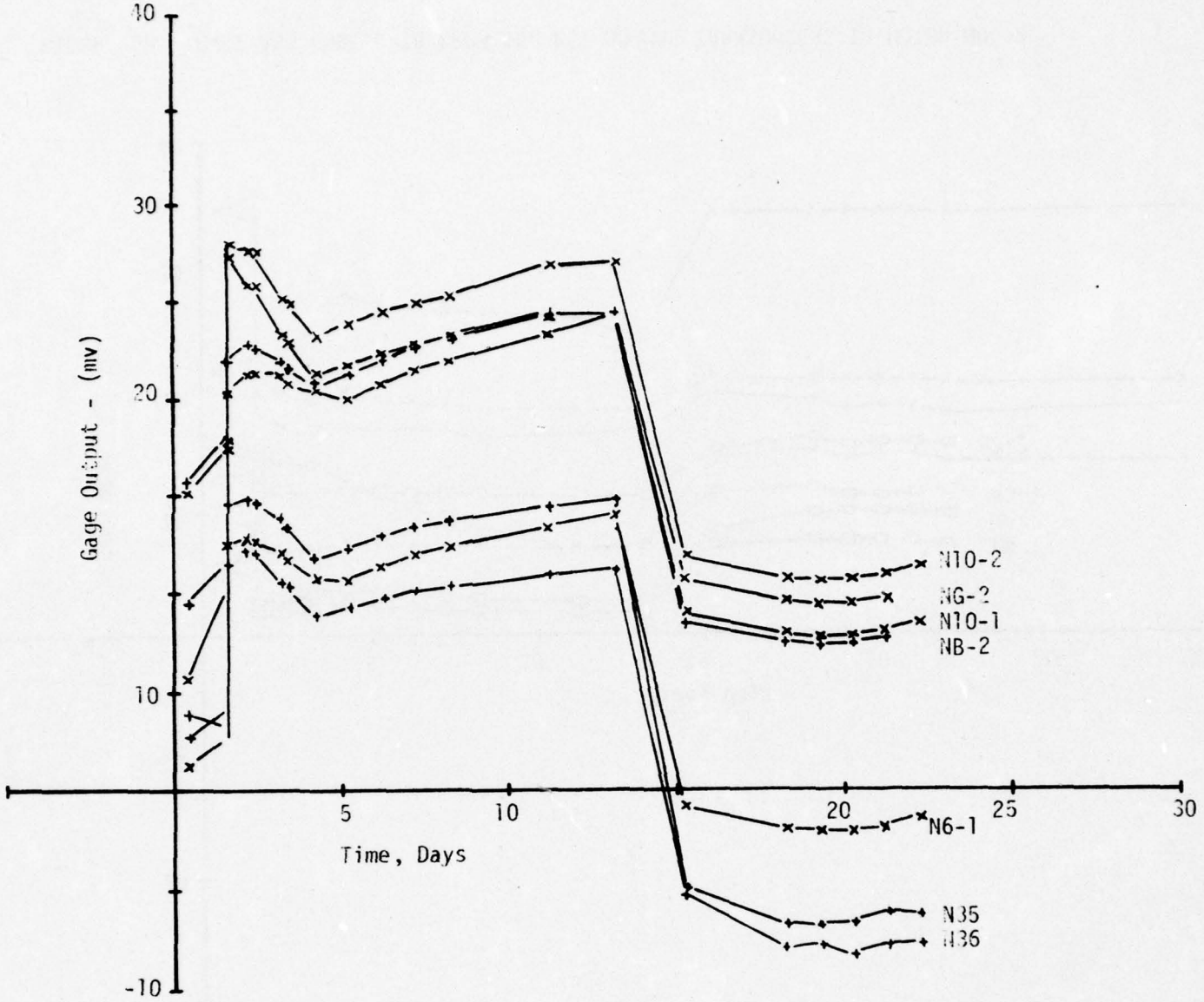

FIGURE 49. CAST AND CURE DATA FROM 150 PSI TRANSDUCERS IN MOTOR NO. 2

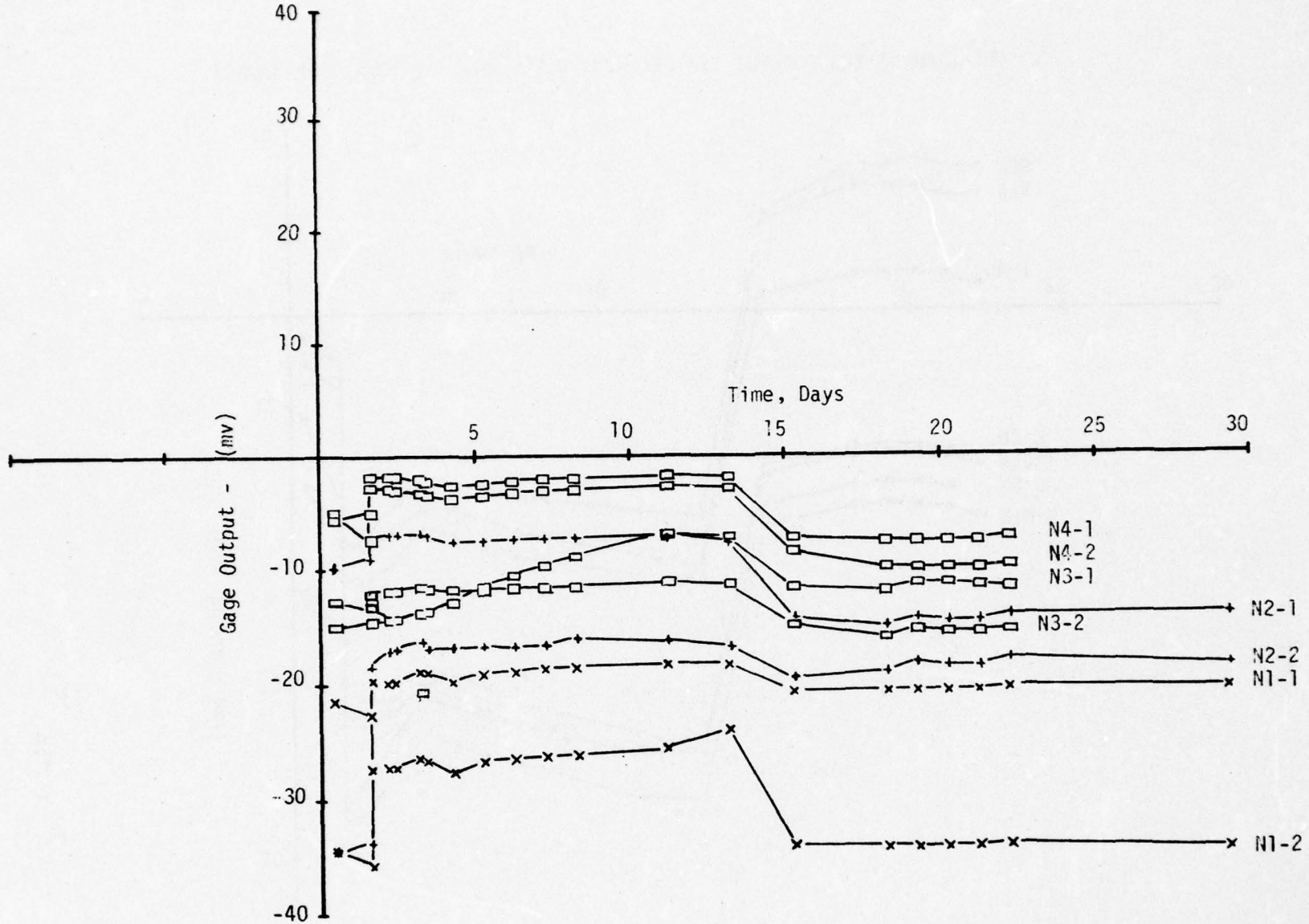

FIGURE 50. CAST AND CURE DATA FROM 450 PSI NORMAL TRANSDUCERS IN MOTOR NO. 2

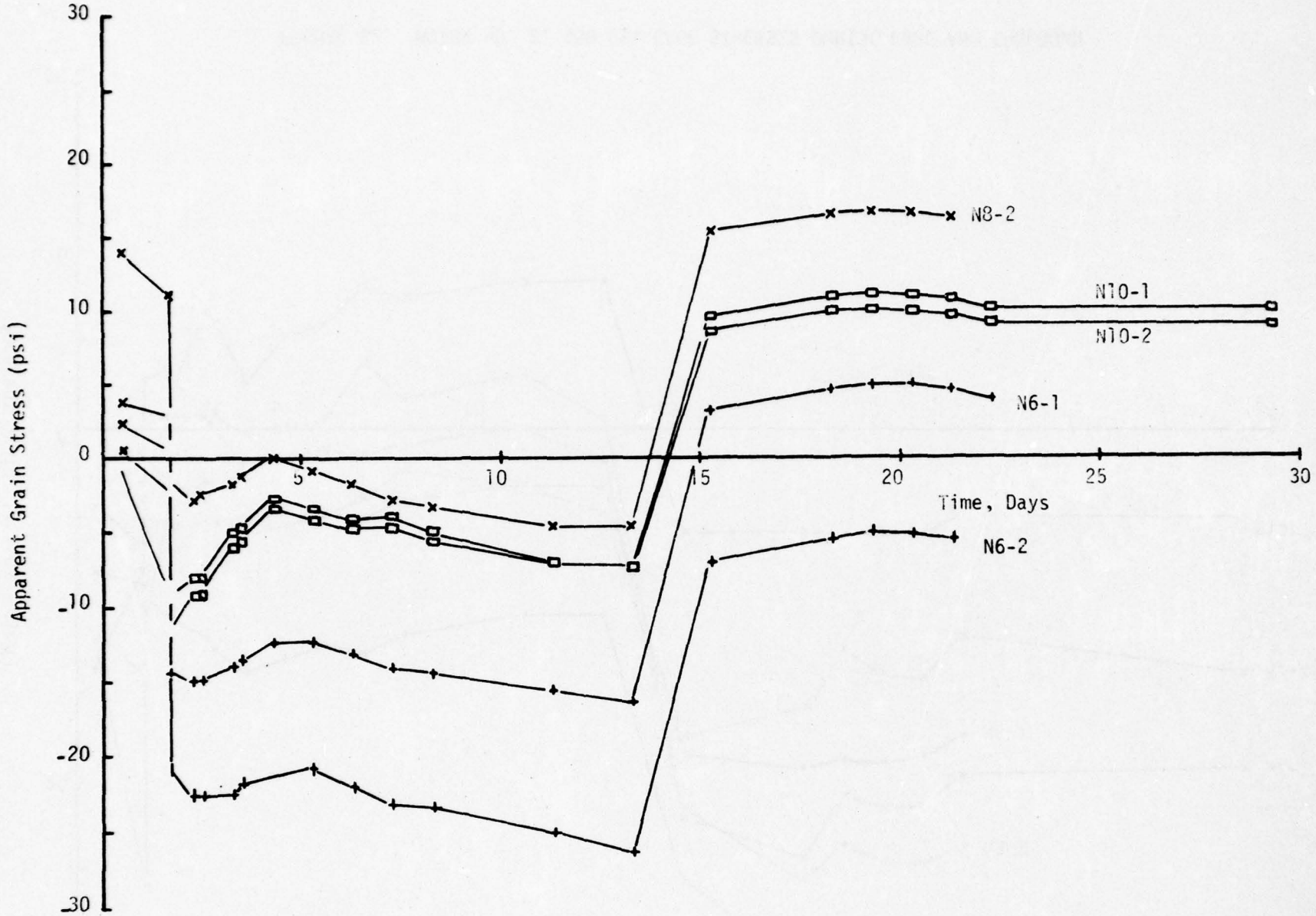

FIGURE 51. MOTOR NO. 2, 150 PSI GAGE STRESSES DURING CURE AND COOLDOWN

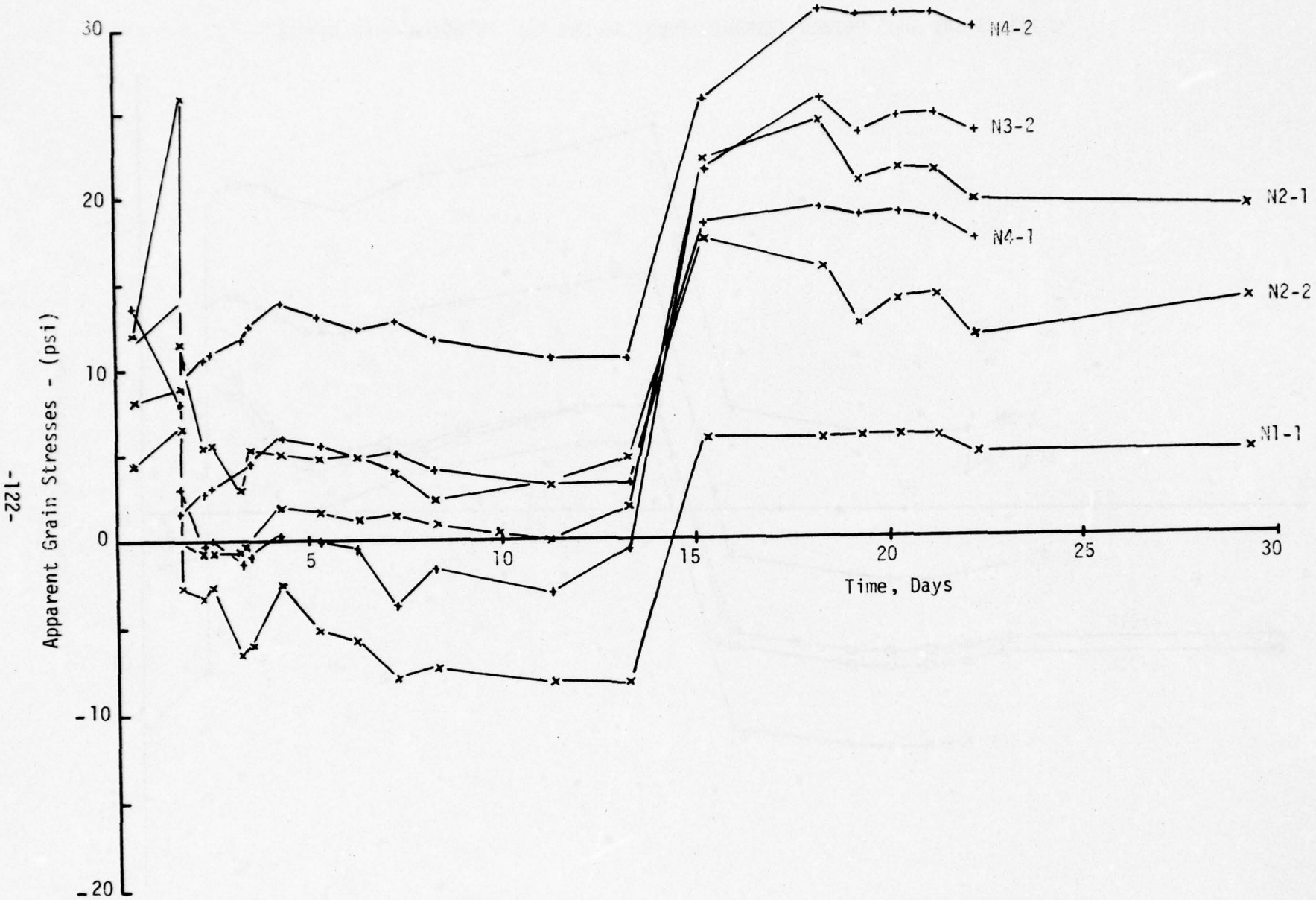

FIGURE 52. MOTOR NO. 2, 450 PSI GAGE STRESSES DURING CURE AND COOLDOWN

D. DATA ANALYSES SHOWING NEED FOR CLOSE ASSESSMENTS

Many factors were involved in revising the program at this point; including questions of the relative accuracy of the gages at expected levels of the measured stresses. But, it is sufficient at this point to show that the two basic calibration parameters of the normal stress transducers were behaving erratically.

The two gage calibration parameters are the sensitivity, b, and the zero load output of the gage, a. Thus, for a stress, σ, applied to the transducer the output voltage, v, is given by

$$v = a + b\sigma \tag{1}$$

The value of b is readily determined from the slope

$$b = \frac{dv}{d\sigma} \tag{2}$$

It will be seen in Section 11 that the stress at the gage is not equal to the pressure applied at the inner-bore of a grain. But, our purposes are satisfied by the approximation

$$b' \approx \frac{dv}{dP_a} \tag{3}$$

where P_a is the pressure at the grain inner-bore

1. Effect of Age on Gage Sensitivity

Table 11 was prepared to show the marked changes observed in the transducer sensitivity measurements over the test program. For reference purposes, also included are the calibrations taken at Konigsberg Instruments, Inc., under vacuum at ASPC, and when mounted in the empty chamber.

The revised program began in June 1974. At that time, more gages had changed to the point that they were no longer considered usable. These are distinguished by the term "Bad" in Table 11. Ten normal stress transducer circuits and four shear stress transducer circuits were considered unacceptable during the 60 $\pm$ 5°F pressure calibration as compared with 6 normal stress transducers during the pressure calibration at 87°F.

TABLE 11

HISTORY OF GAGE SENSITIVITY CALIBRATIONS, MV/PSI

	N1		N2		N3		N4		N5		N6	
	-1	-2	-1	-2	-1	-2	-1	-2	-1	-2	-1	-2
Konigsberg (In Air)												
30°F	0.274	0.268	0.273	0.268	0.270	0.267	0.270	0.274	0.813	0.811	0.808	0.805
80°F	0.275	0,270	0.275	0.269	0.272	0.270	0.273	0.272	0.818	0.813	0.812	0.806
130°F	0.277	0.273	0.276	0.270	0.274	0.270	0.271	0.270	0.822	0.818	0.813	0.810
ASPC (In Vacuum)												
77°F	0.282	0.285	0.274	0.270	0.249	0.277	0.289	0.278	0.808	0.139	0.805	0.811
										0.724 (Repeat)		0.815 (Repeat)
Empty Chamber (Air Atmosphere)												
~75°F	0.265	0.269	0.274	0.162 (Bad)	0.249	0.297	0.276	0.276	0.808	0.756	0.807	0.806
Grain Pressure Calibrations (Approximate)												
87°F												
12-28-72	0.230	0.233	0.118 (Bad)	- (Bad)	0.221	0.192 (Bad)	0.195 (Bad)	0.223	0.732	0.670	0.649	0.743
~90°F												
1-4-73	0.280	0.273	0.215	-	0.193	0.168	0.275	0.275	0.786	0.729	0.779	0.764
60 ±5°F												
6-74	0.299	0.247	0.152 (Bad)	- (Bad)	0.148 (Bad)	0.137 (Bad)	0.233	0.038 (Bad)	0.017 (Bad)	0.660	0.672	0.671
88°F												
11-20-74	0.248	0.286	0.218	-	0.244	0.198	0.280	-	0.836	0.73	0.80	0.784

TABLE 11 (Cont'd)

HISTORY OF GAGE SENSITIVITY CALIBRATIONS, MV/PSI

History	N7		N8		N9		N10		N11	
	-1	-2	-1	-2	-1	-2	-1	-2	-1	-2
Konigberg (In Air)										
30°F	0.799	0.803	0.819	0.821	0.807	0.814	0.821	0.825	0.826	0.823
80°F	0.801	0.805	0.814	0.825	0.812	0.812	0.819	0.813	0.023	0.822
130°F	0.800	0.808	0.822	0.826	0.815	0.813	0.815	0.823	0.825	0.816
ASPC (In Vacuum)										
77°F	0.804	0.811	0.883	0.824	0.802	0.808	0.820	0.838	0.833	0.831
	0.831 (Repeat)									
Empty Chamber (Air Atmosphere)										
~75°F	0.847	0.841	0.829	0.853	0.645	0.805	0.818	0.814	0.824	0.795
Grain Pressure Calibrations (Approximate)										
~87°F										
12-28-72	0.829	0.816	0.810	0.789	0.758	0.728	0.784	0.740	0.829 (Dead	0.764 Short)
~90°F										
1-4-73	-	-	-	-	-	-	-	-	-	-
60 +5°F										
6-74	0.706	0.713	0.081 (Bad)	0.113 (Bad)	0.710	0.727	0.673	0.675	0.725 (Dead	0.724 Short)
88°F										
11-20-74	0.70	0.80	0.760	0.766	0.766	0.780	0.766	0.764	0.734	0.666

Later in the revised program, before the motor was reworked, the motor was warmed to 88°F and again pressure calibrated. Almost all of the gages showed a marked improvement, with only one of them remaining unacceptable (N2-2).

2. Effect of Age on Apparent Zero Load Output Changes

The zero load output could not be conveniently monitored, so a substitute was found in using the gage output at a given temperature. Since the gage output changed greatly, while only small changes in the grain stress could be expected to occur, this reading was a reasonable indicator of gage drift or instability.

Table 12 contains the zero-load output data for the gages. Again, for comparison the actual gage calibration values taken at Konigsberg Instruments, Inc., in vacuum at ASPC and in the empty motor are given. The data taken at 87° to 90°F show very marked changes from test to test.

E. CONCLUSIONS

It was apparent at this stage in the program that the gage measurements were exhibiting marked calibration changes when subjected to different thermal environments.

The overall system needed evaluation, both to correct the problems encountered and to help prevent others from doing the same thing. But, once the problems were corrected then in-situ recalibration techniques for the transducers would be required before the gages could be used.

The roles of the gages, DAS, and the electrical systems on the observed anomalies were to be ascertained through diagnostic studies on the motor and reinforced by laboratory evaluations.

Questions of DAS and transducer accuracies were to be addressed to give the most accurate measuring system possible with the devices. This was to be assured through rigorous certification and operation techniques. The following sections address the questions to the extent that they were pursued on this program.

In this planning the closed envelope restriction was removed from the program and ASPC became directly involved in data acquisition procedures and gage data reduction.

TABLE 12

HISTORY OF CHANGES IN ZERO PRESSURE OUTPUT, MV

	N1		N2		N3		N4		N5		N6	
	-1	-2	-1	-2	-1	-2	-1	-2	-1	-2	-1	-2
Konigsberg (In Air)												
30°F	0.32	-0.24	0.69	0.77	-0.34	-0.89	1.24	-0.18	0.67	0.14	1.28	0.97
80°F	0.39	0.21	-3.16	1.19	0.24	0.36	0.53	-0.29	0.31	0.37	0.08	0.22
130°F	-0.22	-0.30	1.32	1.28	-0.67	0.90	1.08	-0.34	-0.07	0.12	0.40	0.32
ASPC (Vacuum)												
77°F	3.00	-0.25	0.91	-3.00	-2.83	-	1.54	30.54 (-1.86)	-2.10	-0.83	2.33	1.59
Empty Chamber (Air Atmosphere)												
75°F	-5.56	-7.51	2.16	-11.67 (Bad)	-5.13	4.80	-0.76	-1.47	-4.73	-5.84	-7.47	-3.24
Gage Output in Cast Grain												
87°F 12-28-72	-12	-2	-4	-	-16	-12	-6	0	-7	-13	-6	-1
90°F 1-4-73	-12.38	-5.3	-3.85	-	-18.24	-8.51	0	-3.90	-9.84	-16.99	-7.53	-6.02
66°F 6-74	-26.1	15.7	4.5	-	-25.1	19.35	-14.75	-5.3	25.65	-30.18	10.9	-13
88°F 11-20-74	0.1	-31.4	-201.4	-	25.1	-9.5	46.5	-8.6	-68.1	30.2	-13.4	15.6

TABLE 12

HISTORY OF CHANGES IN ZERO PRESSURE OUTPUT, MV (CONT'D)

	N7		N8		N9		N10		N11	
	-1	-2	-1	-2	-1	-2	-1	-2	-1	-2
Konigsberg (In Air)										
30°F	0.13	-0.47	-0.12	-0.54	0.78	0.80	0.28	-0.52	-0.68	-0.08
80°F	0.64	0.30	0.19	0.23	0.34	0.35	0.44	0.53	0.35	0.26
130°F	0.45	0.23	0.07	0.07	0.52	0.34	-0.01	0.79	0.25	-1.68
ASPC(Vacuum)										
77°F	18.71	-0.16	-3.01	-4.89	0.50	-0.15	-4.75	-1.10	-1.64	-2.35
Empty Chamber (Air Atmosphere)										
75°F	-3.45	0.36	2.52	2.50	2.96	-10.52	-3.42	-2.56	3.14	-14.38
Gage Output in Cast Grain										
87°F 12-28-72	0	2	0	0	-6	-15	-8	-10	-1	-21
90°F 1-4-73	-	-	-	-	-	-	-	-	-	-
66°F 6-74	8.6	1.17	1.04	50.6	16.0	-17.9	25.3	-22.6	4.03	-23.8
88°F 11-20-74	361.2	-2.2	-24.1	-1.1	-387.5	19.0	-34.2	23.5	-107.3	-112.5

SECTION 9

MOTOR DIAGNOSTIC EVALUATIONS AND INSTRUMENTATION REWORK

- Revised Program -

In an effort to pinpoint the causes of the system anomalies a critical review of the prior test data was made by all of the concerned parties, and opinions were solicited from a number of experts on semiconductor strain gages. Finally, an expert on electronics and transducers (Thomas T. Yamauchi of the Boeing Company) was employed to serve as an independent consultant. The overall recommendation was to conduct a systematic evaluation of the total measuring system, effect repairs where indicated, develop rigorous DAS calibration and measurement procedures, and support this work with laboratory studies of some of the most probable factors that might produce the erratic gage measurements.

This section provides the results of the systematic tests conducted on the motor, the rework of the electrical system, and the performances of the system components after the rework. The laboratory tests conducted to evaluate gage anomalies are discussed in Section 10.

A. DIAGNOSTIC EVALUATIONS ON THE MOTOR

The diagnostic tests conducted on full-scale Motor No. 1 were designed to isolate and/or identify possible gage and measurement problems. There were 14 diagnostic tests conducted on the motor, beginning with the rather trivial and progressing to the more complex. These tests are summarized below.

1. Visual Inspection

All junction boxes were visually inspected for the following: loose connections, bad solder joints, loose wires, visible corrosion, and loose hardware. Visual inspection did not reveal any obvious faults or problems.

2. Verification of Bridge Completion Circuits

All of the bridge completion circuits were traced-out as per the original schematics. No discrepancies were noted.

3. Electrical Resistance Measurements

Semi-conductor gage resistance readings for the normal stress gages and the shear gages were taken and are listed in Table 13. The gage resistances were read using a digital voltmeter. The three leads from each gage bridge were disconnected at the input terminal strip.

Because of gage self-heating, the resistance values could only be used to assess fairly gross anomalies. Only two transducers evinced problems; one of the two semi-conductor elements of shear gage S-2 was found to be open, while S-13 had a shorted or damaged element.

4. Possible Shunting Paths

The two independent bridges on each of the normal gage diaphragm and the bridges of separate nearby gages were checked to determine if there was shunting between circuits. The results of tests are reported in Table 14. Normal stress gage No. 11 showed a dead short between the common lead of one-half bridge to the common lead of the companion half bridge. The short was probably caused by the common gage lead of one bridge shorting against the other common gage lead. This could occur at the gage stem, in the gage itself, or along the cable bundle. This short undoubtedly affected the output measurements of gage No. 11. No other shunting effects were detected. The measurements of resistance between adjacent bridges of the same transducers and between bridges of nearby stress transducers are also listed in Table 14. These data showed no undesirable shunting effects.

5. Determination of Circuit Interactions

The purpose of this test was to determine whether undesired electrical conductive paths existed between any of the gages. It was conducted by applying shunts to selected channels and measuring the outputs of all channels both before and after application of the shunts. A change in output of any of the channels would indicate interaction.

The shunts were precision resistors selected to produce a mid-range or full-scale output on the selected channels. The shunts were applied in pairs to adjacent channels, then the voltage output of all of the channels was recorded. None of the channels showed significant differences in their readings taken before and after the application of shunts to other gage channels.

It was concluded that there were no interactions between the electrical circuits.

TABLE 13

SEMI-CONDUCTOR GAGE RESISTANCE READINGS

Gage No.	Resistance, ohms	
	Side One	Side Two
N1-1	470	480
N1-2	480	470
N2-1	570	580
N2-2	570	610
N3-1	580	580
N3-2	570	570
N4-1	470	470
N4-2	480	480
N5-1	500	500
N5-2	490	510
N6-1	470	480
N6-2	480	480
N7-1	470	470
N7-2	470	480
N8-1	500	550
N8-2	540	540
N9-1	510	510
N9-2	520	510
N10-1	510	500
N10-2	500	500
N11-1	500	500
N15-1	520	520
N15-2	520	530
S1	360	360
S2	Open	320
S3	360	360
S4	400	400
S5	350	340
S6	360	350
S7	380	380
S8	430	430
S9	350	350
S10	360	350
S11	340	330
S12	350	360
S13	40	400
S14	360	350

TABLE 14

TESTS FOR SHUNTING BETWEEN CIRCUITS

90° Junction Box

Gage Pair Tested	Resistance
N1-1 and N1-2	Inf.
N1-2 and N2-1	Inf.
N2-1 and N2-2	Inf.
S-13 and S-14	Inf.

0° Junction Box

N9-1 and N9-2	Inf.
N9-1 and S-11	Inf.
N9-1 and N10-1	Inf.
N10-2 and N10-1	Inf.
N10-2 and S-11	Inf.
N10-2 and S-12	Inf.
N11-1 and N11-2	Short
N11-1 and S-12	Inf.
N11-1 and S-6	Inf.
N11-2 and S-5	Inf.
S-5 and S-6	Inf.
S-6 and S-7	Inf.
S-6 and S-8	Inf.
S-7 and S-8	Inf.

6. Effects of Varying Circuit Loads

This test was conducted to determine whether there were effects on gage readings due to varying the loads on the common power supply. Two junction boxes with 20 channels of circuit load were powered and recorded, then the power was disconnected from one of the junction boxes, which had the effect of removing the load of ten bridge circuits. The output of the circuits that were still powered and the power supply voltage was recorded. The changes noted ranged from zero to $\pm$ .3 mv which range was typical for repeat measurements at that time.

7. Tests on Bridge Completion Networks

Tests were conducted to evaluate the wiring and the resistors in the bridge completion circuits. No apparent circuit anomalies, other than those gages found to be bad, were detected and no faulty resistors were found. The resistance measurements of the bridge resistors are given in Table 15. These values are all within .5% of those originally specified by the gage supplier.

8. Transducer and System Repeatability and Hysteresis

Two motor pressurization tests to 50 psig at 88°F were conducted two days apart to evaluate the gage and system repeatability and hysteresis. Table 16 presents a summary comparison between the two pressure runs. The apparent sensitivity is the slope of gage output voltage versus motor internal pressure. Zero return is the difference between the gage readings taken before and immediately after the test.

For the normal stress gages, the differences in the apparent sensitivity ranged from about 1% to 24% (for Channel 12). The shear gage apparent sensitivity data were more variable ranging up to a factor of two.

The zero return data were found to be strong functions of the time after test and ranged up to 3.2 mv for normal stress gage N2-1 (Channel 14) and 2.9 mv for shear gage S-13 (Channel 17).

9. Drift Test of All Gages and Circuits

Drift tests of all the gages and gage circuits in the motor were conducted from the period starting 22 November to 10 December 1974. During this period all gages were powered and data were sampled periodically using either a digital voltmeter or an automatic recorder. Table 17 provides a summary of the drift data observed, while Table 18 reduces these observations to give the apparent drift rates. Between the three test periods shown in Table 18 some adjustments were made in the system and a change implemented in the recording instrumentation (manual readings with a precision digital voltmeter were used for the first two readings, while an automatic scanning unit was used for the remaining measurements).

TABLE 15

MEASUREMENTS OF BRIDGE RESISTORS IN SUSPECT CHANNELS

Gage No.	Resistance, ohms							
	R-1	RS-1	R-4	RP	RB_2	R_{z2}	RB_3	R_{z3}
N1-1	5005	3424	5003	5,003	17	29,270		
N1-2	5008	5003	5004	5,004	76	35,040		
N2-1	5009	463	5010	5,011	21	550		
N2-2	5010	605	4888	5,007	-	-	11	
N4-1	5007	1507	5000	5,007	13.8	32,450		
N4-2	5007	1506	5007	5,007	7			
N8-1	5006	3012	5006	5,008	16	-	-	25,490
N8-2	5007	2944	5009	10,020	17	-	-	18,732
N15-1	4997	2504	4996	No Resistor	16	27,990		
N15-2	4997	2435	4997	No Resistor	-	-	7	296,100

	RS-1	RS-2	R-1	R-4	
S-2	3379	3385	4997	3384	
S-6	3060	3064	2180	2179	
S-7	3053	3056	2188	2187	
S-8	3064	3069	2187	2185	(Parallel R4 491,800)
S-9	3056	3059	2176	2177	
S-10	5003	5008	5000	5001	
S-12	3049	3048	2148	2158	(Parallel R1 165,320)
S-13	3045	3039	2057	2127	(Parallel RS_2 158,030)
S-14	3047	3046	2173	2171	

TABLE 16

MOTOR PRESSURE TESTS TO 50 PSIG AT 88°F

Channel No.	Gage No.	11/20 Apparent Sensitivity, mv/psi	11/20 Zero Return, mv	11/22 Apparent Sensitivity mv/psi	11/22 Zero Return, mv
1	N8-2	.77	0	.784	1.1
2	N2-2	GAGE BAD			
3	N10-2	.764	0	.786	.8
4	N5-2	.730	.9	.774	.7
5	N3-1	.244	.7	.234	0
6	N7-2	.814	0	.820	0
7	N6-2	.784	0	.784	0
8	N9-2	.780	0	.772	0
9	N4-1	.280	0	.272	0
10	N1-1	.248	.4	.286	.6
11	N15-1	-	-	-	-
12	N11-2	.666	1.0	.822	.5
13	S-8	.088	.4	.064	0
14	N2-1	.218	.5	.258	3.2
15	S-11	.402	1.0	.410	.6
16	S-6	.076	.6	.120	.5
17	S-13	.612	2.9	.682	1.5
18	S-14	.242	1.4	.162	0
19	N9-1	.766	1.6	.768	.5
20	N11-1	.734	.4	.834	0
21	S-9	.796	.5	.862	.7
22	S-2	-	-	-	-
23	N10-1	.766	0	.780	0

TABLE 16

MOTOR PRESSURE TESTS TO 50 PSIG AT 88°F (CONT.)

Channel No.	Gage No.	11/20 Apparent Sensitivity, mv/psi	11/20 Zero Return, mv	11/22 Apparent Sensitivity, mv/psi	11/22 Zero Return, mv
24	N1-2	.296	.7	.284	.5
25	S-12	.096	.6	-	-
26	S-5	.342	0	.346	.5
27	N4-2	-	0	-	0
28	N5-1	.836	0	.810	0
29	N15-2	.276	0	.272	0
30	S-7	.166	.6	.186	0
31	N8-1	.760	0	.802	.4
32	N6-1	.780	0	.776	.5
33	S-3	.290	.7	.288	0
34	S-4	.184	.5	.140	0
35	N7-1	.70	1.7	.804	0
36	S-10	-	-	-	0
37	S-1	.124	1.6	.056	0
38	N3-2	.198	0	.196	0

TABLE 17

SUMMARY OF DRIFT TEST DATA

Channel No.	Output, mv			
	12/2	12/3	12/5	12/9
1	.2 to .6	0.2	-	-
2	112.3	111.9	-	-
3	24.6	24.6	24.01	24.33
4	32.4	32.3	31.54	31.68
5	27.0	26.8	27.32	27.66
6	-2.1	-1.7	-1.08	- .38
7	16.4	16.4	15.11	14.95
8	18.9	18.8	14.14	18.14
9	36.4	36.3	74.15	123.05
10	24.1	24.2	0	0
11	39.9	39.1	42.85	34.64
12	20.4	20.3	20.29	20.82
13	1.0	.7	-	-
14	-3.4	-3.0	-	-
15	- .1	- .2	-2.65	-5.58
16	3.2	3.0	2.47	3.27
17	-363.4	-362.9	-	-
18	-2.1	-2.0	-	-
19	-13.5	-13.5	-	-
20	1.6	1.6	.93	.20
21	-11.4	-11.5	-9.25	-7.52
22	-	-	-	-
23	-24.9	-24.9	-24.70	-25.09
24	-15.2	-15.4	-16.48	-16.58
25	1.3	1.3	.50	- .68
26	-7.3	-7.3	-5.35	-5.61
27	-9.1	-9.1	-9.36	-9.30
28	-18.4	-18.3	-17.65	-17.79
29	-1.0	- .3	-9.45	-9.66
30	1.0	.9	.47	-1.00
31	-	-5.8	-	-
32	- .7	- .7	-10.61	-10.91
33	-1.6	-1.5	-1.06	- .41
34	2.8	2.3	- .86	- .64
35	- .9	-1.2	-7.05	-7.75
36	1.1	1.3	- .86	-3.85
37	-5.0	-4.8	-2.74	-2.66
38	-10.9	-10.9	-11.35	-11.31

TABLE 18

APPARENT DRIFT RATE FROM 7-DAY TEST PERIOD

Channel No.	Drift Rate, mv/Day		
	12/2-12/3	12/3-12/5	12/5-12/9
1	+0.4	-	-
2	-0.4	-	-
3	0.0	-0.30	0.09
4	-0.1	-0.38	0.02
5	-0.2	0.26	0.07
6	0.4	0.31	0.15
7	0.0	-0.65	-0.06
8	-0.1	-0.33	0.01
9	-0.1	18.93	13.09
10	0.1	-	-
11	-0.8	1.88	-0.42
12	-0.1	0.00	0.11
13	-0.3	-	-
14	0.4	-	-
15	-0.1	-1.23	-0.59
16	-0.2	-0.27	0.15
17	0.5	-	-
18	0.1	-	-
19	0.0	-	-
20	0.0	-0.34	-0.16
21	-0.1	1.13	0.36
22	-	-	-
23	0.0	0.10	0.10
24	-0.2	-0.54	0.04
25	0.0	-0.40	-0.22
26	0.0	0.98	-0.12
27	0.0	-0.13	0.01
28	0.1	0.33	-0.03
29	0.7	-4.58	-0.05
30	-0.1	-0.22	-0.40
31	0.1	-	-
32	0.0	-4.96	-0.06
33	0.1	0.22	0.11
34	-0.5	-1.58	0.03
35	-0.3	-2.93	-0.15
36	0.2	-1.08	-0.63
37	0.2	1.03	0.04
38	0.0	-0.23	0.03

Excluding the obviously faulty channels an average drift rate of about 0.16 mv/day is observed. This converts to about 4% of full scale per month (assuming a full-scale output of 120 mv).

Virtually all of the channels showed some drift, with some very marked changes in eleven of the channels. These data represent the total drift which could include changes from the gages, bridge circuits, and data acquisition systems. Possible drift in the electronics is considered next.

10. Electronics Drift Testing

The electrical drift shown in Tables 17 and 18 occurred in unpredictable ways. Sometimes there was no drift, sometimes a little drift and at other times some quite spectacular steps appeared in the output. The largest observed excursion was that of Channel 9 where the output increased 87 mv over the seven-day test period.

To isolate the sources of this drift it was necessary to redesign the circuits to permit independent assessments of the gages, gage junctions (stainless steel solder joints) bridge completion circuit boards, power supply, and the recorder. Isolation of the electronics was considered first in five sets of experiments.

The gages were completely disconnected from the electronics and replaced with dummy gage circuits made of 0.1% precision resistors wired as half-bridges. These were wire wound precision resistors specifically selected because of their low temperature coefficient. With the transducers disconnected, the measurable drift would have to be attributed to the electronics system.

Five test sets were conducted since only nine of the precision half-bridges were available at the time. Each of the test sets involved drift testing with continuous monitoring. Tables 19 to 22 contain tabulations of the channel output voltage taken at the beginning and end of the drift test period. All of the drift data stayed within the established accuracy of the measuring digital voltmeter used, $\pm$ 0.1 mv, except channels 1, 10 and 31. A rework of the solder junctions in the bridge completion units for those three channels was effected and the drift tests were repeated. This time the three channels performed within the $\pm$ 0.1 mv limits.

The drift data for the total system (Table 18) indicated average drift rates of 4 to 30% per month. In this case, with the gages removed from the circuits, only 2 of the 37 channels tested exhibited drift rates as high as 2.5 to 5% per month.

TABLE 19

TESTS FOR DRIFT IN ELECTRONICS

- FIRST SET (73°F) -

Channel	Gage No.	Output, mv 12/6	12/9
1	N8-2	-30.51	-30.20
2	N2-2	-77.73	-77.71
10	N1-1	27.93	27.93
13	S-8	-.06	-.07
14	N2-1	-69.88	-69.92
17	S-13	6.55	6.54
18	S-14	-.05	-.04
19	N9-1	-18.54	-18.49
31	N8-1	-42.94	-42.30

TABLE 20

TEST FOR DRIFT IN ELECTRONICS

- SECOND SET (72°F) -

Channel	Gage No.	Output, mv	
		12/10	12/11
3	N10-2	33.0	33.0
5	N3-1	40.4	40.4
13	S-8	.90	.90
14	N2-1	-62.0	-62.0
15	S-11	-13.9	-13.9
19	N9-1	-13.0	-13.0
23	N10-1	-.10	-.10
24	N1-2	-16.0	-16.0

TABLE 21

TEST FOR DRIFT IN ELECTRONICS

- THIRD SET (71°F) -

Channel	Gage No.	Output, mv 4 pm 12/11	8 am 12/12	1 pm 12/12
8	N9-2	51.8	51.9	51.9
9	N4-1	98.0	98.0	98.0
10	N1-1	23.4	24.0	23.8
12	N11-2	44.3	44.3	44.3
21	S-9	.20	.20	.20
26	S-5	-11.5	-11.5	-11.5
27	N4-2	-16.6	-16.6	-16.6
30	S-7	-1.3	-1.3	-1.3

TABLE 22

TEST FOR DRIFT IN ELECTRONICS

- FOURTH AND FIFTH SETS (71°F) -

Channel	Gage No.	Output, mv			
		12/12	12/13	12/16	12/17
4	N5-2	-14.4	-14.4		
6	N7-2	-17.1	-17.0		
7	N6-2	18.8	18.7		
16	S-6	.01	.01		
20	N11-1	3.1	3.1		
25	S-12	7.2	7.2		
28	N5-1	-24.1	-24.2		
29	N15-2	12.5	12.4		
32	N6-1	-21.7	-21.7		
33	S-3	-.1	-.3		
34	S-4			-.4	-.5
35	N7-1	-23.0	-23.0		
36	S-10			-5.6	-5.6
37	S-1	2.4	2.3		
38	N3-2			-12.6	-12.7

The obvious conclusion to be drawn from the results of this test series is that the gage leadwire-solder junction combinations were significant contributors to the large system drift initially observed.

11. Gage Self Heating and Power Reversal Effects

These tests were planned to evaluate possible unbalances in transducers due to self-heating of the semi-conductor gages or corrosion of the stainless steel leadwire junctions, which might produce a diode effect in the circuit.

The experiments were performed on Motor No. 1 using a knife switch; thus allowing simple power on-off switching or rapid up and down powering. The measurement circuit for the tests is shown in Figure 53.

A specific reference test was made using a dummy bridge composed of four equal resistors, each having a resistance of 600 ohm, another 600 ohm resistance was in series with the bridge. This dummy bridge caused extreme heating of the bridge, but gave a flat trace when energized with either positive or negative power.

Figure 54 shows effects that are typical of a gage and bridge completion assembly which shows no unusual effects other than differential heating of the semiconductor elements which are in differing environments. When the power is reversed the signal reverses polarity and an equivalent curve is generated. Figure 55, however, shows a more common behavior which is attributed to a diode effect somewhere in the circuit. The diode can be formed by an oxide layer on any metal surface in contact with a different metal.

The diode conducts in the forward direction and under this test condition, it causes no change in the observed result. When power is reversed, however, the diode introduces resistance to the circuit. This resistance causes an offset, but more important, the diode layer is heated by the current causing further offsets as the diode temperature changes. The diode heating effect can either aid or oppose the response produced by the heating of the semiconductor elements, although the diode heating would have a different time constant. The combination of two effects, sometimes opposing and sometimes aiding, could, with differing time constants, superpose to give the effects observed.

There are no clues in the data to determine where a diode exists; but the fact of its existence can be inferred from the data taken. Twelve tests were run, and the diode effect was evident in ten of the twelve. Typical shifts in the warmup data were from two to eight mv in three seconds.

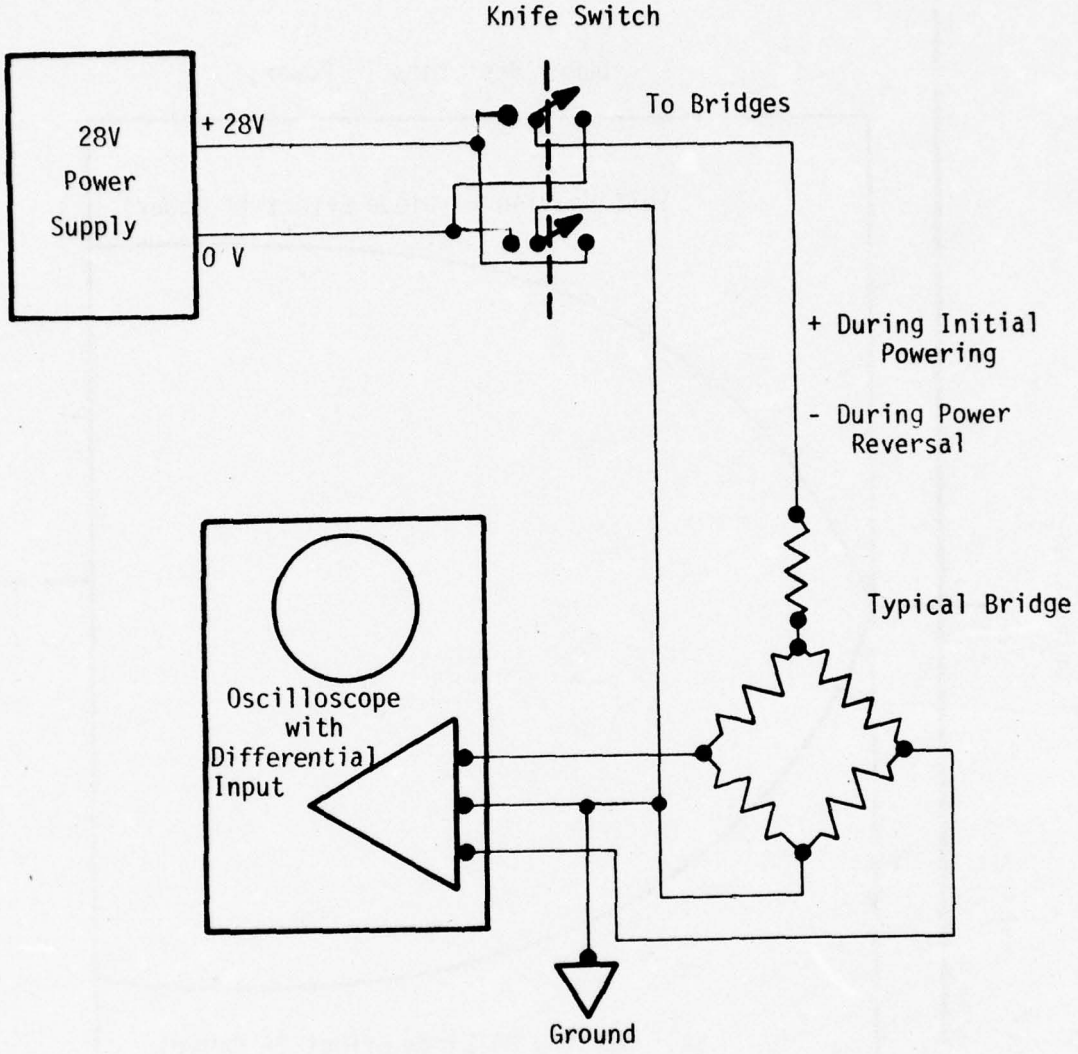

FIGURE 53. MEASUREMENT METHOD FOR GAGE SELF-HEATING AND POWER REVERSAL TEST EXPERIMENTS

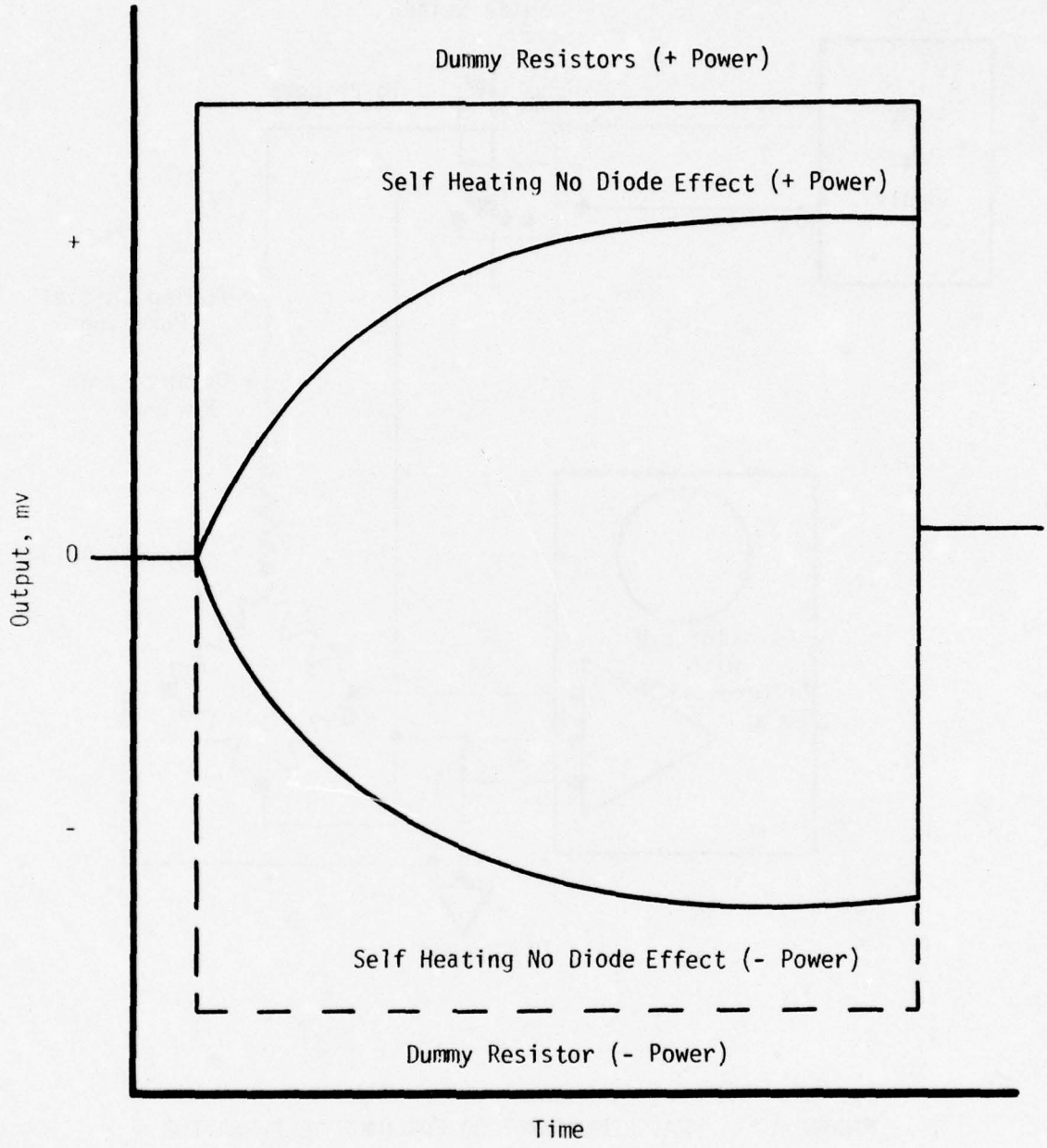

FIGURE 54. SELF HEATING EFFECTS

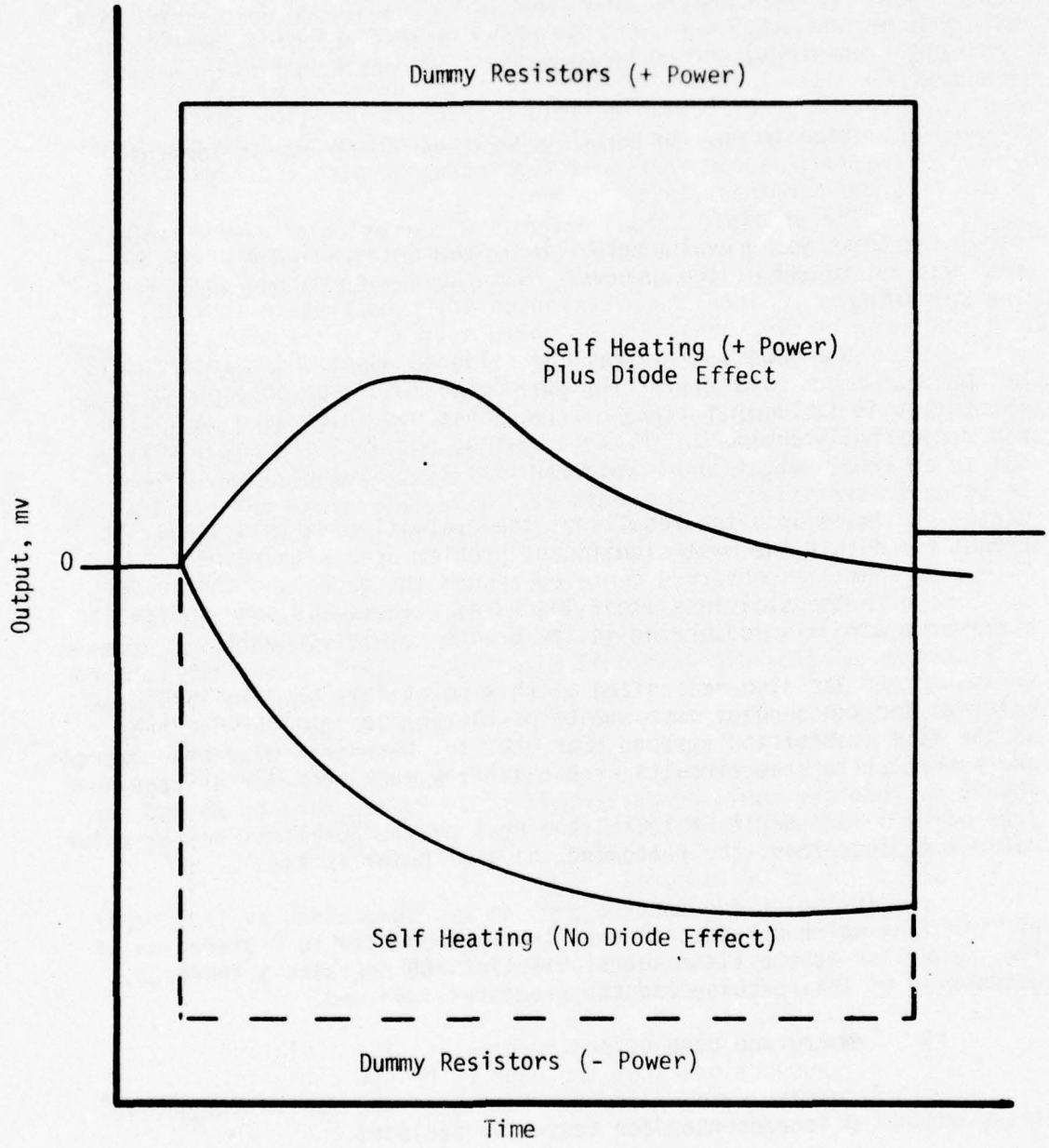

FIGURE 55. SELF HEATING AND DIODE EFFECTS

The self-heating effects are attributable only to the semi-conductor gages since the thermal coefficients of resistors in the bridge completion units are too small. The changes observed would require heating one of the semi-conductor gage elements up to 128°C hotter than its counterpart gage element in the bridge completion unit. With the low current (1/2 watt) resistors used (including some carbon resistors) these temperature differences are considered to be almost impossible.

12. Observations on Leadwire Soldered Junctions at Terminal Strips

The possibly strong effects of corrosion at the stainless steel leadwires was given a brief assessment at this point. The first test was to evaluate the sensitivity of gage output to the quality of the soldering.

Gage N8-2 was selected for observation since moving wires or application of pressure on the case near this gage caused 1 to 2 mv excursions in its output signal. One of the leadwires on this gage was accidentally broken in the pull test so all of the leadwires were cut to an equal length and resoldered. The new junctions were found to be quite sensitive to movements of the leadwires and the terminal strip, so they were resoldered. The resoldered junctions gave an increase of 30 mv in the gage output.

This apparent sensitivity of the soldered junctions was observed again in the laboratory. A gage was obtained which was mounted in a section of flexible case wall with liner covering over the rubber encapsulant. The stainless steel wires came out through the flex case material through a metal tube and were soldered to the junction pads in the same fashion as those on Motor No. 1. When this gage was powered and connected to a recorder, it exhibited the same behavior as gage N8-2. The 10 mv recorder could be driven off scale by touching or moving the lead wires. (It should be noted that most of the junctions on the motor did not exhibit this same phenomenon at this point in time).

The soldered junction problem was compounded by the use of an acid flux which provides an environment conducive to degradation of the connection as the system ages. Section 10B contains a thorough discussion of this problem and the processes involved.

13. Summary and Conclusions

A concise summary of the results of the twelve diagnostic tests conducted is presented for review in Table 23.

TABLE 23

SUMMARY OF DIAGNOSTIC TEST RESULTS

Test No.	Description of Test	Diagnostic Results	Corrective Action Taken
1	Visual Inspection	No apparent problem. No corrosive signs.	As a precaution all solder joints in B.C.U. were touched up, all terminals were tightened.
2	Gage Resistance	No apparent problem. Gages S-13, S-2 bad.	None
3	Checkout of Junction Box Circuits	No circuit discrepancies were noted.	Insure leads are not touching.
4	Shunting Effects	Gage N11 was affected. No other shunting effects were detected.	None possible.
5	Determination of Circuit Interactions	No gage interactions.	None
6	Power Supply Loading Effects	No power supply loading effects.	None
7	Resistor Check	No faulty components.	None
8	Drift Test on All Gages	System drifts observed on all channels.	After system corrections drift rate was reduced to that reported by manufacturer.
9	Drift Test of Electronics	Channels 1, 10 and 31 have slight drift.	Channels excluded in data acquisition.
10	Gage Pressurization Tests	Gage response variation.	Rate dependency detected and reported.
11	Gage Self Heating and Power Reversal Effects	Heating effect and diode effect.	System stabilized for 16 hrs before use. Current applied in one direction only.
12	Junction Observations on Soldered Terminal	Unstable stainless steel solder joints.	Determine and use stable junctions.

The results from test Nos. 1 through 7, and test No. 10 indicate no gross faults, no circuit interactions (with the exception of gage N11), no shunting and loading effects, no faulty resistive components in the B.C.U., no apparent problem with absolute values of the gage resistors) and no massive drift of the electronics (exception Channels 1 and 31). Minor problems detected were very typical of this type of portable-field use instrumentation which has been subjected to environmental conditions not normally encountered in everyday usage, as compared to a temperature controlled, humidity controlled, and permanent installation.

Test No. 9 evaluated total system drift which appears to have occurred in all of the channels, with some very marked changes in eleven of them. Since the electronics drift testing in test No. 10 indicated very little change the observed system drift must be attributed to the gages, leadwires and soldered junctions. Test No. 12 illustrated that marked changes in gage output could be obtained by soldering and resoldering gage leadwire junctions which were sensitive to mechanical disturbances. This suggested, but did not prove, that a problem existed with all of the stainless steel solder junctions.

Based upon the results of the evaluation to this stage, it was concluded that the most significant problem area with respect to the system anomalies observed centered around the gages and the solder junctions with the stainless steel leadwires. There was some indication that errors were also occurring in the bridge completion units.

It was also recognized at this point that no means were available for independent assessments of the bridge completion units and the data acquisition system. For example, there was no way to assure that all of the circuits were equally powered (28.00 volts).

Before continuing with the next phase of the diagnostic evaluation, therefore, the following changes in the system and corrective actions were implemented.

- Rework the soldered leadwire junctions to give the optimum age stability to the stainless steel wire connections.
- Provide diagnostic capabilities for isolating suspect areas of the gage or bridge circuits.
- Upgrade the data acquisition system and implement rigorous operational procedures.

B. REWORK OF THE MOTOR ELECTRICAL SYSTEM

1. Leadwire Junctions and Reference Bridges

The rework of Motor No. 1 began with the removal of all of the soldered junction strips, then replacing with screw type terminal strips. The stainless steel solder junctions were replaced with crimped spade-lug terminals (23) using a tool specially made for ASPC by the Florida Power Tool Company.

The modified junction strip is shown in Figure 56. Three resistors were added to the terminal strip to allow a complete electrical drift and calibration check prior to and following each measurement. At a later date, the work necessary to move terminals from point-to-point and problems associated with this operation prompted a change to rotary switches which further simplified the pre- and post-measurement checks.

The procedures for making electrical checks with the new terminal strip were as follows:

(1) The "zero" readings of the dummy circuit were obtained after moving the completion wires, JB_1 and JB_2, onto the R_z resistors. These two resistors were nearly matched, so the dummy gage circuit would give an output near zero, but differing from zero due to the output of individual bridge completion networks.

(2) The "full-scale" readings of the dummy circuit were obtained with JB_1 still attached to the resistor R_z and JB_2 moved to R_f. The value of the resistance of R_f was chosen to simulate a bridge output near full-scale. Again, the observed output voltage depended upon the individual bridge completion circuit.

The electrical check obtained above is valid within the statistical limitations of the DAS and the stability limitations of the electrical circuits.

2. Standards Added to Each Junction Box

Each of the four junction boxes had a dummy bridge added with a simulated output near 10 mv. A divider was placed across the power supply and one DAS channel to make the output proportional to the gage energization power as an added check to assure that there would be no undetected bridge energization power change.

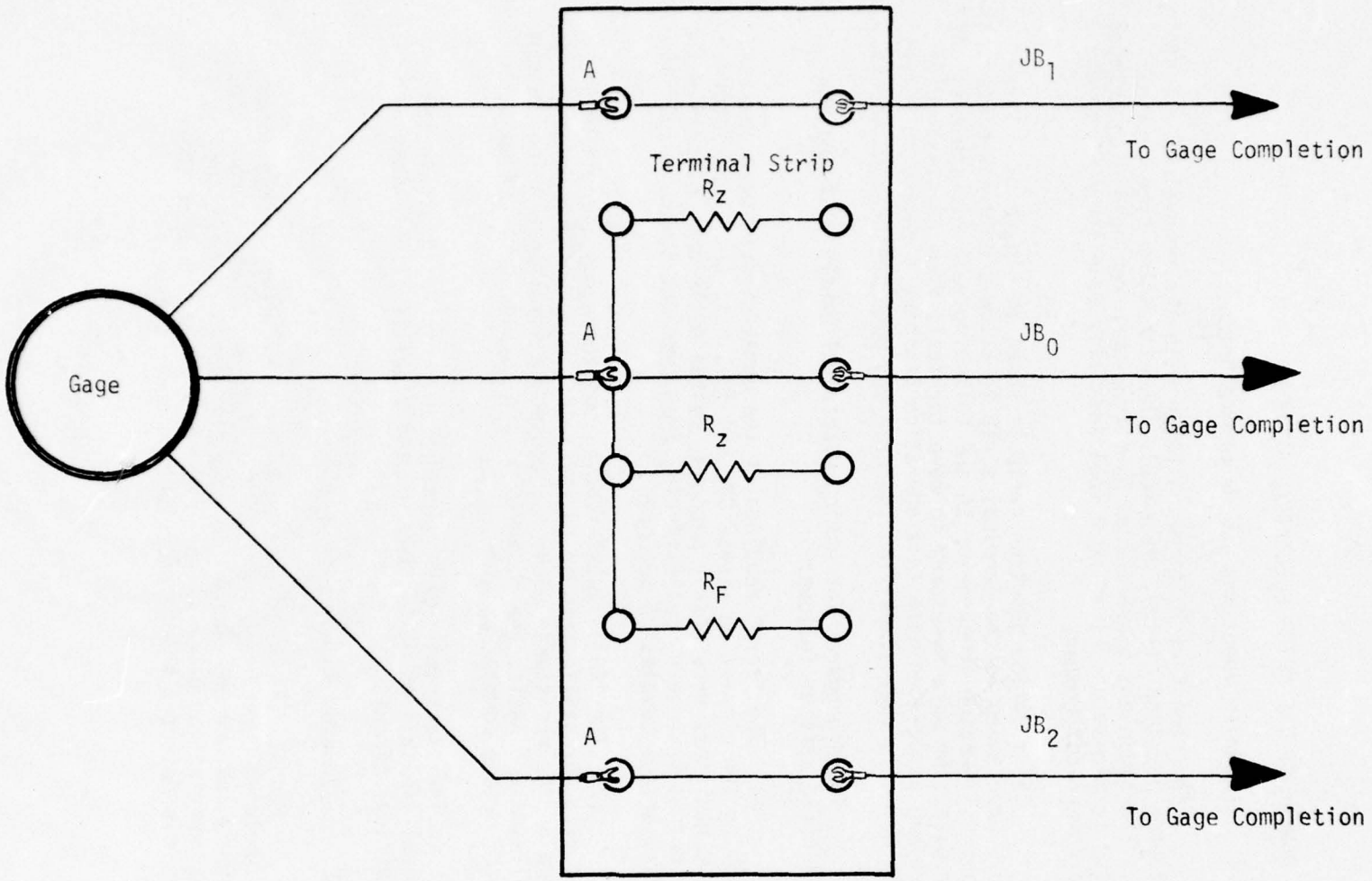

FIGURE 56. NEW TERMINAL STRIP WITH REFERENCE BRIDGE DESIGN

3. Addition of Rotary Switches

Investigations revealed that the repeated manual operation of connecting and disconnecting the spade-lugs to perform the operation (changing from the balanced to the unbalanced conditions) caused fatiguing and eventual breaking of some leadwire joints resulting in different electrical baseline zeroes. An inability to tighten the small spade-lug to the small screw head on the terminal strip in a repeatable fashion also contributed to this problem. The solution was to include precision double-pole, three position rotary switches.

Drift testing was conducted with three of the new switches connected on-line to three gage channels (replacing the manual operation). A typical hookup is shown in Figure 57. The output data were not affected in numerous tests of switching back and forth. Upon demonstrating that the switches were satisfactory and that they improved system performance, they were installed in all channels and a change over from the manual operation was effected.

All resistors were soldered at the switches and the switches were connected on line between the junction box and the transducer as shown in Figure 58. The resistors and switches were then housed in an aluminum chassis. This change was not an electrical circuitry change since the circuits were actually identical to the old ones. The change was simply a procedural step to switch the resistors in and out of the circuits.

C. NEW DATA ACQUISITION SYSTEM

1. Design and Operation

A data acquisition system was desired which could guarantee precision and accuracy of the results within a specified limit of $\pm$ 0.1 millivolts or 3% of the reading, whichever is greater. The required sensitivity of $\pm$ 0.1 mv was to be valid from 1 mv to 100 mv full scale.

The data acquisition system consisted of an available Varian 620 i mini-computer, an interface with an analog to digital converter, and a 64 channel multiplexer, Figure 59. The system was based around a 14 bit analog-to-digital converter capable of performing a conversion in 50 microseconds with an accuracy of $\pm$ .005% of full-scale or $\pm$ 1 least significant bit. The dynamic range of $\pm$ 8192 binary counts and the specified accuracy were well within requirements, provided amplifier/multiplexer combinations of the required low-noise capability could be obtained. Since there was no requirement for measurements to be made at high speed, relatively inexpensive amplifiers and multiplexer switches were utilized. The software in the computer was used to compensate for drift and noise as described in the following paragraphs.

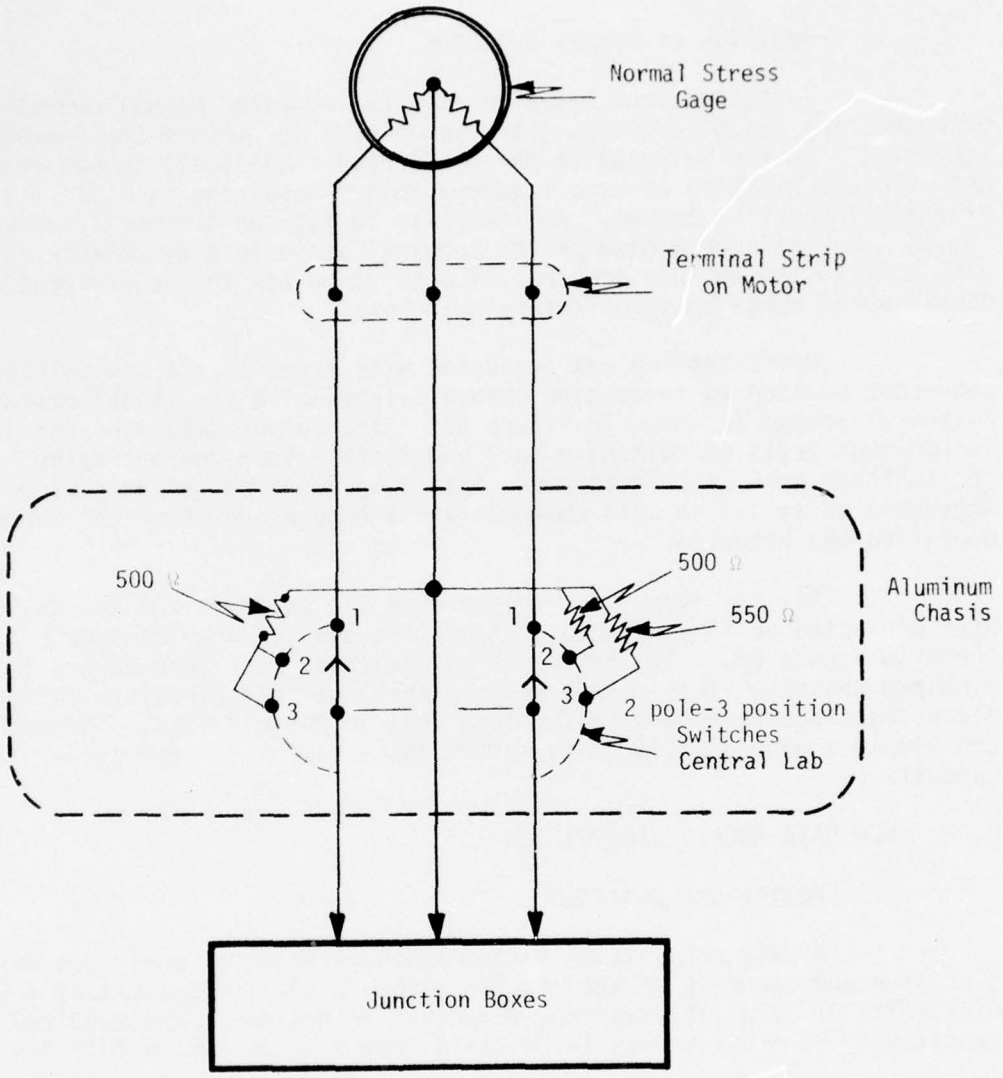

FIGURE 57. TYPICAL NORMAL GAGE SWITCH/RESISTORS HOOKUP

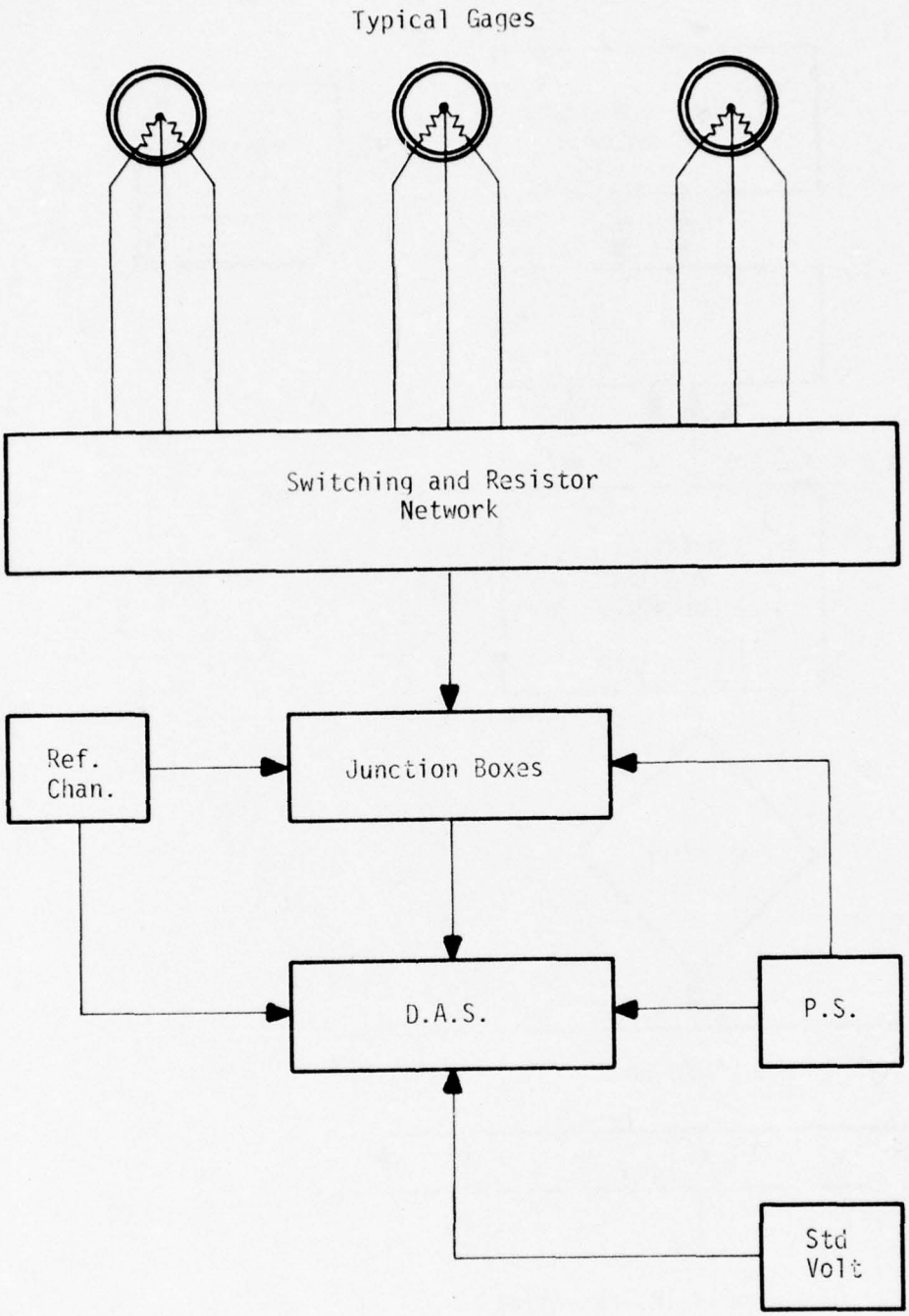

FIGURE 58. BLOCK DIAGRAM OF NEW SWITCHING NETWORK

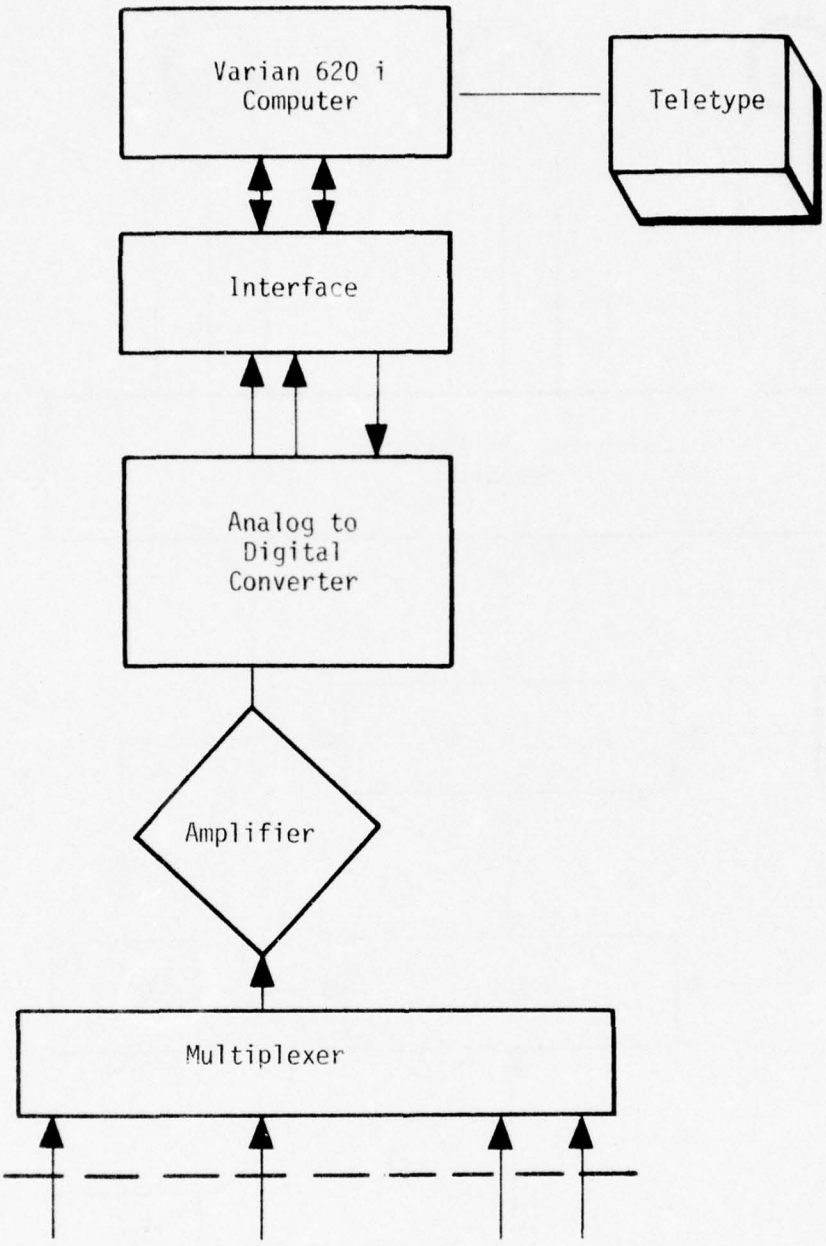

FIGURE 59. DAS BLOCK DIAGRAM

The first step in certifying that the system was satisfactory was to set up criteria for the DAS measurements and then verify that the DAS could meet the criteria through a series of measurements in which comparisons were made with equipment having high accuracy traceable to NBS standards. The full document detailing the certification of the DAS and the 500 ohm and 550 ohm resistors which were to be used as reference bridges is attached as Appendix L.

To summarize the procedures, a sequential series of standard voltages was input to the DAS and its responses to these voltages measured. The actual series of measurements in the ASPC standards laboratory required three days to verify linearity, drift, common mode rejection and accuracy of the DAS.

The resistors used for the bridge simulation bridges were tested in the standards lab over the temperature range of 30 to 150°F. These measurements verified that the temperature coefficients of the resistors were within manufacturing specifications (50 parts/million/°C).

A short assembly language program (Figure 60) was written to contain a list of channel numbers, time information, Δt, and a repeat number, M. Channels could be read in any desired order. A true zero reading preceded each channel reading. The readings on each individual channel and the zero readings would be repeated M times and the resulting difference divided by M before printout. After all of the channels had been read M times and the averages printed, the computer would wait a period of time given by Δt. The entire process would then repeat unless terminated by the operator.

The repeat nature of the readings gave a statistical reduction in noise or scatter in the data which is given by

$$\text{Final Noise Scatter} = \frac{\text{Original Noise Scatter}}{\sqrt{M}}$$

For example, if M = 100, the scatter due to noise in the original results was reduced by a factor of 10.

Both short term and long term drift in the DAS were eliminated by comparing every measurement to a true zero and averaging the difference between the true zero and the channel being measured. Thus, the data were continuously corrected and all readings were maintained within a tight band.

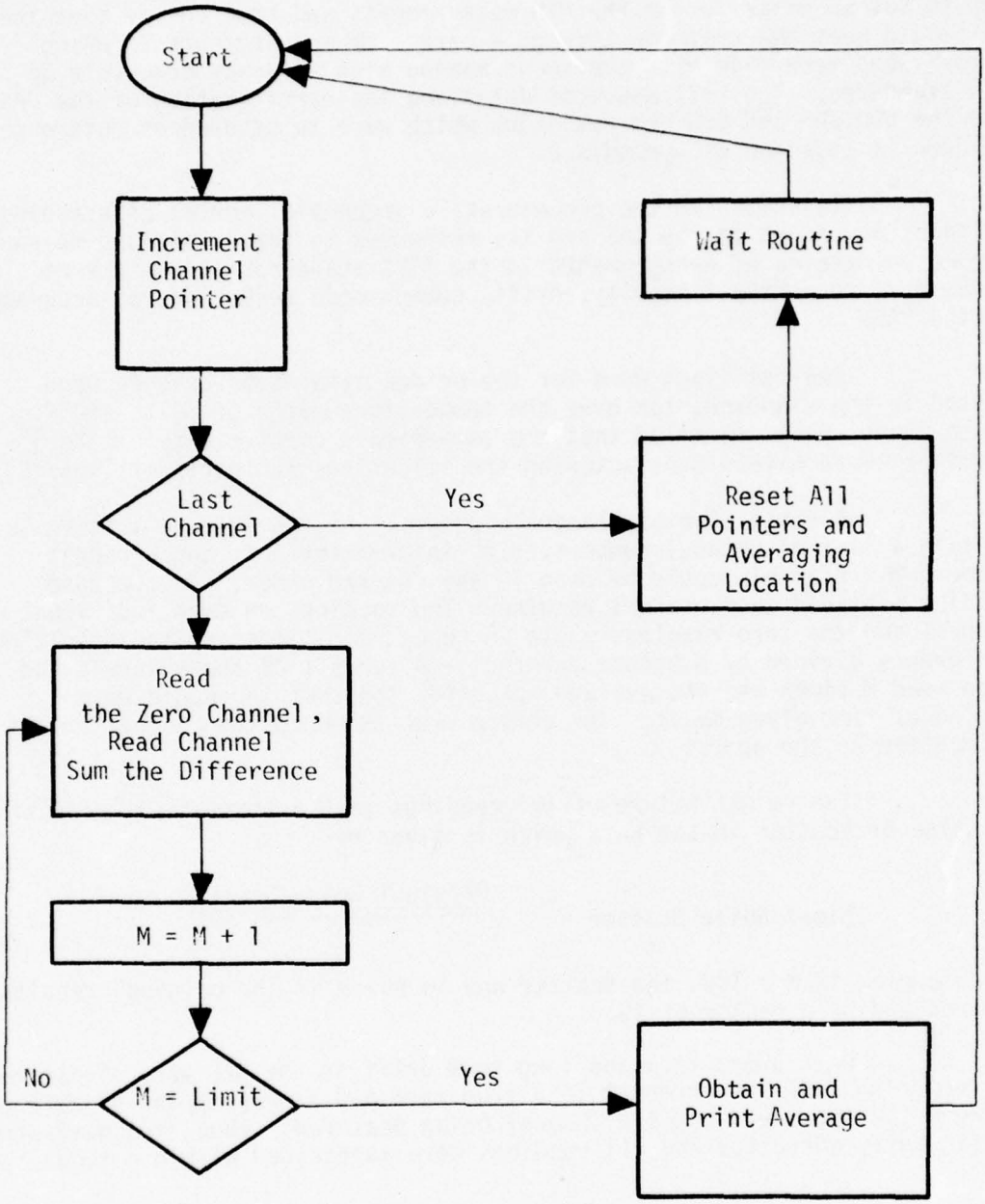

FIGURE 60. FLOW CHART OF PROGRAM

The general design of the DAS revolved around the multiplexers and the analog-to-digital converter. Under worst case conditions, the channel being read is at $+E_{max}$ and the amplifier was at $-E_{max}$. At the instant of switching the slew rate of the amplifier, the integrating capacitor used to reduce noise, the impedance matching networks between amplifier components, and the charges held on the multiplexer gates determine a rise curve as shown in Figure 61. A read delay must be established to allow the system to settle before the analog to digital converter is asked to convert.

Another important factor of the DAS design was common mode rejection. DC common mode rejection is easily obtained as it is only necessary to balance the DC current in both sides of the operational amplifier as shown in Figure 62. An adjustable resistor, R_6, can be adjusted to make both sides of the final amplifier DC symmetrical. If the amplifier is exactly symmetrical then there will be exactly zero output at any common mode voltage.

Unfortunately, the AC common mode is more complex, since the resistance and capacitance must be symmetrical on both sides of the final op-amp stage. To obtain maximum AC common mode rejection, extensive design and balancing of all stages of the multiplexer amplifier system is necessary. This is especially true when a broad frequency range is also specified.

2. Data Acquisition System Certification

The data acquisition system was required to undergo a rigorous test of its operational capabilities. The operational procedure is contained in full in Appendix M. Essentially, it entailed a comparison of DAS output with laboratory standard data which was guaranteed to $\pm$ .02 mv. Channels were first selected randomly and examined at 20 carefully selected voltages on two successive days. Agreement was required to be within $\pm$ 0.1 mv or $\pm$ 1.5% of reading. Other specifications were common mode rejection of 80 DB with a 10 volt AC or DC signal, zero offset of 2 mv and cross talk less than .1 mv.

The actual DAS performances were much better than required with one exception, that being the AC common mode. The 10 V RMS AC had to be replaced with 10 V peak-to-peak, if acceptance was to proceed without expensive trimming of the input to the amplifier. Actual values observed were well within specification on voltages, common mode rejection was 80 DB at $\pm$ 10 volts DC or $\pm$ 10 volts AC peak-to-peak. ($\pm$ 10 volts AC RMS = $\pm$ 14.1 volts peak-to-peak). No measurable DC offset or cross talk were detected.

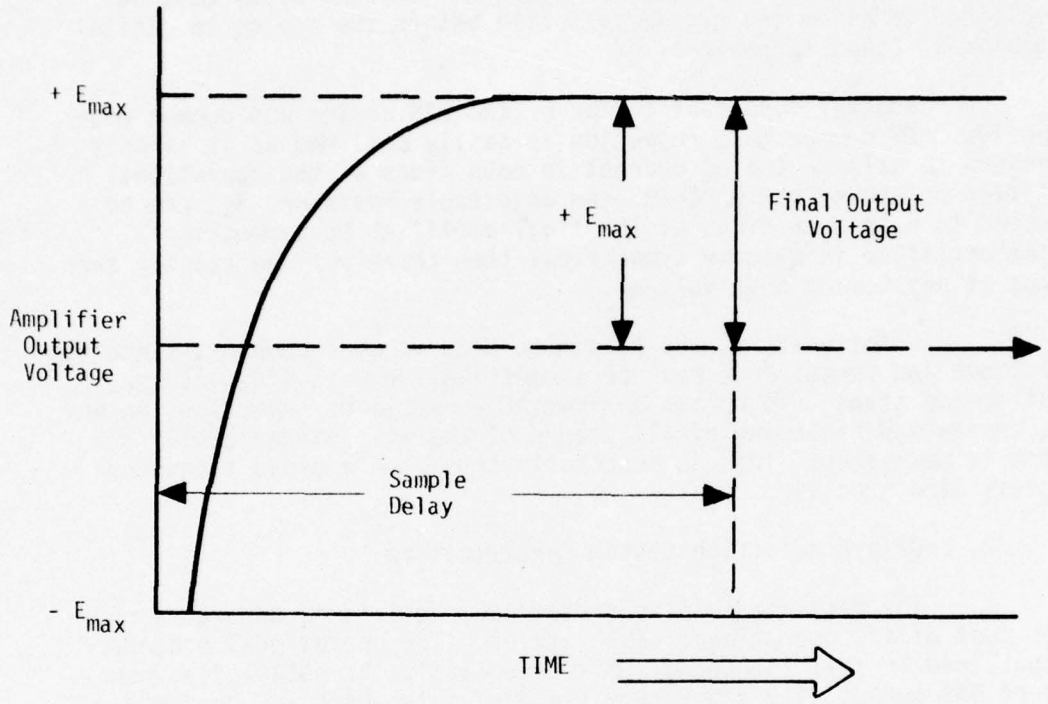

FIGURE 61. OPERATIONAL RISE TIME OF MULTIPLEXER CIRCUITS

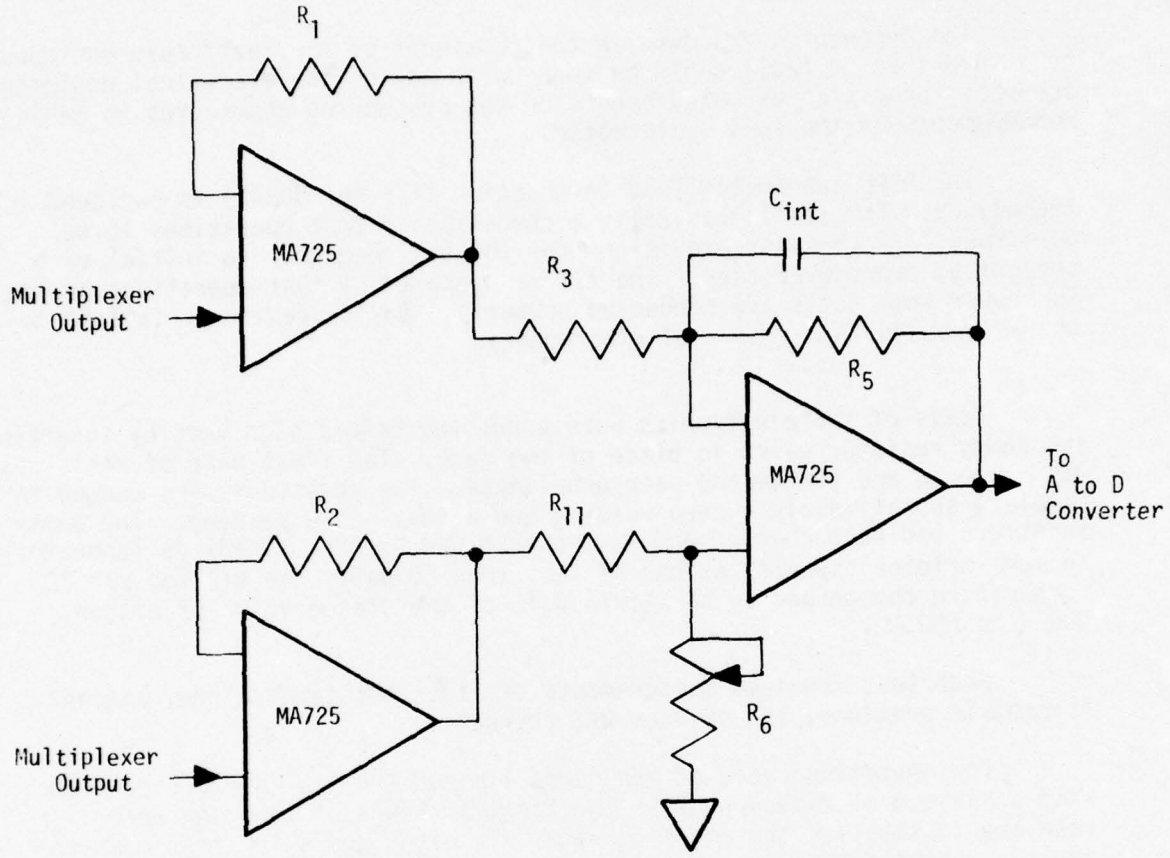

FIGURE 62. CIRCUIT FOR COMMON MODE REJECTION

D. DEFINITION OF NEW OPERATIONAL PROCEDURES

The procedures followed in the remainder of the tests were designed to assure that no fault could be found with any of the electrical equipment, accuracy, precision of measurements or the procedures themselves in making measurements on the full scale motor.

The ASPC Integrated Test Instruction (ITI No. 00845) is included in Appendix N. The ITI is basically a checklist of test operations to be performed. It contains provisions for the test engineer to initial each sequential procedural step. The ITI is prepared by test operations personnel to insure that tests are conducted properly. Any deviation or failure to comply results in a report of discrepancy.

Tests of the electronics were conducted before each test by inserting two dummy resistor pairs in place of the gage. The first pair of resistors was balanced and the second pair unbalanced. The resistors were chosen to simulate approximately a zero reading and a full scale reading. The dummy resistors had been checked and were guaranteed by ASPC standards laboratory to meet original specifications of less than 50 parts per million per °C temperature change and to be within 0.1% of the stated value of either 500Ω or 550Ω.

Each test required measurements of the test temperature, ambient barometric pressure, and of each DAS channel.

The operating cycle of the gages limited them to 24 hours powered with a minimum of 24 hours off. The first 16 hours of powering were required to stablize the gages leaving only eight hours for test measurements. Justification for this procedure was taken from the studies reported in Section 10. Typical voltage output versus powering time data for two gages are plotted in Figure 63. They show that the changes are essentially complete after 16 hours.

The detailed procedures used in the pressure testing of Motor No. 1 are given in Appendix N.

E. EVALUATION OF THE STABILITY OF THE REWORKED SYSTEM

Measurements with the new DAS and the specified procedures were carried out on Motor No. 1 between 4 August 1975 and 21 November 1975. The internal checks made and the certified DAS assured the validity of the data gathered. A test schedule and list of tests carried out is attached as Table 24. The schedule began with drift and stability tests which continued through the entire series. Two pressure calibration tests to 50 psi were included in the series.

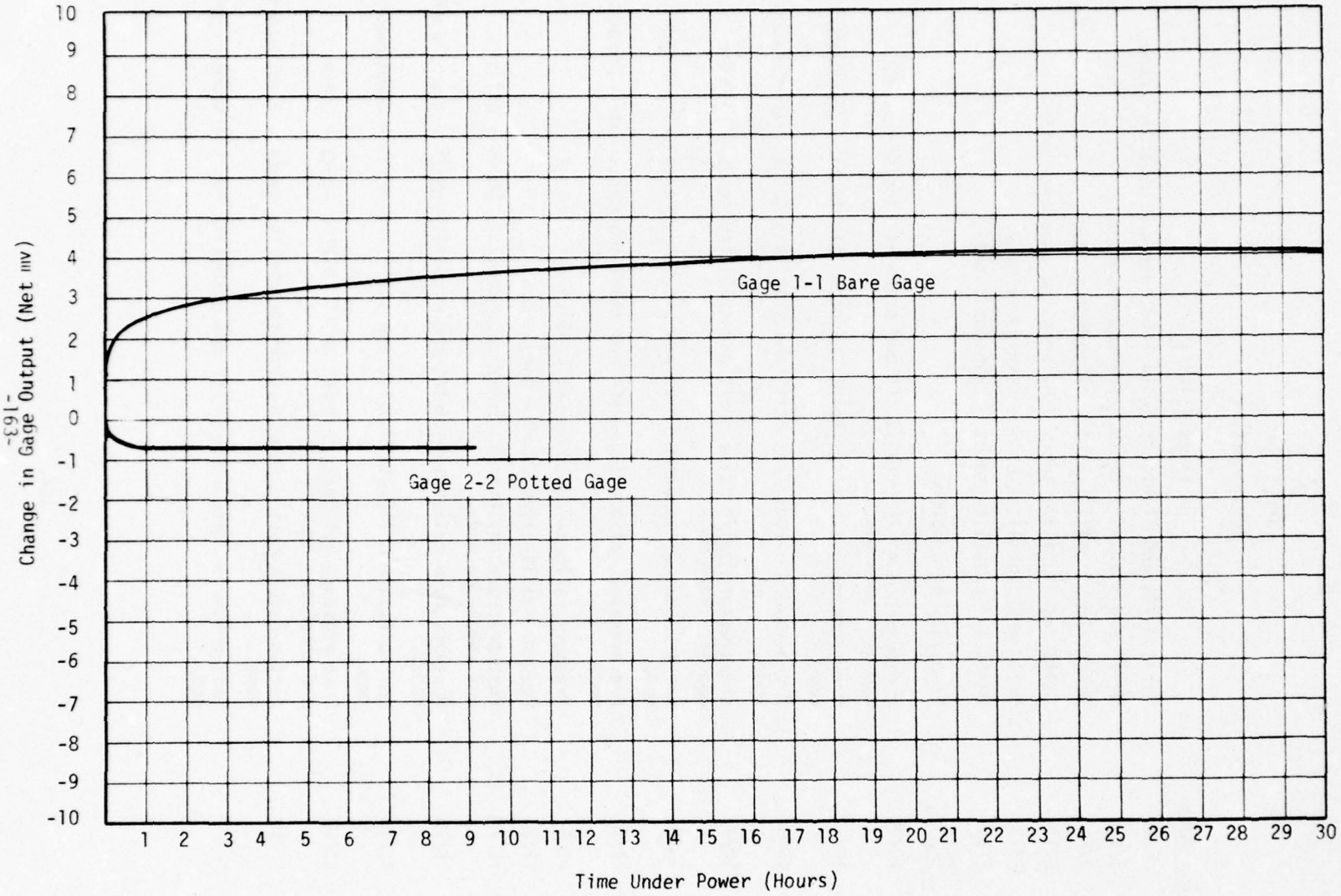

FIGURE 63. SELF HEATING EFFECTS IN POTTED AND BARE GAGE SURROUNDED BY PBD PRE-POLYMER

TABLE 24

TEST SCHEDULE

Test Date	Tests (110°F)
8/4	First drift and stability tests - balance and unbalance mode.
8/6	Drift and stability tests - transducers mode.
8/8	Drift and stability tests - transducers mode.
8/11	Drift and stability tests - balance and unbalance mode.
8/13	Drift and stability tests - transducer mode.
8/15	Drift and stability tests - transducer mode.
8/14 to 10/19	Temporary hold period.
10/20	Pre-pressure calibration drift and stability tests - balance and unbalance mode.
10/22	Pre-pressure calibration drift and stability tests - transducers mode.
10/24	Pre-pressure calibration drift and stability tests - transducers mode.
10/27	Pre-pressure calibration drift and stability tests - balance and unbalance mode.
10/29	Pre-pressure calibration drift and stability tests - transducers mode.
11/3	Pre-pressure calibration drift and stability tests - transducers mode.
11/5	Pressure calibration to 50 psi - first run.
11/7	Pressure calibration to 50 - second run.
11/10	Post-pressure calibration drift and stability tests - balance and unbalance mode.
11/12	Post-pressure calibration drift and stability tests - transducers mode.
11/14	Post-pressure calibration drift and stability tests - transducers mode.
11/17	Post-pressure calibration drift and stability tests - balance and unbalance mode.
11/19	Post-pressure calibration drift and stability tests - transducers mode.
11/21	Post-pressure calibration drift and stability tests - transducers mode.

1. Drift and Stability Tests

Stability of the electrical circuitries and DAS was exceptionally good, excluding stress gage circuits, S-9, N3-2, N8-2, and N15-1. The latter gage circuits were just slightly over specifications by .070, .050 and .080 mv, respectively. The stability of the system, independent of the transducer and stainless steel junctions, was very satisfactory and justifies the considerable effort which was directed toward establishing good system baseline stability.

Figures 64 to 66 summarize the drift data for all gages over a 97 day period. One gage, N15-1, showed a strong anamolous behavior that was noted previously and should be excluded from further consideration. If N15-1 is excluded then the maximum drift observed over a 97 day period is 6 mv and the average drift 2 mv. These values calculate to system drift rates that average about 0.5% FSO/month and reach a maximum of about 1.5% FSO/month, a substantial improvement over those observed before any correction or rework (Table 17).

The drift rates of the reworked system were compared to those measured by Konigsberg, Appendix O. His data show zero pressure drift rates of 0.2 to 0.4% FSO/month for the top 25% of his transducers and 0.6 to 0.8% FSO/month for the top 50%. Thus, the observed drift data are within the manufacturer's range of experience with the gages.

It should be noted, however, that when these drift data are compared with allowable limits for drift which are considered to be consistent with the original objectives of the program (Figures 64-66) the majority of the gages exhibit drift behavior which exceed those limits.

To place this observation in perspective consider that 1% FSO/month converts to 1.2 mv/month which, given an average gage sensitivity of 0.8 mv/psi (150 psi gage), represents about 1.5 psi/month. Since the thermal stresses developed in the Minuteman Stage III motor under normal storage conditions are typically of the order of 5 psi it's obvious that this type of drift behavior is unacceptable for long term testing.

Table 25 shows the readings from the dummy resistor bridges placed in each junction box. The dummy bridges serve two purposes: (1) That the power at each junction box is verified; and (2) that the stability and power supply checks are obtained. Failure of any of the channels 42, 43, 44 and 45 are a signal to stop and repair. Should one of these dummy channels be out all associated data would be invalid.

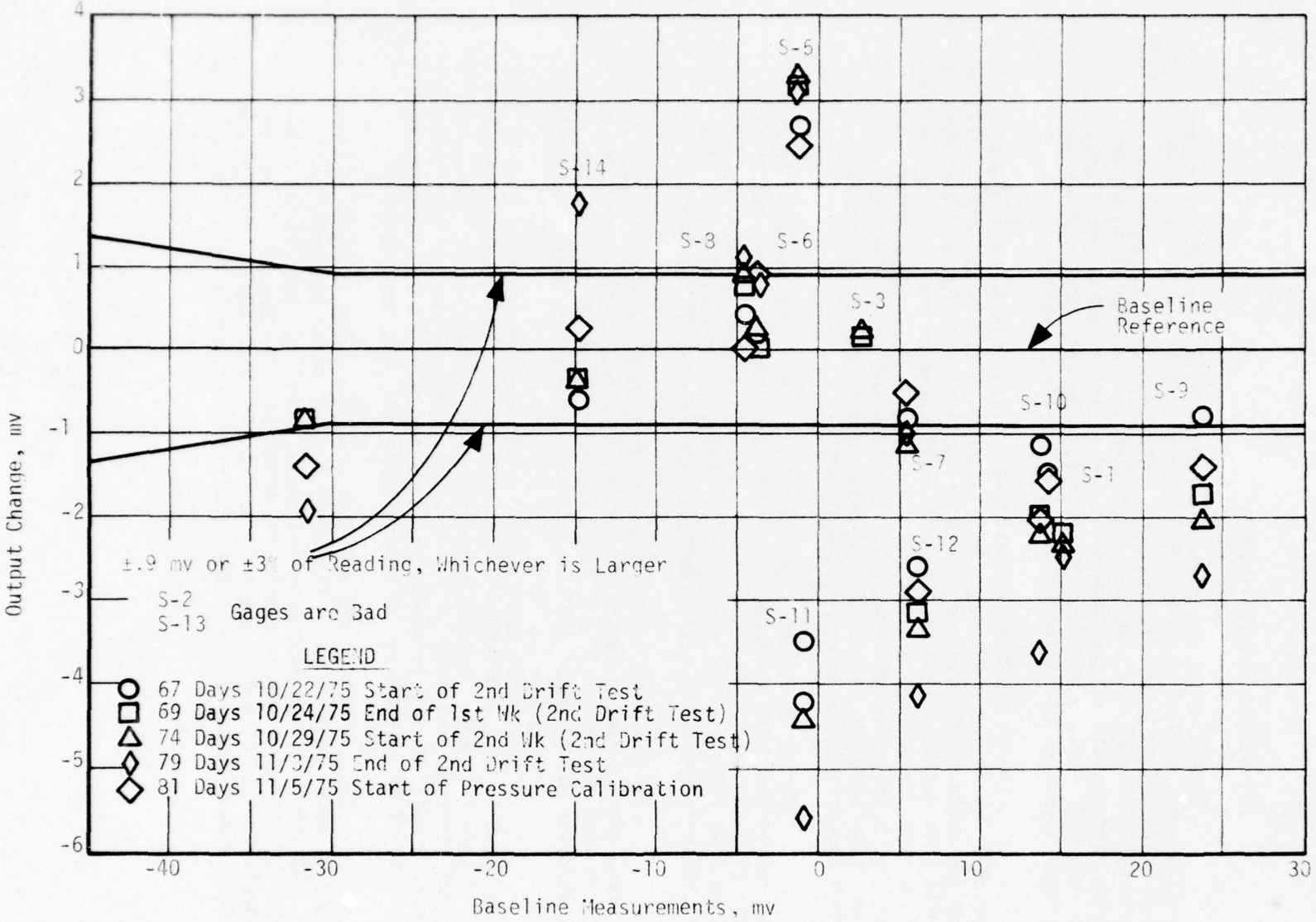

FIGURE 64. DRIFT READINGS FROM SHEAR TRANSDUCERS AT 110°F REFERENCED TO BASELINE (8/6/75 TO 11/5/75)

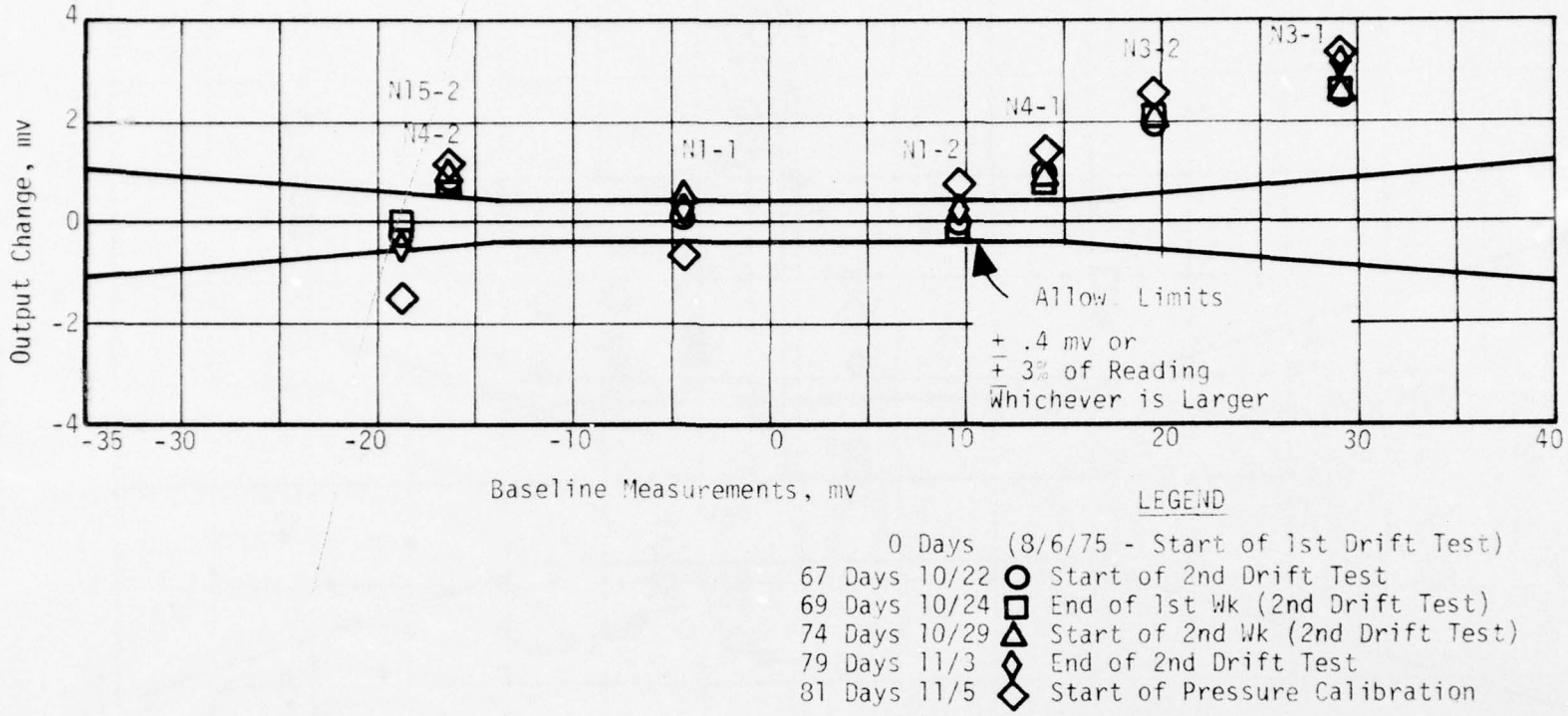

FIGURE 65. DRIFT READINGS FROM 450 PSI NORMAL STRESS TRANSDUCERS AT 110°F REFERENCED TO BASELINE (8/6/75 TO 11/5/75)

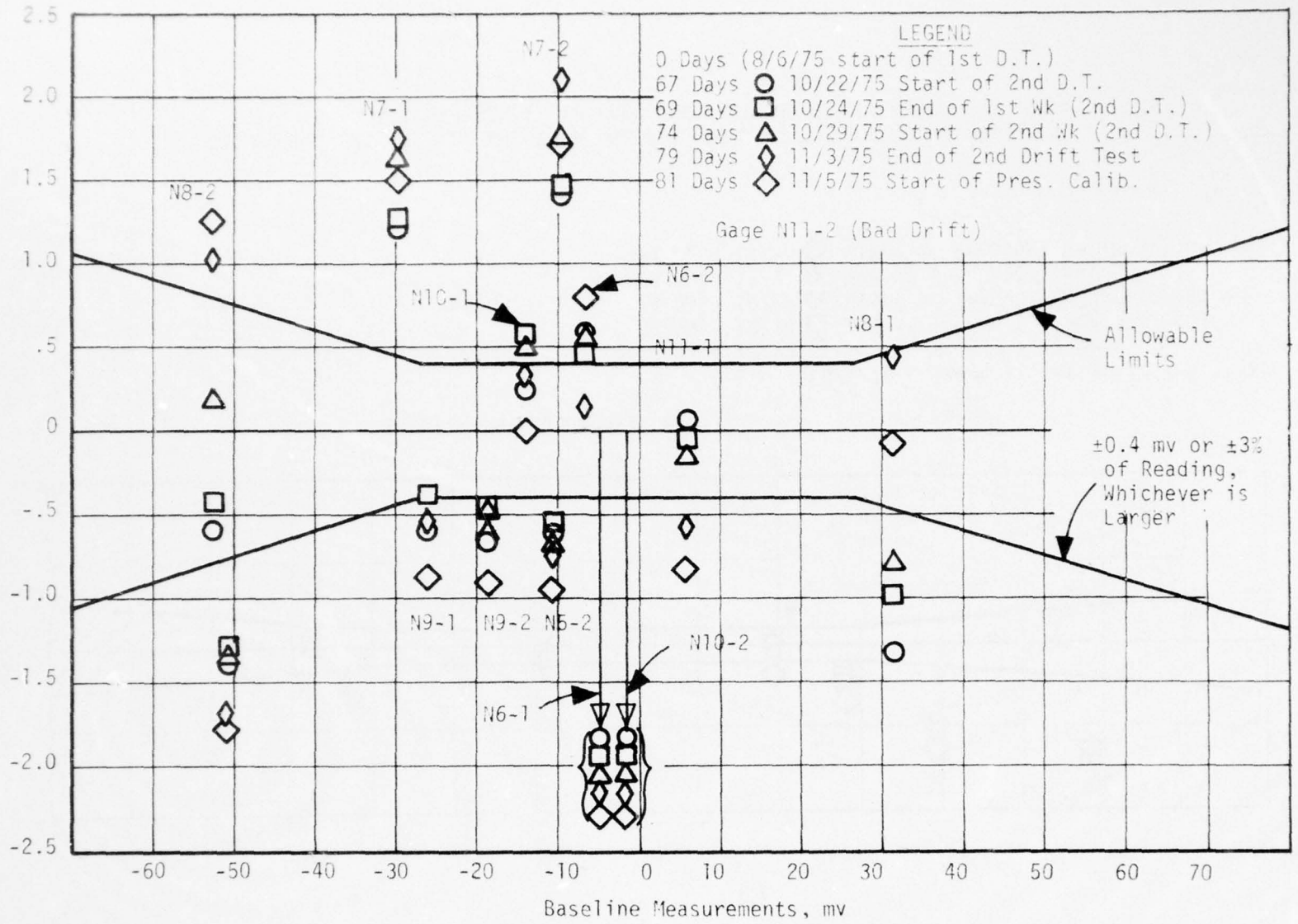

FIGURE 66. DRIFT READINGS FROM 150 PSI NORMAL STRESS TRANSDUCERS AT 110°F REFERENCED TO BASELINE (8/6/75 TO 11/5/75)

TABLE 25

DUMMY RESISTOR POWER SUPPLY INDICATOR

IN EACH JUNCTION BOX

Channel No.	Types of Reference Standard Voltages	Week Starting 8/4	8/11	10/20	10/27	11/10	11/17
42	Dummy Resistors	11.40	11.39	11.48	11.44	11.45	11.40
43	Dummy Resistors	-11.00	-10.97	-11.00	-11.01	-11.06	-11.00
44	Dummy Resistors	-10.78	-10.75	-10.77	-10.70	-10.85	-10.80
45	Dummy Resistors	11.01	11.00	11.10	11.04	11.07	11.01

Figures 67 through 69 are illustrations of the stability of the DAS, bridge completion units and resistors. Figures 67 and 68 display readings with the pair of balanced resistors substituted in place of the gage, while Figure 69 shows the readings with the unbalanced resistors substituted. Gages S-4, S-9, N3-2 and N8-2 were slightly out of specifications. N15-1, the 3-D gage, was badly out of specifications, indicating a faulty circuit.

2. Conclusions

Tests on the reworked system with its accompanying rigorous calibration and measurement techniques have indicated the following:

(1) Rework of the system with the removal of the solder joints eliminated the major source of erratic readings and faulty sensitivity of the gages.

(2) The electronics behaved quite satisfactorily allowing confidence in the data.

(3) Drift in the range of 0.5% FSO/month to an extreme of 1.5% FSO/month occurred in most of the gages over the period of the experiment.

The observed drift in the reworked system is attributed to drift of the gages themselves, and although it appears small relative to full-scale output, a comparison of the drift magnitude with that of the stresses which were to be measured in the majority of motor tests conducted in this program shows that at best an accuracy of $\pm$ 50% could have been expected.

The drift data discussed above are most concerned with only one parameter of the gages, zero stress output. Questions still remained regarding gage sensitivity, viscoelastic gage-grain interactions, dynamic loadings, hysteresis, in-situ recalibrations of the gages, and others. The importance of answering some of these questions lead to the performance of the series of laboratory experiments discussed in the next two sections.

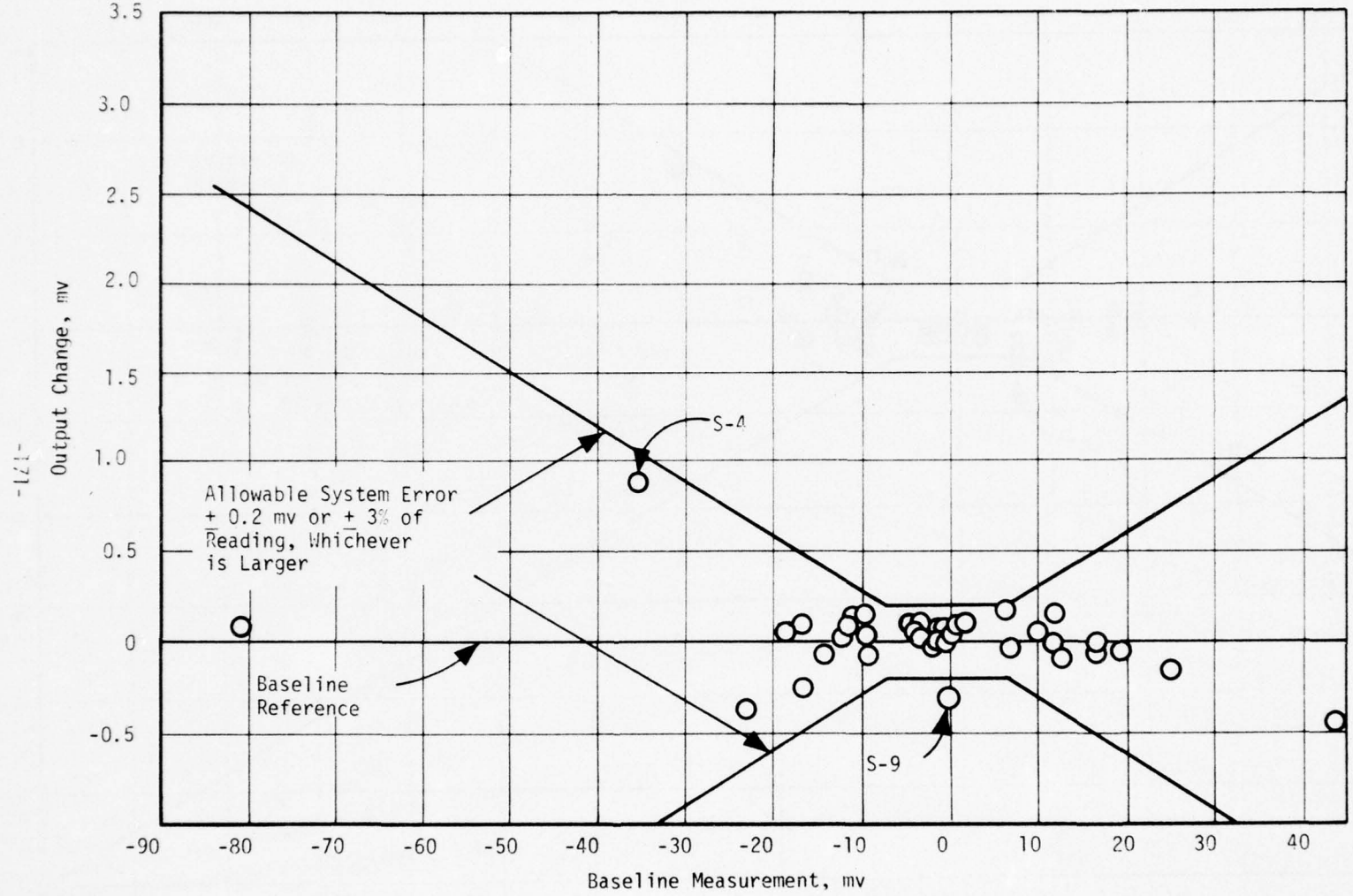

FIGURE 67. DRIFT READINGS FROM TRANSDUCER SIMULATION RESISTORS MEASUREMENTS IN THE BALANCED MODE AT 110°F (8/4-8/11/75)

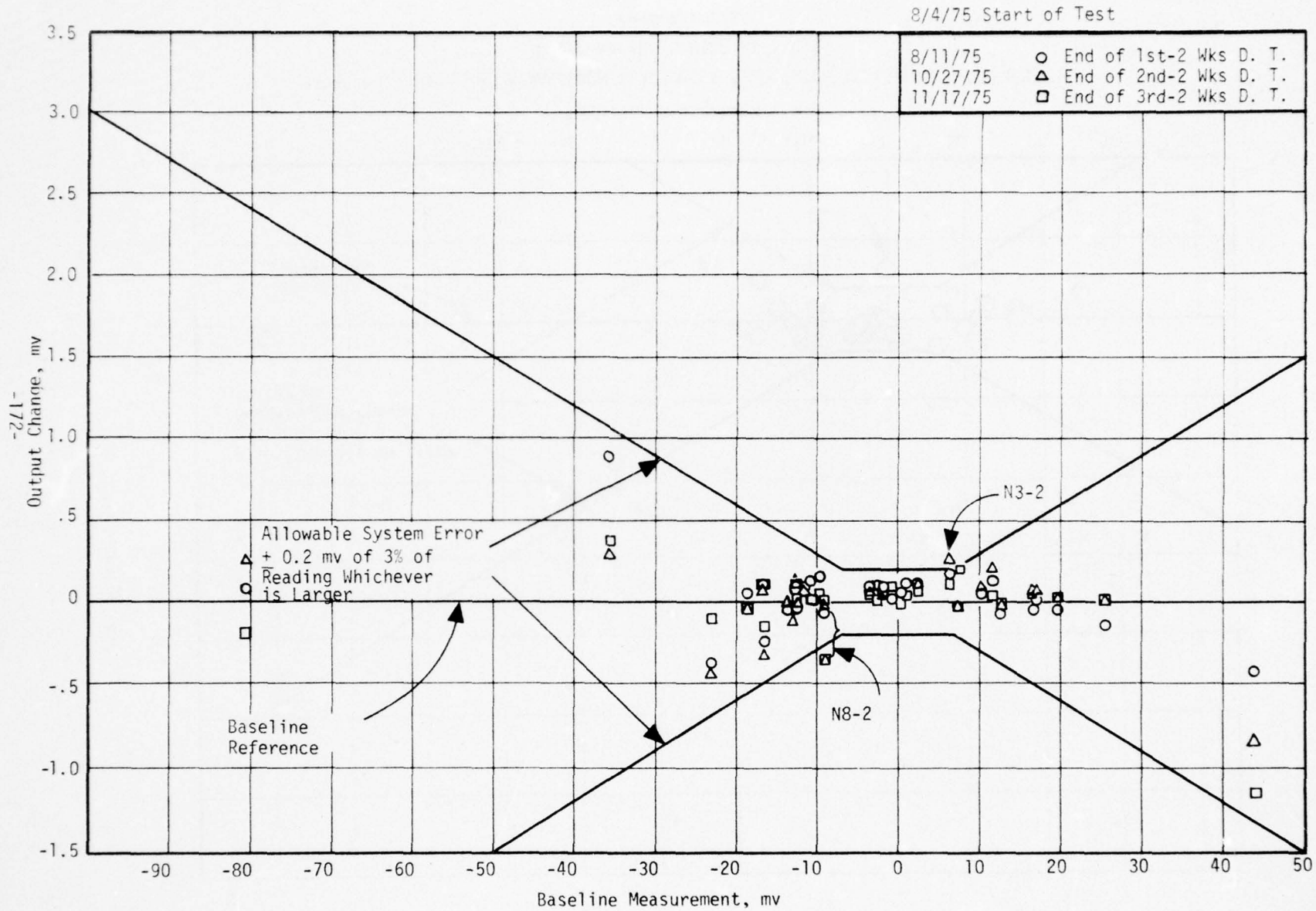

FIGURE 68. DRIFT READINGS FROM TRANSDUCER STIMULATION RESISTORS MEASUREMENTS IN THE BALANCED MODE AT 110°F - EXTENDED TEST

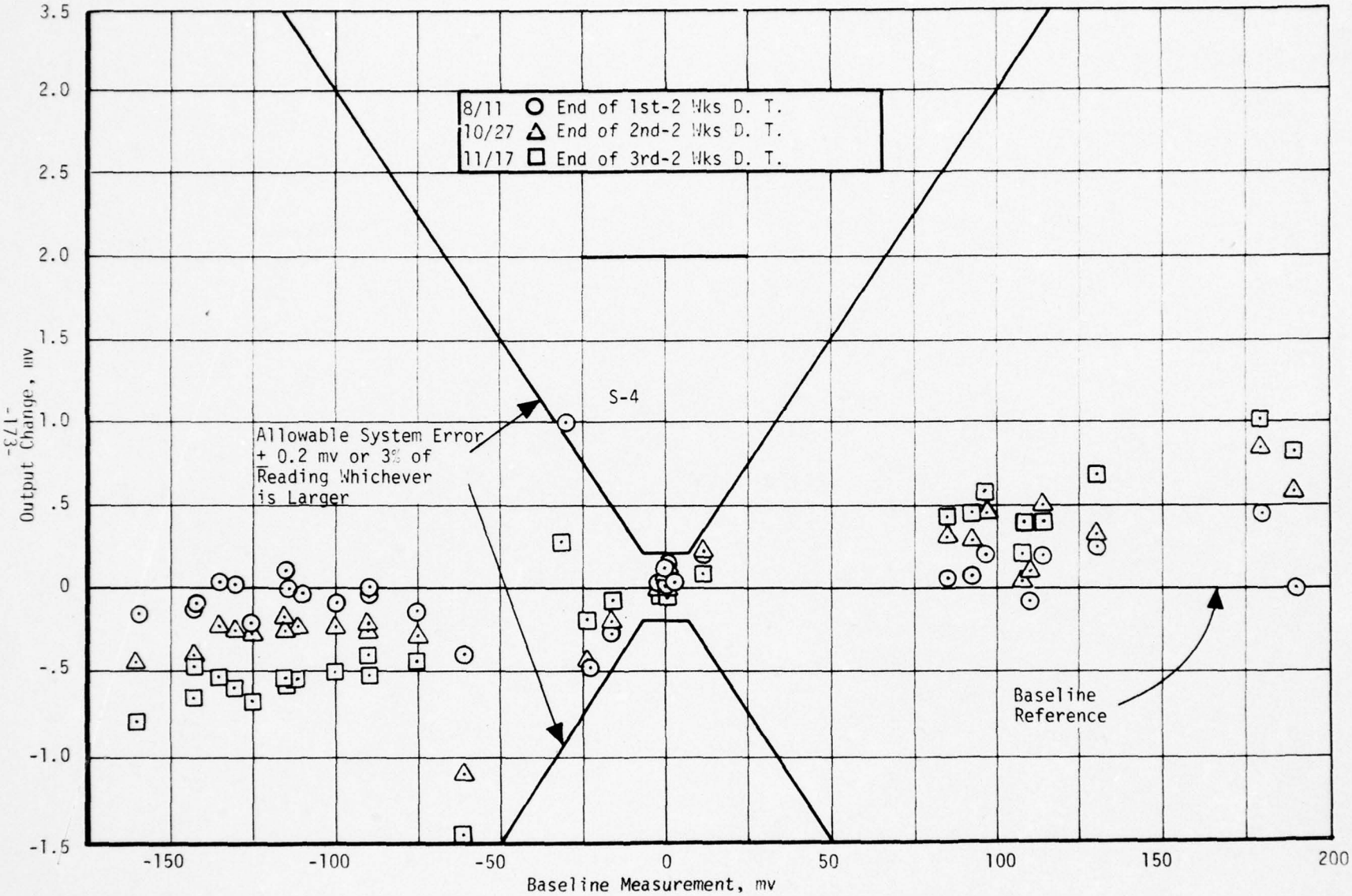

FIGURE 69. DRIFT READING FROM TRANSDUCER SIMULATION RESISTOR MEASUREMENTS IN THE UNBALANCED MODE AT 110°F (8/4/75 TO 11/17/75)

SECTION 10

SOME LABORATORY EVALUATIONS OF

NORMAL STRESS TRANSDUCER ANOMALIES

- Revised Program -

This effort was designed as an exploratory evaluation of normal stress transducers and some of the factors that could modify their behaviors. The studies began with considerations of leadwire junctions then, turning to the transducer itself, considerations were given to semi-conductor gage self-heating, transducer hysteresis and high rate attenuation effects.

The work was conducted in parallel with the diagnostic studies on Motor No. 1 and was somewhat redundant with those efforts. Nevertheless, these laboratory studies brought to light some very interesting aspects of the transducers that should be considered in future transducer development studies. The following discussions were written to serve that purpose.

A. Stainless Steel Leadwire Junctions

As concluded in Section 9, replacing the soldered stainless steel junctions with crimped spade lugs was the major factor in reducing measured drift in the zero stress output of the gages. Some of the background work leading to this corrective action is given below.

1. Nature of the Wire and Junctions

The stainless steel wire was a 33 gage bundle of 15 or 25 strands. This multistrand wire had a resistance of 40 ohms/foot.

The soldered junctions were made on a terminal strip that was attached to the motor case. As shown schematically in Figure 70, the terminal strip had metal solder tabs mounted on an insulating backing. The leadwire junctions were soldered to these tabs.

The supplier delivered the gages with pre-tinned leadwires. The pre-tinning involved a proprietary technique the value of which was not appreciated until the revised program.

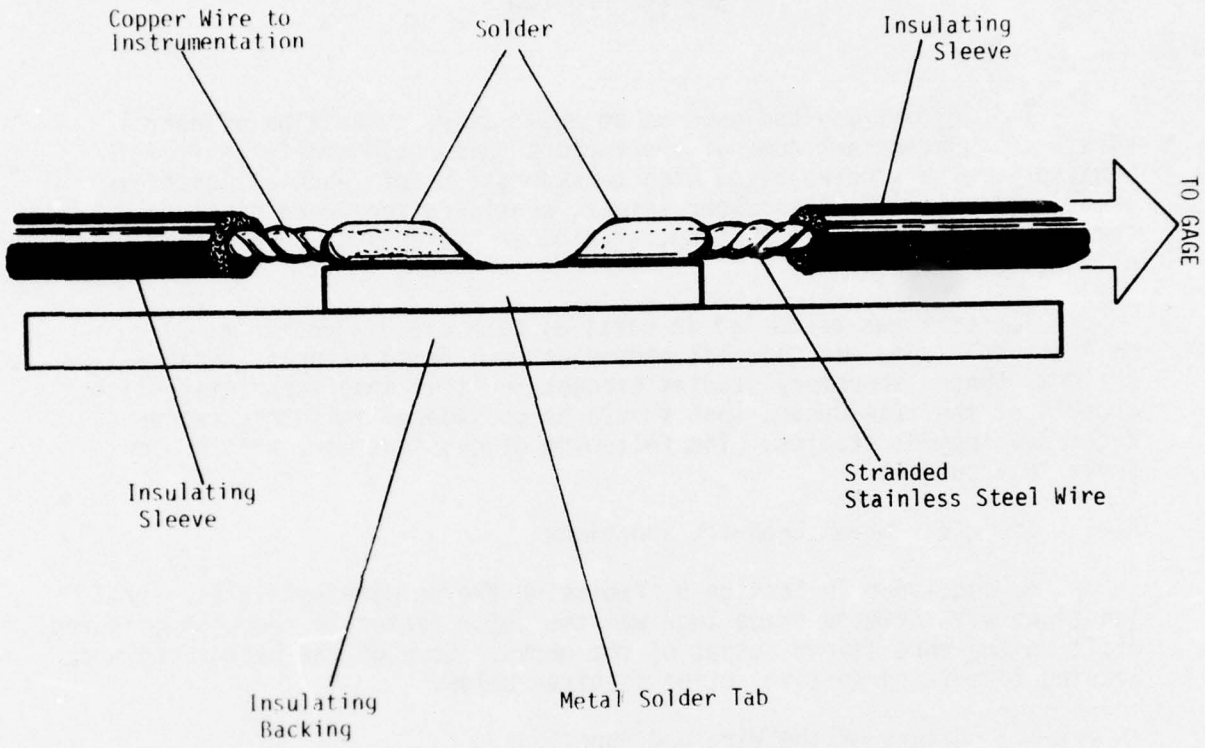

FIGURE 70. STAINLESS STEEL LEADWIRE JUNCTION IN ORIGINAL INSTRUMENTATION

The pre-tinned leads were first soldered to terminals for vacuum calibration of the gages, then they were disconnected, and after installation in the motor, re-soldered to the terminal strip. In this process a few of the leadwires lost their tinning, some were broken, and some were cut to shorter lengths. So it was necessary to strip the insulation and re-tin the ends of these leadwires.

Stainless steel is intractable to normal resin flux solders so that solder joints could only be made if acid flux was used. It was expected that ordinary wiping with a basic solution would remove excess acid and eliminate any residual acid problems. However, the leadwire has a wicking action whereby it holds flux between its many strands. Any unremoved acid has serious long term degrading effects on the junctions; with potentially very large resistance changes. The proprietary technique devised by Konigsberg Instruments, Inc. either prevents or minimizes this wicking action, but ASPC was not made aware of its existence until later in the program.

The degradation of the junction is an oxidative process that is accelerated by moisture (24). The formation of a non-conductive oxide layer between the leadwire and the overlayed solder is the basic feature of this process. This metal oxide can act like a diode when it occurs between dissimilar metals, as in the case of a soldered junction.

The amount of permissible resistance change in a junction was calculated using typical gage circuit parameters. With a limit of $\pm$ 0.1 mv on the gage output, the allowable junction resistance change calculates to be $\pm$ 0.05 ohms. This limit also represents the tolerable unbalanced difference between resistance changes in the junctions associated with the two arms of the gage half-bridge.

2. Tests of Soldered, Crimped and Clamped Junctions

A number of possible leadwire junctions were considered in this program. They were tested in short wire loops with the junctions at both ends. Degradation of the junctions was effected by an accelerated aging which involved high temperature storage in moist air. The test junctions, set up as shown in Figure 71, involved the following test articles:

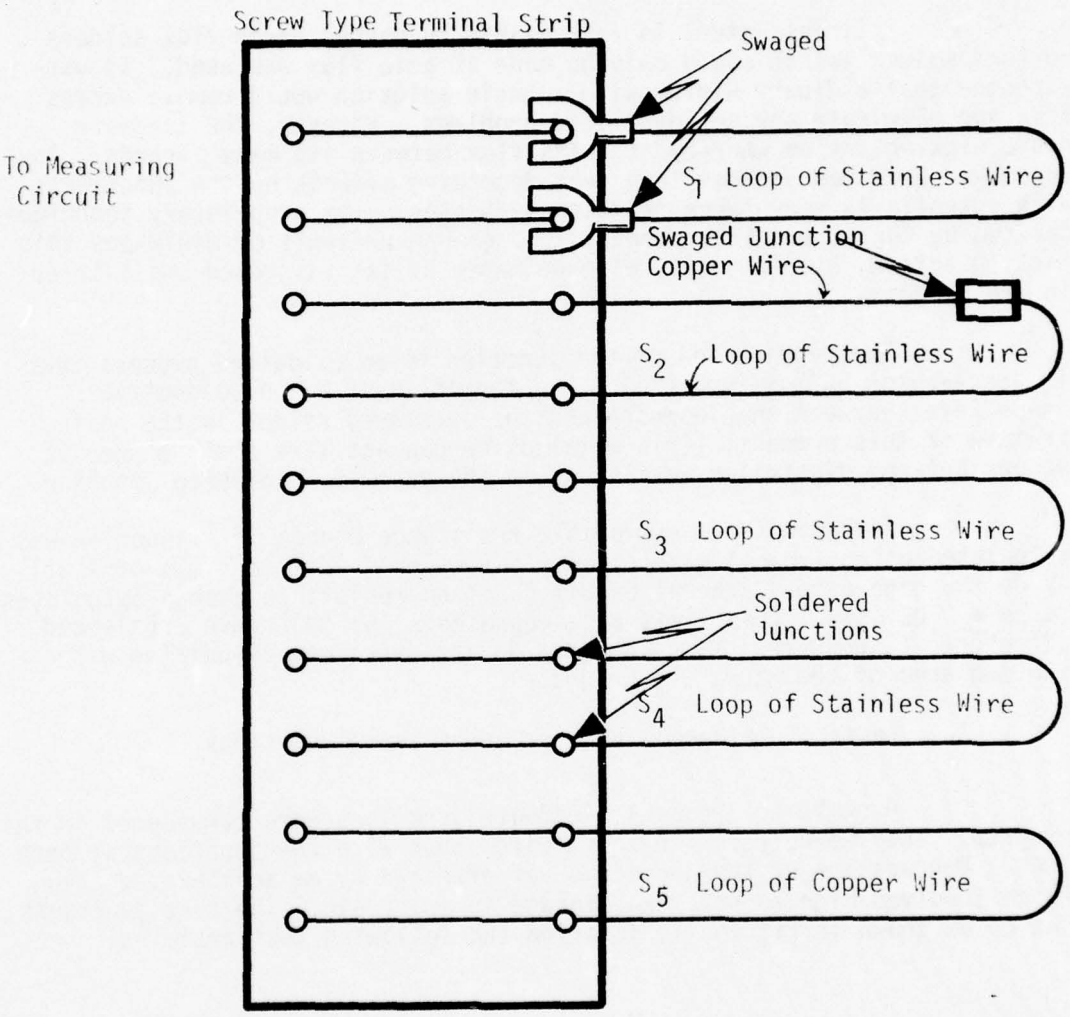

FIGURE 71. DESIGN OF TEST JUNCTIONS

S1 - A loop of stainless steel wire, both ends swaged in spade lugs.

S2 - A loop of stainless steel wire with one end in a swaged interconnection to copper wire and the other clamped under terminal screws.

S3 - A loop of stainless steel wire clamped under terminal screws.

S4 - A loop of stainless steel wire with ends soldered to the spade lugs.

S5 - A loop of copper wire clamped under terminal screws.

This combination of wires and junctions were all attached to a common screw-type terminal strip and was soaked in air at 160°F and 100% R.H. for eleven days in a laboratory oven. At the end of the soaking period, the junctions were removed and allowed to dry out. Figure 72 shows the effect of drying on three junctions and Table 26 gives the tabulated data. The swaged junction tests, S_1 and S_2, did not deteriorate significantly through the test and subsequent drying. On the other hand, the soldered stainless steel junction showed only a small change when first removed from the high humidity, but the resistance increased rapidly with time thereafter. It changed by 13% in the first eight hours. The data are interpreted as an effect of the acid flux catalyzing oxidative degradation of the stainless steel joint.

The ranges of the resistance measurements reported in Table 26 are summarized below.

	Resistance, ohms				
Range	S_1	S_2	S_3	S_4	S_5
Upper Limit	16.47	19.25	15.22	18.20	0.0666
Lower Limit	16.27	19.10	15.04	15.50	0.0625
Delta	0.20	0.15	0.18	2.70	0.0041

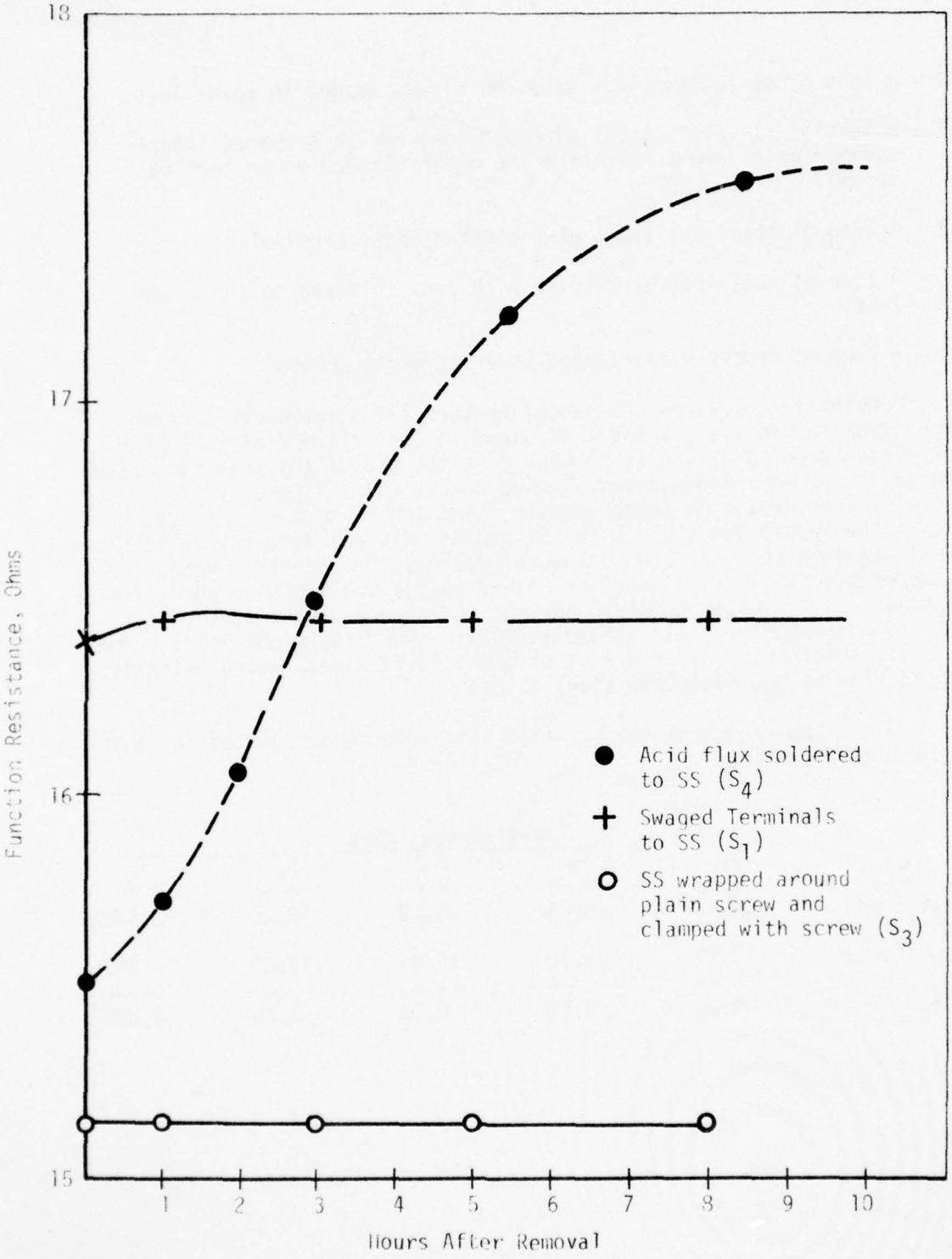

FIGURE 72. THE EFFECT OF DRYING AFTER 9 DAYS AT 160°F AND 100% RH

TABLE 26

RESISTANCE READINGS OF TEST JUNCTIONS IN OHMS

Date	Time	Resistance, ohms S_1	S_2	S_3	S_4	S_5
12/18/74	0900	16.31	19.22	15.19	-	-
12/18/74	1200	16.37	19.25	15.22	-	-
12/19/74	0800	16.32	19.24	15.15	15.51	-
12/19/74	1100	16.31	19.19	15.14	15.50	.0625
12/19/74	1700	16.38	19.18	15.14	15.51	.0625
	Sent units to 160°F at 100% RH at this point.					
12/30/74	Removed from box at 0830					
12/30/74	0905	16.45	19.13	15.10	15.72	.0625
12/30/74	1115	16.45	19.17	15.11	16.51	.0637
12/30/74	1330	16.47	19.25	15.13	17.21	.0627
12/30/74	1625	16.40	19.24	15.15	17.57	.0666
12/31/74	0820	16.27	19.10	15.04	17.47	.0651
12/31/74	1135	16.47	19.20	15.12	17.96	.0651
	Tension experiment: Pulled on each lead then re-measured.					
12/31/74	1135	16.37	19.19	15.13	17.80	.0651
12/31/74	1135	16.41	19.16	15.12	18.20	.0651

These data show that the stainless steel wires with swaged spade lugs and clamped junctions (S_1, S_2 and S_3) are virtually the same, while the soldered junctions, S_4, are distinctly inferior.

The copper wire tests were performed to show that under this aging small changes can occur in these junctions, also. But the changes were quite negligible with respect to gage requirements, $\pm$ 0.05 Ω.

To explain the behavior of S_4 it is suggested that one or more of the strands of the stainless steel wire was completely isolated from the other wire strands, Figure 73. If the soldered length of wire was reduced, such as changing the solder tab from 1/4 in. to 1/8 in. for example, then the maximum change in resistance of the wire that could occur is $\sim$1%. On the other hand, if one strand in eighteen is removed a 6% change in resistance could result. Since a 13% change was observed, it was concluded that at least two strands or the equivalent were isolated from the remainder of the bundle. Further testing showed that more resistance change could be developed by bending the wire near the junctions thus modifying the contact between the strands and the solder. As shown in Table 26, a slight movement of the wire caused a change from 17.8 to 18.2 ohm.

B. FEATURES OF THE NORMAL STRESS TRANSDUCER REQUIRING ASSESSMENT

An exhaustive listing of problem areas has not been attempted here, since a simplified picture is both sufficient and easier to follow. The make up of the transducer is considered first, then a listing of the primary observations is given. Some of the areas noted have been assessed and are discussed in a later sub-section.

1. Make-up of the Normal Stress Transducer

The primary elements of the normal stress transducer are the semi-conductor strain gages, since it is these gages that sense the deformations of the diaphragm and control the electrical output of the unit.

These silicon semi-conductors were bonded both externally and internally to the diaphragms of the normal stress transducers as illustrated in Figure 74. Bonding of the gages was effected using an epoxy adhesive cured at 350°F. Because of thermal expansion differences, cooling the transducer to room temperature produces differential stresses in the semi-conductors and in the diaphragm. Creep of the semi-conductor and the long term drift of the zero stress output of the transducer (Appendix O) are associated with these thermal stresses.

AD-A032 635 AEROJET SOLID PROPULSION CO SACRAMENTO CALIF F/G 21/9.2
FLEXIBLE CASE - GRAIN INTERACTION IN BALLISTIC WEAPON SYSTEMS. --ETC(U)
OCT 76 K W BILLS, S W JANG, H LEEMING F04611-72-C-0055
UNCLASSIFIED ASPC-1953-81-F-VOL-1 AFRPL-TR-76-57-VOL-1 NL

3 OF 3
AD
A032635

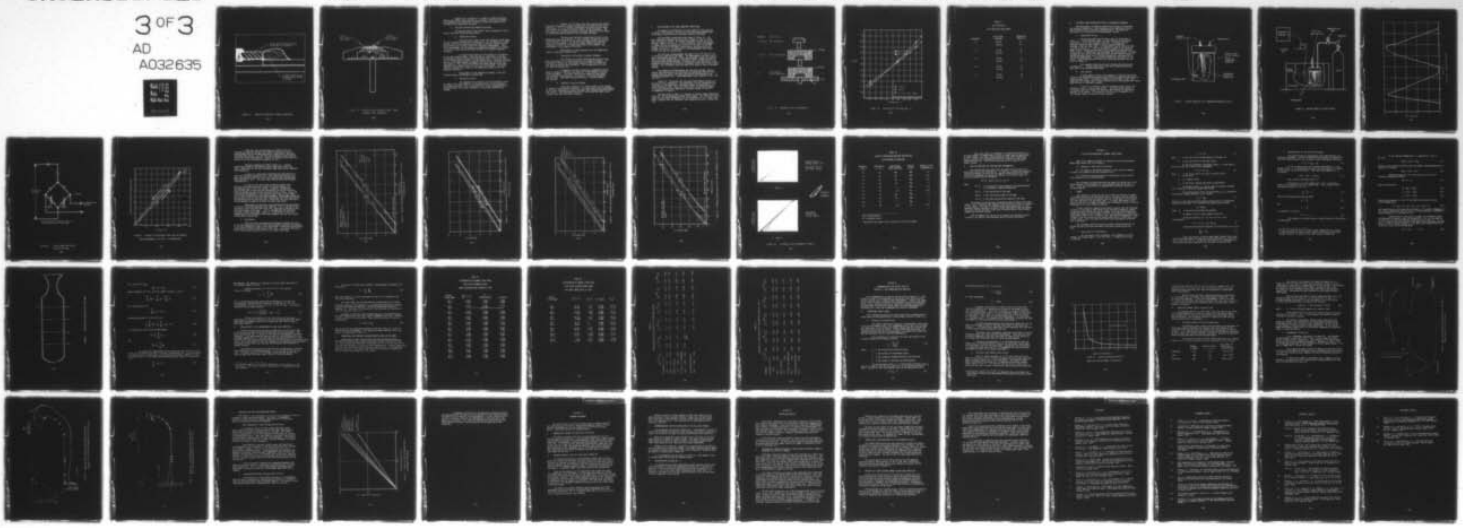

END

DATE
FILMED
1-77

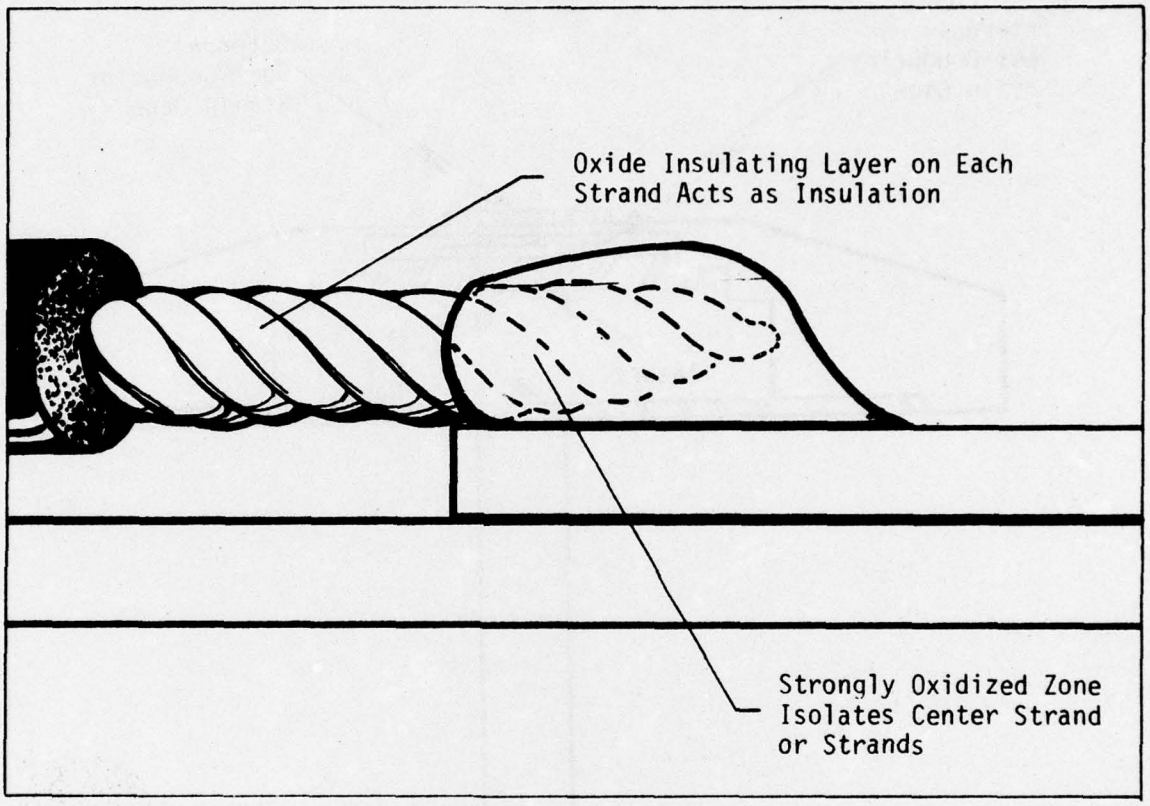

FIGURE 73. SUGGESTED TUNNELING OF STAINLESS JUNCTIONS

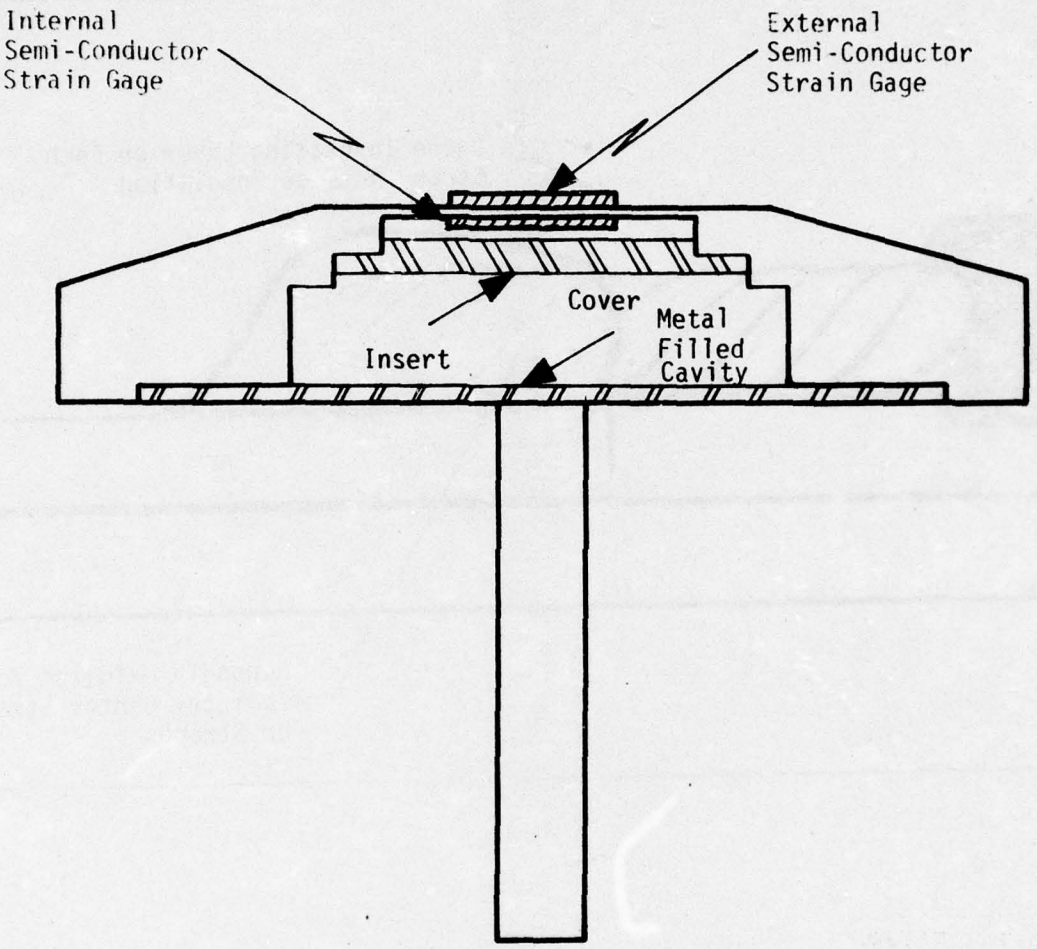

FIGURE 74. MOUNTING OF SEMI-CONDUCTOR STRAIN GAGES ON NORMAL STRESS TRANSDUCER

Embedding the transducer in a rubber or propellant medium exposes the external semi-conductor to a possible corrosive environment. This embedment also introduces viscoelastic interaction effects which increase as the temperature decreases.

2. Possible Problem Areas Needing Assessment

The previous model of the normal stress transducer is sufficient to make the following observations.

a. Temperature Effects

The resistance values of the semi-conductor strain gages are very strongly affected by the temperature. So, the mounting of gages on both sides of the diaphragm places them in different thermal environments which could seriously complicate transducer measurements. Thus, stress measurements in the presence of temperature gradients are probably in error; an error that would become greater as the therm-l gradient increases.

A complicating feature of this problem is self-heating of the semi-conductor gage. Since the gage is effectively a resistor, the passage of current through the gage should cause it to evolve heat, with a corresponding increase in its resistance value. Since the two gages are not in the same thermal environment they should not dissipate this heat equally. Thus, possibly different resistance changes in the semi-conductor strain gages could occur from this self-heating. The effect would be expected to be larger as the temperature change on the semi-conductor increases.

Measurements of the temperature changes in the self-heating process are reported in Section 10C.

b. Hysteresis Effects

One component of transducer drift and hysteresis would be creep of the semi-conductor strain gage relative to the diaphragm. As pointed out before, this is an effect that is both recognized and is now being taken into account (Appendix O) by new gage manufacturing methods.

However, for the gages like those used on the Flexible Case-Grain Interaction program, the questions of hysteresis are still viable ones. As it is presently understood, hysteresis effects would occur because of strong viscoelastic effects in the transducer. The only sources of such effects would be the epoxy adhesive and the rubber (or propellant) potting material that surrounds the gage.

The epoxy was expected to become more brittle as the temperature drops below ambient, so the strongest viscoelastic effects of this material should be at the upper test temperatures (maximum of 130°F) for this program. The IBT-115 rubber potting increases its viscoelastic effects as the temperature drops, which suggests test measurements in the range of 0° to 30°F.

Measurements of gage hysteresis over the temperature range are reported in Section 10D.

c. Attenuation of High Rate Transducer Response

The viscoelastic effects mentioned above have an even more significant role in the attenuation of transducer response. If viscoelastic effects can retard gage responses, then the higher the test rate the greater the retardation. This characteristic is also considered in Section 10D.

A companion to these viscoelastic attenuation effects would be adiabatic heating of the material in the immediate vicinity of the transducer. This would involve local heating of the exposed semi-conductor strain gage by a few degrees, if the pressurization rate was high. Additional heating would occur if casting bubbles were present.

d. Barometric Pressure Changes

Since the transducer is a closed system it will respond to changes in the barometric pressure. For small grain stress measurements, or for tests conducted at various altitudes, these changes could be significant factors. No experimental analysis of this factor was made on the Flexible Case-Grain Interaction program.

C. SELF-HEATING OF THE SEMI-CONDUCTOR STRAIN GAGES

The amount of self-heating in a semi-conductor strain gage was estimated from comparison of precision resistance measurements made on the gages using pulsed and continuous powering techniques.

The transducers tested were those shown in Figure 75. The bare transducer contained two active half bridges 1-1 and 1-2 which were individually tested. The potted transducer also had two active bridges, numbers 2-1 and 2-2. A third transducer, which was embedded in rubber potting and mounted on a section of case wall in the same fashion as the full-scale motor installations, had two active half-bridges, 3-1 and 3-2. At some point in the measurements half-bridge 3-2 was lost due to a broken wire.

The first set of measurements was made at 74 $\pm$ 2°F after 22.5 hr of electrical powering of the gages. The measurements involved a resistance substitution technique. First, the transducer output was measured then a precision decade box was substituted (using a simple switch) for the gage element being evaluated. Following this, the resistance of the decade box was adjusted to bring the transducer output back to the original reading. This resistance value was taken to be equal to that of the gage element.

The second set of measurements was made with the gage held at thermal equilibrium while its resistance was determined using 90 microsecond electrical pulses (the duty cycle was 90 microseconds on and 100,000 microseconds off). These measurements were conducted at 32°, 78°, and 110°F.

Figure 76 illustrates the resistance measurements plotted as a function of test temperature. The temperature rise was determined from the graphs as the temperature difference between the measurements at a given resistance value. Thus, the steady-state, continuously powered strain gage elements gave temperature increases between 11 and 21°F, as summarized in Table 27.

The data given in Table 27 indicate a slightly larger temperature rise, 3°F, for the externally mounted strain gages. This effect was anticipated for the potted transducers, but its occurrence in 1-2, a bare transducer, suggests that the individual semi-conductor may play a strong role, also.

TRANSDUCER	DESCRIPTION
1-1 and 1-2	BARE TRANSDUCER
2-1 and 2-2	POTTED TRANSDUCER
3-1	CASE-MOUNTED, POTTED TRANSDUCER

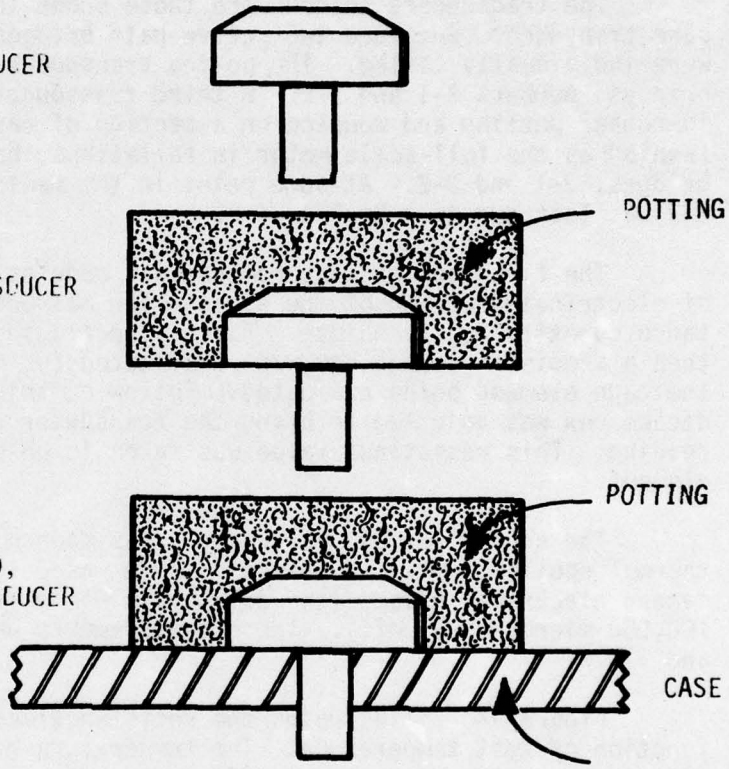

FIGURE 75. LABORATORY TESTS ON TRANSDUCERS

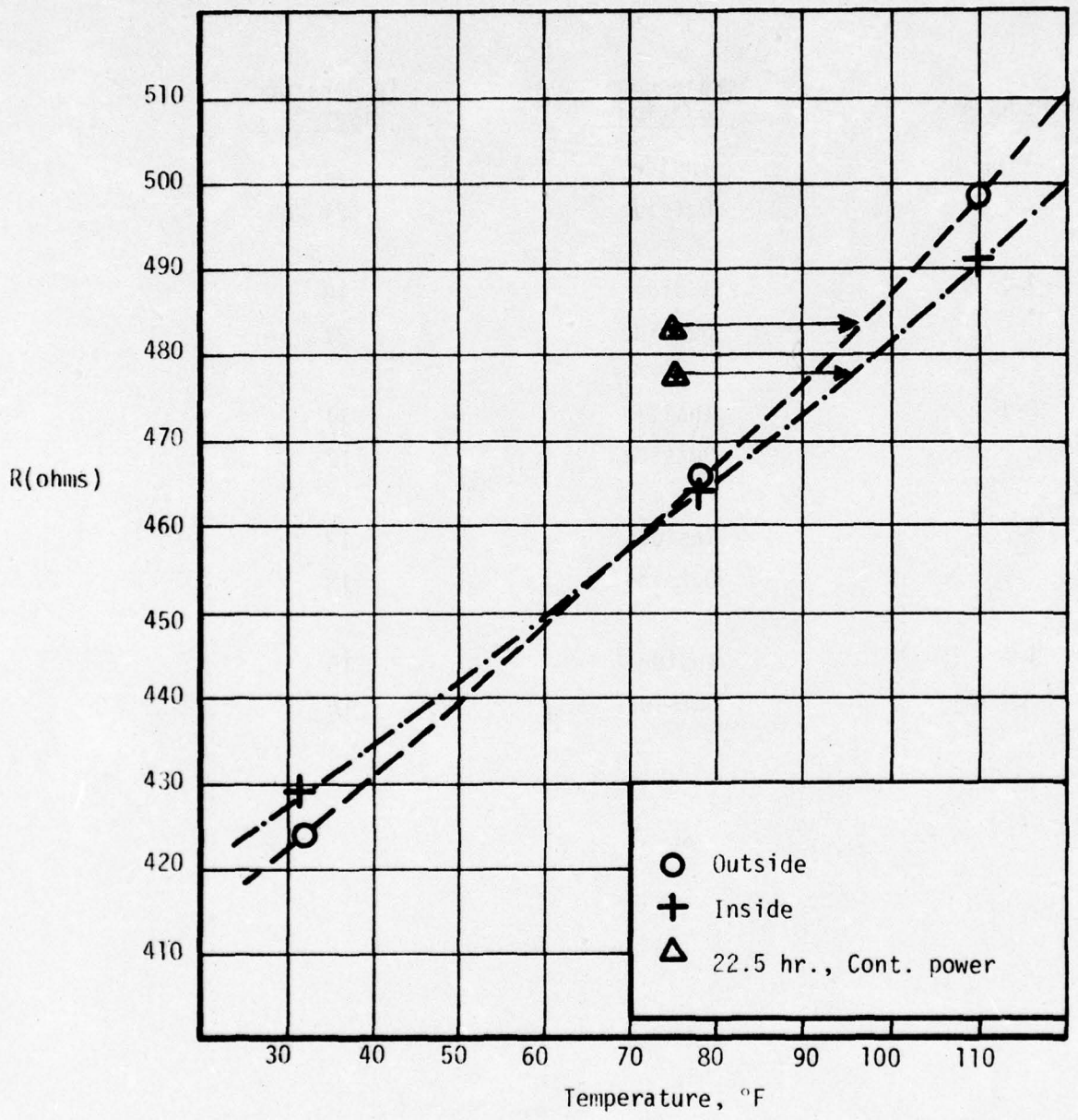

FIGURE 76. THERMAL OFFSET FOR BARE GAGE 1-1

TABLE 27

SELF-HEATING OF

SEMI-CONDUCTOR STRAIN GAGES

Transducer	Strain Gage Location	Temperature Rise, °F
1-1	Inside	21
	Outside	21
1-2	Inside	18
	Outside	21
2-1	Inside	11
	Outside	17
2-2	Inside	13
	Outside	13
3-1	Inside	15
	Outside	16

D. HYSTERESIS AND ATTENUATION EFFECTS IN TRANSDUCER RESPONSES

The measurement, at moderate pressurization rates, of hysteresis and response attenuation in the transducers was accomplished using the pressure bomb and test procedures described below. Following this description is a discussion of the experimental results.

1. Experimental Set-up

The pressure bomb used for these tests is illustrated in Figure 77. The transducers under test were attached to the center post which, in turn, was attached to the cap. A thermocouple was inserted through the bomb sidewall, while a pressure gage was attached to the gas input line. The experimental set-up using the bomb is given in Figure 78. With the transducers mounted in the pressure bomb, suitable connections were made to the recorder and gas pressurization source. A temperature bath surrounded the pressure bomb. Although nitrogen gas was used for the pressurization, various working fluids surrounded the gages under test, including nitrogen gas, ethylene glycol, and liquid polybutadiene. Pressure was effected by hand control of the valves. Typical pressure-time traces for these hand operated runs are given in Figure 79.

The transducer measuring circuit followed the design given in Figure 80. Various power sources and various measuring methods were used in the following experiments.

2. Test Results

A large number of tests were conducted to show that hysteresis occurs in the transducer measurements when they are conducted under moderate pressurization rates. The primary inference from the data is that tests under the still higher rates of motor pressurization could produce very strong modifications of transducer response.

Figure 81 contains a plot of transducer output versus test pressure for unit 3-1 when tested at 32°F. The pressure was applied in 10 seconds, held for 5 minutes at 200 psig, then returned to atmospheric pressure in 10 seconds. The hysteresis in the trace is apparent, as is the residual output of the unit at zero pressure.

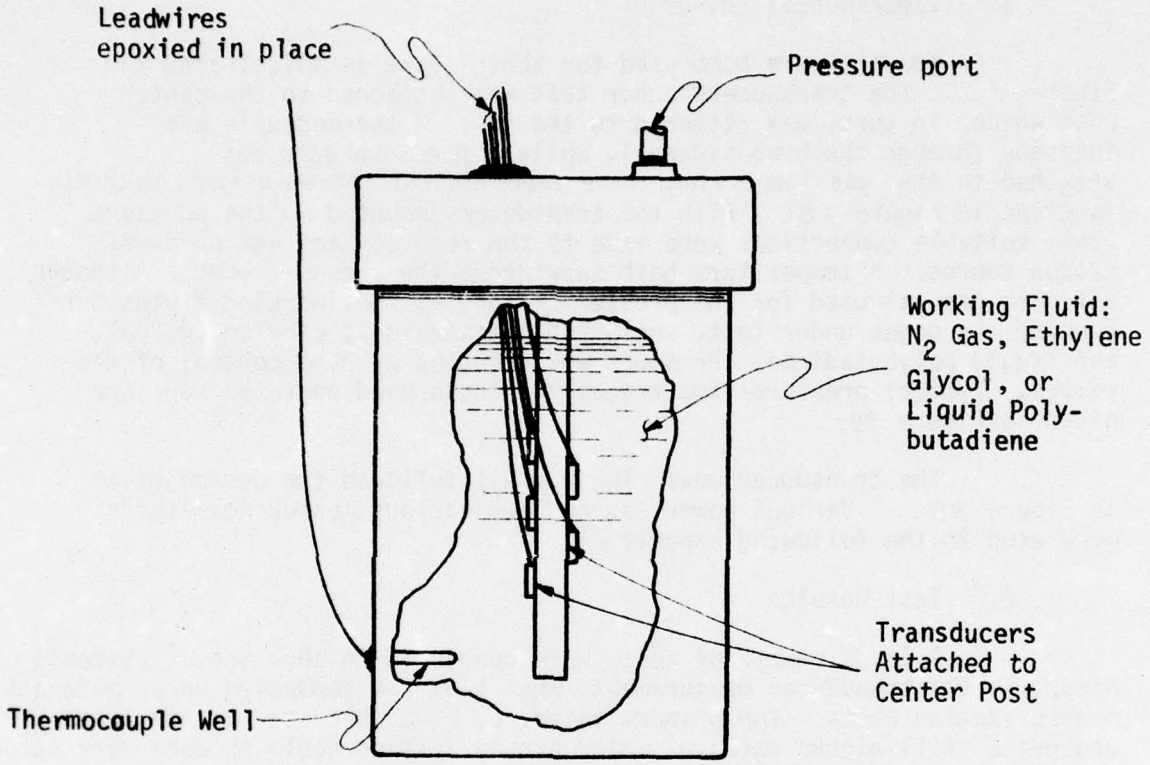

FIGURE 77. PRESSURE BOMB WITH TEST TRANSDUCERS MOUNTED IN PLACE

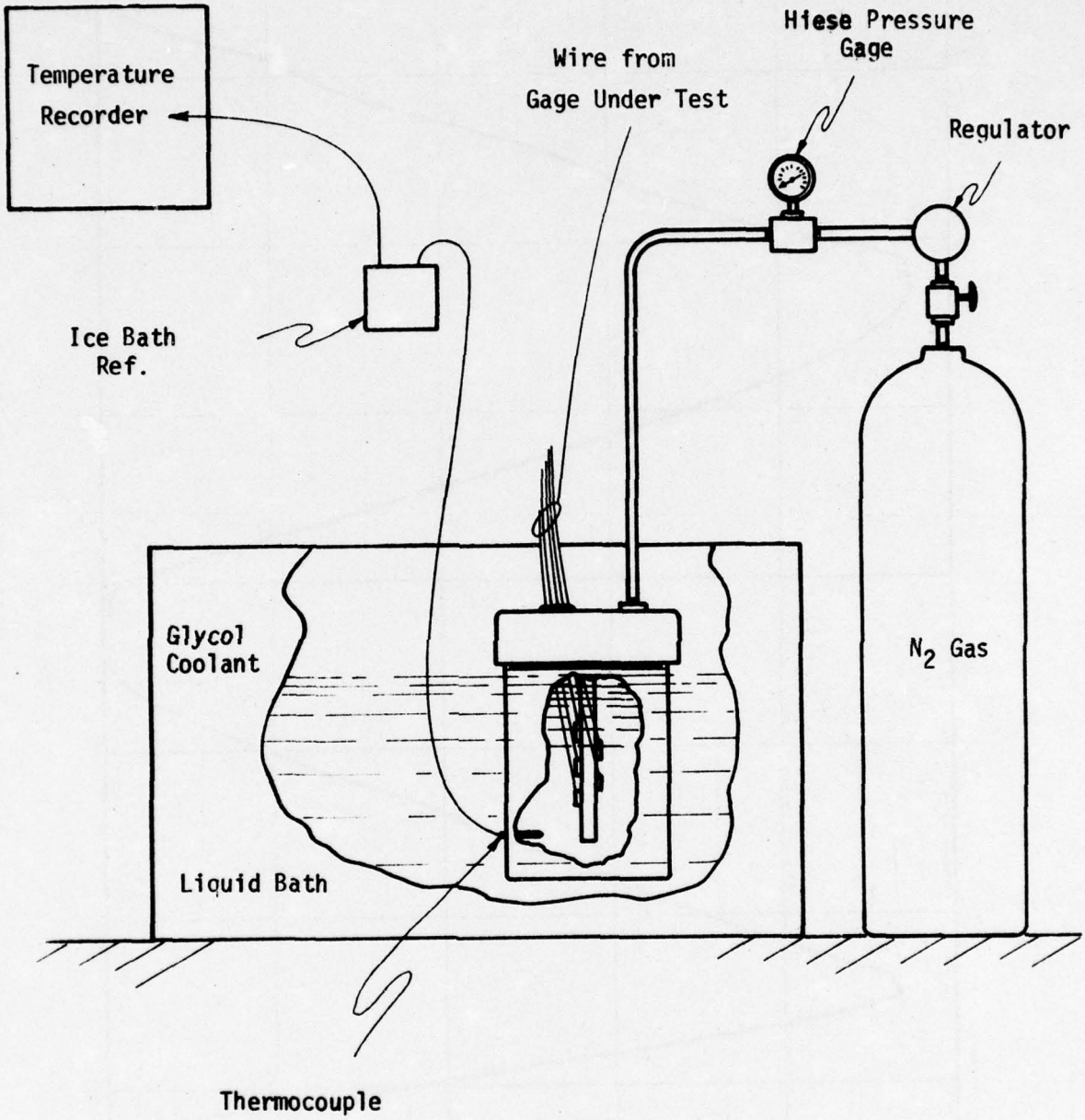

FIGURE 78. PRESSURE BOMB SET UP FOR TESTING

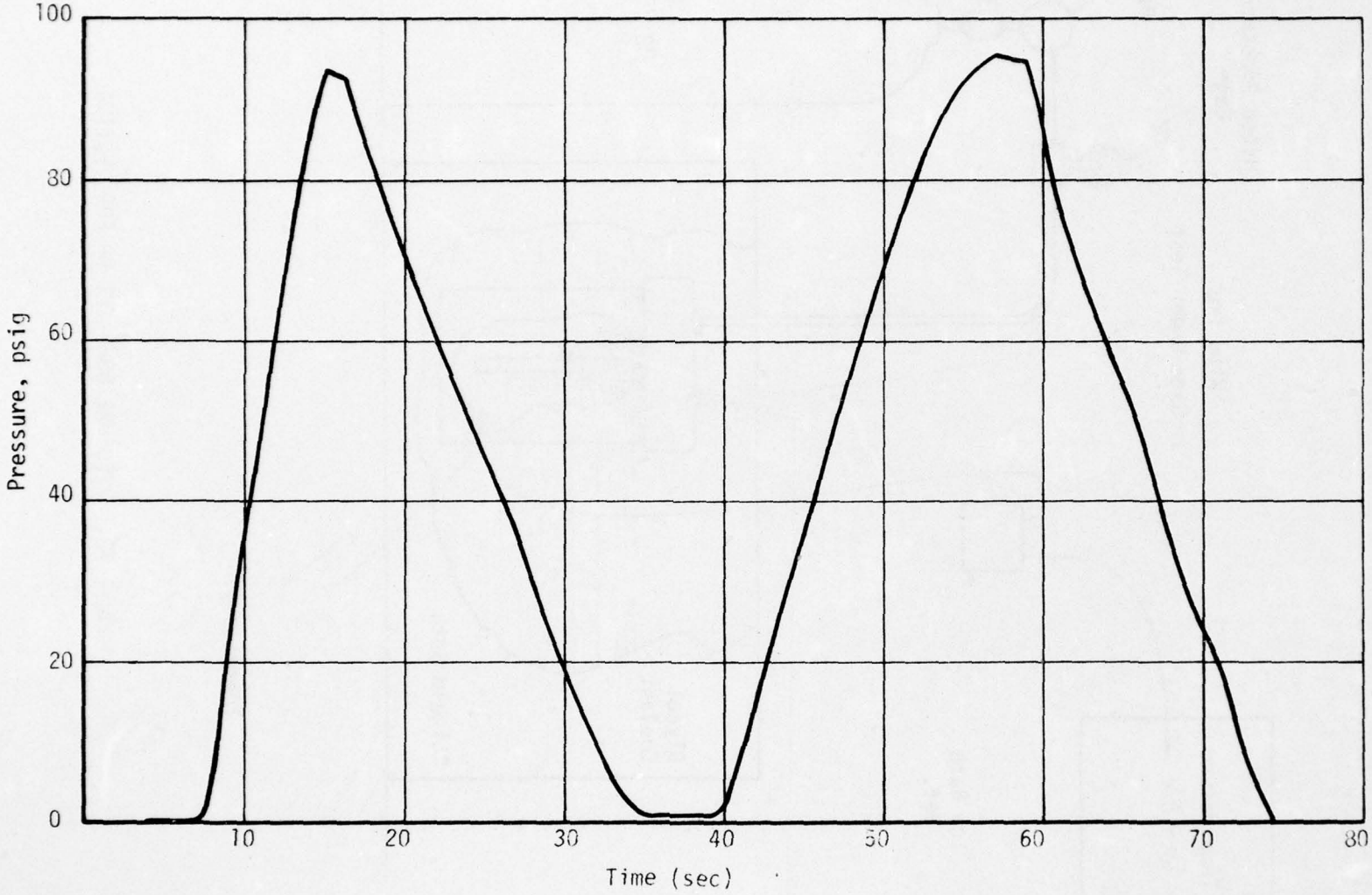

FIGURE 79. PRESSURE TIME TRACE

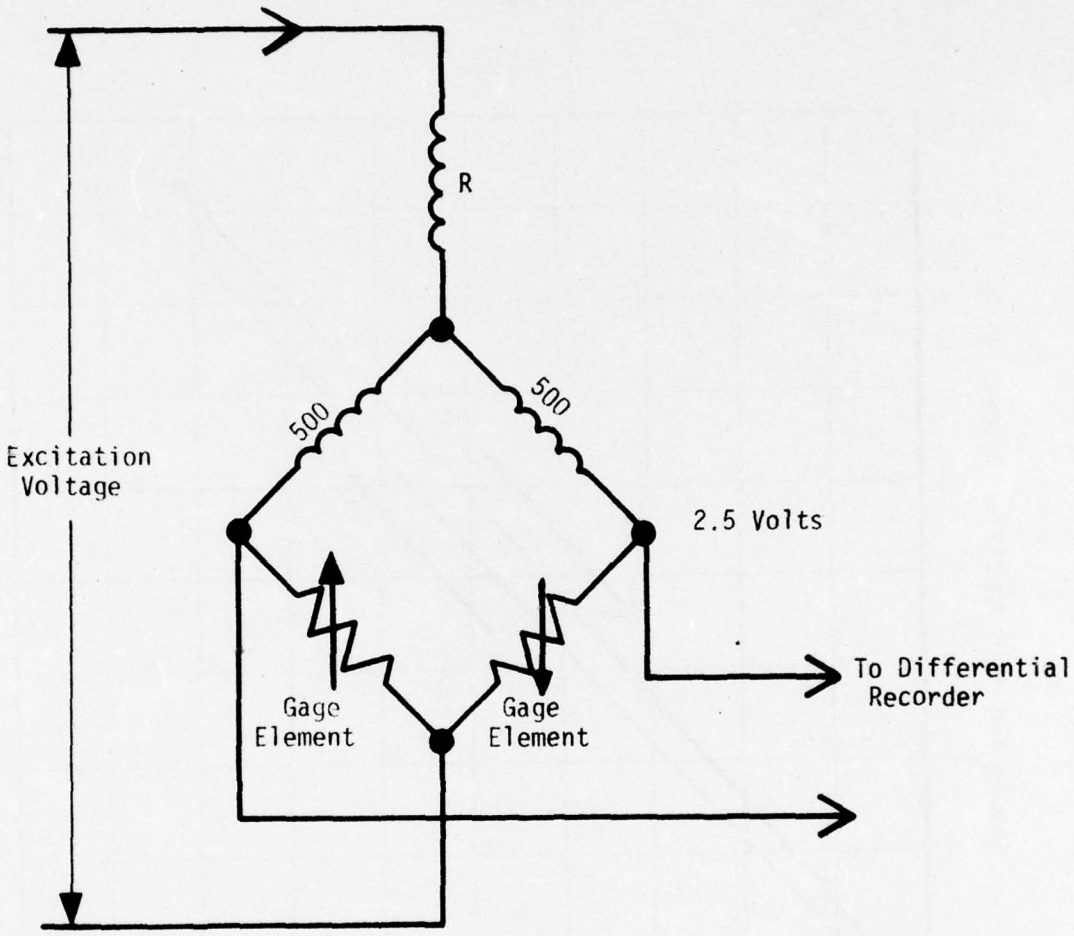

R was adjusted to attain as near 2.5 volts as possible for each gage.

FIGURE 80. BRIDGE COMPLETION CIRCUIT USED FOR EACH GAGE

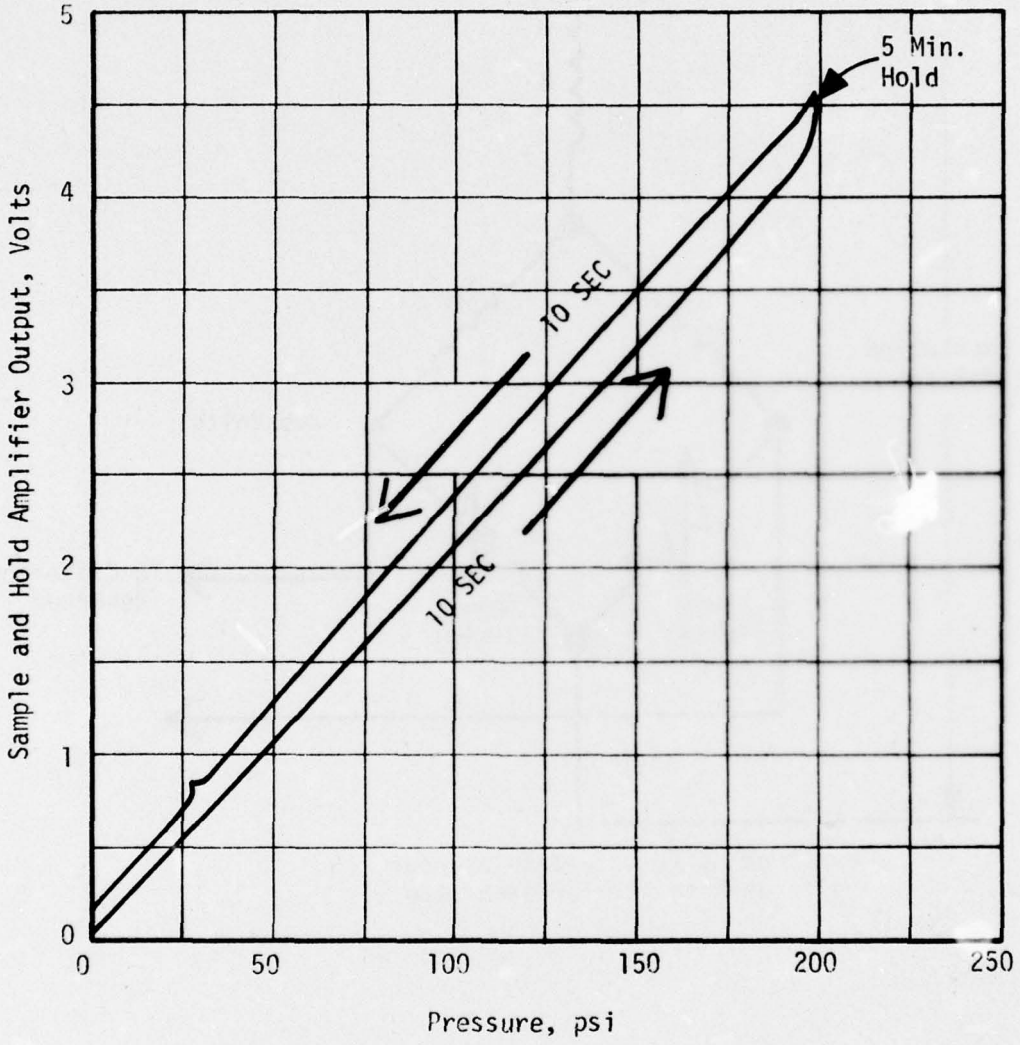

FIGURE 81. HYSTERESIS AND RESIDUAL OFFSET FOR CASE MOUNTED POTTED TRANSDUCER 3-1 AT 32°F - IN NITROGEN GAS

Since this test was performed in a working fluid of nitrogen gas there was concern that adiabatic heating and cooling during pressurization and depressurization, respectively, might have influenced the results. So, the tests were repeated in both ethylene glycol and liquid polybutadiene. Figures 82, 83 and 84 show tests conducted on the bare and potted transducers at 130°F.

The bare transducer at 130°F, Figure 82, evinces significant hysteresis and residual offsets that persist for long times. Other tests on the bare transducer shows these effects decrease with temperature.

Figure 83 illustrates essentially the same behavior at 130°F for the potted transducer, 2-2. But, Figure 84 contains plots where the hysteresis effects at 8°F have significantly increased over those obtained at 130°F. The short time residual offset was markedly increased also.

In some of this testing the transducer output versus pressure traces were distorted, Figure 85, causing concern for the response times of the x-y recorder. Actually, the behaviors near the two ends of the curve are considered to be fairly realistic, while the middle portions of the curve are likely in error. Figure 86 contains two photographs of oscilloscope traces taken in tests where still higher pressurization rates were attempted. Marked gage hysteresis effects may be seen at the point where the pressure was first applied and the pressurization rate was very high. After that, the rate slows down and the hysteresis seems to be about like those seen above.

Measurements of hysteresis were obtained from two transducers, 1-1 and 2-1, using the departure from linearity. This is defined as the deviation of the curve from the center line, expressed as percent of the full-scale output of the gage. Table 28 summarizes the deviations attained in these experiments. There is a large effect of rate and temperature and no noticeable effect when changing from the fully exposed to the rubber covered gage.

3. Conclusions

High rate motor pressurization experiments (minutes per cycle at -9°F and seconds per cycle at 79°F) would require calibration corrections to any data generated by gages of the type tested if linearity and hysteresis errors must be limited to the range of 1% or less. Such errors can run as high as 15% without correction at the 1 sec./cycle rate range.

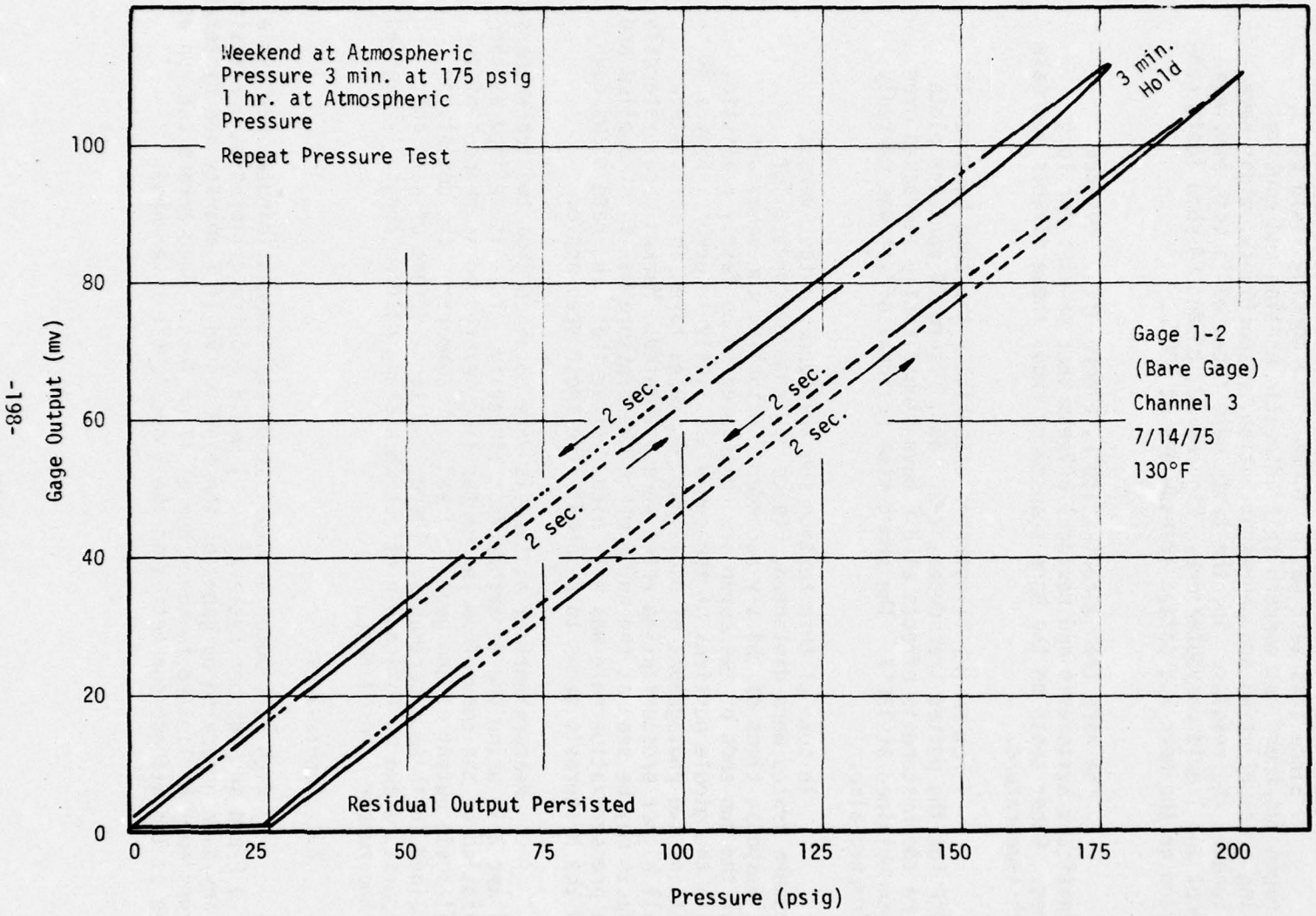

FIGURE 82. HYSTERESIS AND RESIDUAL OFFSET FOR BARE TRANSDUCER 1-2 AT 130°F
- IN ETHYLENE GLYCOL -

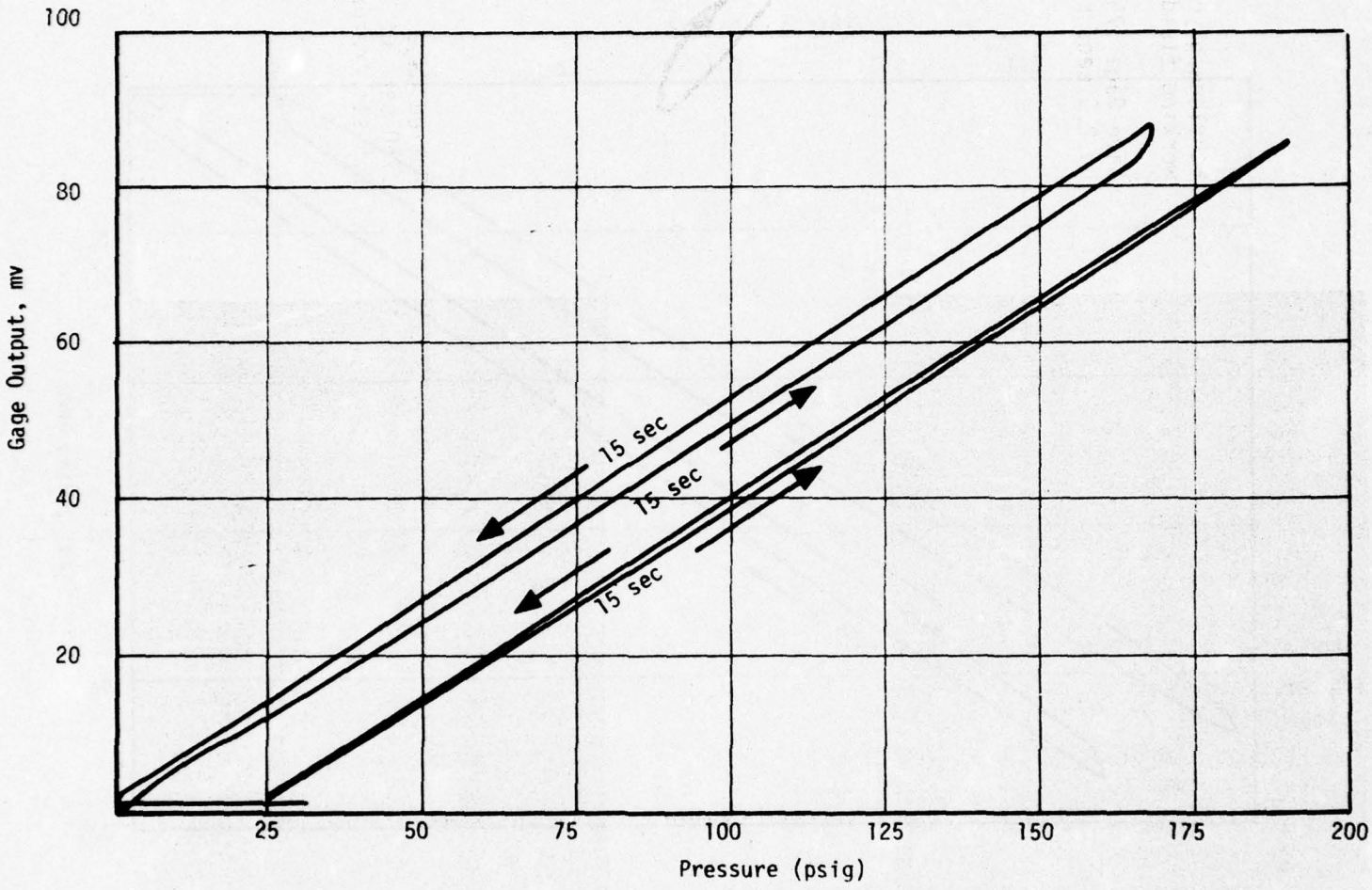

FIGURE 83. HYSTERESIS AND RESIDUAL OFFSET FOR POTTED TRANSDUCER 2-2 AT 130°F

- IN ETHYLENE GLYCOL -

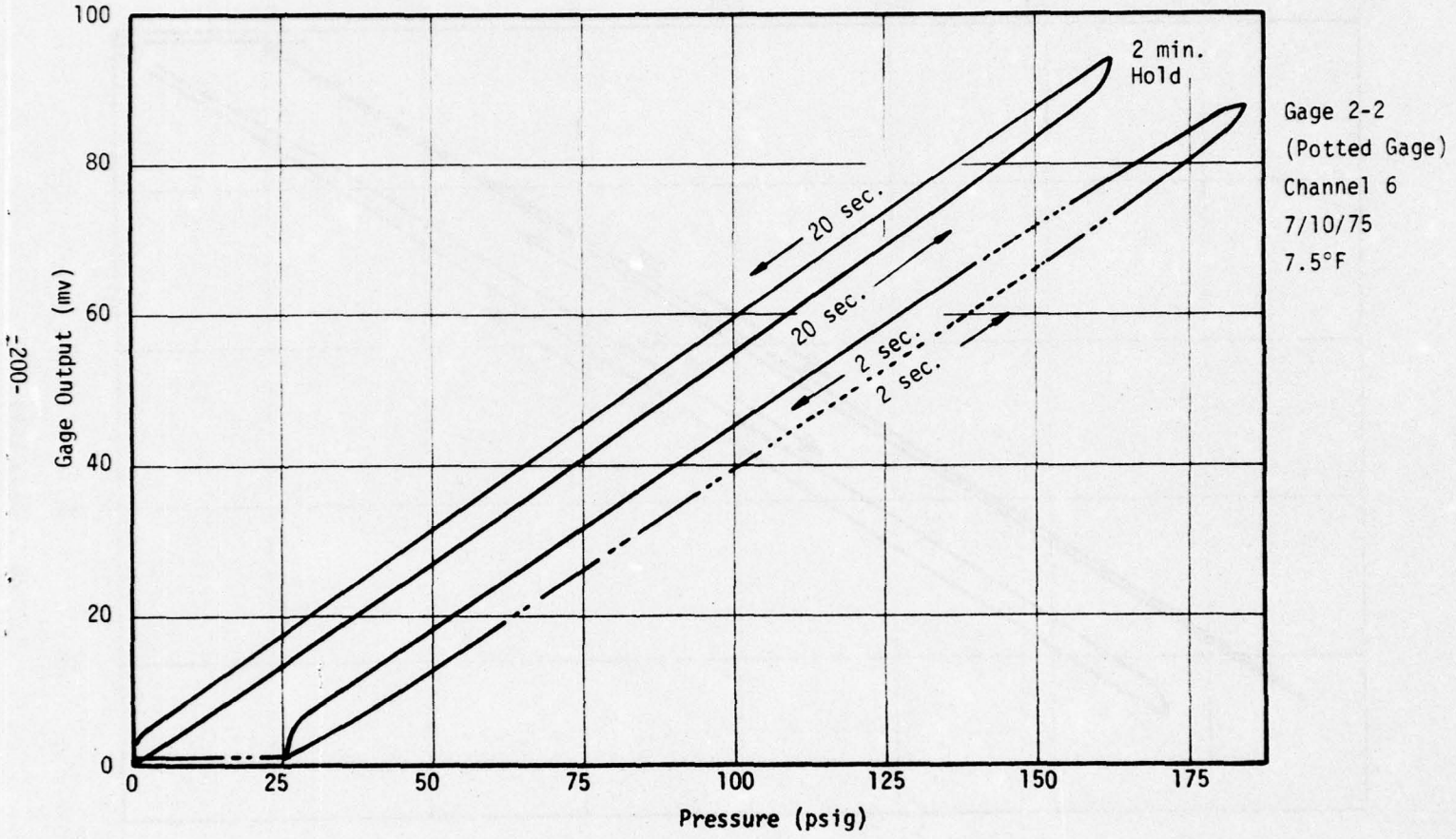

FIGURE 84. HYSTERESIS AND RESIDUAL OFFSET FOR POTTED TRANSDUCER 2-2 AT 8°F
- IN ETHYLENE GLYCOL -

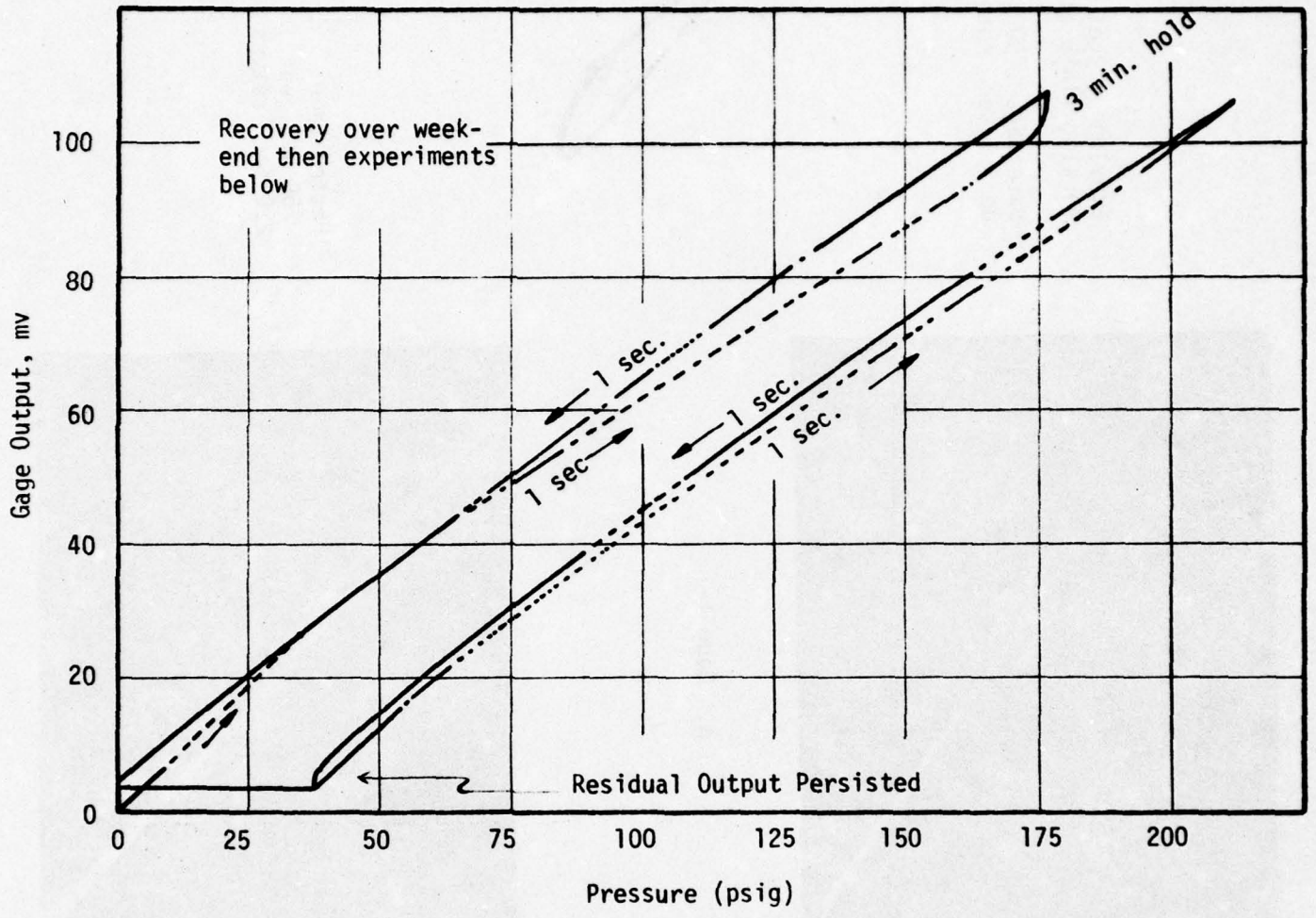

FIGURE 85. HYSTERESIS AND RESIDUAL OFFSET FOR BARE TRANSDUCER 1-1 AT 130°F

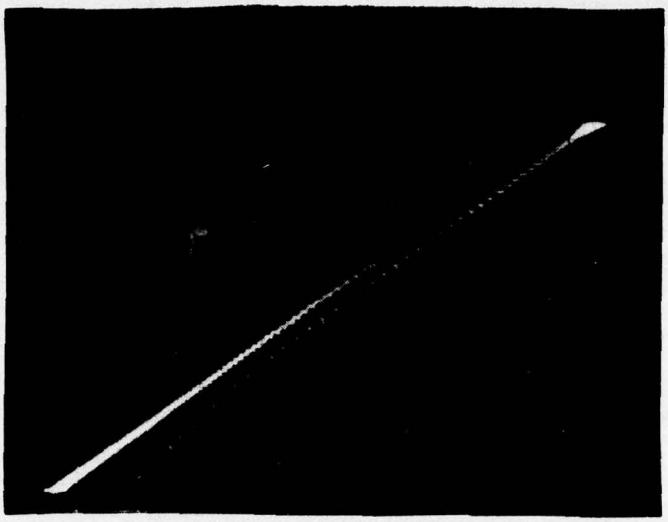

Standard Gage
25 psi/Division

Ethylene glycol
working fluid at 24°C

Bare Gage .750 sec.
up 2.5 sec. return

a. Gage 1-1

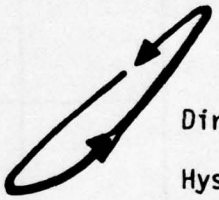

Direction
of
Hysteresis

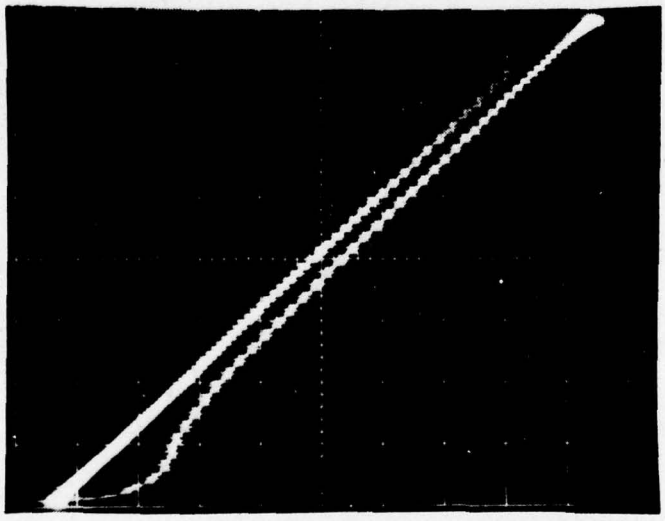

Standard Gage
25 psi/Division

Potted Gage
.750 sec. up
2.5 sec. return

b. Gage 2-1

FIGURE 86. HYSTERESIS TESTS FOR GAGES 1-1 AND 2-1

TABLE 28

EFFECT OF PRESSURIZATION RATE AND POTTING

UPON RESPONSE ATTENUATION

Transducer No.	Temperature °F	Approximate Rate, sec/Cycle	Working Fluid	Departure from Linearity*, %
1-1	-9	120	PBD	1.7
1-1	32	120	PBD	1.0
1-1	32	20	PBD	4.2
1-1	79	30	PBD	.1
1-1	79	7	PBD	1.0
1-1	79	1.5	EG	12.5
2-1	32	120	PBD	1.0
2-1	79	30	PBD	.1
2-1	79	7	PBD	.1
2-1	79	1.5	EG	14.2

PBD is polybutadiene

EG is ethylene glycol

* Deviation from center line as percent of full-scale output.

Gage creep errors are expected in a significant fraction of the gage elements at temperatures of 130°F or higher when the gage element is fully loaded. Long term, high temperature, high stress experiments would be expected to accumulate the errors as a function of the stress, temperature and time. Insufficient data were taken to quantify this aspect, however.

E. GAGE CALIBRATIONS FOR TIME AND RATE DEPENDENCIES

The preceding work has shown that the gages have long term drift and pressurization rate dependencies. In addition, a strong time dependent interaction between the grain and the gage was predicted by Pister (25). These three phenomena are expected to combine to give complex gage calibration relations like the following.

$$V(t,T) = b(t,T)\,\sigma(t,T) + a(t,T) \qquad (4)$$

where

$V(t,T)$ is the measured voltage output of the gage expressed as a function of time and temperature

$b(t,T)$ is the sensitivity of the gage

$a(t,T)$ is the zero stress output of the gage

$\sigma(t,T)$ is the time varying stress applied at the gage

The methods for making these calibrations have not been fully established. But, a procedure that assumes linear viscosity is given in Volume II of this report. This type of calibration would be required for all time dependent loading conditions to which a given application might be exposed. That would include vibration, high rates of pressurization, rapid thermal changes and long term storage.

ASPC recommends that the Air Force support some practical studies to develop the required time-dependent gage calibration procedures.

SECTION 11

IN-SITU RECALIBRATIONS OF NORMAL STRESS GAGES

There are a number of reasons for making an in-situ recalibration. Among those reasons are the following:

(1) Response of gages must be verified.

(2) The gages or the bridge completion circuit may have changed on aging, thus producing new gage characteristics.

(3) Questions regarding gage-grain interactions can be resolved only through an in-situ recalibrations.

The following discussion describes the theory for making the in-situ recalibrations, with an example set of measurements made on the motor at 110°F. These new calibrations are compared with those taken earlier by the gage supplier.

A. THEORY

This approach is based upon the use of internal pressure or vacuum in the motor to define the load sensitivity of the gages, and the establishment of a condition where the thermal stresses in the grain can be assumed (or, even defined) to be negligibly small. A further requirement of the theory is the use of a number of normal stress transducers to give replicate measurements of a given loading condition.

A final constraint imposed by the theory requires that the diaphragm stiffness of the gage be sufficiently large that the viscoelastic aspects of the gage-grain interaction can be ignored. With the limited operating temperature ranges of the strategic missiles the propellant's viscoelastic contribution should not be a problem. But, the very wide temperature ranges allowed in the use of the tactical rockets could yield a significant viscoelastic effect, unless the gages were specifically designed to eliminate this interaction.

The following simplified relations provide convenient methods for estimating gage calibration parameters from motor pressurization test data.

1. Gage Sensitivity Evaluations

For the normal stress transducer, the fundamental relation between the voltage output, v, and the stress, σ, imposed by the grain is given by

$$v = a + b\sigma \tag{5}$$

where a is the zero stress voltage output of the gage, mv

b is the sensitivity of the gage, mv/psi

At the grain bondline, the normal stress, σ, at the gage is seen to be the sum of three stress components.

$$\sigma = \sigma_g + \sigma_T + \sigma_p \tag{6}$$

where σ_g is the stress due to the force of gravity acting on the grain

σ_T is a thermal stress

σ_p is the stress induced upon motor pressurization

The thermal stress, σ_T, may be taken to be nearly constant for a large grain tested at thermal equilibrium.

The pressurization stress at the bondline, σ_p, is related to the internal chamber pressure, p_a, as follows.

$$\sigma_p = -f_n p_a \tag{7}$$

where f_n is the fraction of the internal pressure that is transmitted through the grain web. It is specifically given by the relation

$$f_n = p_b/p_a \tag{8}$$

where p_b is the pressure reaching the bondline

In general, f_n has a value greater than 0.90.

Combining Equations (5), (6) and (7) gives, after rearrangement

$$v = a + b\,(\sigma_g + \sigma_T) - bf_n\, p_a \tag{9}$$

Taking the derivative of Equation (9) with respect to p_a gives

$$\frac{dv}{dp_a} = -bf_n \tag{10}$$

Thus, the slope of a plot of gage output voltage versus motor internal pressure equals the gage sensitivity multiplied by a term that has a value close to 1.0. In general, the value of f_n is adequately calculated from structural analyses of the pressure calibration test.

2. Determinations of the Zero Stress Output

This quantity must be approximated using both empirical and analytical procedures. The basic relation to be used here is Equation (9) with the internal pressure, p_a, set equal to zero (atmospheric pressure).

$$v = a + b\,(\sigma_g + \sigma_T) \tag{11}$$

At the assigned stress-free reference temperature, T_r, the thermal stress, σ_T is arbitrarily set equal to zero*, while σ_g is readily calculated for a given grain design. Thus, upon rearrangement a at T_r is given by

$$a(T_r) = v(T_r) - b(T_r)\sigma_g \tag{12}$$

Thus, we have one known value of a.

The value of a at other temperatures, a(T), is obtained in terms of this quantity, but in an indirect way. This is done by first rearranging Equation (5) to give

$$\frac{v}{b} = \frac{a}{b} + \sigma \tag{13}$$

Then, the following definitions are made.

$$\emptyset \equiv \frac{v}{b} \tag{14}$$

and

$$\alpha \equiv \frac{a}{b} \tag{15}$$

So, Equation (13) becomes

$$\emptyset = \alpha + \sigma \tag{16}$$

This change of variables permits a simplification in the analysis, as shown below.

---

* In practice the motor must be stored at this temperature for a period of time sufficient to allow a nearly complete relaxation of the grain thermal stresses. We prefer to call this process, "annealing".

At the reference temperature, T_r, Equation (16) takes on the form

$$\emptyset(T_r) = \alpha(T_r) + \sigma(T_r) \tag{17}$$

Similarly, after equilibrating the motor at another storage temperature, T, Equation (16) becomes

$$\emptyset(T) = \alpha(T) + \sigma(T) \tag{18}$$

Subtracting Equation (17) from Equation (18) gives the following incremental relation.

$$\Delta\emptyset = \Delta\alpha + \Delta\sigma \tag{19}$$

where, by definition,

$$\Delta\emptyset \equiv \emptyset(T) - \emptyset(T_r) \tag{20}$$

$$\Delta\alpha \equiv \alpha(T) - \alpha(T_r) \tag{21}$$

$$\Delta\sigma \equiv \sigma(T) - \sigma(T_r) \tag{22}$$

Substituting Equation (6) into (22) and making the appropriate subscript changes gives

$$\Delta\sigma = (\sigma_g + \sigma_T + \sigma_p) - (\sigma_g + \sigma_{T_r} + \sigma_p) = \sigma_T \tag{23}$$

This simplification arises from the fact that σ_g is virtually independent of the storage temperature, that the tests are to be conducted at atmospheric pressure where $\sigma_p = 0$, and that $\sigma_{T_r} \equiv 0$.

Consideration is now given to a number of transducers placed circumferentially around a motor at the bondline. That is, the gages are all placed at a given axial distance along the motor, Figure 87. If the grain is symmetrically designed all of the gages should experience the same thermal stress (as shown by Equation (23) we are not concerned here with σ_p and σ_g) Thus, for the various gages

$$\Delta\sigma_1 = \Delta\sigma_2 = \ldots = \Delta\sigma_i \tag{24}$$

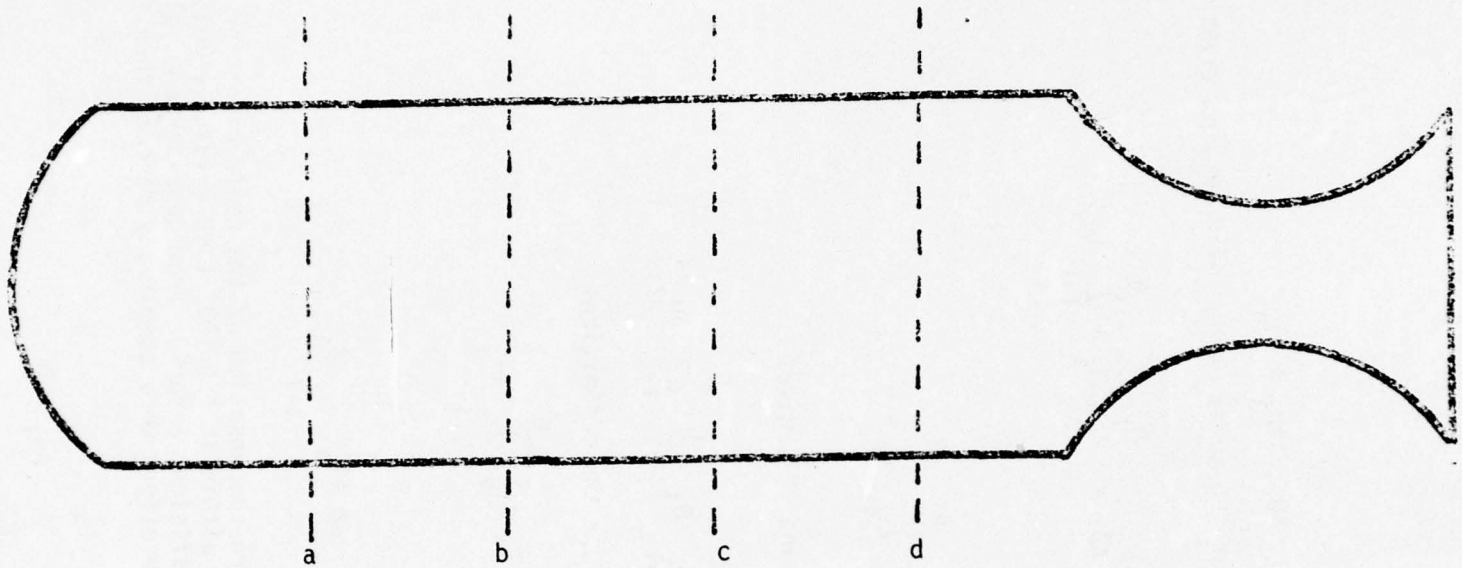

FIGURE 87. DEFINITION OF RELATIVE AXIAL POSITIONS

Also, for the i^{th} gage

$$\Delta\emptyset_i = \Delta\alpha_i + \Delta\sigma_i \tag{25}$$

Summing Equation (25) over the total number of gages, n, gives

$$\sum_{i=1}^{n} \Delta\emptyset_i = \sum_{i=1}^{n} \Delta\alpha_i + \sum_{i=1}^{n} \Delta\sigma_i \tag{26}$$

But, from Equation (24)

$$\sum_{i=1}^{n} \Delta\sigma_i = n\,\Delta\sigma_i \tag{27}$$

Combining Equations (26) and (27) gives

$$\frac{1}{n} \sum_{i=1}^{n} \Delta\emptyset_i = \frac{1}{n} \sum_{i=1}^{n} \Delta\alpha_i + \Delta\sigma_i \tag{28}$$

For convenience, we will use the definitions

$$\overline{\Delta\alpha} \equiv \frac{1}{n} \sum_{i=1}^{n} \Delta\alpha_i \tag{29}$$

and

$$\overline{\Delta\emptyset} \equiv \frac{1}{n} \sum_{i=1}^{n} \Delta\emptyset_i \tag{30}$$

The temperature compensation of the coefficient for the stress transducers was designed to be within 1% FSO/100° (see Reference 26). Also, the effect of temperature on the coefficient α varies from gage-to-gage, although it is not completely random. If the effect were completely random, then for a large value of n:

$$\sum_{i=1}^{n} \Delta\alpha_i \approx 0 \tag{31}$$

Nevertheless, the summation is expected to be quite small* and division by n further reduces its size.

Combining Equations (28) and (31) gives the apparent stress on the gages.

$$\Delta\sigma_i = \frac{1}{n} \sum_{i=1}^{n} \Delta\emptyset_i \qquad (32)$$

The $\Delta\sigma_i$ calculated here may now be used in Equation (25) to get the for each gage. Substituting this quantity in Equation (21) and, then, into Equation (15) gives the desired $a_i(T)$ for the i^{th} gage. This process reduces to the following relation

$$a_i(T) = b_i(T) \left[\frac{a_i(T_r)}{b_i(T_r)} + \Delta\emptyset_i - \Delta\sigma_i \right] \qquad (33)$$

The use of Equations (32) and 33) requires as many gage measurements as possible, with great care taken to exclude data from those gages that have behaved erratically or shown some other form of gage or measurement anomally.

B. APPLICATION TO 110°F MEASUREMENTS ON FULL-SCALE MOTOR NO. 1

Internal pressurization tests were conducted on the full-scale motor at 110°F using the newly certified DAS and motor testing procedures. The motor had been held for 9 months at 110°F during the diagnostic and repair procedures. This temperature had been selected as a good candidate for the reference temperature, T_r, since the motor was cast and cured at 110°F, then held there for four additional months while the propellant post-cure reactions took place. This last storage at 110°F was intended as an annealing process designed to promote residual post cure reactions and accelerate the relaxation of thermal stresses.

The internal pressurization of the motor was accomplished in pressure steps according to the following sequence: 0, 10, 20, 30, 40, 50, 30, and 0 psi. The motor was held for 30 minutes at each pressure during which time the gages were read three times; after 10, 20 and 30 minutes.

---

* For tactical motors at low storage temperatures a finite value of $\bar{\Delta}\alpha$ may be required. The factors involved in generating its magnitude have not been explored.

The analysis of these data involved a rearrangement of Equation (10) which gives

$$\hat{b} = -\frac{1}{f_n}\frac{dv}{dP_a} \tag{34}$$

Where the symbol $\hat{b}$ is used to represent that this is an estimate of the sensitivity parameter.

The slope $-\frac{dv}{dP_a}$, was obtained from the recorded data using linear regression analyses. The fraction, f_n, was obtained from elastic analyses of grain pressurization, Appendix P, using the relationship given in Equation (8). The values of $-dv/dp_a$ and f_n thus obtained are tabulated in Table 29 along with those of $\hat{b}$.

Estimates of the zero stress voltage output, $\hat{a}$, were obtained from the motor pressurization test data taken at atmospheric pressure. Equation (12) was used for this calculation. Rewriting that relation in terms of $\hat{a}$ and $\hat{b}$ gives

$$\hat{a} = v(T_r) - \hat{b}\,\sigma_g \tag{35}$$

The values of $\hat{b}$ were obtained from Table 29 and the values of σ_g from the elastic analysis of Appendix P. The measured voltage readings, $v(T_r)$, σ_g, $\hat{b}$ and $\hat{a}$ are tabulated in Table 30.

C. COMPARISONS WITH PREVIOUS CALIBRATION DATA TAKEN ON THE GAGES

Comparisons of gages sensitivities with those previously taken at Konigsberg Instruments and in gage calibrations at ASPC are given in Table 31. These results show that most of the gages (15 out of 20) are more sensitive now than they were at the time of their manufacture. It would appear that there has been a change in either the gage characteristics or the gage-grain interaction effects. The former seems unlikely, but there is insufficient data to support any hypothesis at this stage.

TABLE 29

DETERMINATION OF NORMAL STRESS GAGE

SENSITIVITY PARAMETER FROM

MOTOR PRESSURIZATION TESTING AT 110°F

Normal Stress Gage	$-\frac{dv}{dp}$, mv psi	f_n, dimensionless	$\hat{b}$, mv/psi
N1-1	0.283	0.956	0.296
N1-2	0.277	0.956	0.289
N2-1	0.104	0.862	0.120
N2-2	← BAD DATA →		
N3-1	0.238	0.956	0.249
N3-2	0.218	0.956	0.228
N4-1	0.281	0.862	0.326
N4-2	0.282	0.862	0.327
N5-1	0.905	0.968	0.935
N5-2	0.722	0.968	0.746
N6-1	0.854	0.962	0.887
N6-2	0.770	0.962	0.800
N7-1	0.819	0.942	0.870
N7-2	0.830	0.942	0.881
N8-1	0.779	0.964	0.808
N8-2	0.943	0.964	0.978
N9-1	0.803	0.968	0.830
N9-2	0.815	0.968	0.842
N10-1	0.912	0.962	0.948
N10-2	0.851	0.962	0.884
N11-1	0.844	0.942	0.896
N11-2	0.818	0.942	0.869

TABLE 30

DETERMINATION OF NORMAL STRESS GAGE

ZERO STRESS VOLTAGE OUTPUT FROM

FULL-SCALE MOTOR TESTS AT 110°F

Normal Stress Gage	$v(T_r)$, mv	σ_g, psi	$\hat{b}$, mv/psi	$\hat{a}$, mv
N5-1	-52.58	1.98	+0.935	-54.43
N5-2	-11.40	1.98	+0.746	-12.88
N6-1	-16.96	1.628	+0.887	-18.40
N6-2	5.555	1.628	-0.800	+6.86
N7-1	-28.29	1.50	-0.870	-26.99
N7-2	-8.005	1.50	-0.881	-6.68
N8-1	32.18	0	-0.808	+32.18
N8-2	-50.64	0	-0.978	-50.64
N9-1	-27.04	-1.98	+0.830	-25.40
N9-2	-19.67	-1.98	+0.842	-18.00
N10-1	-13.97	-1.628	+0.948	-12.43
N10-2	-12.77	-1.628	+0.884	-11.33
N11-1	5.216	-1.50	+0.896	+6.560
N11-2	-77.98	-1.50	-0.869	-79.28

TABLE 31

COMPARISON OF GAGE SENSITIVITY CALIBRATIONS, MV/PSI

	N1		N2		N3		N4		N5		N6	
	-1	-2	-1	-2	-1	-2	-1	-2	-1	-2	-1	16
Konigsberg (In Air)												
80°F	0.275	0.270	0.275	0.269	0.272	0.270	0.273	0.272	0.818	0.813	0.812	0.806
130°F	0.277	0.273	0.276	0.270	0.274	0.270	0.271	0.270	0.822	0.818	0.813	0.810
ASPC (In Vacuum)												
77°F	0.282	0.285	0.274	0.270	0.249	0.277	0.289	0.278	0.808	0.724	0.805	0.811
In Motor (Air Atmosphere)												
~75°F	0.265	0.269	0.274	0.162 (Bad)	0.249	0.297	0.276	0.276	0.808	0.756	0.807	0.806
In-Situ Recalibration												
110°F	0.296	0.289	-	-	0.249	0.228	0.326	0.327	0.935	0.746	0.887	0.800

TABLE 31

COMPARISON OF GAGE SENSITIVITY CALIBRATIONS, MV/PSI (Cont.)

History	N7		N8		N9		N10		N11	
	-1	-2	-1	-2	-1	-2	-1	-2	-1	-2
Konigsberg (In Air)										
80°F	0.801	0.805	0.814	0.825	0.812	0.812	0.819	0.813	0.823	0.822
130°F	0.800	0.806	0.822	0.826	0.815	0.813	0.815	0.823	0.825	0.816
ASPC (In Vacuum)										
77°F	0.804	0.811	0.883	0.824	0.802	0.808	0.820	0.838	0.833	0.831
In Motor (Air Atmosphere)										
~75°F	0.847	0.841	0.829	0.853	0.645	0.805	0.818	0.814	0.824	0.795
In-Situ Recalibration										
110°F	0.870	0.881	0.808	0.978	0.830	0.842	0.948	0.884	0.896	0.869

SECTION 12

RECOMMENDATIONS FOR FUTURE TESTS ON MOTOR NO. 1 FOR COMPARISON WITH ANALYSES

Any recommendation for possible future tests on Motor No. 1, must be made in terms of the magnitudes of the stress levels being measured and the probable error in making these measurements. Clearly, the larger stress levels are more significant with respect to any given measurement error, so test conditions which give large grain stresses are preferred. Considerations of significant stress levels in these measurements are discussed first, then some recommended test plans are presented.

A. SIGNIFICANT STRESS LEVELS

The considerations made here involve statistical considerations of significance and the possibility of large thermal stresses in Motor No. 1.

1. Statistical Considerations

The simplest approach to questions of measurement significance is to use the Student t-test. The recommended form of this test evaluates the significance of the difference between average measured stresses and the analytically predicted values. To keep from being restrictive, the standard deviation for the test measurements is assumed to be unknown and must be calculated from the replicate measurements.

The calculation of t_o from the test data and analytical predictions requires the following relation

$$t_o = \frac{|\sigma_A - \bar{\sigma}|}{\hat{S}/\sqrt{n}} \tag{36}$$

where: σ_A is the analytically predicted stress

$\bar{\sigma}$ is the average of the measured stress

S is the estimated standard deviation from the tests

n is the number of replicate test measurements.

The measured mean stress, $\bar{\sigma}$, is significantly different from σ_A when t_o is greater than the table value of t at the selected confidence level. We will use this fact together with the following definition

$$\Delta \equiv |\sigma_A - \bar{\sigma}| \tag{37}$$

Substituting Equation (37) in (36) gives

$$t < \frac{\Delta}{\hat{S}/\sqrt{n}} \tag{38}$$

or, upon rearranging

$$\frac{\Delta}{\hat{S}} > t/\sqrt{n} \tag{39}$$

Equation (39) provides a simple ratio of the significant stress difference to the testing error in terms of the number of replicate test measurements. A plot of $\Delta/\hat{S}$ versus n is given in Figure 88 for a confidence level of 95%. The curve decreases rapidly as the number of replicates increase from 2 to 4 and $\Delta/\hat{S}$ falls to a value of 1.05 at six replicates. Thus, with six replicate measurements Δ is significant if it exceeds 1.05 $\hat{S}$. This appears to be a good target criterion for both the number of replicates and for the stress difference, Δ.

The replicate measurements could come from repeat tests on the motor or from gages located in the same axial plane in the motor; see Figure 87. The shear stress gages have little redundancy with four sets of paired gages (two replicates for each set).

The normal stress transducers each have two bridges; so paired transducers would give four replicate measurements. There are four sets of paired transducers, with four replicates for each set and one set of three gages (N6, N8 and N10) with six replicate measurements.

From these considerations it is concluded that at least two repeat tests on the motor would be required for the normal stress gages and three motor tests for the shear gages. Considering the difficulties in reproducing large motor tests it is recommended that three replicate measurements be made in the planned experiments.

2. Possibly Large Thermal Stress Levels

There is growing evidence (27 to 30) that propellant moduli taken at low strains (i.e., at 0.25% and below) are much larger than those taken at higher strains (i.e., at 1% and above). The impact of these moduli discrepancies are being felt in comparisons with motor thermal stress* data (31 and 32). The measured stresses given in these motor tests were four and six times, respectively, those analytically predicted.

---

* Acceleration stresses are usually not dependent upon grain moduli and comparisons of these stress measurements with analyses have usually been quite good.

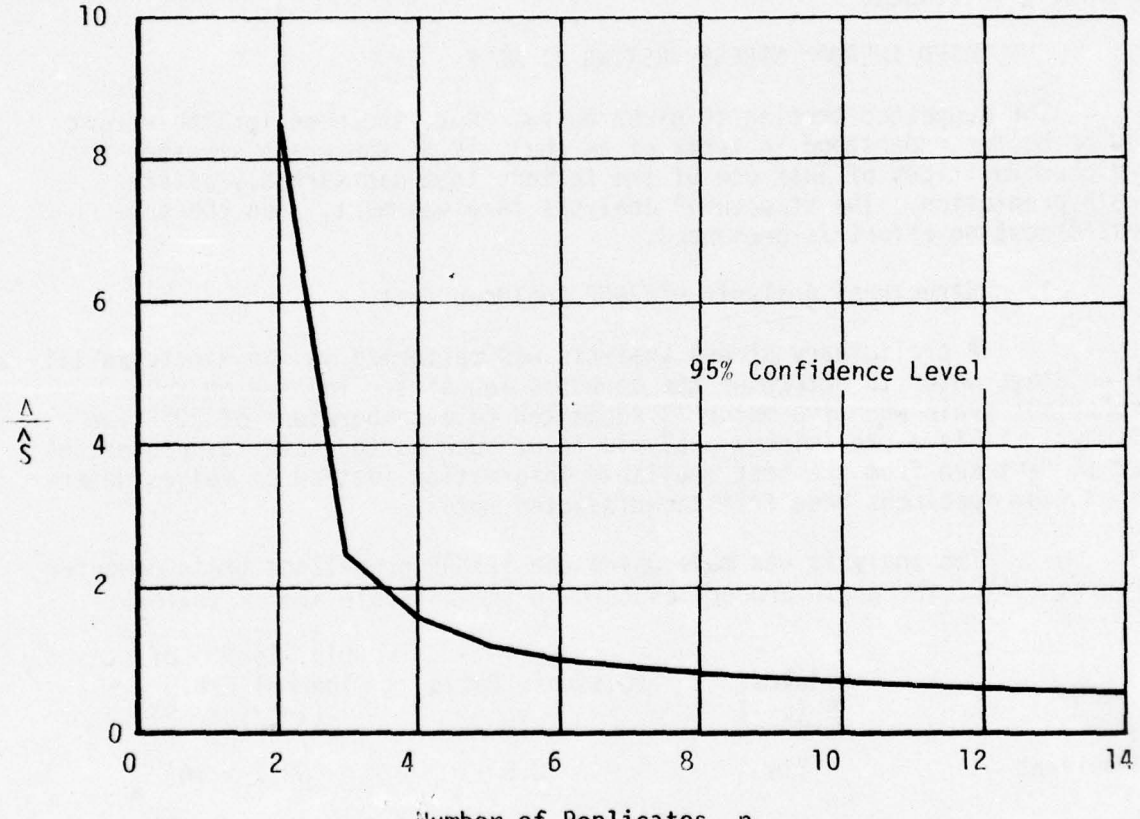

FIGURE 88. STRESS DIFFERENCE-TO-TESTING ERROR RATIO VERSUS NUMBER OF REPLICATES

To predict the creep of a 120 in. grain in vertical storage, Bills and Svob (33) had to use compression tests on large specimens, which gave propellant moduli that were four times those obtained in conventional tensile measurements.

Based on these and other supporting laboratory observations, it is expected that the thermal stress measurements in Motor No. 1 may be higher than expected. If the stress measurements should be as much as a factor of two higher than those predicted, then the stress difference, Δ, will be quite large and the tolerable error in the gage data correspondingly increased.

B. SUGGESTED THERMAL STRESS TESTING AT 30°F

The suggested testing is given below. But, the need for the effort can be better understood in terms of an analysis of the grain stresses and considerations of just one of the factors that can markedly affect their prediction. The structural analysis is given next, then the suggested testing effort is presented.

1. Structural Analysis of 30°F Cooldown Test

A preliminary stress analysis was performed on the Minuteman III Third Stage motor to determine the stresses and strain imposed on the propellant grain when the motor is subjected to a temperature of 30°F for 30 days. It is a preliminary analysis in as much as the material properties had to be taken from the best available information instead of values determined from specimens made from the dissected motor.

The analysis was made using the TEXGAP propellant grain computer program (34). The grain properties used in the analysis are as follows:

	Modulus, E (psi)	Poisson's Ratio ν	Lin. Coeff. of Thermal Exp., α (in./in./°F)
Propellant	216	0.5	53.7×10^{-6}
Liner	300	0.5	53.7×10^{-6}
Insulation	500	0.5	100.0×10^{-6}

The results of the analysis are shown in Figures 89 to 91. Figure 89 shows the inner bore hoop strain distribution when the third stage motor is subjected to a temperature of 30°F for 30 days. The location of the LVDT's are also shown in this figure. Figures 90 and 91 show the propellant-liner interface tensile and shear stress distributions, respectively. The appropriate gage locations are also shown on these same figures.

Over the gages the normal stresses range from about 5 psi to a maximum of about 14 psi, Figure 90. If the propellant in motor No. 1 follows Minuteman experience (35) then the modulus in the grain would be larger than that used here according to the relation

$$E_r(\text{grain}) = 1.319\, E_r(\text{carton}) + 48.270 \qquad (40)$$

where E_r is the relaxation modulus at a specific time

Using Equation (40) the propellant modulus would be increased from 216 psi to 333 psi. This is a 56% increase that would be directly reflected in the grain stresses.

The analysis given above, and the large correction to the propellant modulus, were presented to illustrate both the approximate magnitudes of the grain stresses and the considerable size of just one of the unknowns in making accurate stress predictions. To this may be added the possibly larger effect of strain-level dependence on propellant moduli, as noted previously.

2. Recommended Testing Plan

It is recommended, therefore, that Motor No. 1 be subjected to three thermal cycles from 110°F to 30°F. In each cycle this would require 30 days at both temperatures. The storage at 110°F should anneal the grain and recover the modulus parameters. Reference 36 reports work on the ANB-3066 propellant to show recovery of strain induced damage. This work is summarized in Section 14.C below.

The system measurement errors are expected to be better than 1% of the full-scale output of the normal stress transducers and no worse than 1.5% FSO. This should be quite adequate to assess the expected deviations from analyses.

If gage drift should be considered to be a problem it can be checked at the end of each 110°F storage and all gages normalized to that point for the duration of the cycle.

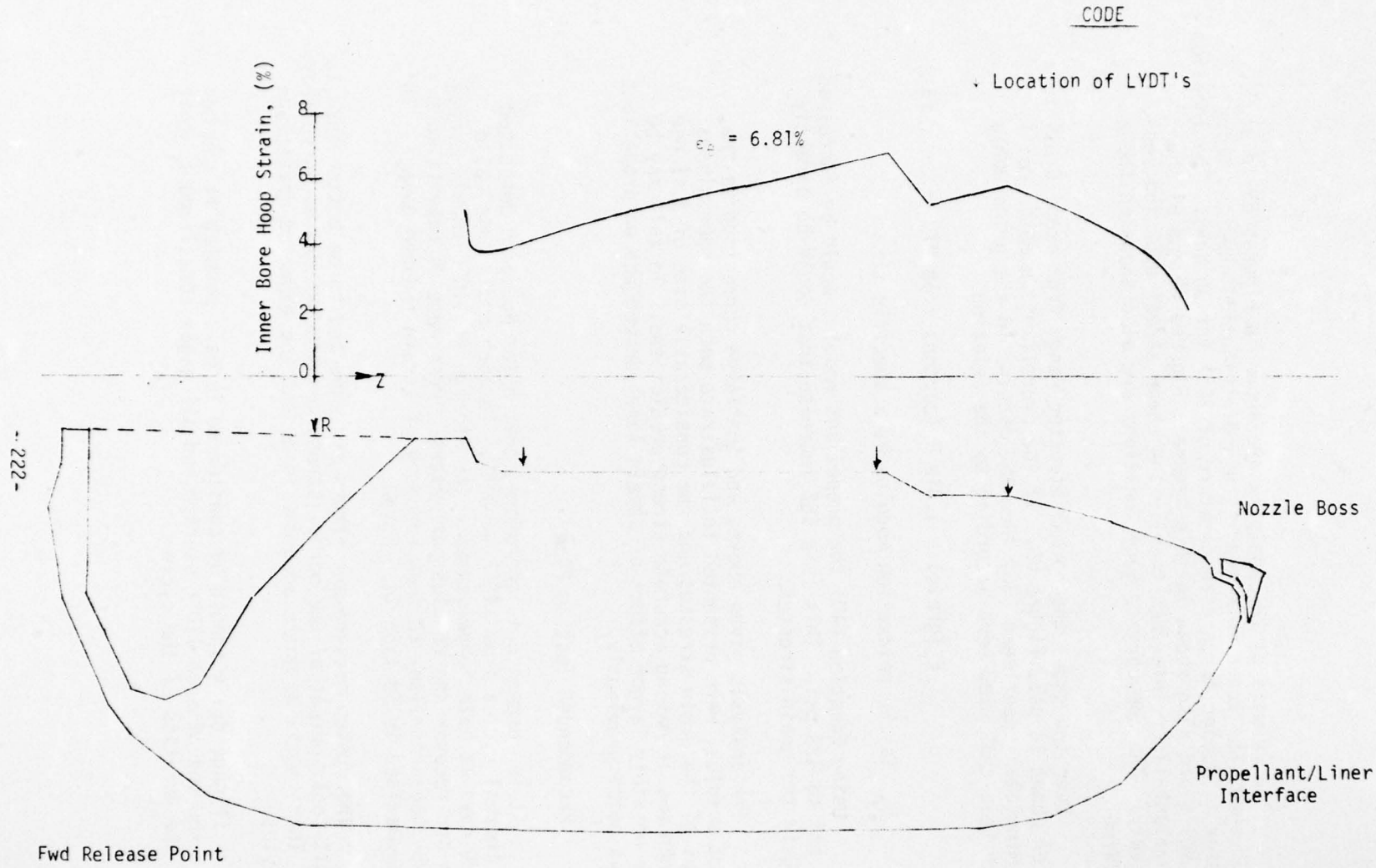

FIGURE 89. INNER BORE HOOP STRAIN DISTRIBUTION, MM III 3RD STAGE III MOTOR SUBJECTED TO 30°F FOR 30 DAYS

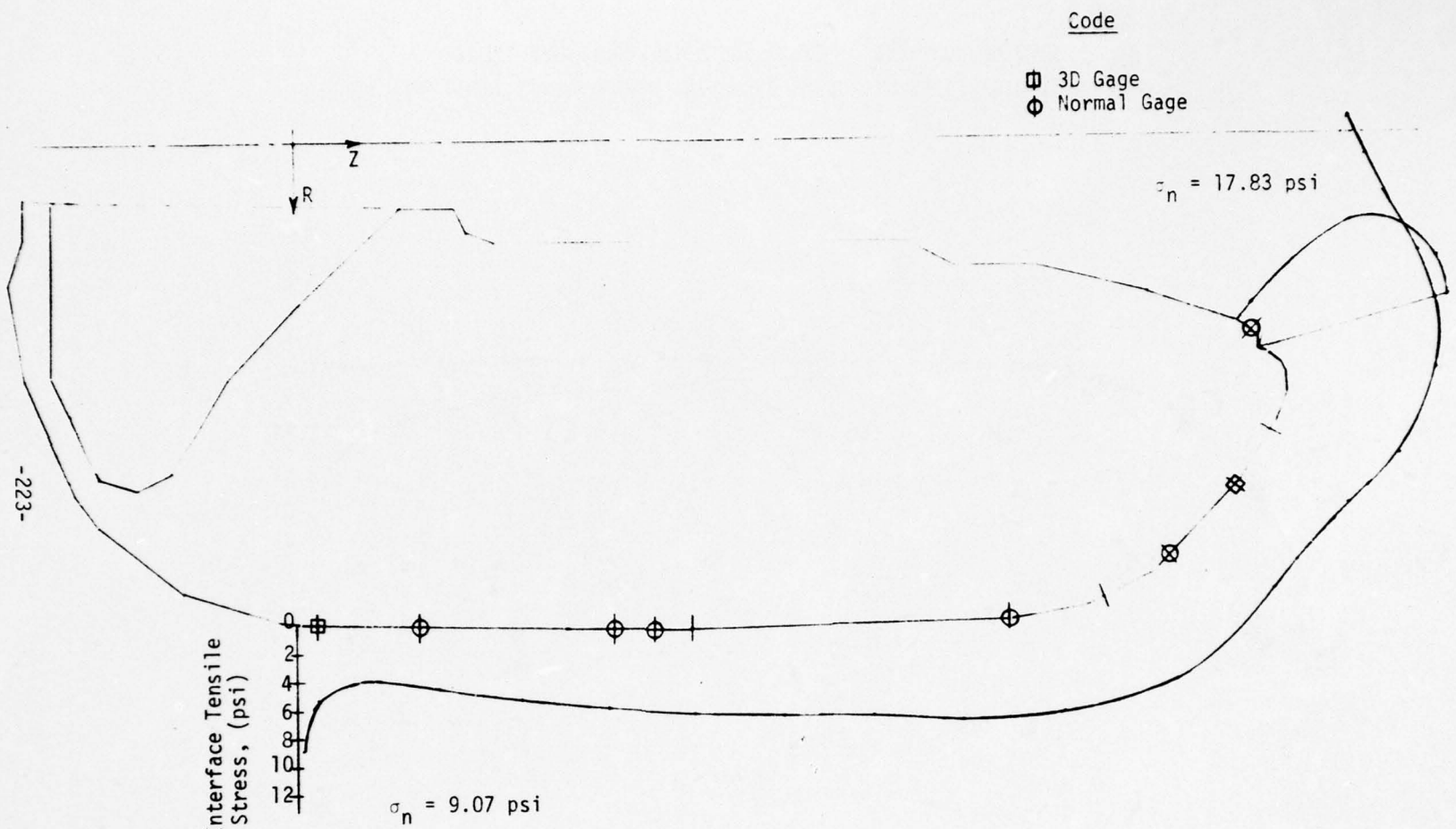

FIGURE 90. PROPELLANT-LINER INTERFACE TENSILE STRESS DISTRIBUTION

MINUTEMAN III 3RD STAGE MOTOR SUBJECTED TO 30°F FOR 30 DAYS

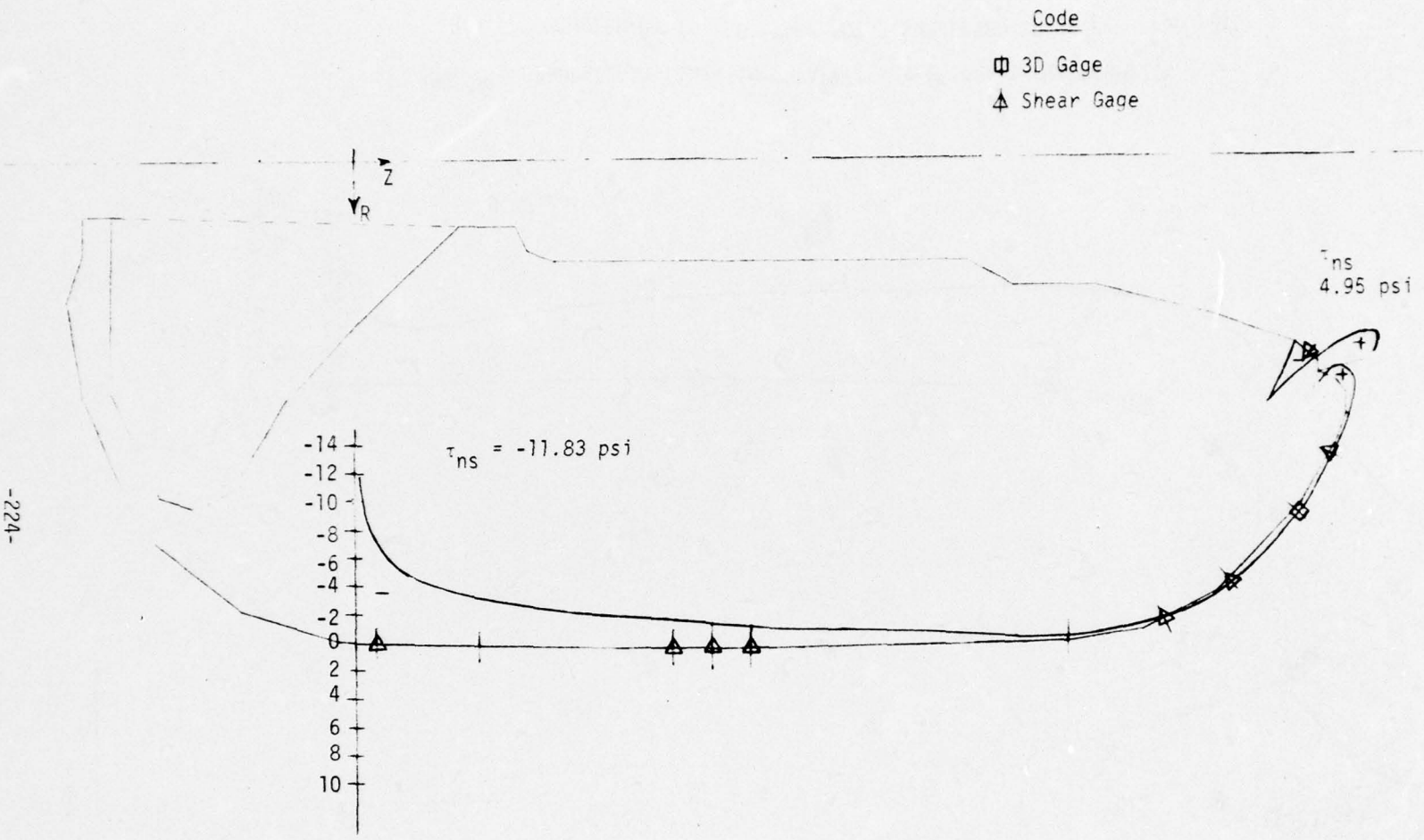

FIGURE 91. PROPELLANT - LINER INTERFACE SHEAR STRESS DISTRIBUTION
MM III 3RD STAGE MOTOR SUBJECTED TO 30°F FOR 30 DAYS

C. SUGGESTED HIGH RATE PRESSURIZATION TESTING

This effort is not recommended as a test of grain response properties, although it might serve that purpose. The effort is recommended primarily to assess high rate response characteristics in the transducers and gage-grain interaction phenomena.

1. Rate Dependency of Both the Gage and the Grain

As discussed earlier in this report the normal stress gages showed viscoelastic response effects; the higher the pressurization rate the greater the response lag in the gage. This effect could be evaluated for all of the transducers in the motor in a series of pressurization tests. Then, they should be dissected from the motor and individually characterized for their rate dependency. The primary purpose of this effort would be to devise general procedures to account for this rate effect in the transducers.

Unfortunately, the grain itself evinces the same kind of rate dependency, and it operates in the same direction as that observed in the gages. Figure 92 illustrates the attenuation effect for a plane section through the grain. If the propellant had no modulus the pressure at the grain inner-bore would immediately reach the case wall. However, the propellant is a stiff material that resists the inner-bore pressure. As the pressurization rate increases the effective stiffness of the propellant increases and less of the inner-bore pressure reaches the case wall.

The resolution of these two rate dependent phenomena (the gage and the grain) requires an additional consideration for the gage-grain interaction. This is a third rate dependent phenomenon whose resolution is essential to the use of these gages under high rates of loading.

2. Recommended High Rate Pressurization Testing

From the point of view of motor testing, it is recommended that the motor be subjected to repeated pressurizations to a maximum of 200 psig, with zero dwell time at the peak pressure. This should involve three pressurization rates conducted three times at each rate.

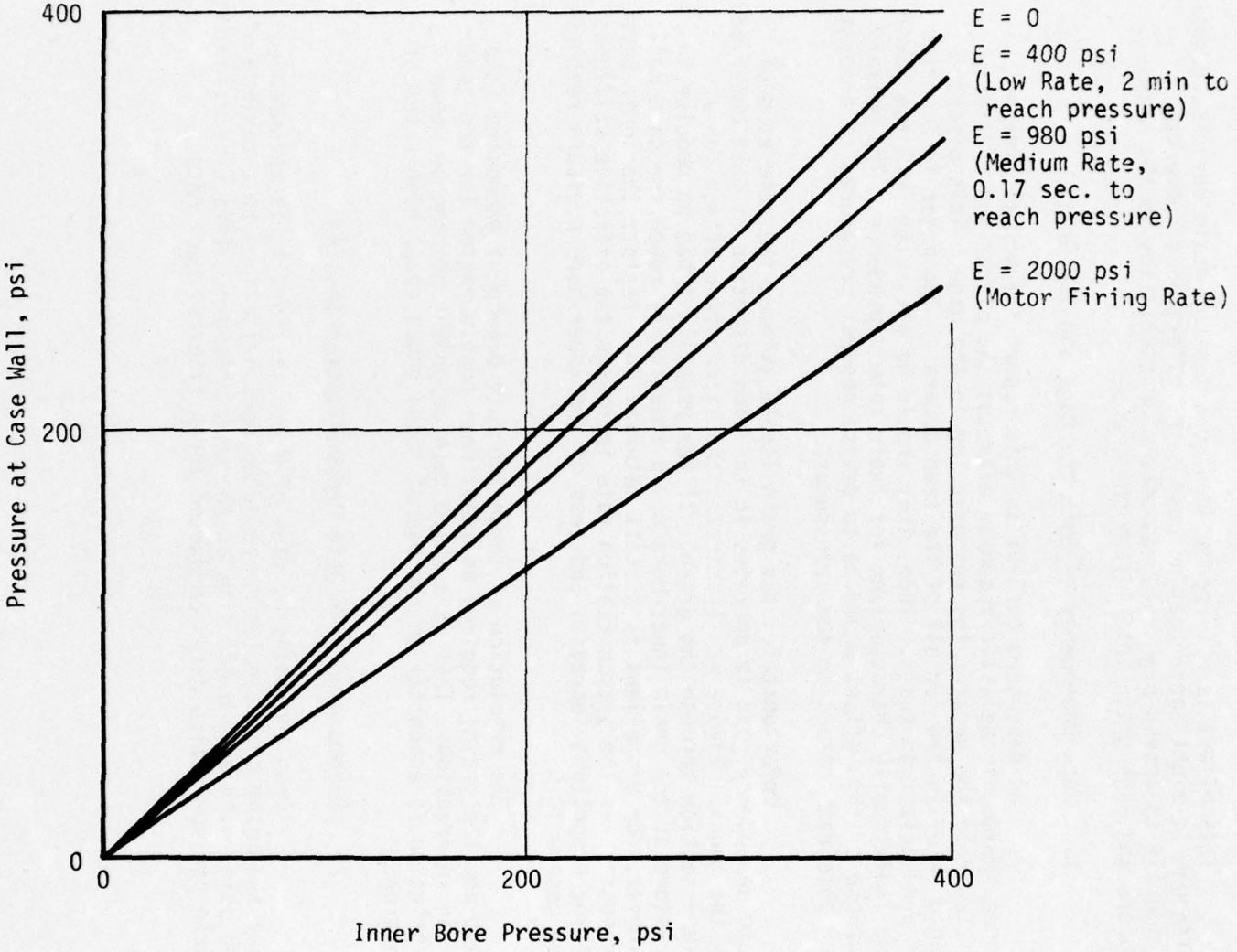

FIGURE 92. EFFECT OF RATE OF PRESSURIZATION ON PRESSURE ATTENUATION

A fundamental assessment of the gage-grain interaction should be conducted before the testing to best define the actual testing approach that would allow corrections for the phenomenon. If this analytical correction is achieved, then the rate dependences of the grain and of the gages can be assessed. This should be confirmed by dissecting the motor and performing individual characterizations on the gages and on the propellant.

SECTION 13

PROGRAM ASSESSMENT

The final efforts of the basic program were to compare the motor test data with the STV results, evaluate the potential value of STV's, and make recommendations for the disposition of the two full-scale motors. These final efforts are reported below.

A. COMPARISON OF MOTOR TEST DATA WITH STV RESULTS

The chores assigned to the STV's on this program (16) were for the most part quite successful. They provided evaluations of gage installation procedures, potting, and gage performances under various motor loading conditions. Unfortunately, the gage measurement anomalies that occurred in the full-scale motor testing prevented any meaningful comparisons with the STV testing. After the system was reworked, the residual gage drift and pressurization rate dependency led to a termination of the program. Thus, there was no real chance to compare test data taken on the full-scale motor and the STV's.

B. POTENTIAL VALUE OF THE STV'S AND THEIR FUTURE USE

The limited experience of this program has shown tests of these motors are potentially much more practical than those on the large motors. The tests are cheaper to conduct, the motors easier to fabricate, and the testing schedules are often shorter, and they can be easily dissected for retrieval of the somewhat expensive gages. In addition, the work can be performed in a laboratory under close supervision of the experimenter.

There are few features of the large motor that cannot be scaled for evaluations in the STV motors. For the most part these are limited to factors associated with the bulk of the large grain. This would include gravitational stresses, large thermal gradients across the web, and patterns of propellant flow that give rise to property gradients (i.e., gradients of propellant density, modulus and strength). But, the first two effects, in most cases, are adequately handled by analysis and do not require gage monitoring, anyway.

The effects of property gradients and flow patterns are little understood at this time and no serious problems identified with them have been established. So, it is doubtful that gages in full-scale motors will be required to monitor their effects.

There are specific design features in full-scale motors that do need experimental stress analyses applied to them, but, the more fundamental questions of the adequacy of present stress and failure analyses need to be addressed first. This function can be conducted most practically by the STV's.

C. RECOMMENDATIONS FOR THE DISPOSITION OF THE FULL-SCALE MOTORS

The recommended disposition of Motor No. 1 is presented in Section 12, which involved thermal and pressurization testing, then motor dissection to recover and calibrate the gages for high pressurization rate sensitivity.

Motor No. 2 would best serve the Air Force as an asset in the Long Range Service Life Analysis studies at OALC. This motor has been stored under conditions similar to those for Motor QT-11 which evinced special liner aging characteristics that need to be better understood.

Another use for Motor No. 2 might be its application to the deflagration-to-detonation transition problem. This motor could be used to monitor the sequence of events occurring in the initial break-up of the grain after the nozzle or forward head is blown off.

It is recommended that the motor be fired for a time between 12 and 15 seconds before the destructive sequence begins.

D. CONSIDERATION OF MOTOR NO. 2

In considering any future experimental stress analysis efforts with full-sclae motors it should be remembered that Motor No. 2 received the benefits of the learning experiences gained from the instrumentation of Motor No. 1, and it has been stored undisturbed since grain cure. It, therefore, represents an asset which would be better suited for the types of tests suggested in this section.

SECTION 14

SUPPORTING ANALYSES

The original interpretation of the major objective of this program was to define the capabilities and limitations of existing, advanced structural analysis techniques. Consistent with this objective it was planned that in Phase IV (Program Assessment) a re-analysis of the Minuteman III, Stage III motor be performed using a non-linear viscoelastic stress analysis and a NASTRAN dynamic analysis, with refinements provided in the areas of flexible case composite behavior, computer programming and propellant properties characterization.

To provide these needed refinements several parallel experimental and analytical efforts were conducted. The results are briefly summarized in the following sections. For more details regarding the composite characterization and propellant damage studies the reader is referred to AFRPL-TR-75-11, dated May 1975.

A. VISCOELASTIC CHARACTERIZATION OF A NON-LINEAR GLASS/EPOXY COMPOSITE INCLUDING THE EFFECTS OF DAMAGE

Isothermal creep and recovery tests were conducted on an epoxy resin and a glass fiber-reinforced composite made from the same bulk resin. The glass/epoxy which was studied included unidirectional and laminated (angle-ply) composites as well as samples removed from a Minuteman III solid rocket motor case. The creep and recovery tests were carried out at a series of stress levels well into the non-linear region at temperatures of 20, 75 and 140°F for several fiber angles. Both the epoxy and glass/epoxy were found to be thermorheologically complex materials with a creep compliance which may be represented by a power law in time.

The linear viscoelastic principal creep compliances were determined for the glass/epoxy using fourth-order tensor transformations. Using the Halpin-Tsai relationships and the "rule of mixtures", the principal creep compliances were compared with those predicted by micromechanics. The experimental results were found to agree very well with the Halpin-Tsai model, except at higher temperatures, and were within the upper and lower theoretical bounds on compliance which were established. The presence of significant crack growth, even at low stress levels, was found to create appreciable softening at higher temperatures.

The non-linear properties were found to depend primarily on the stress normal to the fiber, suggesting a crack opening mode as the essential mechanism. Multiple cycles of creep and recovery showed a disproportionate amount of damage during the first cycle. Crack growth was found to reduce more rapidly with less softening in the laminated ($\pm\ \theta$) composites as a result of the interfacial barrier between the layers. In general, the off-angle composites exhibit considerable softening due to crack growth.

Bending tests conducted on glass/epoxy beam and plate specimens reflect a strong influence of the strain gradient. Linear theory can be used for most of the useful engineering range of application. Non-linear theory, based on unidirectional data, underpredicts the actual stiffness as a result of rapid crack arrest near the outer surfaces.

Multiple cycling effects on the glass/epoxy composite were found to depend on the stress normal to the fiber. The second-order Lebesgue norm (L_2) was found to model multiple cycling effects such as seen in a solid rocket motor case. The L_2 norm, which is a measure of the root mean square of the stress, is proposed as a model for the time-dependent crack growth softening during hydrotesting.

B. GEOMETRICALLY NONLINEAR ANALYSIS OF AXISYMMETRIC SHELLS

The TEXGAP-SA038 program has been modified to include the effects of geometrical nonlinearities during loading of the structure. The new program is available on the UNIVAC-1108 Exec 8 System at ISD and is stored on two tapes; AS 4491 and AS 4492 where one tape is used as a back-up. Various subroutines, which are either new or modified, are linked with the basic linear version of TEXGAP (Reference 34) to form the new non-linear analysis program. The source cards for these modifications are available.

The derivations of the pertinent matrices for the geometric nonlinear analysis modifications, as well as the input instructions which describe the nonlinear option cards required to execute the new program are presented in Appendix Q.

C. RECOVERY OF STRAIN INDUCED DAMAGE IN ANB-3066 PROPELLANT

In the course of the overall "Flexible Case" program the full-scale Minuteman III, Third Stage motor was to be rapidly pressurized to 250 psig then dissected to obtain propellant mechanical properties. But, non-linear viscoelasticity measurements have demonstrated that solid propellants "remember" past deformation histories. Consequently, these histories must be taken into account when planning to characterize the material properties of the grain.

ASPC approached this problem using a series of propellant mechanical property tests designed to assess the effect of motor pressurization on the propellant mechanical properties, followed by evaluations of the effects of annealing time (recovery) in a stress-free condition.

These experiments were conducted to determine how long the propellant cut from the full scale motor would have to be stored before it returned to its original mechanical properties after a short term motor pressurization. Once having eliminated the influence of past deformation by a proper recovery period this propellant could then be characterized for its mechanical properties.

Based on the experimental data contained in this report it was recommended that large propellant blocks from the dissected motor be stored stress-free at room temperature for a period of at least one month. This storage time should be sufficient to eliminate the influence of the pressurization experiment on the propellants mechanical properties. After this period of recovery these blocks could be cut into samples for mechanical properties characterization.

It is important to emphasize that the one-month period cited here is for the specific experimental conditions described. It simply states that one month stress-free storage is required for the material to recover from the effects of a 15 minute relaxation test. What recovery period is required for any other deformation history was not investigated. Past experience would indicate than it is doubtful that recovery of response would occur if the propellant was in a state of tensile stress.

REFERENCES

1. Leeming, H., et. al., Final Report Solid Propellant Structural Test Vehicle, Cumulative Damage and System Analysis, AFRPL-TR-68-130 (October 1968).

2. Burton, J. D. and Noel, Dr. J. S., "Stress State Transducer Development Program," AFRPL-TR-70-102 Final Report on Contract AF04611-68-C-0095 (October 1970).

3. Leeming, H., et. al., "Solid Propellant Structural Test Vehicle and Systems Analysis", Final Report No. AFRPL-TR-70-10, Lockheed Propulsion Co. (March 1970).

4. Leeming, H., et. al., Solid Propellant Structural Test Vehicle Program", Final Report No. AFRPL-TR-72-29, Lockheed Propulsion Company (April 1972).

5. Danieu, D. J., and Ruggles, V. L., "Minuteman STV Stress Analysis and Testing", Final Report No. AFRPL-TR-74-27 (June 1974).

6. Burton, J. D., and Miller, W. H., "Minuteman STV Data Reduction", Contract F04611-72-C-0028, Report No. AFRPL-TR-73-113, Rockwell International (February 1974).

7. Burton, J. D., "Project DAME - Flight and Simulation Testing of a Modified Bomb Dummy Unit", AFRPL-TR-76-60, Rocketdyne Division, Rockwell International Corporation (October 1976).

8. "Simulation Testing of a Modified Bomb Dummy Unit (BDU)", AFRPL-TR-72-107 (December 1972).

9. Briar, H. P., and Bills, Jr., K. W., "Development of an In-Situ Transmitter for Solid Rocket Propellant Surveillance", Final Report No. AFRPL-TR-72-93 (December 1972).

10. Briar, H. P., and Bills, Jr., K. W., and Schapery, R. A., "Design and Test of the Operational In-Situ Gage for Solid Propellant Surveillance", Final Report No. AFRPL-TR-76-36 (June 1976).

11. Leeming, H., and Briggs, W., "Development of a Three Dimensional Stress Gage for Propellant Gages", Final Report No. AFRPL-TR-74-48 (February 1975).

12. Weingart, N., "Operations Manual for the Portable Data Acquisition System", Contract No. F04611-72-C-0083, Syscon Report No. R-2050-30 (July 8, 1974).

REFERENCES (CONT.)

13. Pritts, O. R., et. al., "Simulated Air Launch Environment", Final Report No. AFRPL-TR-74-47 (October 1974).

14. (Unpublished) "SRAM Aging and Surveillance Instrumented Motor Program", Lockheed Propulsion Company (August 1974).

15. Mastrolia, E. J., and Michigian, H. J., "Demonstration of Ambient Temperature Cure", Final Report No. AFRPL-TR-73-68 (August 1973).

16. Jang, S. W., Bills, Jr., K. W., and Leeming, H., "Flexible Case-Grain Interaction in Ballistic Weapons Systems", Special Report No. AFRPL-TR-75-7 (October 1975).

17. (Unpublished) "Hydrotesting of 13 Minuteman III Stage Three Fiberglass Chambers", Aerojet-General Corporation Report (Not dated).

18. Becker, E. B., and Brisbane, J. J., "Application of the Finite Element Method of Stress Analysis of Solid Propellant Rocket Grains", Report No. S-76 Vol. 1 and 2, Rohm and Haas, Co., Huntsville, Alabama (January 1966).

19. Wyle Laboratories Test Report No. 51144 (Unpublished), "Environmental Test Program on Minuteman III Third Stage Motor Part Number 52-TET-1 for Aerojet-General Corporation" (30 October 1968).

20. Leeming, H., "Techniques for Measuring Stress, Strain and Temperature in Solid Propellant Motors", Special Report AFRPL-TR-71-131 (November 1971).

21. Day, E., (Unpublished) "Minutes of AFRPL Flexible Case-Grain Interaction Program Technical Interchange Meeting" (22 August 1974).

22. "Polaris A-3 First-Stage Chamber Preparation and Hydrotest for Structural Evaluation of Through-the-Forward-Head Instrumentation", Final Report, Aerojet Solid Propulsion Company, Report No. POL 71416 (12 March 1971).

23. Hollingsworth Solderless Terminal Co., "Private Communication" (January 15, 1975).

24. Latimer, W. M., The Oxidation States of the Elements and Their Potentials in Aqueous Solutions, P. 209, Prentice-Hall, New York (1939).

25. Pister, K. S., and Leeming, H., "Stress Measurements in Solid Propellant Motors", JANNAF Mechanical Behavior Working Group 8th Meeting 1969, Vol. I, p. 365 (March 1970).

See Also: Appendix A of "Techniques for Measuring Stress, Strain and Temperature in Solid Propellant Motors", Special Report No. AFRPL-TR-71-131 (November 1971).

See Also: Fitzgerald, J. E., and Hufferd, W. L., "Interaction of a Diaphragm Pressure Gage with A Viscoelastic Halfspace", JANNAF Mechanical Behavior Working Group 8th Meeting 1969, Vol. I, p. 367 (March 1970).

26. (Unpublished) "PS 60: Specification and Discussion "FLUID" Calibration and Temperature Compensation of Normal Stress Transducers", Konigsberg Instruments, Inc., Drawing No. PS 60 (Undated).

27. Francis, E. C. and Carlton, C. H., "Some Aspects of Composite Propellant Nonlinear Behavior in Structural Applications", ICRPG/AIAA 3rd Solid Propulsion Conference, AIAA Paper No. 68-519 (June 1968).

28. Farris, R. J., "The Character of the Stress-Strain Function for Highly Filled Elastomers", Trans. of the Soc. of Rheology 12:2, 303-314 (1968).

See Also: Farris, R. J., "The Influence of Vacuole Formation on the Response and Failure of Filled Elastomers", Trans. of the Soc. of Rheology, 12:2, 315-334 (1968).

29. Adicoff, A., and Lepie, A. H., "Effect of Tensile Strain on the Use of the WLF Equation", J. App. Poly. Sci., 14, p. 953 (1970).

30. Schapery, R. A., and Webb, L. D., in "Solid Propellant Structural Test Vehicle Program", Report No. AFRPL-TR-72-29, pp. 191 to 265 (April 1972).

31. Bills, Jr., K. W., Campbell, D. M., Sampson, R. C., and Steel, R. D., "Failures in Grains Exposed to Rapid Changes of Environmental Temperatures", Aerojet Report 1236-81F, Contract N00017-68-C-4415 (September 1969).

32. Leeming, H., et. al., "Solid Propellant Structural Test Vehicle, Cumulative Damage and Systems Analysis", Final Report No. AFRPL-TR-68-130, p. 91 (October 1968).

33. Bills, Jr., K. W., and Svob, G. J., "Establishing Mechanical Properties Criteria", Bulletin of the 4th Meeting, ICRPG Working Group on Mechanical Behavior, Vol. I, p. 269 (October 1965).

34. Dunham, R. S., and Becker, E. B., " TEXGAP - The Texas Grain Analysis Program", The University of Texas, TICOM, Report No. 73-1 (August 1973).

35. Woodman, D. D. (Unpublished), "Pressure Cure/Aged Bond Summary Report", Aerojet Solid Propulsion Co., Report No. 0162-111-MD-F (20 November 1962).

36. Farris, R. J., and Beckwith, S. W., "Flexible Case-Grain Interaction in Ballistic Weapon Systems", Special Report No. AFRPL-TR-75-11 (May 1975).